CONDITION MONITORING OF TRANSFORMERS: THE ACOUSTIC METHOD

by

Adrian Darryl Moodley

submitted in fulfillment of the requirement for the degree of

MASTER OF SCIENCE

in

ELECTRICAL ENGINEERING

at the

UNIVERSITY OF KWAZULU NATAL

SUPERVISOR: Dr. D.A. Hoch

March 2007

ACKNOWLEDGEMENTS

My sincere gratitude and appreciation to the following:

My supervisor Dr. D.A. Hoch for all his guidance and support.

The laboratory assistant Mr. Geoffrey Bennett for all his support and assistance.

The workshop staff at the University of Kwazulu Natal for all their guidance, assistance and support.

Mrs. Beverly Bennett for all her support.

My family, Andrew Moodley, Premie Moodley, Alicia` Moodley and Sheldon Moodley, for their advice, support, and guidance.

Managers, colleagues and friends from Mittal Steel South Africa for their advice and support.

ABSTRACT

Partial discharges (p.d.'s) are a major source of the progressive deterioration of insulation in high voltage equipment. The existence of this phenomenon is a major cause for concern, as it results in the eventual breakdown of high voltage equipment. Several approaches (e.g. gas-in-oil analysis, electrical p.d. detection methods, R.F. measurements) are currently used to detect p.d.'s, but each of these methods has their associated limitations.

Due to the limitations of the aforementioned approaches, it necessitated the development of a consistent and reliable method for the detection, examination and localization of p.d.'s. This precipitated the development of the acoustic emission method, which essentially involves the examination of the acoustic emissions that emanate from high voltage units. The examination of these acoustic emissions enables many deductions about the present condition of a transformer to be made. The principle employed here is: p.d.'s always produce mechanical stress waves, where the frequency content of the pulses varies with the particular liquid being stressed.

It has been shown that the simultaneous application of both the acoustic method and the electrical method for p.d. detection and localization is more effective and accurate than the individual use of either of these methods. In addition, this combined method is less prone to false alarms.

It is the purpose of this document, to provide the following:

- Review of partial discharges and their occurrence in high voltage equipment with a focus on high voltage transformers.
- Review of the fundamental properties of dielectric liquids, and the prebreakdown and breakdown phenomena observed in these liquids.
- Review of transformer oil and its breakdown characteristics.
- Review of the fundamental concepts in Acoustics.
- Review of the electrical, mechanical and physical properties of the different types of insulation used in transformer units.
- Review of the Electrical and Acoustic Methods of partial discharge detection and localisation.
- Simulations: Conducted using a finite element modeling package. These simulations consist of the following models:
    - Two dimensional simulations.
    - Two dimensional simulations with multiple p.d. sources.
    - Three dimensional simulations.
- Experimental testing on a specially designed test cell. This experimental testing involved the following objectives:
    - Evaluation of the dielectric strength of transformer oil.
    - Evaluation of the various factors influencing the dielectric strength of dielectric liquid.
    - Combination of the electrical method and the acoustic method of partial discharge detection and localization.
    - Evaluation of factors influencing the accuracy and reliability of the acoustic method of partial discharge detection and localization.
- Experimental testing on an oil-filled 11kV distribution transformer. The testing method employed involves the simultaneous application of the electrical method and the acoustic method of partial discharge detection and localization.

LIST OF SYMBOLS AND ABBREVIATIONS

Except where otherwise stated, the following symbols and abbreviations are used in this document.

Symbol	Meaning
μs	microsecond
cm	centimeter
f	frequency
g	grams
H.V.	high voltage
Hz	hertz
I_m	mean current
kHz	kilohertz
km	kilometer
kV	kilovolt
kΩ	kilo-ohm
m	meter
MHz	megahertz
mm	millimeter
ms	millisecond
ns	nanosecond
p.d.	partial discharge
Pa	pascal
pC	picocoulomb
Q_i	injected charge
r_p	radius (point electrode)
s	second
ε	dielectric constant
Ω	ohm

TABLE OF CONTENTS

CHAPTER 1: INTRODUCTION

Transformers are major capital items, and the cost due to a failure, is high in both direct costs and downtime. The early detection of problems is essential in order to reduce losses due to failure. It is for this reason that transformers are monitored frequently using a variety of methods. At the factory, manufacturers have the ability to use electrical methods in order to determine the presence or absence of partial discharges (p.d.'s) in high voltage power transformers. The information provided by these electrical methods is very useful, but this information cannot be used to locate the source of the p.d's. These electrical measurements are also very susceptible to electro-magnetic interference and therefore cannot be used on the field on in-service transformers. In addition, the sensitivity of electrical p.d. detection methods has been shown to decrease with increased capacitance of the test object. [22]

Another frequently used method is the gas-in-oil analysis, which indicates internal partial discharges or arcing. The detection of combustible gases in transformer oil has been used routinely, in order to monitor the health of transformers. A shortfall of the gas-in-oil method is that it provides historical data, which is not representative of the instantaneous condition of the unit. A long delay can occur between the development of a p.d. source and the evolution of sufficient gas to warrant concern. In addition, this method does not provide sufficient information in order to determine the origin of the discharge. It therefore only indicates the existence of a problem.

R.F. measurements may also indicate the existence of a problem, but not the location or cause. Without knowing the location or possible cause of a problem, much time and money may be wasted by investigating problems without attaining any success.

Essentially, p.d.'s are pulse-like in nature. They result in a localized, instantaneous release of energy. A fraction of this released energy heats the material next to the p.d. and can evaporate some of it. This results in the formation of a small explosion [14], which excites mechanical stress waves (acoustic waves)[15], which propagate within the transformer. The discharge therefore acts as a point source for acoustic waves. These stress waves/acoustic emissions travel through the insulating transformer oil, and may subsequently be detected at the transformer tank wall. Several acoustic emission sensors are usually located on the transformer tank wall, and hence by measuring the relative time of arrival of the stress wave at each of the sensors, the location of the source of the p.d. may be ascertained. [14]

Note from the above, that acoustic emission sensing offers an excellent, real time solution which provides information, firstly, about the detection of the p.d. and secondly about the location of the source of the p.d. Acoustic Methods can also be made to be immune to electro-magnetic interference which occurs on the field during "live" testing. It has therefore proven to be the method of choice for many companies. There also exist many instances where the combination of the acoustic and electrical methods of p.d. detection has proven to be more effective than either method individually, in avoiding false alarms, which are common in on-line monitoring. These false alarms may occur in the acoustic signals due to environmental factors such as rain or hail, and may also occur in the electrical method due to electrical signals caused by corona.

The research contained in this document investigates partial discharges, and their occurrence in liquid dielectrics. Furthermore, the characteristics of liquid dielectrics are explored in order to investigate the various prebreakdown and breakdown phenomena that occur in stressed liquid dielectrics. The electrical and acoustic methods of partial discharge detection and localization are investigated and simulated using software. All the aforementioned concepts are then evaluated experimentally using a specially designed test cell and the results obtained as well as conclusions reached have been completely documented.

SECTION A: LITERATURE REVIEW

CHAPTER 2
PARTIAL DISCHARGES

The following chapter examines the phenomenon termed "Partial Discharges" and the mechanisms that underlie them.

2 Definition and classification of partial discharges

Partial discharges are most commonly referred to as electric discharges that do not bridge electrodes. A dielectric in the form of a solid, liquid or gaseous insulator is typically present between the partial discharge and one (or both) of the electrodes.
In transformers discharges are due to electric arcing which vaporizes the dielectric fluid in the discharge path and creates a bubble cavitation effect (examined in following sub-sections).

Common examples of the above type of discharges are:

- Discharges which take place in a solid dielectric (here, both electrodes are shielded from the discharges by the solid).
- Discharges that occur on a surface (where at least one electrode is shielded by a solid dielectric).
- Discharges around a sharp point at high voltages (here, the discharge is shielded from one electrode by a column of non-ionized gas).

However small, each of the above discharges may be, over time they cause progressive deterioration, which in turn leads to failure of the equipment.
Partial discharges belong to the broader group of gas discharges. In gas discharges the gas molecules become ionized by the impact of electrons, and the newly formed electrons gather speed in an electric field, hence ionizing more molecules on impact. This results in an avalanche of electrons being formed. A passage of current through the gas is formed when the electrons in the avalanche and the ions that are left behind, begin moving towards the electrode. The following is a diagrammatic representation of the above-mentioned relationships:

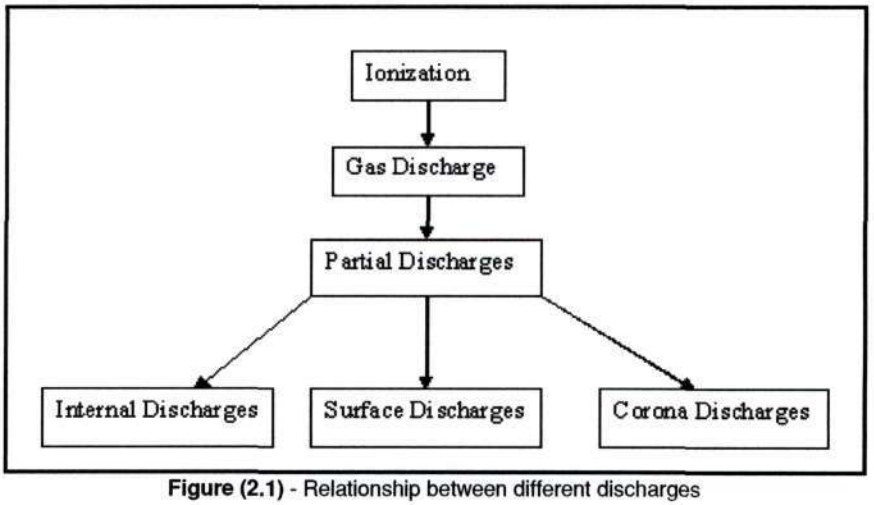

Figure (2.1) - Relationship between different discharges

Description of terminology used in figure (2.1):

- **Ionization**: Is any process by which an atom becomes electrically charged.
- **Gas Discharges**: Passage of current through gases by avalanches of electrons.
- **Internal Discharges**: Refers to discharges that occur in inclusions or cavities within a dielectric.

- **Surface Discharges**: Refers to discharges that occur at the surface of a dielectric.
- **Corona Discharges**: Discharges that occur in the strong inhomogeneous field around a sharp edge or point of an electrode.

There are instances where it is not possible to classify a partial discharge into one of the above types. Figure (2.2), depicts the intermediate state between a surface discharge and an internal discharge. (**Note:** If the space is reduced, until it is eventually closed, the discharge will become an internal discharge).

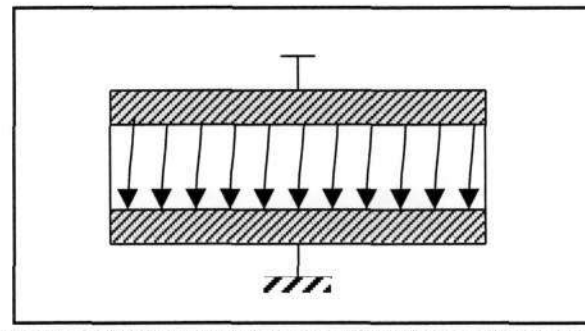

Figure (2.2) - Illustration of the intermediate state between a surface discharge and an internal discharge

2.1 Overview of internal discharges

Internal discharges in a dielectric occur in inclusions that have a low dielectric strength. The material contained in the inclusion, breaks down at a stress that is low, when compared with the breakdown strength of the dielectric that surrounds the inclusion.
Due to the fact that the dielectric constant of the material in the inclusion is typically lower than that of the surrounding dielectric, this causes the electric stress in the inclusion to be higher than that in the dielectric, which ultimately causes the inclusion to break down even earlier.

Gas filled cavities frequently occur in cast resins, plastics, impregnated paper, etc. The stress that is present in the dielectric, when the discharges first occur, depends on the stress in the cavity and also the breakdown strength of the cavity. The following are cases where the stress in the cavity can be easily calculated:

- When the situation occurs, where there is a flat cavity that is situated perpendicular to the electric field, then the stress in the cavity is given by:
  ε × the stress in the dielectric
  (where ε is the dielectric constant of the insulating material).

- If there is a case where the cavity is spherical, the stress in the cavity is given by
  $$\frac{3\varepsilon}{(1+2\varepsilon)} \times \textit{stress in the dielectric} \qquad (2.1)$$
  (**Note:** The equation tends to 1.5 times if ε is large. [1]).

- If the cavity is long and parallel to the electric field, the stress in the cavity is approximately equal to the stress in the dielectric.

The kind of gas present in the cavity, the gas pressure and the dimensions of the cavity, all determine the dielectric strength of the cavity. The breakdown voltage for a given gas is derived by using the Paschen curve for this particular gas. The Paschen curve depicts the breakdown voltage of a given gas as a function of the electrode spacing multiplied by the gas density.

The Paschen curve can also be modified, in order to depict the stress at which the gas breaks down. In this case, the gas pressure is taken as a parameter and the electrode spacing is taken as a variable.

Inclusions can occur in extruded plastics or cast resin insulation, etc. These inclusions may consist of dirt, paper or other foreign particles, and these inclusions may be impregnated in the material, hence resulting in the formation of inclusions of reduced strength. After the breakdown of an inclusion, a gas is produced and gas discharges occur. Note, that after the first breakdown, the breakdown voltage is lower and lower for subsequent breakdowns.
It was observed that a local field of concentration occurs at the edges of a metal splinter, hence attaining the breakdown strength of the dielectric, even if the splinter is deeply embedded in the dielectric. This causes a small portion of the dielectric to break down causing a gas filled cavity to be formed.

Oil filled cavities commonly occur between layers and in butt gaps of the oil-impregnated paper insulation such as in transformer windings and in cables. The stress that occurs in an oil-filled cavity can be calculated in a similar fashion to the calculations that were performed in order to calculate the stress in a gas-filled cavity.

- For a cavity that is flat and lies in a direction that is perpendicular to the electric field, the stress in the cavity is $\frac{\varepsilon_2}{\varepsilon_1} \times$ *the stress in the dielectric*, where ε_1 is the dielectric constant of the oil, and ε_2 is the dielectric constant of the solid dielectric.
- For the case where the cavity is spherical, the stress is given by
$$\frac{3\varepsilon_2}{(\varepsilon_1 + 2\varepsilon_2)} \times \textit{stress in the dielectric} \qquad (2.2)$$
- For a cavity that is long and flat, and parallel to the electric field, the stress in the cavity is equal to the stress in the dielectric.

The breakdown stress of oil is not as well known as that of a gas, because it is strongly dependant on contamination and the amount of dissolved gas present. From the Cigre' report of *De Vos* and *Vermeer* [56], it was established that when oil breaks down, gas bubbles are produced and gas discharges take place in these bubbles (examined in later sub-sections). Due to the fact that a liquid is able to absorb gases, balance is reached between the formation of gas and the absorption of the gas by the liquid. As a result, these discharges either stop, increase or become stable.

2.2 Overview of surface discharges

Surface discharges occur when there is a stress component parallel to a dielectric surface. This is applicable to bushings, end of cables, the overhang of generator windings, and cases where a discharge from outside hits the surface. The discharge affects the electric field. Consequently, the discharges extend beyond the area where the original surface component of the electric field was large enough to cause discharges.

2.2.1 Discharges in air

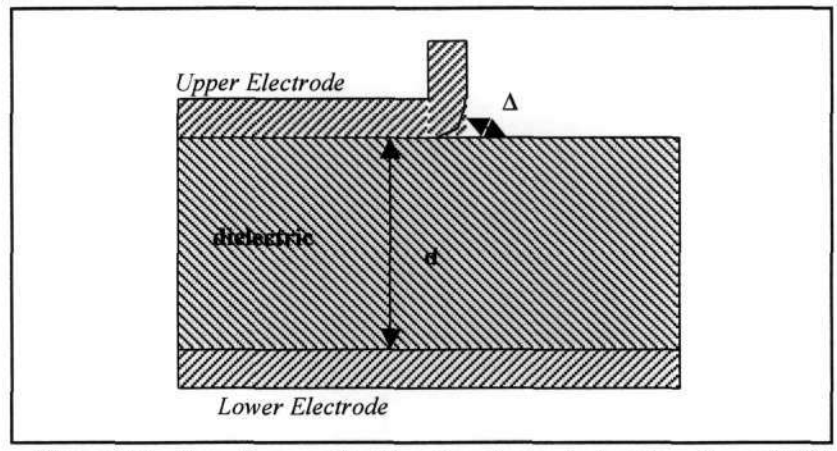

Figure (2.3) – Plane-Plane configuration of an air gap , Δ , in series with a solid dielectric

The air-gap, Δ, which is in series with the solid dielectric **d**, breaks down as shown above. The inception voltage is given by:

$$V_i = \Delta E_i + \frac{dE_i}{\varepsilon}$$, where E_i is the breakdown stress of the air gap Δ. (2.3)

If the breakdown voltage of the air-gap (U_i) is now introduced, the equation becomes:

$$V_i = U_i + \frac{d}{\varepsilon\ \Delta} U_i \quad (2.4)$$

The above formula has a minimum, which is where the gap actually breaks through. Mason[1], developed the following empirical formula for this minima (i.e. the inception voltage of an electrode edge in air). This is given by:

$$(V_i)_{edge} = 4.15 \sqrt{\left(\frac{d}{\varepsilon}\right)\frac{293}{T}} \text{ units} = (kV_{rms}) \quad (2.5)$$

where:
d = thickness of the insulation (mm)
T = Temperature (°K)
E= dielectric constant

Note: the above empirical equation produces results that are correct to $(\frac{d}{\varepsilon})$

Halleck[1], discovered that if the radius of curvature of the electrode edge, is smaller than 1mm, then the inception voltage, (V_i), is decreased by approximately 10 to 20 %. This is due to the concentration of field lines.

Observe figure (2.4). If the upper electrode is separated from the dielectric, then the breakdown voltage is no longer given by the empirical formula, but now it is given by the actual distance Δ. This holds only if Δ is less than the result of the empirical minima equation.

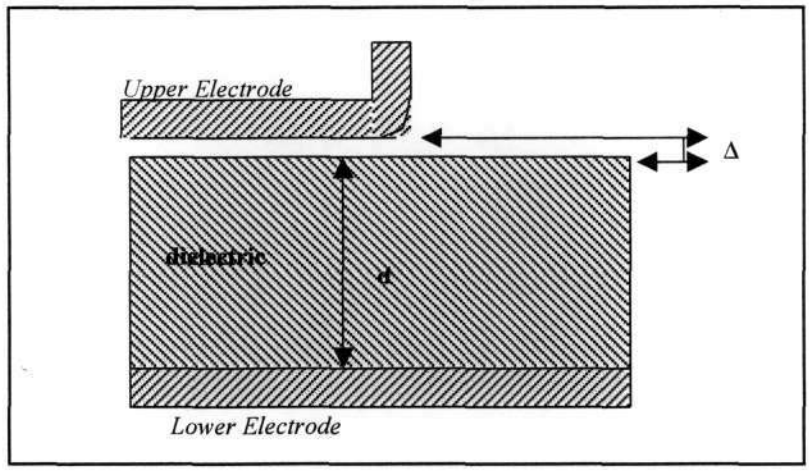

Figure (2.4) – Separation of the upper electrode from the dielectric

2.2.2 Discharges whilst under oil

Similar formulae as for discharges in air could be used, but in this case the breakdown voltage of the oil gap (U_i), is not known precisely. This is due to the fact that the breakdown stress of air is greatly affected by contamination and moisture. Kappeler [1], conducted investigations on the inception voltage of electrode arrangements as found in capacitors and bushings. From these experiments, it was concluded that the inception voltages in air are lower than those following from the formula:

$$V_i = U_i + \frac{d}{\varepsilon \Delta} U_i \qquad (2.6)$$

The apparent cause of this was due to the field concentrations at the edges of the thin capacitor layers.

2.3 Overview of corona discharges

Corona discharges occur around sharp points or edges at high voltage, and they occur sooner at negative voltage than at positive voltage. With alternating current voltage they often occur during the negative half-cycle of the sine wave only.

2.3.1 Negative corona

G.W. Trichel[1] noted that if a positive ion appears in the vicinity of the point, it is attracted by the electric field and moves towards the point. The ion hits the electrode and releases one or more electrons, which cause a cloud of positive ions, near the point and negative electrons traveling away from the point (by the Townsend Mechanism). Radiation occurs and results in photo ionization at the surface of the point and a lateral extension of the ionized region occurs until the cathode spot is formed from which the corona discharge emanates.

At a large distance from the cathode, the electrons slow down and attach themselves to the oxygen molecules in air. Two regions with space charge have now been formed; a positive space charge has been built up in the closest vicinity of the point, by the slow positive ions that are left after the ionization of the air molecules. A larger distance away, the negative ions, which are formed by adhesion of the electrons to the oxygen molecules, cause a negative space charge. This entire process ensues in a time of the order of 10^{-8} seconds, at a distance of 0.1 mm from the point.

A luminous region, commonly called negative glow, appears in the strong field that lies just outside the point. In the region of the negative charge, a faint glow is present (termed the positive column). The Faraday dark space is located between the two luminous parts. The Faraday dark space corresponds to a region of little stress where no ionization takes place.

2.3.2 Positive corona

Discharges occur in a narrow channel when the point is positive. When the inception voltage has been attained, an avalanche of electrons is formed and this causes a distribution of particles, where the electric field at the head of the electron avalanche is increased. Photons come into this increased field and start new avalanches and hence streamer discharges are formed (Depicted in figure (2.5)).

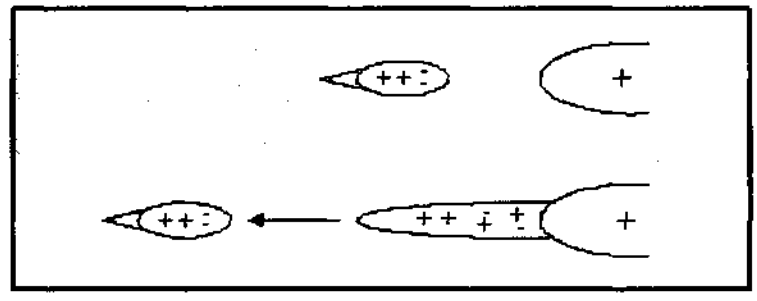

Figure (2.5) - The development of a streamer discharge

2.3.3 Recurrence of corona discharges

At D.C. voltages, negative corona discharges recur regularly and the impulses are equal in size. The repetitive frequency is strongly dependant on the voltage.

However, positive corona discharges recur irregularly. They occur in outbursts of small and large discharges. The rate of repetition increases with an increase in voltage. At A.C. voltages, corona discharges occur initially only in the negative cycle of the high voltage sine wave. They are equal in size and their number increases to a first approximation linearly with the applied voltage. At higher voltages, discharges also occur in the positive half-cycles.

2.4 Summary of partial discharges

In the transformer, partial discharges occur as follows:

- Partial Discharges in the solid insulation. These could occur in the paper, pressboard, wood etc. They may also occur within the insulation due to cavities, impurities etc (principle was discussed earlier). They could also occur on the boundary surface of insulating materials (surface discharges; discussed previously), or between metallic and insulating surfaces.
- Partial discharges in the oil, between sharp or insufficiently rounded-off live metal parts and some neighboring metallic objects of different potential. (Corona partial discharges; described earlier)
- Partial Discharges that occur between metallic objects of undefined potential to parts of fixed potential.
- Partial Discharges caused by bubbles, contamination or moisture. This type usually occurs between the oil and some insulating material or between oil and metal.

The partial discharges that occur in solid insulation, dramatically affects the dielectric strength of high voltage equipment such as transformers. They exert a prolonged destructive force, which results in the progressive deterioration of the dielectric strength of the insulation. They can cause damage either directly or indirectly. In the direct case they result in turn-to-turn faults but it is more probable that they will lead to an indirect fault which refers to the short-circuit stress at a spot within the transformer where the dielectric strength has previously been weakened by partial discharges. P.D.'s that occur within, or on the surface of solid insulation, poses a real danger to high voltage equipment.

CHAPTER 3
LIQUID DIELECTRICS

3.1 Background

'Electric breakdown', refers to the final stage in a succession of irreversible processes which occur when any electrically stressed dielectric (solid, liquid, gaseous or vacuum) is suddenly traversed by an arc ('main stroke').[30] This arc refers to a highly conducting and luminous channel which is capable of carrying huge current between the electrically stressed conductors. The origin of any electric breakdown is a localized current flow. Electric breakdown in solids and liquids can also be attained through the action of an intense light beam, typically produced by a laser.

Electric breakdown is preceded by a wide variety of inter-correlated phenomena. The processes that characterize these prebreakdown phenomena are:

- Ionic processes
- Electronic processes
- Optical (light emission) processes
- Thermal processes (boiling, change of phase)
- Shock waves (mechanical stress waves/ acoustic emissions)
- Hydrodynamic processes (flow, cavitation processes)

In order to obtain a closer view of the underlying processes that result in the occurrence of the aforementioned prebreakdown phenomena, the physical properties of dielectric liquids is examined in this chapter.

3.2 Physical properties of liquids

Typically, most materials are solid at very low temperatures, and gaseous at high temperatures. In order to facilitate the understanding of the basic processes in the liquid state, the liquid being examined is considered either as a solid or a compressed gas. Practically, there are two significant temperatures:

a). The melting temperature (T_m)

b). The boiling temperature (T_b)

Both of the aforementioned temperatures are dependant upon the ambient pressure (p).

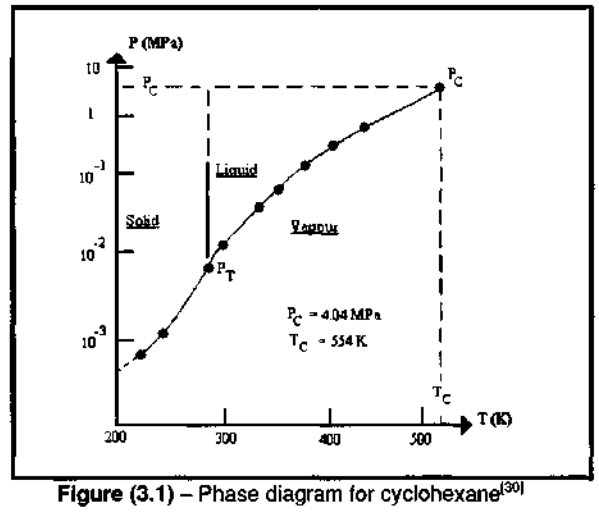

Figure (3.1) – Phase diagram for cyclohexane[30]

Figure (3.1) depicts the phase diagram for cyclohexane. The triple point, (P_T), is the intersection of the three equilibrium curves between the pairs of phases. At temperatures below the melting temperature (T_m), the solid has a lower vapour pressure than the liquid and hence cannot exist in equilibrium with it.

Figure (3.2), depicts the mass per unit volume (ρ) vs. temperature (T). It shows the schematic static curve at thermodynamic equilibrium. Note in the liquid-vapour phase change, an increase in the temperature results in a decrease in the mass per unit volume of the liquid (ρ_l), but an increase in the mass per unit volume of the vapour (ρ_v). The critical temperature (T_c), refers to the point at which $\rho_l = \rho_v$. This point marks the upper temperature above which the liquid phase cannot exist. "This is the reason that the p(T) diagram ends at the critical point P_c; above T_c, the medium possesses its own 'fluid' properties."[30]

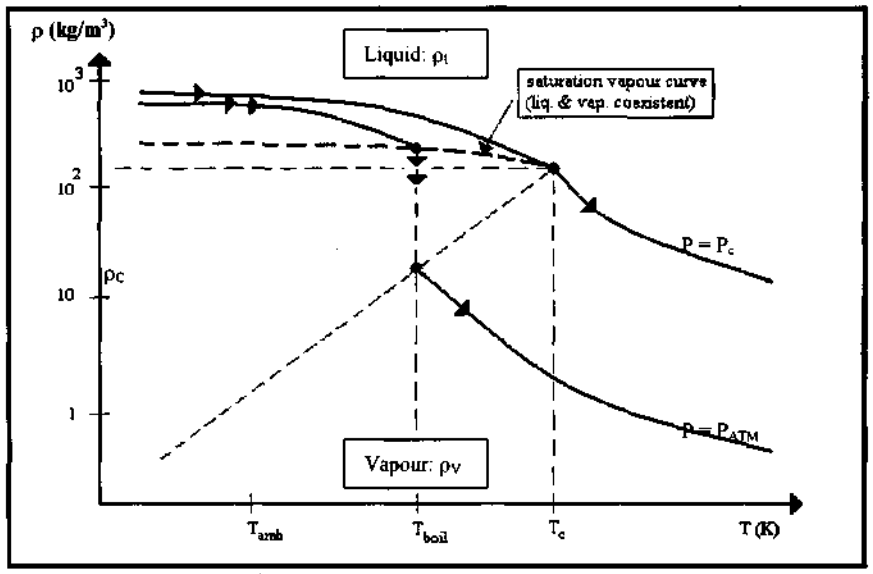

Figure (3.2) – *Mass per unit volume (ρ) Vs temperature (T): Schematic static curve at thermodynamic equilibrium* [30]

The influence of the mass per unit volume and the temperature on the properties of liquids is essential in order to examine problems such as phase change, bubble elongation, fluid flow and particle motion (examined in later sub-sections).

3.2.1 Mass per unit volume

The mass per unit volume of hydrocarbons does not vary much at room temperature and atmospheric pressure. It typically ranges from 600 kg/m^3 to 1000 kg/m^3. As depicted in Figure (3.2), for a given pressure the mass per unit volume of a liquid weakly decreases with an increase in temperature. In comparison, the mass per unit volume of the vapour increases to a large extent. Large deviations to the aforementioned are expected out of thermal equilibrium.

3.2.2 Superficial tension (A)

The superficial tension does not vary much from one liquid to another. It is typically approximately 40×10^{-3} Nm^{-1} and decreases as the temperature is increased. It vanishes at the critical temperature. [30]

3.2.3 Viscosity

"The dynamic viscosity of the liquid, (η_l), does not significantly increase with pressure, even if the pressure increases above the critical point."[30] It decreases with an increase in temperature. In the case of a vapour, the viscosity (η_v) varies approximately as p/T . At atmospheric pressure $\eta_v << \eta_l$. "The kinematic viscosity $v = \eta/p$, appears for instance in the Reynolds number $R_e = v\phi/v$, characterising the motion of a fluid (or body) at a velocity v, ϕ being a characteristic length. At atmospheric pressure, for many liquids, $v_v \approx v_l$." [30]

3.2.4 Specific heat (C_p) and latent heat of vaporisation (L_v)

The specific heat and the latent heat of vaporisation vary with temperature and pressure. "At constant pressure, C_p, feebly increases when the temperature is increased, whereas L_v decreases and vanishes at the critical point."[30] The amount of energy necessary to evaporate one mole of liquid is:

$$W = L_v + \int_{T_a}^{T_b} C_p(T)dT \tag{3.1}$$

where: T_a is the ambient temperature.
T_b is the boiling temperature
L_v is the value at T_b.

3.2.5 Cavitation

In instances where a liquid is heated under constant pressure or when its pressure is decreased whilst maintaining a constant temperature (by static or dynamic methods), this causes vapour filled or gas and vapour filled bubbles or cavities to grow. "This is termed 'boiling' is the temperature is increased, and 'cavitation' when the pressure is reduced."[30] Cavity growth is a dynamic phenomenon and can be explosive. In addition powerful shock waves can be produced.

3.2.6 Velocity of sound (c)

This parameter refers to the speed of propagation of small pressure and density changes in a compressible medium. [30] "The velocity of this compressible wave in a liquid is given by:

$$c = \sqrt{\frac{\lambda}{\rho_l}} \tag{3.2}$$

where λ is the adiabatic elastic modulus."[30] The velocity *(c)* of the wave is constant, but the intensity of the wave decreases as it propagates by means of geometrical spreading and interactions with the medium. "The sound wave obeys the laws of reflection and refraction and produces light scattering."[30]

3.2.7 Shock waves

This type of wave is also a compression wave, but it occurs as the result of large pressure changes, which in turn cause discontinuities in pressure, specific mass, as well as velocity. "Its initial velocity is higher then c, but quickly tends to c."[30] Shock waves can occur as a result of explosions, lightning, or the motion of an object at a velocity higher than c. Shock waves travel as velocities equal to that of the object.

3.2.8 Physical and electronic properties of various hydrocarbons

The following table depicts the physical and electronic properties of a number of hydrocarbons at a temperature of 20°C. [30]

Liquid	ε_r	ρ_l $kg\,m^{-3}$	η 10^{-3} Pas	N $10^{-21} cm^{-3}$	k_e cm^2/V_s	V_0 eV	T_b K	T_c K	p_c MPa	ρ_c kg/m^3
n-pentane	1.84	626	0.24	5.2	0.16	0.0	309	410	3.33	237
n-hexane	1.89	660	0.33	4.6	0.09	0.04	342	508	2.91	233
cyclohexane	2.02	779	1.02	5.6	0.4	0.01	353	554	4.04	273
n-decane	1.99	730	0.92	3.1	0.025	0.18	447	618	2.12	236
iso-octane	1.94	692	0.50	3.7	7	-0.18	374	544	2.57	244

Table (3.1) – Physical and electronic properties of various hydrocarbons at 20 °C

3.3 Behaviour of electric charge carriers

3.3.1 Electronic processes in liquid and gaseous hydrocarbons

Typically, there are strong electron and molecular interactions in dense media. The mean free path of electrons in dense media is in the order of molecular dimensions. "For many hydrocarbons, the electron energy in the conduction band of the liquid with respect to the vacuum level (V_o), is closer to zero (or slightly positive) at room temperature."[30] In other non-polar molecular liquids, it is possible for V_o to reach high negative values (e.g. –0.62 eV in tetramethylsilane), or intermediate negative values (e.g. –0.18 eV in isooctane). In the case of high negative values of V_o, the delocalised electron interacts weakly with the molecules of the liquid and the electron is quasi free. [30]

It is also possible for electrons to become 'trapped' in localised states, which consequently results in a wide variation in electronic mobilities at low fields (<50 kV/cm) and at room temperature. The electronic mobilities can be seen to be high in 'fast' liquids (e.g. 90 cm^2/Vs in tetramethylsilane), and low in 'slow' liquids (e.g. <0.2 cm^2/Vs in several n-alkenes.) [30] The mobility is of an intermediate value in isooctane (7 cm^2/Vs).

"In gaseous hydrocarbons, electronic mobilities at low fields are constant; they vary linearly as $1/N$ (N, number of molecules per unit volume; $N = A_N \rho / M$; A_N is the Avogadro number; ρ: mass per unit volume; M: molecular mass). In high fields E, the drift velocity approaches a constant value in the range 10^6 to 10^7 cm/s (10 to 100 km/s) for E/N ratios around 3 to $5x10^{-17}$ V cm^2."[30] A 'hopping model' describes the transport properties of trapped electrons in liquids. This model predicts a "temperature and field-dependant relationship for electron mobility."[30] If λ is the mean distance between traps, at low field strengths the mobility follows an exponential increase with temperature (T) given by [30]:

$$k_e \prec \exp(-W_a / KT) \tag{3.3}$$

where: W_a is the activation energy.
K is the Boltzmann constant.

The following equation describes the increase in mobility with the field E: [30]

$$k_e(E) = k_e(E=0)\frac{\sinh(e\lambda E / 2KT)}{(e\lambda E / 2KT)} \tag{3.4}$$

where: e is the electronic charge

"For $\lambda \sim 10^{-9}$ m, an exponential increase of k_e, is expected when $E > 1$ MV/cm."[30] The electron velocities in liquid hydrocarbons eventually reach the values measured in gases (e.g. 10 to 100 km/s), at fields, which lie in the range of 2 to 7 MV/cm. This is in direct contrast with 'fast' liquids where electrons reach their maximum velocity at much lower field strengths. An electron is termed as 'hot' when its electronic temperature is greater than the temperature of the medium. Note that the lifetime of excess electrons in ultra purified liquids can far exceed 1ms, and this can typically be longer than their transit time between the electrodes. "However, they readily form negative ions by attachment to electron scavengers. If K_s is the kinetic constant of capture of the scavenger and n_s is its density, the attachment time is $\tau_s = 1/K_s n_s$.
In hydrocarbons, the value of K_s ranges from $\sim 10^{11}$ *to* 10^{14} $mol^{-1}s^{-1}$."[30]

3.3.2 Influence of light

Photoionisation in gases is an efficient means of supplying an abundant source of electrons far ahead of prestreamers (or luminous avalanches). Photoionisation also contributes to the development of fast streamers i.e. 10^3 to 5×10^3 km/s in air in plane-plane or point-plane gaps of approximately 2 cm, reaching 5×10^4 km/s in long sparks (> 10m) or lightning strokes. [30] From previous research [30] it was noted that the highest streamer velocities measured in liquids (point-plane gaps), were not much greater than 100km/s, whereas in comparison the highest electron velocities, and the streamer velocity in transformer oil in uniform field gaps (a 1 cm gap subjected to a 1 MV impulse voltage, and a 50 cm gap subjected to a 10 MV impulse voltage), was noted to be in the region of 2×10^3 km/s. This raises the question of the influence of light upon discharge development in liquids.

3.3.3 Electroconvection

"Electroconvective motion of an insulating fluid induced by the presence of space charge (ionic or electronic) can develop in a very brief time: $t_H < 50\eta/\varepsilon E^2$ (< 1μs in low viscosity fluids)" [30] The upper limit for the apparent mobility is the electrohydrodynamic (EHD) mobility which is given by: $K_H = (\varepsilon/\rho)^{1/2}$. (3.5)

Due to the fact that in ionic liquids, $K_H = 1.5\times10^{-3}\ cm^2/Vs$ (higher than the ionic mobility but lower than the electronic mobility), the flow velocity could reach values in the region of 60 m/s for fields in the region of 4 MV/cm. [30] Liquid motion induced by EHD phenomena, could produce pressure fluctuations. In addition cavitation may occur if the pressure is "locally reduced to below the vapour pressure of the liquid, leading to a gas generation; according to the Bernoulli's theorem, a velocity of 15 m/s could produce a lowering of the pressure by 0.1 MPa."[30] However, it was shown [30] that this mechanism is not responsible for bubble generation near a sharp point.

3.4 Prebreakdown phenomena in liquid dielectrics

3.4.1 Background

Partial discharge detection and localization techniques are centered on the recognition and interpretation of the phenomena, which occur prior to, as well as during the process of electrical breakdown. This section examines the most typical and prevalent prebreakdown phenomena.

The mechanisms responsible for breakdown in dielectric liquids has for long been the subject of many speculations. The phenomena involved in the prebreakdown phase (i.e. the events which precede arc development) is very complex, and therefore much difficulty has been encountered with regards to the development of a unified theory which is able to explain all experimental results. However, two main concepts have been proposed [31] for electrical breakdowns. These are:

- Bubble processes.
- Electronic processes.

It has been experimentally proven [31], that the physical nature of streamers is gaseous. However, spectroscopic analysis of the light emitted by streamers has indicated that electronic processes are also present. These are examined in the following sections.

3.4.2 Electronic and gaseous processes

Neither the electronic nor the gaseous mechanism can be considered singly during the prebreakdown phase of dielectric liquids. The following mathematical model has been proposed by researchers[31], to explain the prebreakdown processes that can occur, and to evaluate the propagation velocity of streamers based upon energy considerations.

The total energy of the system (W_T), which is electrical energy, is consumed in different forms i.e.:

- Vaporisation
- Chemical Decomposition
- Capillary Energy due to the gas
- Liquid interface
- Displacement
- Ionisation

Consider the amount of energy used in streamer displacement to be denoted by W_c. Therefore:

$$W_c = \beta W_T \tag{3.6}$$

where: $0 < \beta < 1$

In addition, consider that the streamer consists of n branches, and assume that each of these branches can be described by a cylindrical channel. Based on this information: [31]

$$\sum_{j=1}^{n} \frac{1}{2}\left(\rho \pi r_j^2 dl_j\right) v_j^2 = \beta \sum_{j=1}^{n} q_j E_j dl_j \tag{3.7}$$

where: r_j is the radius of the branch.
dl_j is its displacement.
v_j is its velocity.
q_j is its charge.
E_j is the electrical field at its head.

"If the energy W_c is not used to push the liquid for the streamer to move, ρ will be the volumic mass of the gaseous phase."[31] Therefore the velocity corresponding to each displacement (dl_j) of the streamer can be obtained from equation (4.2) as:

$$v_j^2 = \frac{2}{\pi r_j^2}\frac{\beta}{\rho} q_j E_j \tag{3.8}$$

or:

$$v_j^2 = \frac{2}{\pi r_j^2}\frac{\beta}{\rho}\left(\int i_j dt\right) E_j \tag{3.9}$$

where the term i_j refers to the streamer current at any time.

Consider a slow streamer, where the current consists of several pulses. Here, the total electrical charge is the sum of all the elementary charges that can be deduced from the integration of the current pulses. Each elementary charge contributes to the propagation of the streamer. "When a discharge occurs, there is light emission and the electrical field drops to a level which is unable to maintain the discharge."[31] The energy that is deposited by this discharge assists in the propagation of the streamer. The electrical field corresponding to each charge can be calculated using: [31]

$$E_j = \frac{\sigma}{\varepsilon} = \frac{q_j}{2\pi\varepsilon r_j^2} \tag{3.10}$$

where: q_j is the elementary charge corresponding to the jth current pulse.

Σ is the surface charge density at the live head of the streamer (approximated to a half sphere of radius r_j).

Consider typical values of r_j = 5μm [41] and q_j = 1 pC[40], with equation *(4.5)* E_j is evaluated as 3.2 MV/cm. "This field is in the same range as calculated for the initiation of a bubble which would lead to a slow streamer."[31] For this case the vaporization mechanism would be dominant. [31]

For the case of the fast streamer, the frequency and/or amplitude of the current pulses are very high and hence the current is roughly continuous. Here, q_j could reach values of tens of pC. Such high values may be capable of producing field emission or field ionization.

Combining equations (4.4.) and (4.5), yields the following relationship:

$$v_j = K_j q_j \tag{3.11}$$

$$\text{where: } K_j = \left(\frac{\beta}{\varepsilon\rho}\right)^{1/2}\left(\frac{1}{\pi r_j^2}\right) \tag{3.12}$$

$$\text{and } q_j = \int i_j dt \tag{3.13}$$

Note the close relationship between the streamer current (the charge) and its propagation velocity. [31]

The following observations were recorded during experimental testing (from reference [31]):

- The charge corresponding to the current between two consecutive current pulses (the conducting current) is negligible when compared to that corresponding to a pulse.[31] This implies that the field and velocity will also be negligible. As a result the "propagation is not uniform and the velocity is not constant: i.e. the streamer propagates by steps."[31] The streamer propagation tends to be continuous, and the streamer velocity tends to increase as the frequency of the current pulses increases. This increase in

frequency can be achieved by increasing the applied voltage, or via the addition of an electronic scavenger to the liquid (in the case of a slow bush-like streamer).

- The electronic scavenger additive acts by increasing the current pulse frequency and reducing the time duration between consecutive discharges. It also increases the electrical charge, which in turn assists in the propagation of the streamer. This results in an increase in the average propagation velocity. "The streamer becomes more energetic and then more filamentary."[31]

3.4.3 Summary

Electronic scavenger additives and hydrostatic pressure can act simultaneously on the prebreakdown phenomena in dielectric liquids.[31] Therefore, the single action of either the electronic or gaseous mechanisms is not possible.

3.5 Liquid dielectrics: Propagation and structure of streamers

3.5.1 Background

The formation of a breakdown channel, in solids, liquids and gases, requires the conversion of matter at low temperature, to conducting plasma at high temperature.[44] The formation of this breakdown channel is typically preceded by events known commonly as "streamers". During this event the optical refractive index of the stressed channel is different from that of the surrounding liquid. The structure of this "streamer" is very similar to structures observed in other insulation media i.e. solids and gases. The term "streamer" as used in the context of liquid dielectrics also includes other structures such as monochannel patterns.[45]

3.5.2 Properties of streamers

Streamers are characterized by various different structures, depending on the prevailing environmental conditions.[45] Streamers produce typical shapes of current transients and emitted light signals, which are followed by shock waves.[45] The conductivity of streamers is dependant upon the mechanisms that are involved in the propagation. Streamers are highly conducting. Studies have shown [45], using Kerr effect measurements, that the total voltage drop across a streamer is less than 10% of the total voltage across the electrodes. Streamers extinguish when the electric field becomes too weak. When streamers collapse, they produce a string of "micro-bubbles" [45] which dissolve in the liquid.
Streamers that originate from the positive electrode are typically 'fast' or 'filamentary', whilst those emanating from the negative electrode tend to be 'slow' and 'bushy'.[45] Typically positive streamers are in the region of 10 times faster than negative streamers. However various researchers [45], noted that transformer oil is an exception to this rule, as positive and negative streamers seem to have velocities which lie in the same range. Depending on the propagation velocity of the streamers, and the polarity of the voltage, streamers may be classified into 1 of 4 different modes i.e. (1^{st}, 2^{nd}, 3^{rd} and 4^{th}), where each of these propagation modes correspond to a given inception electric field.

The chemical characteristics of the dielectric liquid, (pure or contaminated, pressure, temperature, etc.), as well as the electrode geometry and amplitude of the applied voltage, all have a significant impact on the characteristics (structure, current, velocity, mode of propagation), of streamers.

3.5.3 The effect of voltage polarity on the characteristics of streamers

The polarity effect manifests differences in the following parameters:

- Generation of streamer.
- Structure of streamer.
- Propagation velocity of streamer.

Both positive and negative streamers pass through several 'propagation modes', on their way to the counter electrode. Experimental research shows [45] that a positive streamer typically passes through three consecutive stages *i.e.* primary, secondary and tertiary, whilst a negative streamer passes through just two propagation stages. However, the appearance of each structure is dependant upon the field inception. [45]

3.5.3.1 Positive streamers

As the applied voltage ($V_{applied}$) is increased across the electrode gap, the formation of positive primary streamers (PPS) is first noted. The inception field of these primary streamers is approximately 2.0 MV/cm. These primary streamers exhibit an intensified branching [45], and occur in an umbrella-like structure. The propagation velocity of these PPS is in the range of 2 to 3 km/s. Prior to reaching the counter electrode, very fast events bridge the remaining gap and cause breakdown.

"Higher voltage levels lead to a reduced time to breakdown and to the formation of a positive secondary streamer (PSS)."[45] The inception field of these secondary streamers is approximately 12 MV/cm. These PSS occur as an extension of the primary structure with the highest branching, and have a complex spatial structure consisting of a bright main channel (radius in the order of 60 to 90 μm), bright lateral stems with a top zone of ionization in the shape of brush-type structure (having a 0.7 to 1.2 mm radius) which in turn consists of not less than 20 weak luminous streamers with a radius of 3 to 6 μm. These secondary streamers propagate with a significantly higher velocity, which is in the region of 32 km/s. **Shock waves** are noted at the streamer fronts. [45]

Both slow and fast positive streamers extend by jump through a zone of ionization. This jump is accompanied by a streamer flash and an increase in the ionization current at the moment of the flash by up to 0.05 to 0.5 A. [45] The frequency of the flashes is directly proportional to the average field ($E_{average}$) where $E_{average}$ = ratio of $V_{applied}$ and length of electrode gap. Typically $E_{average}$ ranges from 1.7 to 5kV/cm for fast streamers.

If the electrode gap is highly overstressed, this results in a short mode 1 (primary streamer), an earlier mode 2 (secondary streamer) and an ultra high speed tertiary streamer (PTS). Tertiary streamers are often luminous and possess only minor differences in structure from secondary streamers. These minor differences include the fact that tertiary streamers are less branched and often filamentary. The velocity of PTS can exceed 100 km/s. [45]

3.5.3.2 Negative streamers

Negative streamers typically occur in two consecutive modes *i.e.* primary and secondary streamers.[45] Negative primary streamers (NPS) show different structures depending on the strength of the electric field. NPS have an inception electric field of > 2.5 MV/cm[45]. The following structural behavioural patterns were observed at varying electric field strengths according to reference [45]:

- **At low field strengths**: The streamer branches propagate in both paraxial (paraxial propagation velocity ≈ 1 km/s) and lateral directions and completely bridge the gap. The diameter of the branches of the streamer is approximately 30 to 70 μm.[45] Any further increase in the electric field strength results in an increase in the propagation velocity of the streamer, as well as an intensified growth of branches[45]. The main streamer branches obstruct the progress and in some instances even suppresses the growth of smaller side streamers.[45]
- **At high electric field strengths**: The streamer pattern appears as a compact and bushy structure with many branches at high field strengths. The propagation velocity is approximately 1 to 3.5 km/s.
- **At very high electric field strengths**: Researchers[45] noted that for very high field strengths, only one branch bridges the electrode gap. The velocity of the streamer is in excess of 100 km/s. For gap distances larger than 40mm, the researchers reported that a secondary stage was observed. The structure of the negative secondary streamer (NSS) is also dependant upon the electric field strength.[45]

3.5.3.3 RF voltage tests

"Positive and negative streamers are formed alternatively when the streamer inception voltage is exceeded."[45] The growth rate of the electric fields determines the mode of propagation to occur *i.e.* in the case of positive polarity; primary, secondary and even tertiary streamers may occur, whilst for negative polarity; primary and secondary streamers may occur.

"For cosine waveforms with frequencies up to 1 MHz, a positive primary streamer starts and propagates towards the counter electrode."[45] As the applied voltage drops below the extinction voltage, the streamer stops. Further decreases in the voltage cause the brightness of the streamer to decay and the faint branches disappear.[45] As the voltage passes through the zero crossing, "a negative streamer is formed at the tip of the positive streamer."[45] This implies that the positive streamer changes instantaneously into a negative streamer as the voltage crosses zero.

Due to the alternating polarity of consecutive half waves, the following observations were recorded as listed in reference [45]:

- The straight branches of the umbrella-like positive primary streamers disappear and several main branches are generated.
- Umbrella-like structures occur at the tips of the bush-like negative primary streamers.

Note: At very high frequencies, new streamer patterns cannot occur due to the fact that the conversion from one polarity to another requires a finite time *i.e.* all charge carriers of opposite polarity have to be removed, before a change of streamers pattern can occur.

3.5.3.4 Streamer current and light emission

"Transient current pulses are generally accompanied by light emission pulses."[45] The current signal can be measured through the medium of a voltage across a non-inductive resistor that is placed in series with the test cell. Optoelectronic techniques may also be used to measure the current signal.[45] Optical detectors (fast photodiode) or photomultiplier tubes may be used to detect the light emitted by the streamer.

CHAPTER 4
BREAKDOWN OF TRANSFORMER OIL

4.1 Background

Liquid dielectrics are typically used as insulating media in high voltage equipment. This is due to the fact that they can fill up any volume that needs to be insulated. In addition, they can be easily circulated and can therefore be used to dissipate the heat that is generated in the given system. Transformer oil is the most commonly used liquid dielectric. The most profound disadvantage of liquid dielectrics is that they are easily contaminated.

The following chapter provides an examination of the factors that affect the dielectric strength of transformer oil. Some of these contributing factors, which are examined, include:
(1). The stabilization phenomenon.
(2). Oil and electrode pretreatment.
(3). The effect of oil velocity.
(4). The effect of capacitance parallel to the test cell.
(5). The effects of electrode area and gap spacing.

4.2 Review of recommended experimental techniques

The experimental procedure reviewed below, is an account of the experimental research procedure adopted in reference [32].

4.2.1 Electrode selection for dielectric testing

The types of electrodes that should be utilised for dielectric testing is dependent upon the gap spacing to be investigated. The following choices are recommended [32]:

- **Investigation of gap spacings in the range of 0.1mm to 0.5mm**:
  Small mild electrodes, each approximately 10mm in diameter are recommended for these investigations. The oil should be allowed to enter the test gap via a small hole in the centre of the lower electrode. The gap spacing between these electrodes should adjustable (possibly with the aid of a micrometer).

- **Investigation of gap spacings in the range of 1mm to 4mm**:
  Bruce profile brass electrodes (flat area of 2.56 cm^2) are recommended [32] for these investigations. [32] The gap spacing should be adjustable (possibly with the aid of feeler gauges).

- **Investigation of gap spacings in the range of 1mm to 6mm**: Large mild steel coaxial cylindrical electrodes are typically used for these investigations. These electrodes cover areas in the range of 30cm^2 to 1240cm^2. [32]

It is essential that the electrodes be cleaned prior to testing in order to remove impurities. The preparation of the electrodes should be as follows [32]:

- Initial wash in trichloroethylene.
- Standard surface polishing with a 1000 grade silicon paper.
- Second wash in a mixture of hot water and soap solution, using a synthetic sponge.
- Rinses in hot and distilled water.
- The electrodes should then be dried in a laminar flow cabinet.
- Final wipe with a lint free lens tissue with acetone and finally trichoroethylene.

- The rest of the electrode assembly should be washed in hot water and soap solution and then rinsed as described above, after each test.

4.2.2 Oil handling, processing and quality control

Quality grade transformer oil is typically used for this type of experimental testing. The oil should be kept clean and dry. Prior to the oil being allowed to enter the test vessel, it should be passed through a filter into an evacuated degassing column. This ensures sufficient air removal as well as partial drying.[32] The test cell should be positioned lower than the degassing column, so that when sufficient oil is processed it may be transferred to the test cell by gravity.[32]
The quality of the transformer oil should be regularly controlled during the course of the experimental work, due to the fact that the reliability and reproducibility of results is dependant upon the oil quality. This check can be performed with a "standard motor-operated Foster oil test cell having standard VDE electrodes and a gap spacing of 2mm."[32]

4.2.3 Review of possible electrical testing specifications

The tests as conducted in reference [32] were performed with a sine wave ac voltage at 50Hz. The high voltage supply was provided by a 100 kV, 5 kVA transformer. "The applied voltage was raised in all tests uniformly at a rate of 2 kV/sec."[32] In order to prevent carbonization of the test sample and pitting of the electrodes due to the prolonged flow of the fault current, a circuit breaker should be connected to the primary of the transformer in order to remove the fault current. The current in the secondary of the transformer can be limited by a series electrolytic resistor placed between the high voltage transformer and the test cell. [32]

4.3 Review of previously obtained experimental results

The following is a review of the experimental results as documented in reference [32].

4.3.1 Stabilization phenomenon

Researchers[32] noted that after successive tests, the average dielectric strength of the oil reached a stable or plateau level. This stabilization was noted to be influenced by a variety of factors such as (1) electrode area, (2) gap spacing, (3) oil quality, (4) energy released in the gap, (5) electrode pretreatment, and (6) time between breakdowns. [32]

Electrode Area: The following results were recorded based on the electrode areas: [32]

(1). Large cylindrical mild steel electrodes: The values were noted to stabilize after approximately twenty breakdowns. [32]

(2). Brass Electrodes: The values were noted to become stable after approximately ten breakdowns.

(3). Small steel electrodes: The values stabilized after approximately five breakdowns.

"It is suggested that stability may be attributed to the removal of surface irregularities by successive breakdowns."[32] However, another possibility arises due to the fact that the electrodes may have absorbed gas whilst polished and dried in open air. Therefore the stabilization could have been attributed to the gradual removal of this absorbed gas due to successive breakdowns. [32]

Oil Quality: The following results were recorded based on the oil quality: [32]
The quality of the oil in the test gap can be changed by "continuous circulation or by changing the filter porosity."[32] Researchers [32] noted that the continuous circulation of the oil in the gap (at a velocity of 3 cm/s) resulted in an "increase in the percentage difference between the first breakdown value and the plateau level, without altering the number of breakdowns before reaching the plateau level."[32] This seems to also be an indication that the stabilization process is mainly associated with the "removal of surface irregularities."[32] It was also noted [32] that the change of the oil filter porosity (from 6μm to 15μm) only resulted in a slight percentage difference between the first value and the plateau level. [32]

Surface roughness of electrodes
With reference to tests performed on the Bruce Electrodes, it was demonstrated that the stabilization is dependant upon the roughness of the electrode surfaces. "The rougher the electrode surfaces, the longer the stabilizing period."[32] From the experiments [32] it was seen that Bruce electrodes that were polished with 320 grade emery paper, reached the plateau level after approximately 15 to 20 breakdowns, whilst those polished with 1000 grade emery paper reached the plateau level after approximately 10 breakdowns.

This seems to confirm previously drawn conclusions that successive discharges seem to remove the most prominent surface irregularities that may be present on the electrode surfaces. The results demonstrated in reference [32] are in disagreement with the previously drawn conclusion [33], which states "stabilization is owing to the removal by successive discharges of small fibers suspended in the oil within the test gap."[33] This disagreement arises from the fact that the oil sample was replaced after each breakdown measurement.

However, the creation of an insulating layer on the surface of the electrodes (due to chemical transformations) is also possible. "Therefore a higher applied voltage may be necessary to

overcome this barrier."[32] It is also highly possible that the circulating oil will not be able to dislodge this layer.

4.3.2 Oil quality

The impurities, which may be present in transformer oil, can be categorized into 4 groups:

(1). Dust or fibre particles already present in the liquid. These impurities tend to lower the dielectric strength of the oil. Due to the fact that they are extremely small they tend to escape the filtration process.

(2). Particles produced by previous discharges. These could be minute metallic particles, which are removed from the electrode surfaces during breakdown, or carbon particles, which are formed due to the decomposition of the transformer oil.

(3). Deliberately introduced additives, which serve to alter the electrical properties of the transformer oil.

(4). Water.

"Conducting impurities, and/or impurities with a higher dielectric constant that the liquid, are attracted into regions of high electric stress and eventually form a bridge."[32] This bridge will eventually result in breakdown.

Researchers[32] also revealed that increasing the filter porosity (from 6μm to 15μm) resulted in a decrease in the mean dielectric strength of the oil of approximately 12 %. Bruce electrodes were used for these tests with gap spacing of 1mm, 2mm, and 4mm. [32]

An increase in the number of purification cycles of the oil caused an increase in the mean dielectric strength of the oil. This fact is a likely result of the fact as the number of purification cycles increase, the distribution of particle sizes moves to smaller values. Brass electrodes were used for these tests with a gap distance of 1mm. "After 2, 5, and 8 purification cycles an increase in the mean dielectric strength of 8% after 5 cycles, and 10% after 8 cycles was observed when compared to the mean dielectric strength after 2 purification cycles.
It was also noted [32] that the continuous flow of the oil at a velocity of approximately 3 cm/s resulted in an increase in the mean dielectric strength. A 15% increase in the mean dielectric strength was noted for the brass electrodes (gap spacing of 1, 2 and 4mm), whilst a 25% increase was noted for small mild steel electrodes (gap spacing in the range of 0.1 to 0.5 mm). In the case of the large steel cylindrical electrodes, an increase of 8% was noted (gap distances of 1, 2, 3 and 6mm). There are two possible reasons, which could account for these results:

- The motion of the oil delays the formation of particle bridges (as described previously), between the electrodes.
- The "oil flow impedes the entry of impurities into the gap."[32]

As noted as reference [32], the oil circulation did not affect the standard deviation and the skewness of the dielectric strength distributions in any way. [32] This finding is in direct contrast with the results obtained by other researchers [34], where it was claimed "a normalization of the dielectric strength distribution takes place as a result of the oil flow and as the velocity is increased."[34]

The increase in the circulation speed (3 cm/s) resulted in a change in the mean dielectric strength. The increase of the mean dielectric strength is not indefinite. As the oil circulation increases, it results in the flow becoming increasingly more turbulent. This turbulent flow will in turn, result in a pressure difference in the liquid that will result in the formation of bubbles, which reduce the dielectric strength.

4.3.3 External capacitance

"The source impedance seen by the test gap includes two separate capacitances:
(1). The capacitance of the voltage power source, and
(2). The self capacitance of the test cell."[32]
These two components affect the discharge current waveform during breakdown. [32] The capacitance of the voltage power source cannot be changed, as it is an intrinsic property of the power supply. The capacitance of the test cell is dependant upon the electrode area and the gap spacing and is a very important parameter for the stabilization phenomenon since "electrode damage and oil deterioration are affected by the current waveform and its energy dissipated in the gap" [32]. This capacitance may be modified by the addition of various values of capacitances in parallel with the test cell. In reference [32], it was established that a capacitance of 570 pF connected in parallel with the test cell, with Bruce Electrodes, increased the dielectric strength of the oil. This increase may be accounted for by "assuming that the energy released in the gap, when a breakdown occurs, is optimum for destroying the most prominent protrusions on the electrode surfaces."[32] Therefore the energy which is released in the test gap makes the surfaces of the electrodes smoother, hence increasing the plateau dielectric strength of the oil.

The optimum value of the capacitance is dependant upon the actual test cell, as well as the distance of the capacitance from it. [32] Note, that capacitance values which are less than the optimum value will probably not smooth out the protrusions on the electrode surfaces, whilst a capacitance value in excess of the optimum value will result in excessive electrode damage and oil deterioration.

4.3.4 Effects of the electrode gap spacing on dielectric strength

AC Dielectric Strength: According to reference [32], tests were conducted using brass electrodes, and small steel electrodes for gaps varying between 0.1mm and 4mm. In addition, tests with gap spacings varying between 1mm and 6 mm were conducted using the large steel electrodes.
The aforementioned tests were conducted using static oil (changed after each breakdown), as well as continuously circulating oil (3 cm/s).

Summary of results:
It was demonstrated [32] that the mean breakdown voltage varied linearly with the logarithm of the gap spacing according to the expression:

$$v = Kd^n \tag{4.1}$$

where: K is a constant
: d is the gap spacing
: n is an exponential factor between 0 and 1.

For the experimental results, as achieved by researchers in reference [32], it was calculated that the value of the exponential factor, n, is approximately 0.7. This implies that the breakdown voltage is less than proportional to the gap spacing.
It is widely accepted that the effect of the gap spacing on the dielectric strength is a complex phenomenon due to the fact that an increase in the gap spacing could possibly increased the number of impurities entering the gap which could in turn reduce the dielectric strength of the liquid (impurities act as nucleation sites).

4.3.5 Effects of the electrode area on dielectric strength

"It is well known that the dielectric strength of oil increases with decreasing electrode area."[32] Experiments conducted in reference [32], showed that a non-linear relationship exists between the dielectric strength and the logarithm of the electrode area. It was observed that the dielectric strength levels off with increasing electrode area.
It was in these researchers (and several other researchers) that the area effect is weaker than the gap spacing effect. [32] The following reasons could account for this finding:

- The strong gap effect may be attributed to the "impressed voltage, which increases as the gap increases, thus creating more decomposition products and electrode damage."[32]
- It has also been suggested that weak links (present in the oil volume or electrode surfaces), as well as physical size factors have an effect on the dielectric strength. However, the possibility exists that the physical size factors may prevail in initiating breakdown, as it is more sensitive to gap spacing than the electrode area.

Note: It has also been recorded that the stronger dependence of dielectric strength on gap spacing rather than electrode area is also true for solid insulating materials.
Further research is to be conducted to examine the exact cause for the area effect being weaker than the gap spacing effect.

4.3.6 Summary

The results discussed above show that:

- The dielectric strength is dependant upon factors such as stabilization, electrode area, gap spacing, oil velocity and self-capacitance of the test cell.
- It was noted that the stabilization process is very strongly dependant upon the electrode area and its roughness.
- The oil flow was shown to be an important factor, even for cases where the velocity was only a few cm/s.
- It was demonstrated that the connector of external capacitance parallel to the test cell had a beneficial effect on the dielectric strength.
- Furthermore, it was found that there exists a stronger dependence of dielectric strength on gap spacing rather than electrode area is also true for solid insulating materials. A possible reason for this is "due to the faster accumulation of large particles in the gap entering the stressed volume via the non-uniform field region at the electrode edges."[32]

However, further research is necessary in order to completely ascertain the cause for the dominance of the gap spacing effect over the electrode area effect.

4.4 The effect of the electrode gap on breakdown in dielectric liquids

4.4.1 Background

The concept of "Dielectric Strength" is a frequently used term in the electrical insulation industry. The concept of the dielectric strength assumes that "the breakdown voltage of a material, when divided by the sample thickness, is constant and thus a material characteristic."[48] However, it is a well-established fact that the ratio of the breakdown voltage to the thickness of a sample is not a constant, but instead increases nonlinearly with an increase in the thickness of the sample. This is particularly true for uniform field conditions, whereas a much more complicated relationship exists for non-uniform field conditions where polarity effects have to be accounted for.

Historically, experiments examining the dielectric strength of insulating liquids were conducted with electrode gap spacings < 1mm, due to the unavailability of power supplies that are able to supply high impulse voltages to produce breakdown in larger gaps. These studies were also centred on uniform field conditions. As more capable power supplies became available, researchers were able to use larger gaps in order to simulate conditions similar to those that are experienced during in-service conditions. However, the assumption that was commonly made (particularly in the testing of hydrocarbon systems) was that the breakdown voltage under positive polarity would always be lower than under negative polarity. [48]

The effect of the electrode spacing on the breakdown voltage at both polarities was however studied by some researchers. [49, 50, 51, 52] In these studies, comparisons were made between conventional hydrocarbons and perfluorinated ones.[48] The findings showed a significant polarity effect on the breakdown voltage as a function of the electrode separation.[48] The results for the different hydrocarbons are listed below:

- For aliphatic hydrocarbons (n-pentane, n-hexane) and aromatic hydrocarbons (benzene, toluene), the breakdown voltages were recoded to be higher when the point electrode was a cathode than when it was an anode.[48]
- For chlorinated hydrocarbons, and perfluorinated hydrocarbons, the difference in the breakdown voltages at both positive and negative polarities was very small. In some case the breakdown voltage for the positive polarity was higher than the breakdown voltage at the negative polarity.[48]

Note: The above results were obtained with gap spacings of 1 to 5mm, 10 to 250μm, and 10 to 1000μm.

Recent work[53, 54], which involved the investigation of the polarity effect in perfluoro polyethers (gap spacings of 5 and 10mm), showed that the breakdown voltage for the positive polarity was equal to or higher than the breakdown voltage for the negative polarity.

"It appears that the presence of atoms having strong electron affinity influences the charge carrier discharge process. In the presence of these electronegative atoms, the breakdown voltages with the point an anode are affected to a larger extent than for the reverse polarity."[48]

4.4.2 Summary

The following table provides a summary of the experimental results obtained by Nitta and Aihara[49]. These tests were performed with various hydrocarbons, under non-uniform test conditions (due to the fact that under uniform field conditions it is very difficult to determine at which electrode breakdown initiated [48]).

Liquid	Gap Spacing	Cathode (*kV*)	Anode (*kV*)
Carbon tetrachloride	1	16.0 ± 3.8	14.1 ± 2.6
	3	21.8 ± 3.0	21.0 ± 2.6
	4	28.8 ± 2.4	28.0 ± 2.3
n-octane	1	20.4 ± 3.1	13.3 ± 3.3
	2, (3)	38.3 ± 4.9	18.4 ± 1.3
	3, (5)	49.8 ± 2.4	26.0 ± 2.0
Chloro-benzene	1	18.8 ± 2.6	18.3 ± 2.6
	3	27.3 ± 2.0	25.5 ± 2.1
	5	35.5 ± 0.9	37.0 ± 1.9
Toluene	1	20.4 ± 2.5	16.0 ± 2.8
	3	42.3 ± 3.4	21.8 ± 4.8
	4, (5)	48.0 ± 2.4	25.0 ± 3.1

Table (4.1) – Effect of gap and polarity on 50% breakdown voltage

Note: The bracketed number indicates the gap spacing for the needle anode when the gap for the cathode was different.

From Table (4.1), for the liquids containing chlorine, no polarity effect is observed as both polarities produce approximately the same breakdown voltages. These voltages are noted to increase with increasing gap spacing.

However, the two simple hydrocarbons (n-octane and toluene), display a strong polarity effect. An increase in the gap spacing produces a significant increase in the negative breakdown voltage, but the positive breakdown voltage has a considerably smaller increase. It was noted that the negative and positive breakdown voltages of the simple hydrocarbons become approximately equal at gaps < 0.5mm. [48] Previous research [52] has shown similar results on n-hexane, decane, perfluoro hexane, and perfluoro pentane (using gap spacings ranging from 10μm to 1000 μm). As listed in reference [52], the positive and negative breakdown voltages for the simple hydrocarbons become equal at a gap spacing of approximately 0.5mm. The perfluorinated hydrocarbons showed approximately no polarity effect.

4.5 Vapour bubble formation in dielectric liquids

4.5.1 Background

The following section provides a review of documented research that examines the electrical conduction of purified non-polar liquids as a function of various parameters. A point to plane electrode geometry is the preferred electrode configuration used by the researchers for the experimental testing.

The generation and dynamics of the vapour bubbles were examined as a function of the following parameters:

- The injected energy.
- The hydrostatic pressure.
- The nature of the liquid.

Different hydrocarbons were examined with respect to the aforementioned parameters and the results were compared.

4.5.2 Review of possible experimental techniques

The liquids listed in Table (4.2) were selected for the experimental testing [34]. The properties of these liquids are shown below:

	n-decane	n-pentane	Cyclohexane	Iso-octane	Néohexane	TMS
Teb (Patm)°K	447.3	309	353	374.4	322.8	299.6
Tc (°K)	617.7	469.6	554	544	489.2	460
Pc (MPa)	2.12	3.33	4.04	2.57	3.067	3.4
Cp(Téb) J/mol. °K	398.2	172.6	185.2	281.3	199.18	208.2
Lv(Patm)J/mol	39250	25749	30096	35095	26205	25050
η (CP) 20°C	0.92	0.24	1.02	0.503	0.4	0.243
ρg/cm^3	0.73	0.62	0.72	0.708	0.649	0.648
Ke (cm^2/V.S)	0.025	0.16	0.4	7	12	90

Table (4.2) – Properties Of Liquids under examination

The liquids shown in table (4.2) were purified and transferred into the test cell by vacuum distillation. [34] The spacing between the electrodes was varied from 0.5mm to 3mm. Coaxial test cells (having a well-defined characteristic impedance of 50Ω), were used in order to measure significant current pulses without incurring reflections or oscillations in the nanosecond range. [34] A nitrogen-operated piston could be used to pressurize these cells up to a maximum pressure of 12 MPa.

4.5.2.1 Measuring techniques

An oscilloscope was used to obtain time-resolved measurements of the conduction current and of the light intensity. Stabilized voltage sources and sensitive current meters were used. [34] The temporal study of bubble growth and collapse was optically achieved by recording the variations in the intensity of the transmitted light beam (a 5 mW He-Ne laser) due to the scattering by the bubble, with the aid of a fast photo-diode. The signal, which is obtained, characterizes the amount of light that is intercepted by the bubble. This intercepted light is proportional to the cross-section of the bubble.[34] "The simultaneous acquisition of the injected

charge and the photo-diode signal was effected using an oscilloscope connected to a calculator. This device is capable of processing a series of measured values."[34]

4.5.3 Review of experimental results

4.5.3.1 Liquids with low thermal electronic mobility

The following is an account of the results obtained for cyclohexane, propane, n-pentane and n-decane *i.e.* liquids with low thermal electronic mobility.
For values of the point radius > 0.5μm, when the DC negative voltage is increased, it was noted that current pulses start to appear abruptly above a given threshold value of the applied voltage ($V_{threshold}$) which corresponds to a critical value of 7 MV/cm of the electrical field at the point. However, according to calculations performed with the Fowler-Nordheim equation, the field value required for field emission is 20 MV/cm (continuous current, independent of P), in the same liquid. The following characteristics of the current pulse stage were recorded: [34]

- Duration of current pulses < 4ns.
- Frequency *(F)* of current pulses was in the kHz range, and it increased with the applied voltage and is proportional to the mean current ($I_m=QF$).
- The injected charge per pulse was calculated based upon the tip radius of curvature R_{point}. This was independent of the applied voltage and the hydrostatic pressure (in the range of 1 to 12 MPa).
- A low standard deviation was noted between the elapsed time between two successive pulses at a given applied voltage and Q_i.

Conclusions associating vapour bubble formation with current pulses

Based upon the aforementioned results, the following conclusions were drawn as listed in reference [34]:

- For cases where the hydrostatic pressure is below the critical pressure $P_{critical}$ of the liquid, each current pulse induced the generation of a single bubble near the point electrode. The current pulse regime is independent of the pressure (P), and each of the bubbles appeared after a current pulse. Drawing from the fore-mentioned, it was concluded that the bubble is a consequence of the current pulse.
- It was also noted, that each bubble initiated by a current pulse, follows a common pattern, i.e. growth to a maximum radius (R_{max}), then collapse which is followed by rebounds. The maximum radius (R_{max}) of growth is in the micrometer range.
- For a given pressure, R_{max} is independent of the applied voltage V (*where* $V \geq V_{threshold}$), but proportional to the injected charge per pulse (Q_i) and therefore to the point radius (R_{point}).
- As the hydrostatic pressure is increased, it was noted that the volume and lifetime of the bubble was considerably reduced. However, the time sequence of events remained qualitatively the same.
- **"Shock waves** are radiated during the growth, collapse and rebound phases of the bubble."[35] Although no more bubbles are noted above the critical pressure of the liquid ($P_{critical}$), one shock wave is associated with the current pulse still remains.
- At pressures below the critical pressure ($P < P_{critical}$), erosion of the tip of the point electrode was observed. This indicates that this erosion is related to the bubble regime. "This erosion is presumably a consequence of the phenomenon of cavitation erosion which is generally attributed to the pressure pulse associated with bubble collapse."[36,37]

Correlation with theoretical predictions

The results obtained for both the growth and collapse phases, can be described by the Rayleigh Theory. The experimental lifetime of the first bubble was plotted against the pressure (P), and a good correlation existed with the value calculated by the Rayleigh Relation:

$$t_1 = 1.83 R_m \left(\frac{\rho}{P}\right)^{0.5} \tag{4.2}$$

where: ρ is the material density.
The above correlation proves that the growth and collapse dynamics are controlled by the liquid's inertia.[34]

The injected energy (W) and consequently the maximum radius of bubble growth (R_{max}), can be calculated from the measured values of the injected charge per pulse (Q_i) and the threshold voltage ($V_{threshold}$) as a function of the hydrostatic pressure (P), by:

$$R_{\max} = k\left(\frac{W}{P}\right)^{\frac{1}{3}} \tag{4.3}$$

where: k is a coefficient which depends upon the thermodynamic characteristics of the liquid according to the relation:

$$k = \left(\frac{3RT_b}{4\pi}\left(L_v + \int_{T_0}^{T_b} C_p(T)dT\right)\right)^{1/3} \tag{4.4}$$

where: R is the gas constant.
T_b is the boiling temperature at the pressure P.
: T_o is the ambient temperature.
: $C_p(T)$ is the specific liquid heat capacity.
: L_v is the latent heat of vapourisation at temperature T_b.

"This relation is obtained with the crude assumption that the vapour pressure in the bubble at it's maximum radius R_{max} equals the applied hydrostatic pressure P."[34] In reference [34], it has been proven that there exist a good correlation between the theoretically calculated radius $R_{max\text{-}calc}$ (calculated with equations (4.3) and (4.4)), and the experimentally obtained maximum radius $R_{max\text{-}exp}$ for all values of W and P. The ratio $\left(\frac{R_{\max-\exp}}{R_{\max-calc}}\right) \approx 0.85$ for cyclohexane.

4.5.3.2 Liquids with high thermal electronic mobility

The following is an account of the results obtained for Isooctane, Neohexane and Tetramethylsilane (TMS) i.e. liquids with high thermal electronic mobility.

It was observed[34] in TMS, that above a threshold electric field ($E_{theshold}$) of approximately 4 MV/cm ($E_{threshold} \approx 7$ *MV/cm* for previously examined liquids), a current instability occurred. It appeared that this current instability was connected with the appearance of the current pulses. These current pulses were irregular in duration, amplitude and frequency. The frequency was very low (*from 0.1 to ~ 10 kHz*), and independent of the mean current. Unlike the previous case with cyclohexane, in TMS the charge per pulse (Q_i) is not a "characteristic parameter of the phenomenon."[34]

In isooctane and neohexane, a threshold value for the electric field ($E_{threshold}$) of approximately 5 MV/cm was recorded. These results obtained for these liquids were strongly identical to the

results obtained for cyclohexane. In these liquids, for pressures less than the critical pressure for the liquid ($P < P_{critical}$), the bubble formation was related to each current pulse and the growth and collapse phases could also be strongly described by the Rayleigh Theory. However, a deviation was noted with regards to the correlation between the theoretically predicted maximum radius of growth (R_{max}) and the predicted value. The ratio $\left(\frac{R_{\max-exp}}{R_{\max-calc}}\right) \approx 0.4$ for TMS and 0.7 for isooctane and neohexane.

In all the liquids (from cyclohexane to TMS), for positive points with $R_{point} > 0.5$ μm, no regular pulse regime was noted, and the current displayed a gradual rise with the voltage (i.e. no current instability). "However, when an erratic current pulse occurs, it also induces the formation of a bubble."[34]

4.5.3.3 Transition to a slow negative streamer

For conditions around atmospheric pressure and large point radius values (R_{point}), a burst of current pulses correlated with the formation of successively growing bubbles after the first pulse. [34] "This burst shows a current shape characteristic of the propagation of a bush-like streamer."[34] It has a random occurrence, and the number of pulses comprising the burst (n) as well as the probability of its appearance was noted to decrease rapidly when the applied hydrostatic pressure increases. Above a pressure of 1 MPa, only the regular regime of a single current pulse i.e. single bubble generation was noted.

The maximum radius of a swarm of bubbles (produced by a current burst of n pulses) was noted to be roughly in agreement with the value calculated from:

$$R'_{\max} \cong \sum_{i=1}^{n} R_{\max}(i)$$

where: R_{max} is the radius calculated from equation (4.3) and (4.4).

4.5.4 Discussion of results

The experiments conducted by researchers (reference [34]) as listed above show that a bubble is created by a rapid and localized injection of energy. Analyses of the experimental results have shown that most of the electrical energy is converted into heat which is used to evaporate the liquid. However, various other energetical processes must also be present i.e.:

- Ionization
- Decomposition
- Vaporization
- Light emission
- Work against the external pressure
- Surface tension
- Shock wave energy
- Viscous losses.

Therefore the total injected energy must be calculated by incorporating each of the above processes i.e.

$$W_{tot} = W_i + W_d + W_v + W_\lambda + W_P + W_\sigma + W_w + W_\eta$$

The magnitude of the various terms listed above can be estimated once the electrical characteristics of the current pulse, the bubble dynamic and the maximum bubble radius (R_{max}) are known. These terms were determined as:

- $W_i \cong E_i Q_i$ where $E_i \approx 10$eV. Therefore, the ionization energy W_i is approximately less than 1% of W_{tot}.
- The analysis of the decomposition products and the determination of the emitted light intensity (from 200nm to 1100 nm) showed that both W_d and W_λ are approximately less than 0.1% of W_{tot}.
- The pressure work is equal to the kinetic energy of the system. $W_p = 4\pi R_{max}{}^3 P/3$. It was proven that W_p was approximately 7% of W_{tot}.
- $W_\sigma = 4\pi\sigma R^2$ and was approximated to be $\leq$ 1% of W_{tot}.
- The terms W_w and W_η have been proven [38, 39] to be negligible.

Therefore, with consideration to the above, it can be noted that most of the injected energy is used to evaporate the liquid. In addition, the bubble generation only occurs for values of the applied pressure less than the critical pressure of the liquid. This indicates that, "the responsible mechanism of this formation is indeed local boiling due to the high power density near the point ($\sim 10^8$W/cm^3)."[34]

Cyclohexane, Propane, N-Pentane, N-Decane

The liquids mentioned above have similar electronic properties, *i.e.* a low-field electron mobility ($<10^{-4}$ m^{2}V^{-1}s^{-1}) which indicates a localized state of electrons, but different physical properties (T_b, P_c, L_v, *etc*). Therefore, the mechanism of corona discharges has identical characteristics in these liquids. The injection of energy occurs in a very low volume over a short period of time, which in turn induces an intense heat in the region of the point until reaching a super-critical state in the liquid. "In this case the frequency of nucleation being infinite, a bubble is produced after each current pulse."[34]

Iso-octane, Neohexane, Tetramethylsilane

The above liquids have high to very high thermal electronic mobility (quasi-free electrons). This in fact explains the characteristics of their current and light emission pulses. "the distance around the point where light emission is detected, which must e proportional to the depth of the electronic multiplication zone and consequently of the heating zone, is 2 to 3 times larger in isooctane and neohexane and 4 to 6 times lager in TMS than in cyclohexane."[42] Considering this, the injection of energy (related to the current pulse) therefore occurs in a greater volume and over longer periods of time. This explains the decrease of the ratio (R_{exp}/R_{mth}) with the increase of K_e.[34]

4.6 Summary

In the cases described in section (4.5.4), the liquid's inertia is the major limiting mechanism of the bubble dynamics. A possible reason for the very rapid damping of the bubble oscillations corresponding to large energy losses, can be deduced by taking into account the heat and mass transfer at the vapour/liquid interface. [38]

The following relationship between the generation of vapor bubbles and conduction phenomena (as a function of pressure and nature of the liquid) was observed:

- The initial bubble generation is a result of a current pulse caused by an electron avalanche in the liquid phase.[34]
- The erosion of the needle is a result of bubble collapse due to "cavitation erosion phenomena."[34]
- The ratio (R_{mexp}/R_{mth}) is a function of the thermal electronic mobility K_e of liquids.
- The transition to a slow negative streamer was observed to be as a result of successive discharges, which occur in the vapour phase of the preceding bubbles that in turn produce a string of bubbles.

CHAPTER 5
TRANSFORMER INSULATION

5.1 Background

The purpose of insulation in a transformer is to isolate the parts that are at differential potentials from one another. Oil impregnated and cellulose-based products; primarily paper and pressboard are the most important materials, of optimum dielectric strength that are used in high voltage power transformers.

Phenol-based paper has been used as the internal insulation (due to high mechanical strength). However, due to its poor creepage strength, modern designs have introduced oil resistant enamel as the interturn insulation. It is however, less capable of withstanding mechanical stresses caused by thermal displacements and short-circuit forces.

In smaller power transformers, silicone oil is used as the insulation mechanism. Nylon-papers are used instead of Kraft paper. Nylon-papers have superior properties due to the use of polyamide fibres and flakes in their manufacture. The most important property is their high thermal stability, and excellent dielectric strength (retained at even very high temperatures). Their preferred used should be in large power transformers that are required to carry frequent, large overloads of short duration (causing temperature in windings to exceed 200° C for short periods). The disadvantage of nylon paper is its high cost factor.

Experimentation has been conducted using high pressure (5 bar) SF_6 gas, instead of oil, as an insulating medium in transformers. According to results of experiments, transformers, which use SF6 gas, can be manufactured with foil-windings, with plastic foil insulation placed between turns, and with cooling being provided by vertical cooling ducts running between the foil windings. The advantage of this insulation is that the interturn insulation can be subjected to a much higher degree of interturn dielectric stress, than on conventional oil-impregnated paper interturn insulation. This allows a significant decrease in the dimension of the windings. The thermal stress of the insulation may be much higher, which permits the application of increased current densities without necessitating the change of cooling mechanisms. The units themselves can therefore be smaller in physical size, which facilitates their transportation. Another advantage is that pressboard insulation hardly ages in SF_6 gas.
The problem arises in designing a tank to actually withstand the high pressure exceeding 5 bars. From an economical perspective, this insulation is not the optimum solution.

After discussing all of the above types of insulation, so far the most popular and most widely used are the oil-impregnated paper and oil-impregnated pressboard insulation.
They are being used in transformers of the highest voltage ratings, due to their high dielectric strength, their excellent cooling properties and the possibility of their easy regeneration. It is not probable that they will be replaced due to these excellent properties.

5.2 Properties of insulating transformer oils

The chemical, electrical and physical properties of insulating oils in transformers are specified by the relevant standards. The I.E.C. standard concerning the insulating oils of transformers and apparatus [2] specifies the following:

- 3 classes of oil are specified. They are distinguishable by their flash points, pour points and kinematic viscosity. The following is a summary of the 3 classes of oil:

	Class I	Class II	Class III
Flash point	$\geq$ 140 ° C	$\geq$ 130 ° C	$\geq$ 95 ° C
Pour point	$\leq$ -30 ° C	$\leq$ -45 ° C	$\leq$ -60 ° C
Kinematic Viscosity	$\leq$ 16.5 mm^2s^{-1}	$\leq$ 11 mm^2s^{-1}	$\leq$ 3.5 mm^2s^{-1}

Table (5.1) – Characteristics of various classes of transformer oils

- The density of insulating oil, of a satisfactory quality (at 20 ° C) should be below 0.895g cm^{-3}.
- The oil should not contain any inorganic acid, corrosive sulphur, alkali soluble in water, or mechanical impurities. It should also be transparent.

Note: Most of the above properties should not change under operating conditions.

The following are the parameters, which typically change due to operating conditions such as moisture and gas absorption, mechanical impurities, etc.

- Breakdown voltage at 50 Hz (or 60 Hz) when the transformer is filled, should be at least 200 $kV.cm^{-1}$.
- Interfacial tension at 25 ° C, should be at least 40 x 10^{-3} Nm^{-1}
- Loss factor (tan δ), at 90° should be less than 50 x 10^{-4}
- Permittivity (ε) = 2.2

The most important property of the oil (with regard to insulation design) is its dielectric strength. This may reach 4000$kV.cm^{-1}$ (for oils purified to a very high level under laboratory conditions). In practice it is expected to be approximately 200 $kV.cm^{-1}$, in the case of maximum attainable purity.

During the service life of a transformer, the deterioration of the dielectric strength has to be observed. If the breakdown voltage of the oils drops below 140 $kV.cm^{-1}$, the oil should be changed or alternatively regenerated. Any fall in the dielectric strength of the insulating oils, can be attributed to moisture, gases or solid impurities in the oil.

5.3 Properties of pressboard

Pressboard is used in the manufacture of insulating cylinders and moulded pieces. Transformerboard (special type of pressboard), is made of high-grade sulphate cellulose, and is generally used in large power transformers Transformerboard combines the excellent electrical characteristics of soft paper, with the excellent mechanical properties of hard-paper insulation. The manufacture of pressboard involves compressing several thin paper layers in a wet condition without using any bonding material. The thinner individual layers, the better the quality of the pressboard. In transformerboard there are approximately 35 layers of 30μm thick paper sheets per millimeter. The dielectric strength of pressboard that is impregnated with oil under a pressure of 2.7×10^{-2} mbar lies within the range of 200 to 250 $kV.cm^{-1}$.
The field strength for the inception of a partial discharge is about 70 to 80 % of the above value. Pressboard has a loss factor of approximately 40×10^{-4} at 20 ° C, and approximately 70×10^{-4} at 130 ° C. It has a permittivity of 4.4 to 4.5. The surface field strength permissible for pressboard is lies in the range of 5 to 30 $kV.cm^{-1}$ (depends on creepage distances; the higher values apply to shorter distances).
Applying a 50 Hz voltage at the above field strength will not result in any partial discharges occurring.

Note: There is a distinct difference between partial discharges that occur in the pressboard and that, which occurs inside the insulation. The p.d.'s, which occur in the pressboard, appear in the experimental measurements with a higher intensity than those that occur inside the insulation, due to the fact that their time to breakdown is considerably longer. However there is an important issue: The p.d.'s, which occur inside the insulation, might be of lower intensity but they are detrimental to the insulation and typically cause a breakdown sooner or later. This successfully explains why transformers that exhibit a lower p.d. level during tests soon become defective in service, while those with higher p.d. levels continue to operate successfully for untold years.

The mechanical properties of pressboard are excellent. The aging properties of pressboard were found to be favorable.

5.4 Properties of paper insulation

Paper insulation typically has a thickness of 30 to 120μm, and densities of 0.7 to 0.8 $g.cm^{-3}$. An important characteristic of paper is its tensile strength. For paper, this is expressed in units of the so-called "tensile length", where the tensile length is the length of a suspended paper tape (of uniform width and thickness), where its weight will just cause a rupture in the tape under the tensile force produced by its dead weight. Insulating paper typically has a tensile strength of 6 to 8 km.

The dielectric strength (at 50 or 60 Hz) has a value in the range of 100 to 150 $kV.cm^{-1}$ (in dry conditions, when applied in a thin layer). The dissipation factor is 10 to 30×10^{-4}. Its resistivity is 100 to 600×10^{6}, and its permittivity is approximately 2. Under the effects of water, heat and oxygen the properties of paper deteriorate i.e. subjected to aging. Provided the paper retains its mechanical strength, and does not disintegrate into pieces, it still remains electrically satisfactory. There are methods available for determining the factor of degradation within the paper.

5.5 Properties of oil paper insulation

Typically, the dielectric strength of laminated paper, which is impregnated with oil, is very much above that of either of the two components. The purpose of the paper is to split the oil into two minute gaps. The paper is actually a tangled mass of fibres that is not fully compressed. This permits the oil to fill up the spaces between the fibres and sheets. This forms extremely

thin oil spaces where the dielectric strength is very higher than that when measure between thick-layers of the same oil. Therefore, it is correct to say that the dielectric strength of oil-impregnated paper is defined by the strength of the small oil spaces.

The dielectric strength of the oil-impregnated paper of new transformers is typically 200 to 400 kV/cm. Its permittivity is approximately 3.5. However, the dielectric strength is drastically affected by heat and moisture. Moisture also leads to the aging of the paper.

If perfect degasification of the paper is not performed, then gas bubbles and cavities will be present in the insulation. The dielectric strength of the paper will decrease due to these gas bubbles, and due to the fact that the permittivity of air is lower than that of paper, a considerably higher electric stress will exist in the cavities in the paper. The resulting flashovers and discharges that occur in the cavities, do not cause breakdown of the dielectric strength of the entire insulation, and are hence termed partial discharges. However partial discharges result in the local progressive deterioration of the insulation.

Another source of partial discharges from the paper will be the gas bubbles that develop under the effect of high field strengths, from the moisture in the paper. These gas bubbles may appear, depending on the moisture levels, at a field strength as low as 10 kV/cm. Under the effect of moisture, partial discharges may take place in the insulation. Once the partial discharging process, has started, it makes itself independent on the initiating conditions and starts to spread owing to its chemical and physical effects.

Therefore, the moisture and gas content in transformers should be kept as low as is practically possible, throughout the manufacturing process, and this situation should be monitored throughout the life cycle of the transformer.

5.6 Summary

With reference to Chapter 2, partial discharges may occur in the Power Transformer as follows:

- Partial Discharges in the solid insulation. These could occur in the paper, pressboard, wood etc. They may also occur within the insulation due to cavities, impurities etc (principle was discussed earlier). They could also occur on the boundary surface of insulating materials (surface discharges; discussed previously), or between metallic and insulating surfaces.
- Partial discharges in the oil, between sharp or insufficiently rounded-off live metal parts and some neighbouring metallic objects of different potential. (Corona partial discharges; described earlier)
- Partial Discharges that occur between metallic objects of undefined potential to parts of fixed potential.
- Partial Discharges caused by bubbles, contamination or moisture. his type usually occurs between the oil and some insulating material or between oil and metal.

The partial discharges that occur in the solid insulation, dramatically affects the dielectric strength of the transformer. They exert a prolonged destructive force, which results in the progressive deterioration of the dielectric strength of the insulation. They can cause damage either directly or indirectly. In the direct case, e.g. they can lead to a turn-to-turn fault. It is more probable that they will lead to an indirect fault e.g. short-circuit stress at a spot within the transformer where the dielectric strength has previously been weakened by partial discharges. P.D.'s that occur within, or on the surface of solid insulation is definitely hazardous.

CHAPTER 6
PARTIAL DISCHARGE DETECTION

Partial Discharges result in the production of many different types of phenomena. These phenomena may be used for detection purposes. The various types of phenomena associated with partial discharges are depicted below:

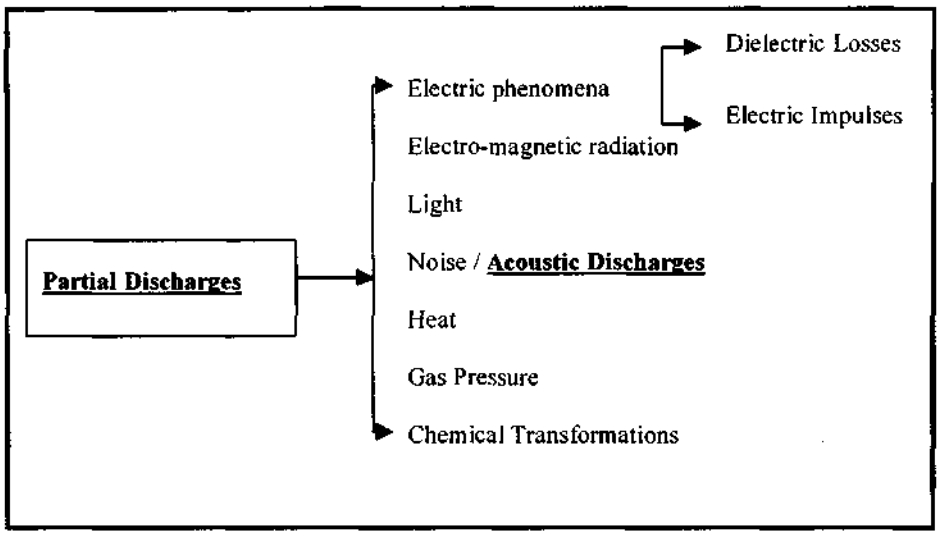

Figure (6.1) - Phenomena produced by partial discharges

"Acoustic discharges" has been highlighted, because it is main area of research for this project.

Useful Terminology

- **Detection**: Concerns the determination of the presence or absence of partial discharges. Several methods may be implemented. The voltage at which the discharges appear may also be determined.
- **Measurement**: Involves the determination of the magnitude of the partial discharges. Several electrical methods may be utilized.
- **Location**: Establishing the place(s) where the partial discharges occur. The choice of method depends on the nature of the investigated object. Noise or light produced by discharges may also be used as methods.
- **Evaluation**: Assessment of danger involved by discharges.

Electrical p.d. detection methods are the most commonly used methods. However other methods based on various other partial discharge induced phenomena (from figure 6.1) have also proved to be informative. Electrical partial detection methods have been applied over a wide range of circumstances [15]. This method has limitations, typically as a result of electromagnetic interference. On the field these types of interfering signals cannot be controlled as they are under laboratory conditions. They therefore pose a problem. Also, the sensitivity of partial detection methods decreases with increased capacitance of the test object [15]. This makes electrical partial detection methods not very sensitive when they are used with apparatus having a large capacitance. Additionally, it has been noted that electrical detection methods are not very useful when it comes to locating the sources of partial discharges.

Comparatively, acoustic p.d. detection, has several advantages over the electrical methods[15]. Firstly, acoustic methods can be configured to be immune to electromagnetic interference. This is a major benefit, because during field testing there are several interfering signal present, which would greatly reduce the sensitivity of the method. Also, the sensitivity of the acoustic methods does not vary with the objects capacitance, as is the case in the electrical methods. An important

benefit of the acoustic method is that it provides an indication of the p.d. source within the complex setup of the transformers.

Experimentation has also revealed that under some circumstances, electrical and acoustic methods can be combined, and the results are very good. This is often used in the localization of p.d. sources. They have also been combined during the online detection of p.d.'s in order to avoid false alarms, where would have resulted from either method separately.

The following chapters identify all the mechanisms involved in p.d. detection and localization using acoustic methods.

ACOUSTIC METHOD OF PARTIAL DISCHARGE DETECTION AND LOCALISATION

CHAPTER 7
FUNDAMENTAL CONCEPTS IN ACOUSTICS

'Sound propagates through a medium by means of wave motion' [14]. When the disturbance occurs in a liquid medium it results in local changes in pressure (p), which in turn results in local changes in density (ρ) and the displacement of molecules in the medium. The general differential equation of acoustic wave motion is derived from 3 basic equations that describe continuity, conservation of momentum, and elasticity of the medium. This equation is given by:

$$\nabla^2 p = \frac{1}{c^2}\frac{\partial^2 p}{\partial t^2} \tag{7.1}$$

'The elastic wave equation has a tensor form with three orthogonally polarized plane wave solutions for any direction of propagation' [14]. This equation is best described in the limit of plane harmonic pressure waves, given by:

$$p(x,t) = p_0 \sin(\omega t \pm \frac{\omega x}{c}) \tag{7.2}$$

The pressure wave above is shown to vary with both time and position. At any given value of x (*position*), the value of the excess pressure repeats itself f times a second. This results in a period of the wave equal to $T = \frac{1}{f}$. (7.3)

For all t, the pressure wave repeats itself with the space interval $\lambda = \frac{c}{f}$ along the direction of propagation. (7.4)

The elastic properties of a liquid directly determine the velocity of sound in that liquid[14].
Forces act on every "small volume" (particle) of the liquid. The net sum of all these forces is what causes the particle to move (say, with a velocity *v*).

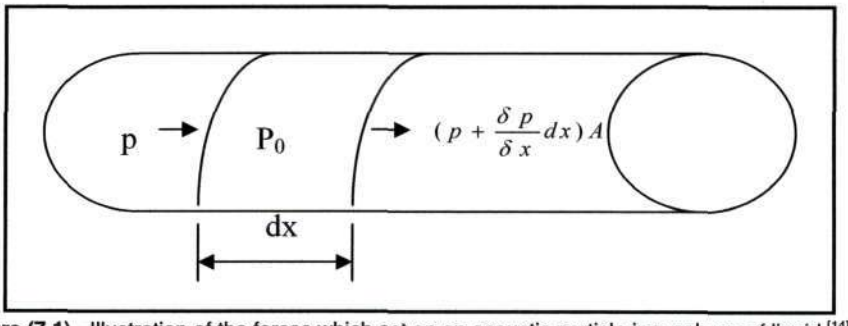

Figure (7.1) - Illustration of the forces which act on an acoustic particle in a column of liquid [14].

where: A = area of tube [14].

The ratio between the sound pressure and the velocity of the particle is called the "*specific acoustic impedance*", which is analogous to electrical impedance, given by:

$$\vec{z} = \frac{\vec{p}}{\vec{v}} \tag{7.5}$$

In the case of planar waves, this acoustic impedance becomes a scalar $z = p_0 c$, and this is now called the characteristic impedance of the medium. Note, that the relationship between the

propagation of the wave and the individual particle movement is determined by the parameters of the material

The time average of the acoustic energy flow through the medium (acoustic intensity (W/m^2), is an important equation which is given by :

$$I = \overline{vp} = -\frac{p}{2p_0c} = \frac{Vp_0c}{2} \tag{7.6}$$

where: p = peak pressure; V = peak velocity

7.1 Signal absorption

Several mechanisms e.g. spreading of the acoustic wave, acoustic absorption and scattering of the wave front cause the intensity of a wave to decrease as a function of the distance from the source, as it propagates through a medium. [14].
For lossless media, the intensity of a spherical wave decreases inversely to the area of the wave front, and in a cylindrical wave the intensity of the wave decreases inversely with the distance from the source. This is not valid in the near region of the source. This reduction in intensity is termed "spatial attenuation".

7.2 Refraction / reflection

Refraction and reflection occurs when acoustic waves propagate through media of different densities or elasticities. The energy of the transmitted wave is reduced.

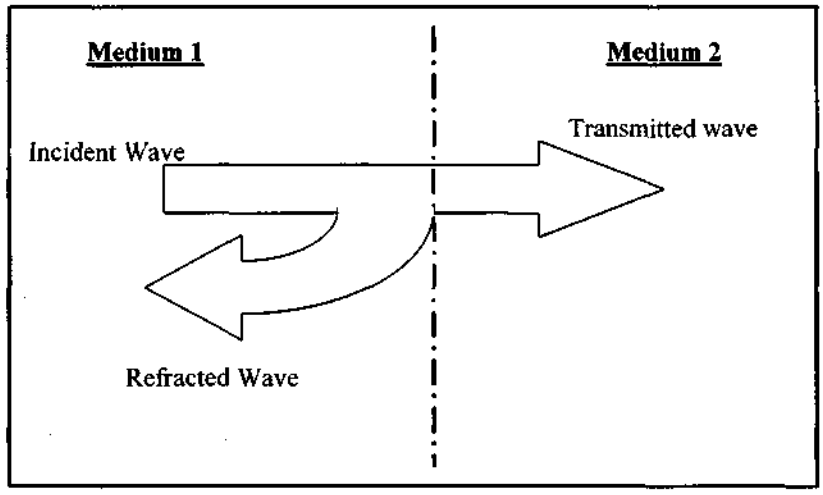

Figure (7.2) - Transmission and reflection of a wave that is incident, normal to an impedance discontinuity [14].

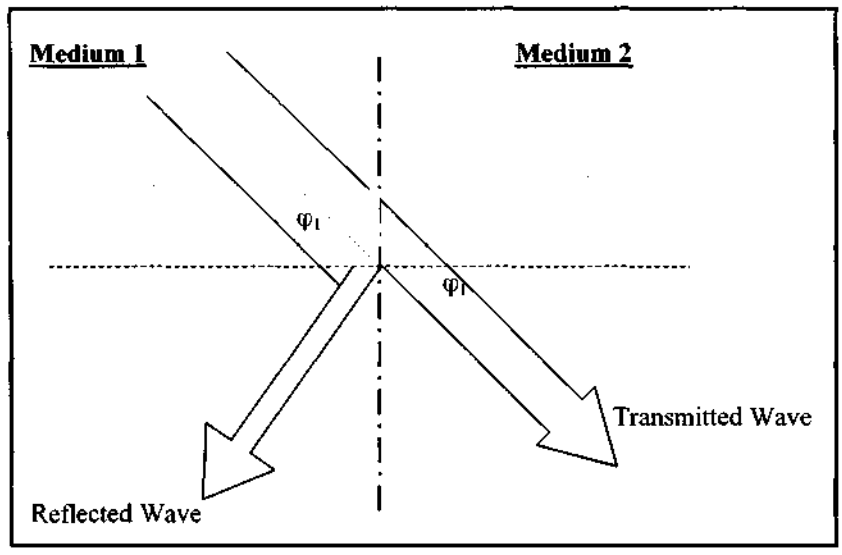

Figure (7.3) - Refraction of a wave that is incident to the discontinuity at an oblique angle [14].

'The transmission co-efficient is determined by the difference in acoustic impedance for the two media' [14]. This is given by:

$$\alpha_{Transmission} = \frac{I_t}{I_i} = \frac{4Z_1Z_2}{(Z_1+Z_2)^2} \tag{7.7}$$

For a given pressure wave, the transmission co-efficient between oil and steel is 0.11, and the transmission co-efficient between air and steel is 0.0016.

When the incident wave strikes the boundary obliquely, the angle of the transmitted wave is 'governed by the required coincidence between the incident and transmitted wave along the interface' [14]. Snell's Law describes this as:

$$\sin(\frac{\phi_t}{c_t}) = \sin(\frac{\phi_i}{c_i}) \tag{7.8}$$

7.3 Wave diffraction

Acoustic waves bend around corners and obstacles. This occurs as a result of wave diffraction. The bending of the acoustic waves because of diffraction becomes less obvious as the wavelength of the wave decreases relative to the dimensions of the obstacle. Diffraction is called scattering when many obstacles are present.

7.4 Losses

Losses that occur in homogenous media are mainly divided into three types:

- Viscous losses
- Heat conduction losses
- Losses due to molecular exchanges of energy

'Ultimately, all acoustic energy is degraded into thermal energy' [14]. Losses result in exponential decreases of intensity, with distance along the sound propagation path. This is described by:

$$I(x) = I_0 e^{-2\alpha x} \tag{7.9}$$

where 2α is the intensity absorption coefficient.

Sound waves are scattered in inhomogeneous materials due to the occurrence of gas bubbles in either the solid or liquid. The losses due to scattering may be extremely large, hence reducing the intensity of the wave.

7.5 Acoustic characteristics of liquids

The velocity of sound in liquids varies from approximately 900m/s to 2000m/s [14]. Usually only pressure waves can propagate in liquids due to the small viscosity and shear forces. With the exception of water, the velocity of sound decreases monotonically with temperature in most liquids (i.e. approximately 2 to 6 m/s per °C)

The absorption in liquids increases with the square of the frequency, where the losses are proportional to and dominated by the viscosity.

7.6 Parameters that affect the velocity of sound in transformer oil

It was found that the speed of acoustic waves propagating in transformer oil differed from previously specified values in literature [14]. After several investigations were conducted, it was noted that the velocity of acoustic waves in transformer oil was not constant, but dependant upon a relationship which involved the temperature of the oil, the gas and moisture content of the oil, and the frequency content of the signal.

Motivation for experimentation: Usually tests are conducted on transformers on the factory floor. Under these types of conditions, the transformers are not at their normal operating temperatures and the temperature of the oil is fairly equal to the temperature of the factory environment. Under these circumstances, the value of the speed of sound in transformer oil, as quoted in literature is fairly accurate. However, whilst testing "on-line" transformers, the localization techniques used for locating p.d's turned up erroneous results [17]. It was found that these errors were apparently due to the fact that the acoustic waves were in fact traveling at a different speed in the transformer oil than what was previously anticipated.

More specifically, it was found that the sonic velocity of oil varied with temperature [17]. A vast amount of experimental work was conducted to verify the above. The opportunity was also

taken to determine whether or not other oil-related characteristics could also influence the sonic velocity of oil. The parameters, which were the focus of the evaluation, were:

- Oil temperature
- Oil moisture content
- Oil gas content
- Frequency content of the propagating signal.

'A typical naphthanic based transformer oil was used in these experiments and in order to maintain consistency, all the oil was taken from the same barrel.' [17]
The following are the results of the experimentation.

7.6.1 Temperature effects

The frequency of the acoustic waves, which were of particular interest in the experiment, was 150 kHz. Acoustic filters were used to attain waves only in this frequency range. Vacuum degassed and dried oil were used. The sonic velocity of these acoustic waves was measured in the temperature range of -30 °C to 130 °C.

The result of the experimentation was that it was clearly evident that the temperature of the oil played a major role in the velocity of the propagating acoustic waves through the oil [17]. It was also noted that there exists a limiting maximum velocity of the acoustic waves, at very low temperatures (when the oil approaches the consistency of grease).
However, the velocity decreases rapidly as the temperature rises. It was also noted that at a temperature of 130 °C, the lower velocity limit had still not been attained.

7.6.2 Moisture content

Oils with different moisture level contents were used in this investigation. The range of moisture levels in the oils tested, were 6 ppm to 76 ppm. The temperature of the oil was kept constant at 60 °C, and once again the frequency content of the signals of interest was 150 kHz.

The results of the experimentation showed that the addition of moisture to the oil reduces the sonic velocity. This effect is not as significant as the effect of temperature changes on the sonic velocity [17].

7.6.3 Gas content of the oil

Vacuum dried and degassed oil were used to prepare samples, which were then saturated with gases such as ethane, methane, carbon dioxide, hydrogen and acetylene. The signal frequency was once again chosen to be 150 kHz.

It could be noted from the experimentation that any absorbed gas present in the oil, results in a small but measurable decrease in the sonic velocity. The sonic velocity was shown to not respond equally to all gases. It was also suggested that there exists an inverse relationship between the molecular weight of a gas and the corresponding effect on its velocity [17]. Carbon dioxide, having the largest molecular mass of all the gases tested, experienced the least effect, whilst hydrogen, being the lightest of all the gases tested, experienced the largest effect. This theory is still to be confirmed.

7.6.4 Frequency content of the signal

Measurements were made using ultrasonic transducers of different resonant frequencies. Dry and degassed oil at a constant temperature of 60 °C, was used as the medium. The test was conducted at 150kHz, 250kHz, 600kHz, 800kHz and 1 Mhz.

It was found that the higher the frequency content of the signal, the faster it would propagate through the transformer oil.

7.6.5 Summary of results

In order to obtain a high degree of accuracy, the effect of all of the previously mentioned parameters must be taken into account. However, in various cases it was found that a reasonable approximation to the true effective sonic velocity could be realized by only taking into account the temperature of the oil, as well as the frequency content of the propagating signal, as these two parameters have the most significant effect on the sonic velocity.

7.7 Acoustic properties of solid materials

Solids typically support both longitudinal (pressure) and transverse (shear) wave types. These wave types are usually excited simultaneously. Generally, the velocity of the shear wave is approximately 50 % of the velocity of the pressure wave. When sound is transmitted from a semi-infinite liquid into a semi-infinite solid, the pressure wave in the liquid generates both a pressure and a shear wave in the solid.

Acoustic properties of most solids are reliant upon the composition of the solid, as well as the production process involved. The absorption coefficient of the solid can vary over several decades. Losses of the propagating signal commonly occur on the boundaries of inhomogenities. These losses dramatically reduce the sensitivity of the measurements. These losses also place a maximum limit to the thickness of a test object that may be investigated.

Material	Density [g/cm^3]	Pressure Velocity [m/s]	Shear Velocity [m/s]	Absorption [dB/m]
Aluminium	2.7	6300	3100	4x10 ^{6}@50 kHz
Iron	7.8	5900	3200	-
Cast Iron	6.9 to 7.3	3500 to 5800	2200 to 3200	100 @ 2 Mhz
Filled Epoxy	1.15	2600	1100	1000 @ 2 MHz
Unfilled Epoxy	1.2	2700	1200	-
Copper	8.9	4700	2300	-
Glass Silicate	2.2	6000	3800	6.5 x 10^{-7} @ 50 kHz
Impregnated Crepe Paper	Approx. 0.9	1500 to 1600	-	Approx. 200 @ 400 kHz
Impregnated Pressboard	1.25	1950	-	-

Table (7.1) - Acoustic properties of selected solids [14]

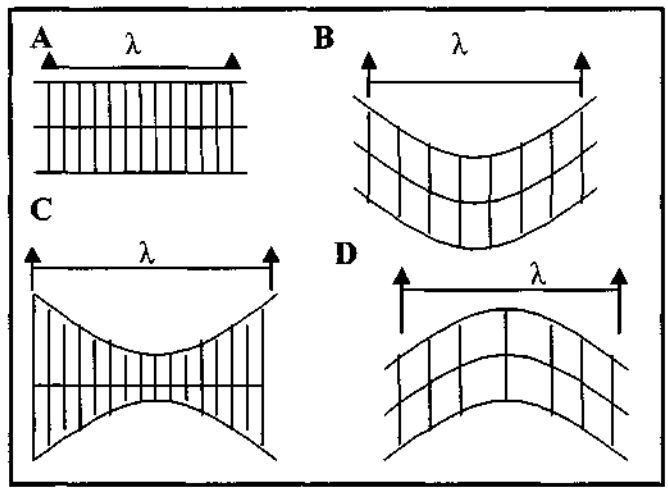

Figure (7.4) - Illustration of the particle displacement for (A) pressure wave, (B) shear wave, (C) semi-longitudinal wave, (D) flexural wave

Flexural waves in plates apply to p.d. detection in transformers. In the case of a plate, the phase velocity is strongly dependant on the frequency and plate thickness. 'For lower frequencies, the velocity increases with the square of the frequency, but at higher frequencies it is close to the velocity of the transverse wave (typically 2500 to 3000 m/s for a metal). [17].

The requirement of co-incidence, between the wave in the plate and the wave component parallel to the plate, restricts the transmission of a signal from the pressure wave to the plate. Dispersion of the flexural wave in the plate, results in the above requirement only being met for certain combinations of frequency and angle of incidence. This in turn results in higher frequencies being fed into the plate with near normal incidence, whereas lower frequencies are fed in at more oblique angle.

'At very low frequencies, where the phase velocity in the plate is smaller than the velocity of the pressure wave, total reflection occurs [14]. It is important to note that for low frequencies, the propagation velocity of the flexural wave is equal to twice the phase velocity, while at high frequencies, the propagation velocity and the phase velocity of the flexural wave converge.

The following diagram depicts the signal transmission from a liquid to a plate. Note that a requirement for the transfer of the acoustic energy from the liquid to the plate is that the two wave fronts in both media should coincide. Figure (7.5) depicts that the pressure wave in the liquid is in phase with the flexural wave in the plate.

See overleaf for figure 7.5.....

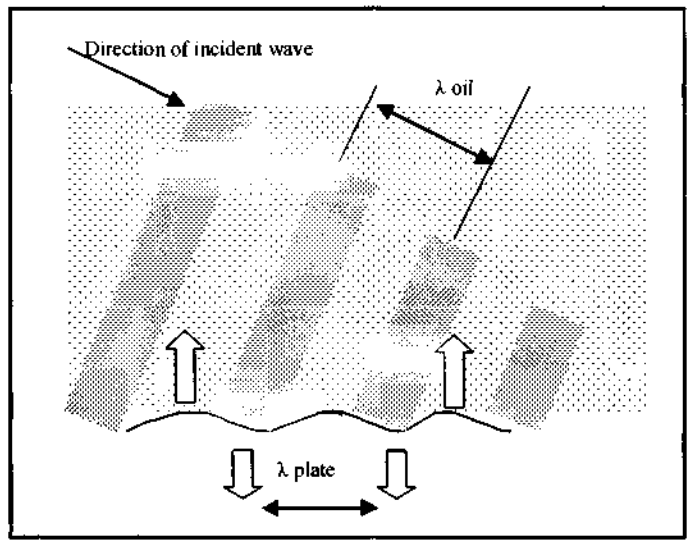

Figure (7.5) – Signal transmission from liquid to plate

7.8 The Acoustic Discharge Detection Method

The principle of acoustic discharge detection stems from the fact that mechanical signals emanate from the discharges. 'The discharge appears as a small "explosion", which excites a mechanical wave that propagates throughout the insulation.' [15]. These waves impinge on the tank wall. Therefore, the wave may be detected by suitable sensors, and the output can be analysed on a data acquisition system. However, locating the source of the p.d. is more involved due to the following factors:

- The transformer has a complicated inner geometry.
- The effects of attenuation, reflections and refractions that occur as the signal passes through the transformer.
- Reverberation within the tank of the transformer.
- Changes made to the signal whilst traveling through or along a tank wall.

The shape of the detected signal is dependant on the detection apparatus used, the sensor, and the source e.g. in the event of a discharge occurring in the insulation, a fast front pulse is emitted. This pulse has a spherical wave front. In the case of oil and oil-impregnated insulation, this emitted pulse is actually a pressure wave that is longitudinal in nature.

7.9 Sensors

Piezo-electric transducers conventionally designed for acoustic emission purposes are generally used to "listen" to acoustic emissions. Certain modifications generally have to be made to the device. E Howells, and E.T. Norton [3], experimented with the device and recognized that the response spectra from the manufacturer for the transducer might have been generated using transient transverse (shear) waves as the forcing function. As another possibility the response spectra could also have been generated using continuous longitudinal (compression) waves as the forcing function. Now, a problem arose, because the acoustic emissions due to partial discharges in a transformer, are transient signals and due to the fact that most of their propagation path is in oil, transverse waves are not possible. It was therefore necessary for them to recalibrate each transducer in order to determine its response to *longitudinal* transients. They achieved this by placing the sensor face-to-face with a longitudinal transducer, which acted as the forcing function. The driver used for this purpose was a heavily dampened five MHz barium titanate unit. This type of unit is typically used for ultrasonic inspections. It is a resonant unit whose output below 1.5 MHz is especially flat in the frequency domain. The driver was then pulsed electrically and the output from the sensor was amplified and filtered (to exclude signal beyond 1 Mhz) and then observed on the oscilloscope. A frequency analyzer was then used to process the transient. 16 spectra were averaged in order to exclude random noise.

A characteristic of piezoelectric crystals are that they are sensitive to electrical and magnetic field, however, any influence of the electrical and magnetic fields can be negated by utilizing the concept of differential transducers, where two identical crystals are mounted in the transducer such that their outputs are 180 ° out of phase. Since these fields influence both crystals their subsequent signals cancel out. Only one crystal is actually in contact with the transformer wall during the testing. This method has proven successful even in dramatically noisy environments.

The sensitivity of these transducers varies inversely with the temperature. This temperature dependence for a type D140B transducer is illustrated in figure (7.6). During cold conditions any variation can be compensated by adjusting the power amplifier gain.

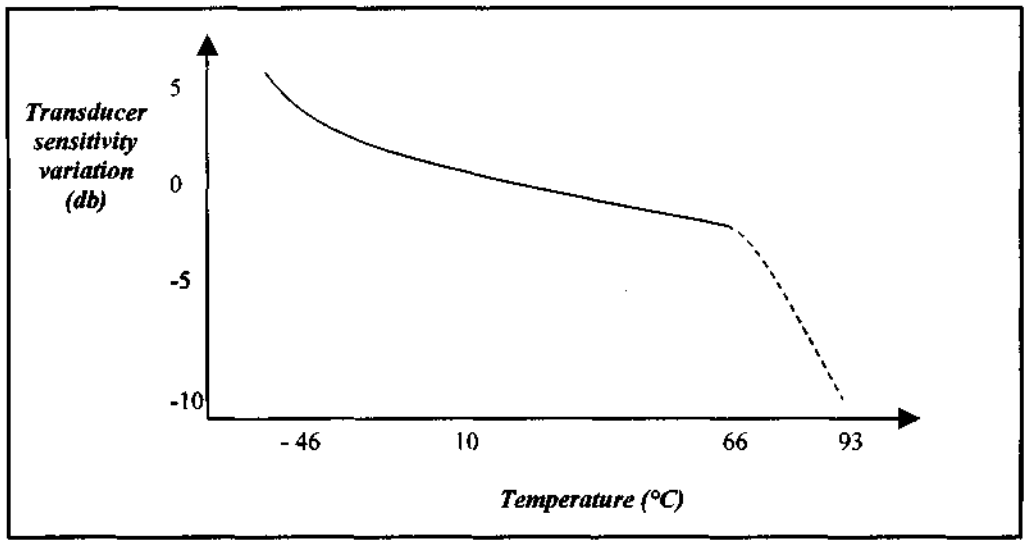

Figure (7.6) - Transducer Sensitivity Vs temperature[3]

7.9.1 Attachment of sensors

When attaching the sensors to the walls of the transformer, a thin layer of grease should be applied to the measuring surface of the transducer, in order to improve the contact. By eliminating any air-space between the transducer and the tank, an increase in sensitivity and better reproducibility was obtained. This concept was experimentally proven by D. Train, A Mercier and D. Thorne [4].

7.9.2 Inaccuracies associated with magnetic noise (magnetostriction)

The operation of the transformer is associated with magnetic noise. This magnetic noise is caused by a phenomenon termed "magnetostriction" (change of dimension of sheets forming the core). In other words, if a piece of magnetic sheet steel is magnetized it will extend itself. However when the magnetization is removed, the sheet steel will revert to its original condition. A transformer is magnetically excited by an alternating voltage and current. It becomes extended and contracted twice during a full cycle of magnetization. Note that these expansions and contractions are generally not uniform, and hence varies all over a sheet. These extensions, which occur, are dimensionally small.

Howells and E.T. Norton [3] experimented in order to determine if there was any relationship between magnetic circuit noise and partial discharge signals. The outcome of this experimentation was that magnetic circuit noise (due to magnetostriction) is not in any way related to partial discharge signals. The two signals were found to be substantially different in both the time and frequency domains. Therefore the magnetic circuit noise can safely be ignored.

In the time domain, the signals may be separated by the signal-to-noise ratio and the pulse shape. In the frequency domain, the use of a high-pass filter will nullify the magnetic noise signals caused by magnetostriction in the transformer core.
The high pass filter may be introduced as follows:

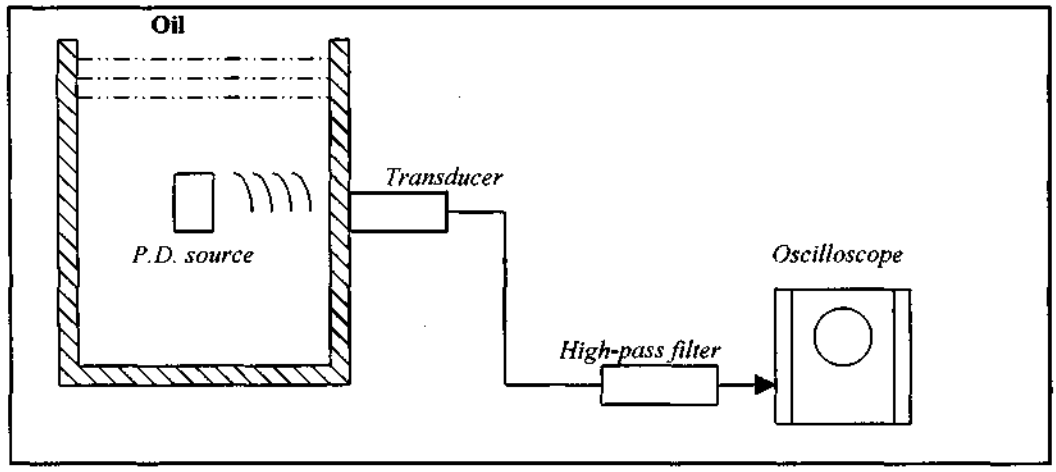

Figure (7.7) - Experimental Setup using High Pass filter

7.9.3 Positioning of sensors

As discussed previously, the form of the emitted pressure wave is changed once it impinges onto the walls of the transformer tank. The original oil-borne pressure wave is transformed into (1) a steel borne pressure wave, and (2) a steel borne shear wave together with a slight flexural oscillation of the wall at low frequency (typically below 10 Khz).

If a sensor was mounted on the transformer wall, it would respond to all of the above signals. However, these signals may be distinguished from each other by using a wide-band transducer amplifier system. The position of the transducer in relation the discharge site, will determine the order of arrival of the signals.
Example:. If the transducer is close to a normal to the wall through the discharge then the direct oil borne pressure wave will be the first to arrive, followed by the wall borne wave and lastly by the wall borne shear wave.

Away from the area in the vicinity of the normal, a transducer will firstly respond to the pressure wave emanating from the steel, and then either the pressure wave in the oil or the shear wave in the steel, depending on the distance from the normal. The term, area of direct reception is used to refer to the area around the normal. The shape of the areas of direct reception varies with the geometry of the surface, i.e. for a flat surface it is a circle whilst for a cylindrical surface it is an ellipse. The size of the area of direct reception is most reliant on the length of the normal through the discharge. The perimeter is defined as, the locus of all possible transducer positions, where the direct oil borne pressure wave arrives at precisely the same instant of time as the steel borne pressure wave. The locus is termed to be isochronic.

From the above theory and definitions the following relationship has been derived:

$$\sin\alpha = \frac{V_{OIL}}{V_{STEEL}}$$

where α refers to the critical angle between the normal to the wall on the perimeter of the area of direct reception and the line from the perimeter to the discharge site. V_{OIL} and V_{STEEL} are the respective velocities of those in the mediums of oil and steel.

7.9.4 Sensitivity

The r.m.s. sound pressure, at a distance of 100 mm away from a 1 pC discharge is 0.2 Pa. This pressure 1 metre away should be approximately 0.02 Pa, for spherical waves. In the case of practical power transformers, the discharges are actually tens to hundreds of pico-coulombs. Therefore in choosing sensitivity for a transducer, the case of choosing a transducer that is sensitive enough to measure 0.2 Pa pressure waves should be more than adequate.

7.9.5 Frequency range

Cavities within paper insulation could typically result in acoustic discharges, which range up to 300 kHz [7]. They tend to be concentrated between 100 and 200 kHz. Also, the effect of magnetostriction (core noise), oil circulation disturbances and other environmental noise, has to be taken into account. These types of noise typically centre around 50 kHz. Therefore a good design decision would be to have a sensor that is preferably more sensitive above 100 kHz. [7, 8].

CHAPTER 8
LOCALISATION OF THE PARTIAL DISCHARGE SITES USING ACOUSTIC TECHNIQUES

To obtain the maximum benefit, it is necessary not only to detect the partial discharges, but also to locate the source of the discharge.

Generally there are two basic propagation paths from the source of the acoustic wave to the sensors, which are on the walls of the transformer. The first path is the direct path in the oil. Say the acoustic wave propagates along this path at a speed of v_{oil}. The other path refers to the mixed path where the acoustic wave propagates first through the oil, and then through the steel plate. Say the wave propagates at a speed of v_{steel} .The propagation velocity of the acoustic wave through the steel is greater than the propagation velocity of the acoustic wave through the oil. However, the amplitude of the direct-path wave is much greater attenuated than that of the mixed path wave. This is due to the significant attenuation, which occurs to the signal in the steel plate. It is therefore a wiser decision, to choose the propagation time of the direct-path wave as the basis in order to determine the propagation time from the source of the partial discharge to each sensor.

The following is a representation of the system, using four acoustic sensors (S_1 to S_4).Also S_1 has been chosen as the reference sensor which will trigger the other sensors. It has been assumed that the propagation time to the sensor S_1 is T. P(x,y,z) is a representation of the source of the partial discharge.

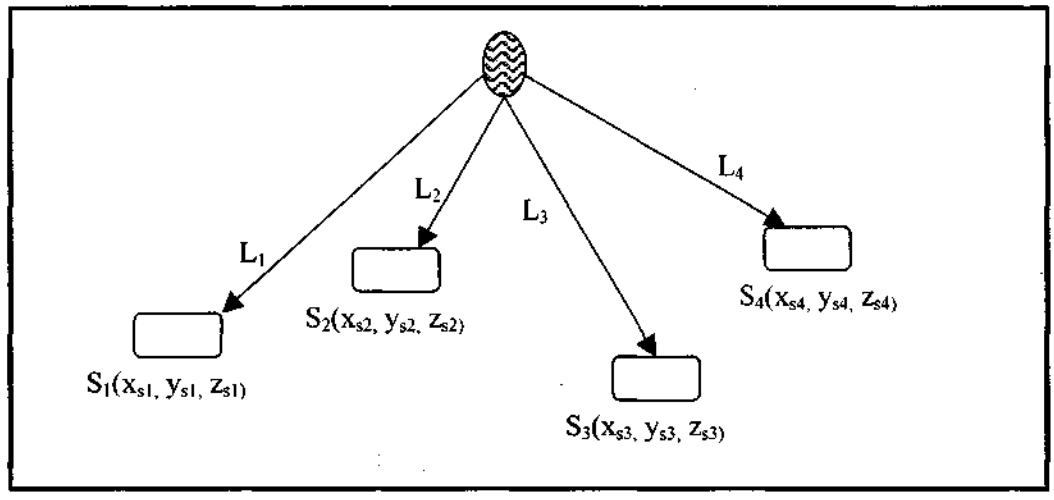

Figure (8.1) - Representation of system

The distance from P(x,y,z) to each of the four sensors can now be calculated using the following formulae:

1) $L_1 = v_{oil} * T_1 = v_{oil}\, T$
2) $L_2 = v_{oil} * T_2 = v_{oil}\, (T + \tau_{12})$
3) $L_3 = v_{oil} * T_3 = v_{oil}\, (T + \tau_{13})$
4) $L_4 = v_{oil} * T_4 = v_{oil}\, (T + \tau_{14})$

Where $\tau 1n$ is the time delay between the sensor (S_1) and sensor (S_n). Now, the relationship between the position of the partial discharge site can be associated as follows (by using the distance formula):

$$(x - x_{s1})^2 + (y - y_{s1})^2 + (z - z_{s1})^2 = (v_{oil}\, T)^2$$

$$(x - x_{s2})^2 + (y - y_{s2})^2 + (z - z_{s2})^2 = (v_{oil}\, (T + \tau_{12}))^2$$

$(x - x_{s3})^2 + (y - y_{s3})^2 + (z - z_{s3})^2 = (v_{oil}(T + \tau_{13}))^2$

$(x - x_{s4})^2 + (y - y_{s4})^2 + (z - z_{s4})^2 = (v_{oil}(T + \tau_{14}))^2$

Now the above equation have to be solved for x, y, z, and T. (**Note:** Assume that τ_{1n} are known). The least squares algorithm may now be used to solve for the unknowns.

$$x = \frac{1}{N}\sum_{i=1}^{N} x_{si} + \frac{1}{N}\sum_{i=1}^{N} \frac{(T + \tau_{1i})(x - x_{si})v_{oil}}{[(x - x_{si})^2 + (y - y_{si})^2 + (z - z_{si})^2]^{\frac{1}{2}}}$$

$$y = \frac{1}{N}\sum_{i=1}^{N} y_{si} + \frac{1}{N}\sum_{i=1}^{N} \frac{(T + \tau_{1i})(y - y_{si})v_{oil}}{[(x - x_{si})^2 + (y - y_{si})^2 + (z - z_{si})^2]^{\frac{1}{2}}}$$

$$z = \frac{1}{N}\sum_{i=1}^{N} z_{si} + \frac{1}{N}\sum_{i=1}^{N} \frac{(T + \tau_{1i})(z - z_{si})v_{oil}}{[(x - x_{si})^2 + (y - y_{si})^2 + (z - z_{si})^2]^{\frac{1}{2}}}$$

$$T = \frac{\sum_{i=1}^{N}[(x - x_{si})^2 + (y - y_{si})^2 + (z - z_{si})^2]^{\frac{1}{2}}}{\sum_{i=1}^{N} v_{oil}}$$

Hence, the above method succeeds in determining the co-ordinates of the discharge site P(x,y,z).

CHAPTER 9
ELECTRICAL DETECTION

The presence of a cavity/inclusion in a dielectric can be diagrammatically depicted as follows:

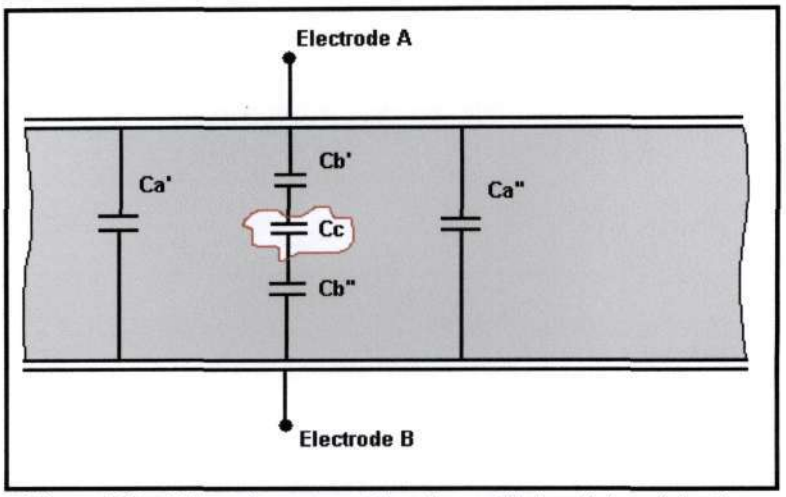

Figure (9.1) – Schematic representation of a gas filled cavity in a dielectric

Figure (9.1), depicts a dielectric material present between two electrodes, A and B. A gas filled cavity has been included in the dielectric. This cavity will become the origin of partial discharges if the applied voltage is increased. This is due to the fact that the "field gradients in the void are strongly enhanced by the differences in the permittivities as well as the shape of the cavity."[1]

The behaviour of internal discharges at a.c. voltage can be examined conveniently with the following analogue circuit.

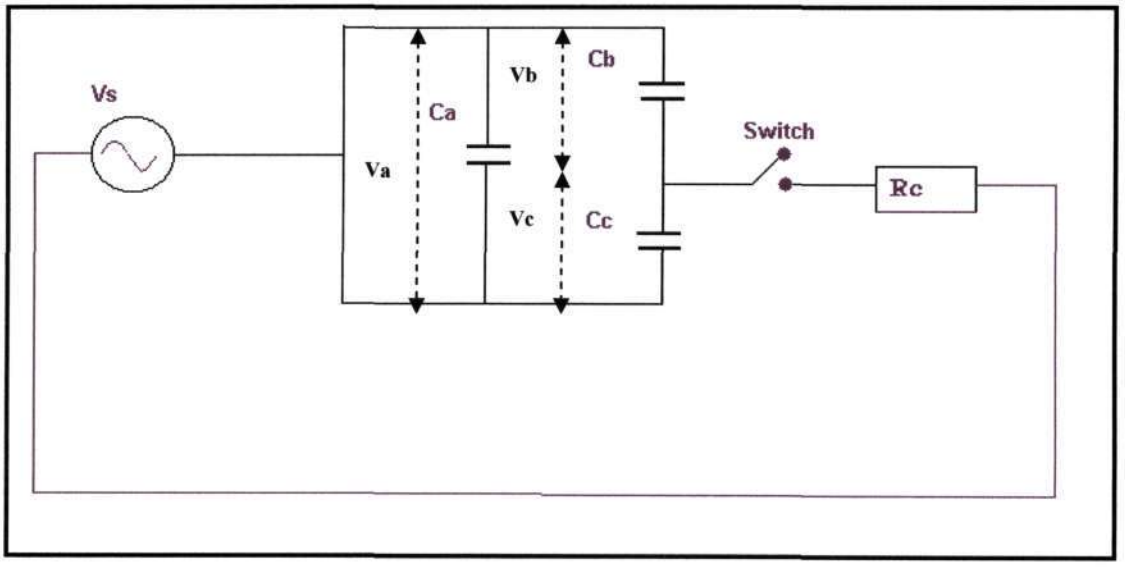

Figure (9.2) – Equivalent Analogue Circuit

The simple capacitor arrangement of figure (9.2), comprises of the dielectric material between electrodes A and B, as well as the gas-filled void. The capacitance across the void is denoted by C_c. The voltage across this void is given by V_c. The above circuit was simulated using PsCad software. The switch was controlled by the voltage across the void.

The following waveform was attained from the circuit simulation:

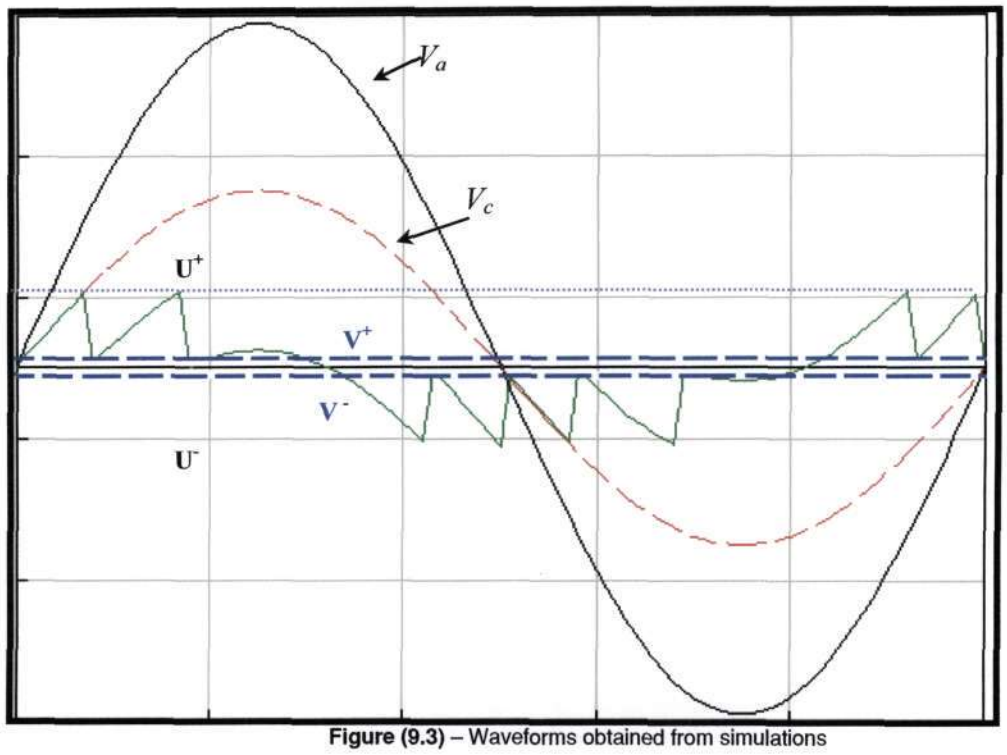

Figure (9.3) – Waveforms obtained from simulations

The voltage across the dielectric is given by V_a, while the voltage across the void is denoted by V_c. When the voltage across the void reaches the breakdown voltage, denoted by U^+, a discharge occurs in the void. Note that the breakdown voltage U^+, can be ascertained from the Paschen curve (considering a gas filled void). The voltage across the void then drops to V^+(in an extremely short time, approximately 10^{-7} sec)[1], when the discharge extinguishes. This is extremely short compared to the duration of the 50Hz sine wave. The voltage drop can thus be regarded as a step function. [1] Once the discharge has extinguished, the voltage across the void begins to rise again. "This voltage is determined by the superposition of the main electric field and the field of the surface charges at the cavity walls left behind after the last discharge."[1] These fields attempt to counteract one another.

When the voltage across the void reaches U^+ again, a new discharge occurs. This process occurs several times. The voltage across the cavity decreases during the negative part of the cycle. In these instances the breakdown voltage now becomes U^-. Regularly recurrent discharges are formed in this way.
"The discharges in the cavity cause current impulses in the leads of the sample."[1] These impulses were experimentally noted to be concentrated in regions where the voltage applied to the sample increases or decreases the most. [1]

There exist a great variety of circuits that can be utilized to detect these current impulses. All these circuits can be reduced to the following diagram:

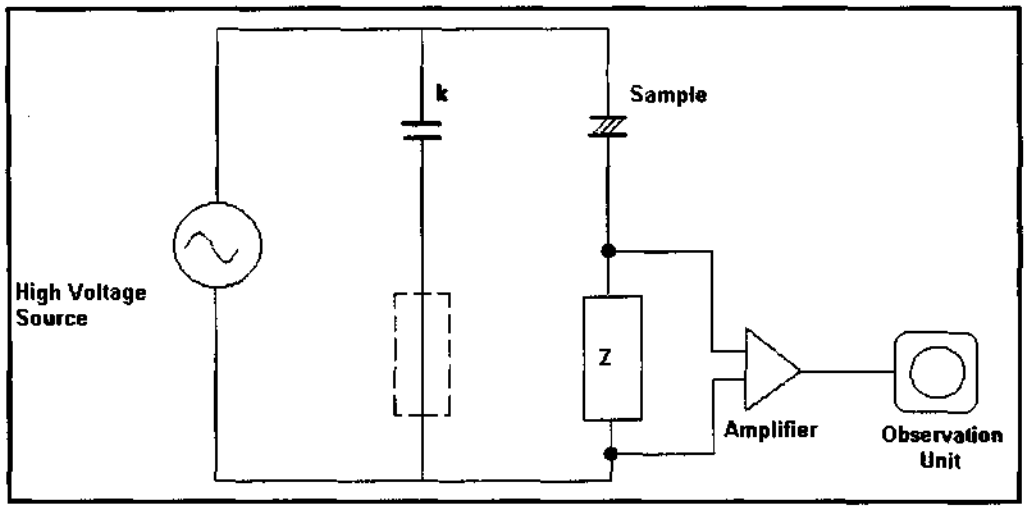

Figure (9.4) – Basic Circuit used for Electrical Discharge detection [1]

The circuit depicted in figure (9.4), comprises of the following components:

- A high-voltage supply, with a sufficiently low level of background noise, to allow the measurement of the specified partial discharge magnitude at the specified test voltage.
- A sample that is affected by partial discharges.
- A coupling capacitor **k**, which facilitates the passage of high frequency current impulses. This capacitor should be of low inductance design. [22] It should exhibit a sufficiently low level of partial discharges at the specified test voltage, in order to allow the measurement of the specified partial discharge magnitude. It is possible to tolerate a higher level of partial discharges from the coupling capacitor if the measurement system is capable of distinguishing between the discharges from the test object and the coupling capacitor and measure them separately.
- An impedance Z, across which voltage impulses occur. These voltage impulses are caused by the current impulses in the sample. The impedance may also be placed in series with the coupling capacitor **k**. Both the methods of connecting this impedance are electrically equal (the same voltage appears across the impedance) assuming that the impedance of the H.V. source is large.
- An amplifier.
- An observation unit.

Further Note: In practice the connection of the impedance, **Z**, may be of significant importance. In instances where the sample is large, **Z** , is very often placed in series with the coupling capacitor **k**, so that the large current of the sample does not pass through the impedance **Z**.[1]

Two common impedances are used: (1) A resistor shunted by a parasitic capacitor C, or (2) An oscillatory circuit (LCR). Laplace Transformation can be utilized to calculate the voltage impulses, which occur across these impedances. These two cases are described overleaf.

Case (1) – RC impedance

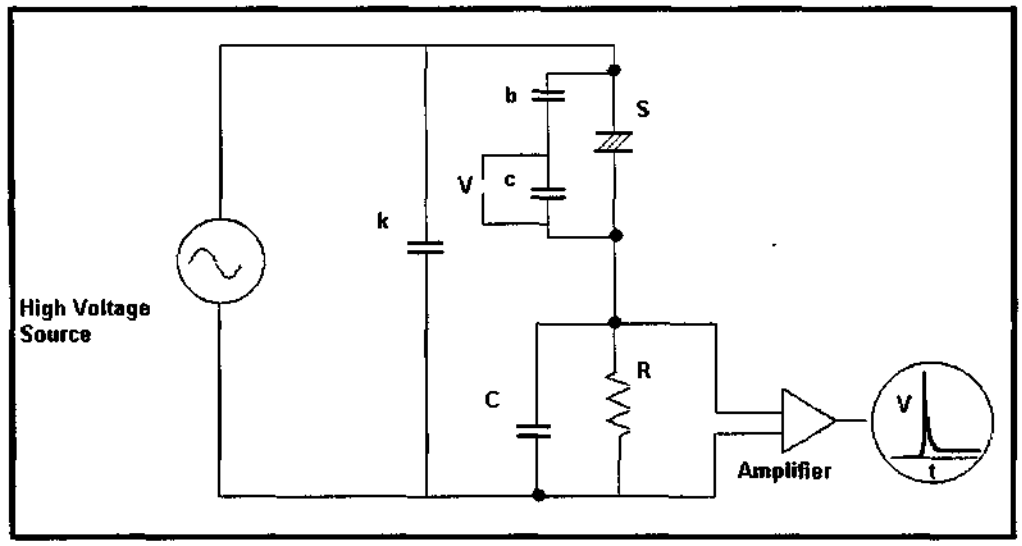

Figure (9.5)- Circuit with RC Impedance – Response Depicted[1]

Figure (9.5), depicts the case where the impedance is made up of a resistor, which is shunted by a parasitic capacitance *C*. The result (depicted) illustrates that the impulse appears to be unidirectional. This impulse is given by: [1]

$$V = \frac{q}{(1+\frac{C}{k})S + C}.\exp(-t/Rm) \tag{9.1}$$

where: q is the magnitude of the partial discharge which causes the impulse.

$$Q = b.\Delta V \tag{9.2}$$

In addition m (in equation 9.1), can be calculated as:

$$m = \frac{Sk}{S+k} + C \tag{9.3}$$

Case (2) – LRC impedance

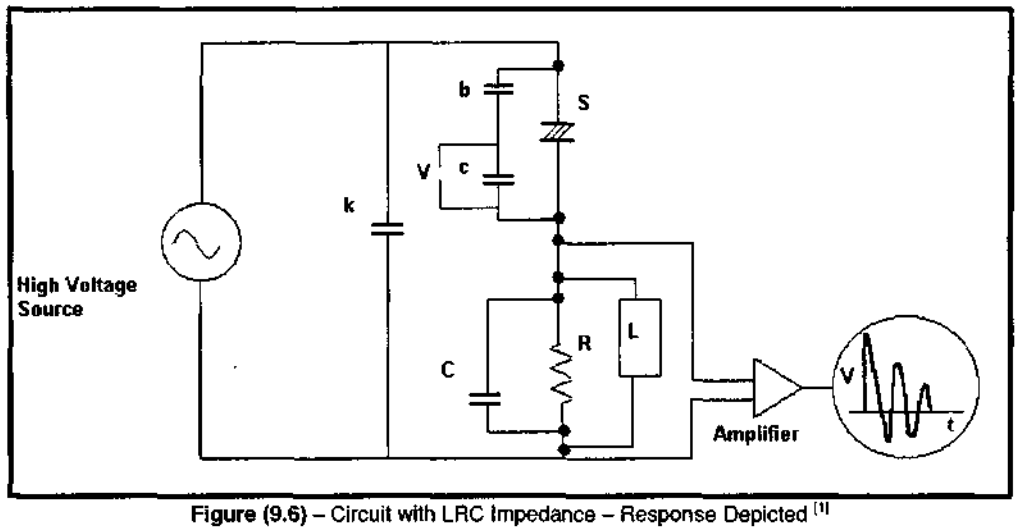

Figure (9.6) – Circuit with LRC Impedance – Response Depicted [1]

Figure (9.6), depicts the case where the impedance is made up of an oscillatory LRC element. The impulse is an attenuated oscillation, which has the same crest voltage as in case (1). This impulse is given by:

$$V = \frac{q}{(1+\frac{C}{k})S + C}.\exp(-t/2Rm).\cos\omega\ t \tag{9.4}$$

Note, m can be calculated from equation (9.3).

$$\text{And } \omega = \sqrt{\left(\frac{1}{Lm} - \frac{1}{4R^2m^2}\right)} \tag{9.5}$$

9.1 Electrical detection methods

The various electrical detection methods can be categorized into the following three groups:

- The current impulses that are formed in the leads of the sample are transformed into voltage impulses, which are amplified and examined. These methods are commonly referred to as straight detection methods.[1]
- The impulses referred to in the previous statement, are examined but special measures are implemented in order to remove disturbances caused by discharges that are in the high voltage source, leads, bushings, terminals etc. These methods are referred to as balanced detection methods.[1]
- This method involves the measurement of the power, which is dissipated by the current impulses. These methods are commonly referred to as loss detection methods.[1]

There are two important parameters that characterize each of the above methods. These are sensitivity and resolution. The sensitivity is defined by the "smallest discharge that can just be detected."[1] In terms of electrical methods, the sensitivity depends largely on the capacitance of the test object.
The resolution is defined "by the number of impulses which may be distinguished in one quadrant of the 50 Hz sine wave."[1]

9.1.1 Straight detection methods (with RC circuits)

The following circuit was published[1] for the testing of transformers:

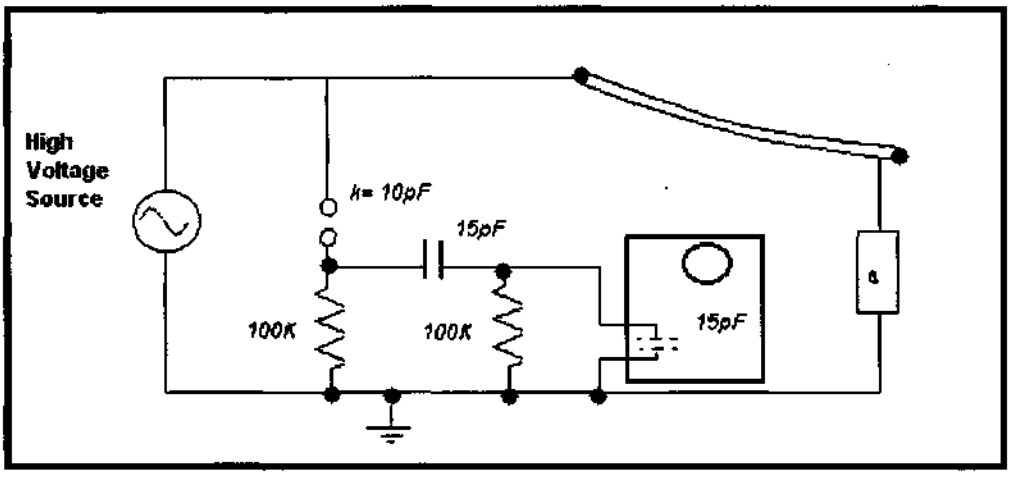

Figure (9.7) – RC circuit for discharge detection in transformers

In the circuit depicted in figure (9.7), the coupling capacitor is formed by a sphere-gap. The detection resistor is placed in series with the coupling capacitor and hence forms part of a high pass filter that rejects the 50 Hz mains frequency. A broadband amplifier is used, and the impulses are observed with the aid of an oscilloscope. The transformer is connected to the circuit by means of a corona-free high voltage bar.[1] The implementation of detection by means of a resistor yields an equal response to all oscillations which may be generated by the discharges in the transformer windings. The sensitivity of the circuit has been estimated to be 20-50 pC in a sample with a capacity of 1 nF.[1]

9.1.2 Straight detection methods (with LCR circuits)

The following circuit describes a typical straight detection method, which utilizes an LCR circuit.

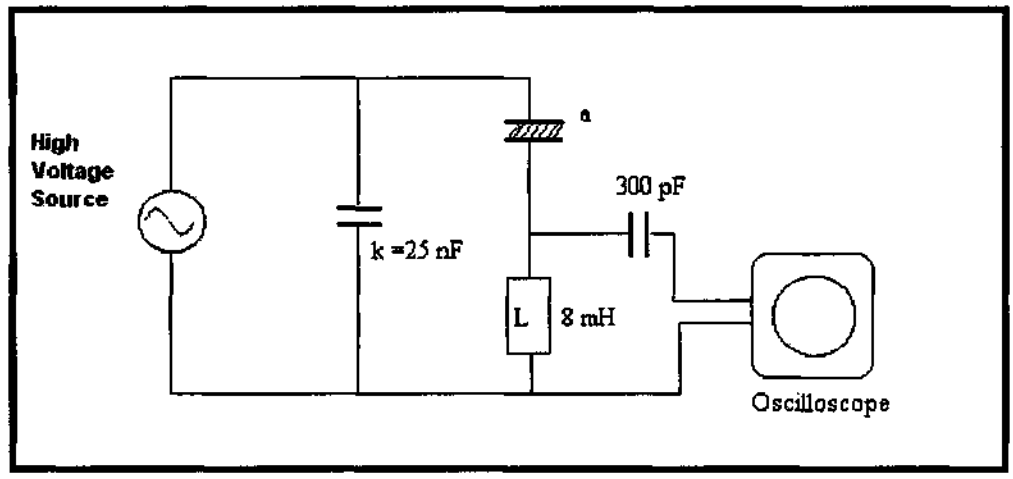

Figure (9.8) – LRC circuit for discharge detection in transformers

The above circuit shows a small coil (L), which is placed in series with the sample. The reason for the introduction of this small coil is mainly to eliminate the 50 Hz test frequency. The values of *a, k* and *L*, determine the frequency of the attenuated oscillations which will occur over L. This frequency varies with different samples. The sensitivity of this circuit is approximately 20 pC for an object of 1000 pF. "The resolution is determined by the attenuation of the oscillatory impulses and is thus given by the quality of the coil."[1]

9.1.3 Optimum straight detection method

The following circuit achieves optimum sensitivity and reproducible results. [1]

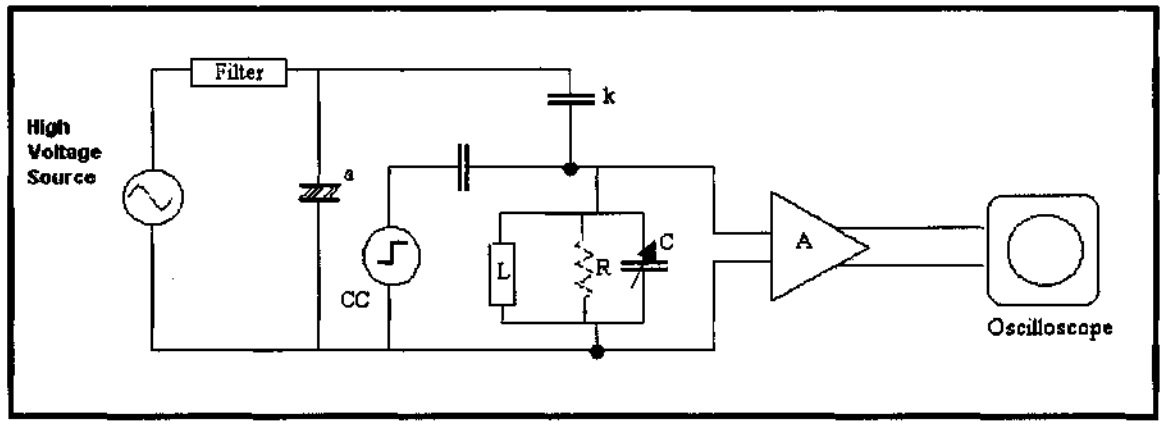

Figure (9.9) – Optimal circuit

The following components are used in the above circuit:

- **k** - Discharge free coupling capacitor.
- **a** – Earthed sample.
- **LCR** – Detection impedance, interchangeable in order to achieve optimum sensitivity.
- **A** - Amplifier (bandwidth = 10 kHz).
- **CC** - Calibration impulse. This is used to calibrate the discharge impulses.
- **Filter** - Blocks disturbances from the mains and from the transformer.

The high voltage source in the above circuit is discharge free. A series of LCR elements has been included so that optimum sensitivity can be achieved for a number of capacity ranges.[1] By varying C, the frequency of the oscillation can always be tuned to the midband frequency of the amplifier. The sensitivity is high. In an object of about 1000pF, a discharge of about 0.02 pC may be detected [1]. The bandwidth of the amplifier is 10 Hz, which allows for a resolution of 35 impulses per quadrant of the 50 Hz wave. The calibration circuit is a very important part of this circuit. A calibration impulse of known charge is injected into the circuit. This impulse can be varied such that the picture on the screen can be made as high as that of the observed discharges. In this way an estimation of the discharges (in pC) can be ascertained.

SECTION B - SIMULATIONS

CHAPTER 10
FEMLAB SIMULATIONS

10.1 Background of software package

In order to model the entire process, of the occurrence of a partial discharge within a transformer tank, and then track the propagation of the acoustic wave from the discharge source, to the transformer tank wall, a finite element modeling program called "Femlab" was used. Femlab is an interactive environment for modeling and solving scientific and engineering problems based on partial differential equations. [20].

Femlab applies the finite element method, to solve partial differential equations. This method is run in conjunction with "adaptive meshing" [20] and error control. Several numerical solvers are also available.

10.2 Boundary conditions

There are two types of boundary conditions that can be specified in Femlab. These are the **Neumann** Boundary condition, and the **Dirichlet** boundary condition.

10.2.1 Neumann boundary condition

The Neumann boundary condition is given by the equation:

$$n.(c\nabla u - \alpha u\gamma) + qu = g \qquad (10.1)$$

It can be noted from equation (10.1), that the Neumann boundary condition sets the gradient in the direction normal to the boundary. For the case where the type of problem involves the solution of the wave equation, $\propto$ and γ are zero. For this wave equation problem, equation (10.1) becomes:

$$n(c\nabla u) + qu = g \qquad (10.2)$$

In Femlab, values for g and q have to be specified. The variable u, refers to the acoustic pressure. If it is desired, to make the tank totally reflecting, then g = q = 0, should be set.

10.2.2 Dirichlet boundary condition

The Dirichlet boundary condition enables the user to define the value of the function, on a particular boundary. It is defined by the following equation:

$$n.(c\nabla u + \alpha u\gamma) + q.u = g - h^T \mu \qquad (10.3)$$

or: $h.u = r$ (10.4)

For this problem, equation (10.4) is usually used. It can be noted from equation (10.4), that the Dirichlet boundary condition sets the value of u (represents the acoustic pressure in this project).

10.3 Subdomain settings

The parameters relating to each subdomain have to be set under the tab "Subdomain settings". The equation being solved is:

$$d_a.u^{"} - \nabla.(c\nabla u) = f \qquad (10.5)$$

where

d_a is the mass coefficient.
u is the acoustic pressure
f represents the source term
c is the velocity of sound in the domain being described.

10.4 Two-dimensional simulation models

The following two-dimensional models investigate the occurrence of a partial discharge within various geometries containing dielectric liquid.

10.4.1 Model: 1

Note that in chapter 7, it was stated that, "Sound propagates through a medium by means of wave motion"[14]. Therefore, in order to model the system, the wave equation was selected. The wave equation is a type of classical partial differential equation.

Next, the geometry of the model had to be constructed. Figure (10.1), shows the first model that was constructed:

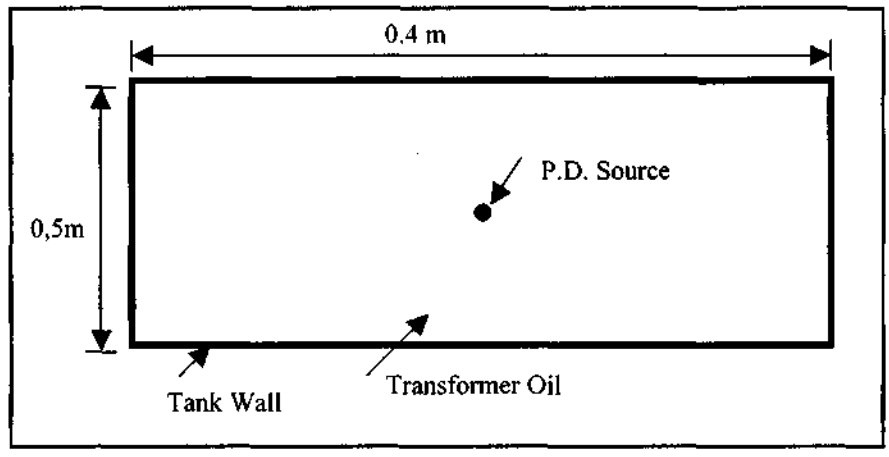

Figure (10.1) – Setup of simplified model

Note that the dimensions are arbitrary. The p.d. source was placed at co-ordinates: **(x,y)** =(0.2, 0.25).

For the first simulation, a simple model was considered. The tank was set to be reflective, i.e. not permit any energy to pass through the tank walls. Consequently, the tank walls were set with the Neumann boundary condition with g = q = 0.

Next, the p.d. source was set to emit a pulse of constant magnitude. It was therefore set with Dirichlet boundary conditions, with r =100, which specifies that the function would have a value of 100 on the boundary of the source of the partial discharge.

The speed of sound in transformer oil was set at 1400 m/s (assuming factory conditions). The mass coefficient for the domain, d_a, was set to be 1.The source term was set to zero.
The model was then meshed. When acoustic waves are being modeled, it is important to ensure that there are enough mesh points in order to resolve the waveform accurately. This also ensures that effects such as interference are modeled correctly. In order to achieve this, it is recommended that there be 8 mesh points per wavelength. [20] This can be achieved by setting the maximum mesh size to be 11.3/15 in the Max Edge size, general dialog box under mesh parameters.

The system was then simulated for 20 milliseconds, in steps of 10 microseconds. The results are documented below.

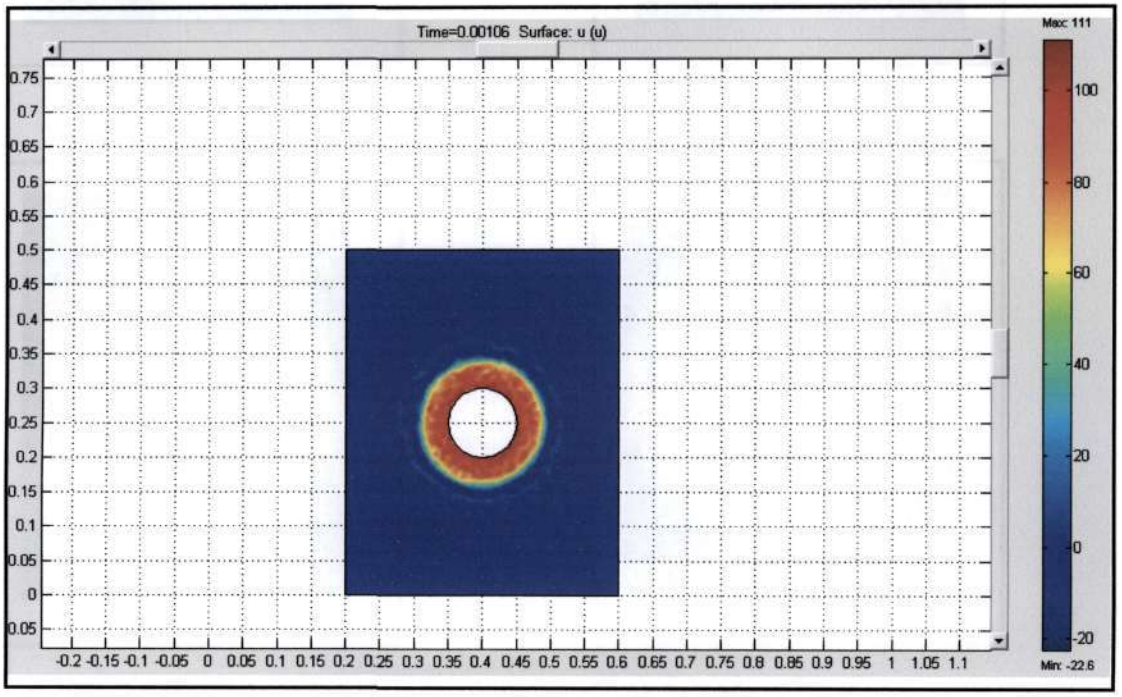

Figure (10.2) - Initial propagation of acoustic wave from p.d. source

Figure (10.2), represents the initial propagation of the acoustic wave from the p.d. source. The intensity of the p.d. was set to 100 N/m^2 under the boundary conditions tab. The intensity of the p.d. was specified to be constant for all time.

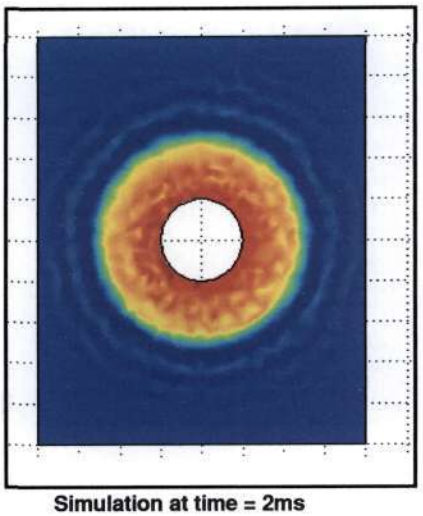

Simulation at time = 2ms

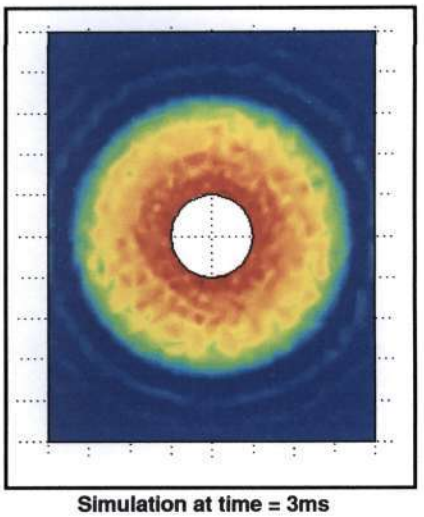

Simulation at time = 3ms

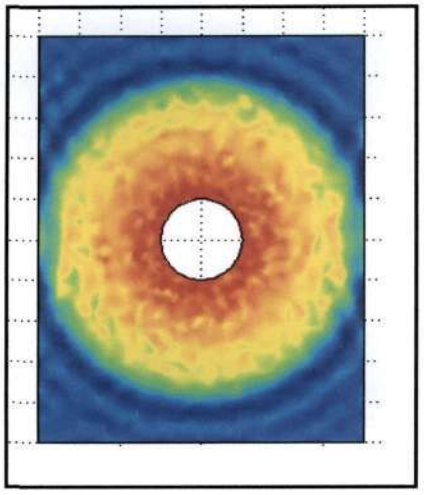

Simulation at time = 3.8 ms

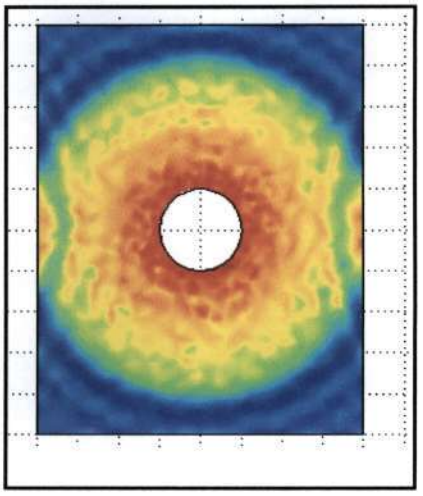

Simulation at 4.2 ms

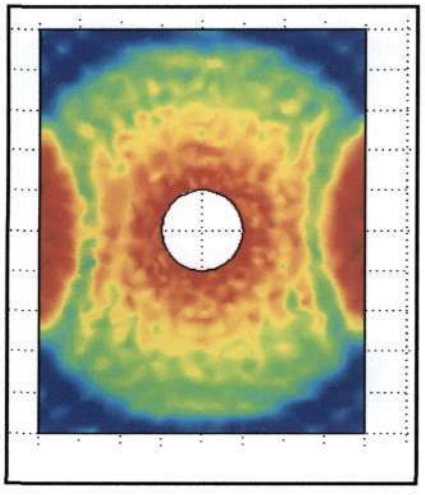

Simulation at time = 5ms

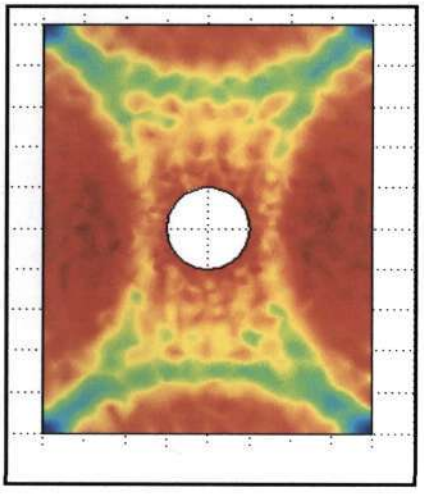

Simulation at time = 6.6 ms

Note that at times 4.2 ms, 5 ms and 6.6 ms, reflections at the transformer tank wall can be observed.

A sensor was placed on the tank wall at **(x,y)** = (0.2, 0.25) and a cross-section plot of the acoustic pressure in the x-direction was taken.

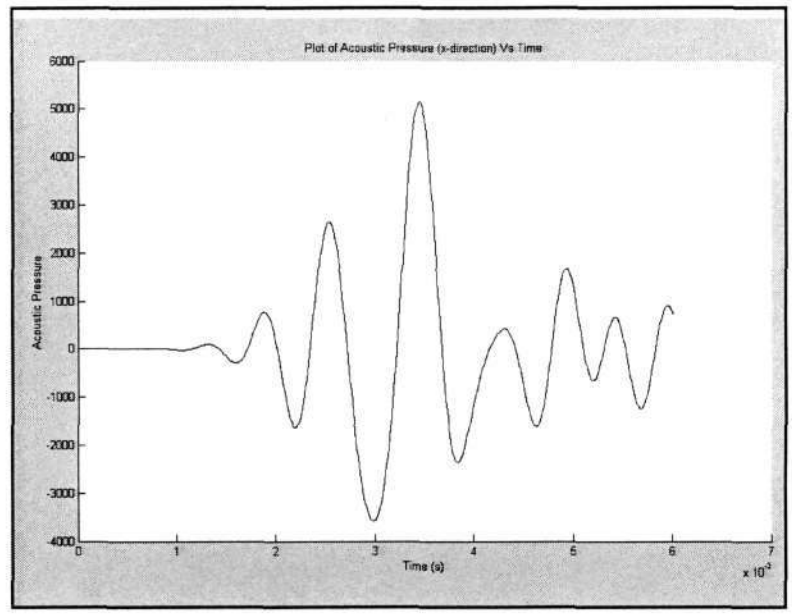

Graph (10.1) – Plot of Acoustic Pressure (x-direction) Vs Time

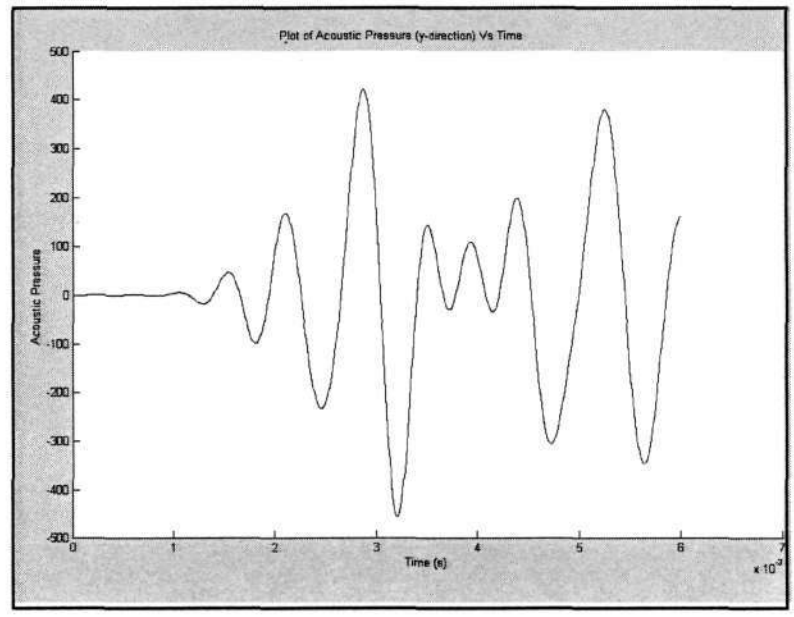

Graph (10.2) – Plot of acoustic pressure (y-direction) Vs time

With reference to Graph (10.1), note that the time taken for the first ripple to reach the surface of the transformer tank wall is approximately 1.1 milliseconds. Now, in the model that was constructed, the distance between the source of the p.d. and the transformer wall is 0.15m metres. Therefore: $speed = \frac{dis\tan ce}{time} = \frac{0.15}{1.1*10^{-3}}*10 = 1363.6\ \ metres/\sec$

This correlates well to the speed of sound in transformer oil that was set in the software i.e. 1400m/s.

10.4.2 Model: 2

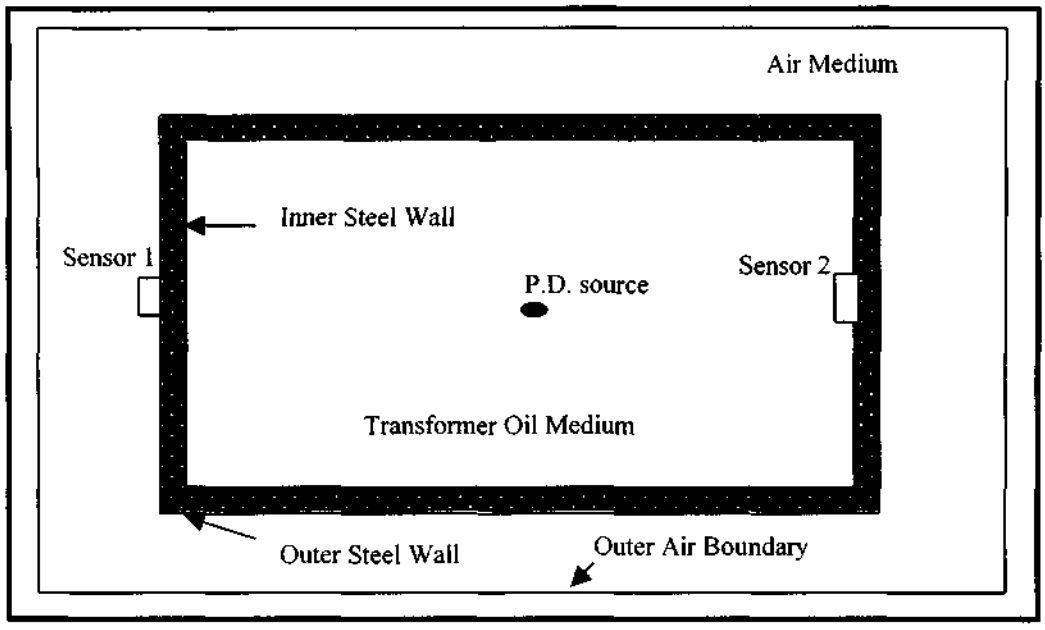

Figure (10.3) - Illustration of the construction of model 2

The outer air boundary of the model was specified to have the Dirichlet boundary condition. The function was set to be zero, at this outer air boundary. The inner and outer steel walls of the transformer tank were both set with the Neumann condition, with the condition $q > 0$. This condition specifies that the walls will absorb and reflect the incident acoustic waves. The p.d. source was then set with the Dirichlet boundary condition to emit a pulse of constant intensity of 100 N/m^2.

Subdomain Settings: The velocity of the sound in the different subdomains were set as –

- Speed of sound in air: 333.33 m/s
- Speed of sound in the steel wall: 3200 m/s
- Speed of sound in the transformer oil: 1400 m/s

The mass coefficients for all three subdomains were set at 1. The model was then simulated for 20 milliseconds with a step size of 5 microseconds.

The sensor was positioned at different locations, in order to check the differences between the acoustic pressures at different positions in the tank. In the first instance, the sensor was placed at the interface between the steel wall of the transformer tank, and the air (depicted as sensor position 1). In the next instance, the sensor was moved to the interface between the steel wall and the transformer oil. The following are the cross-sectional plots that were recorded.

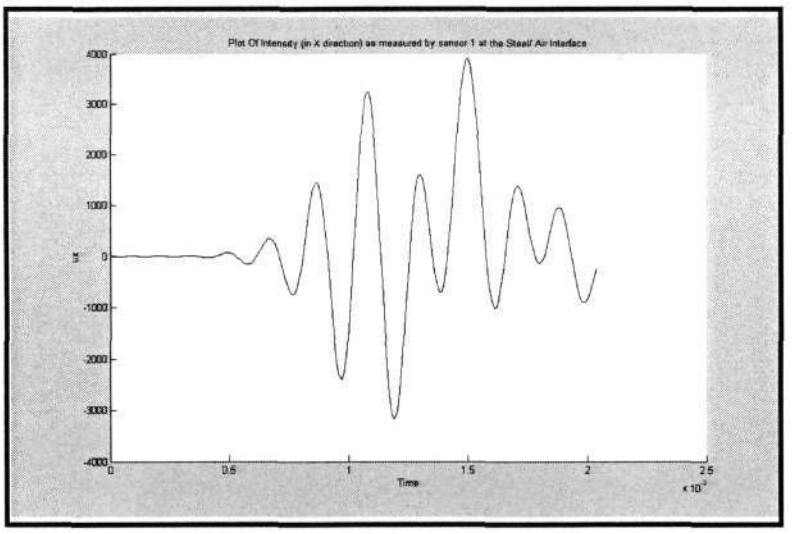

Graph (10.3) – Plot of intensity of acoustic wave at steel/air interface

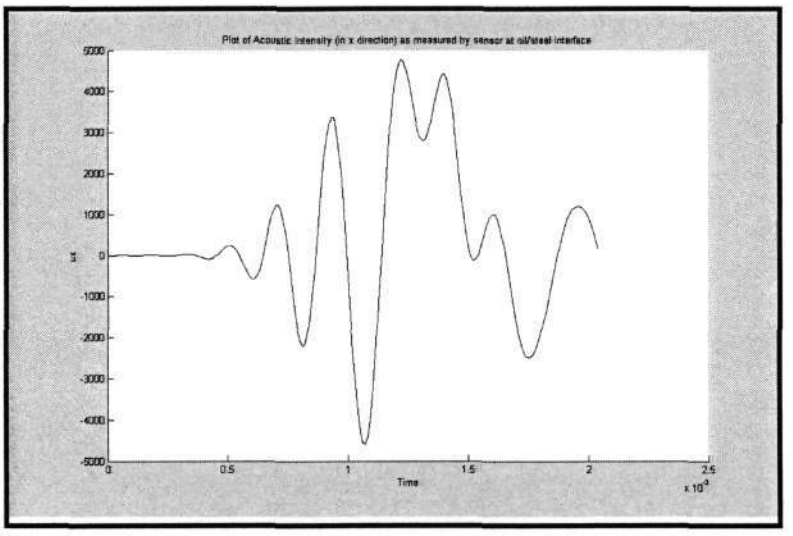

Graph (10.4) – Plot of intensity of acoustic wave at oil/steel interface

In order to illustrate the effect of attenuation of the incident acoustic wave, due to the steel wall, Graph (10.3) and Graph (10.4) were plotted on the same set of axes (see overleaf).

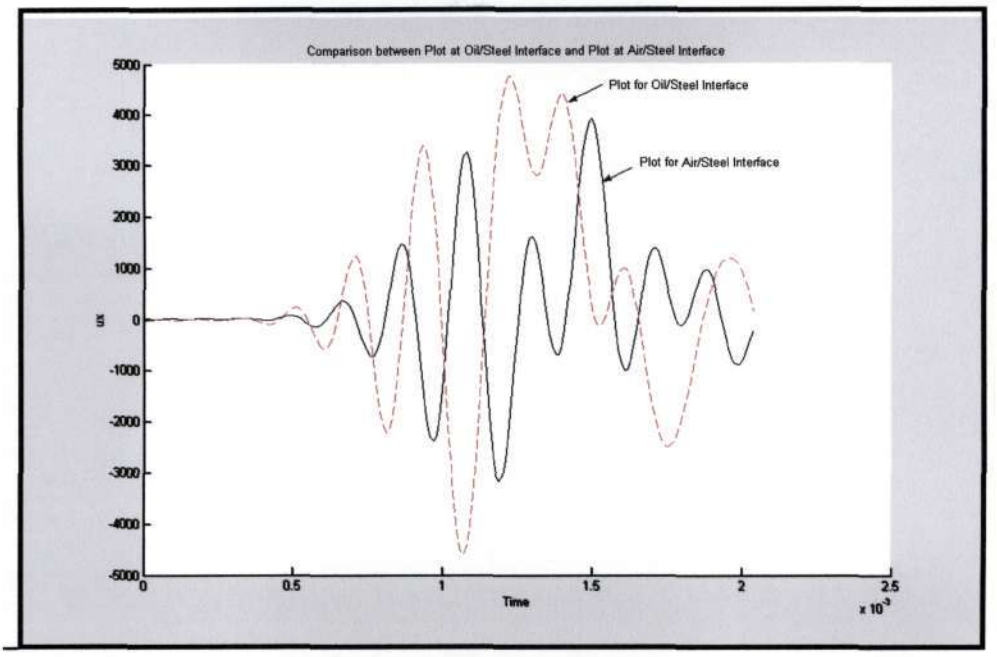

Graph (10.5) - Comparison between plots for steel/air interface and oil/steel Interface

Graph (10.5), highlights the fact that the wave is attenuated as it passes through the steel wall of the transformer tank. Note that the amplitude of the wave that is incident at the Oil/Steel interface is larger than the amplitude for the Steel/Air interface.

10.4.3 Model 3:

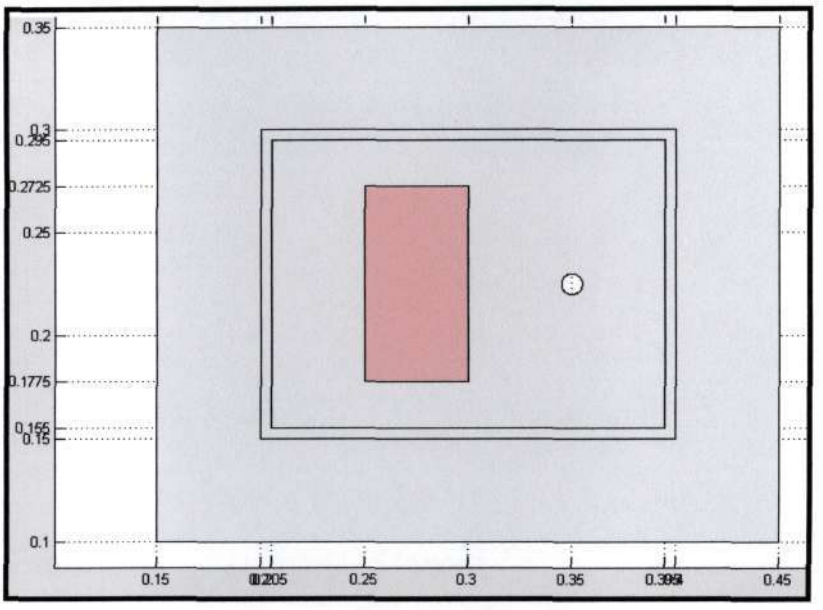

Figure (10.4) - Layout of model 3. Inclusion of iron core

Figure (10.4), depicts the geometrical layout of the model implemented for the third simulation. The model consists of five regions:

- The outer air region
- The narrow tank wall (steel) region
- The inner transformer oil medium
- The inner iron core region
- The point source (partial discharge)

The following boundary conditions were imposed on the model:

- The value of the function was set to be zero, on the outer extremities of the air boundary. The region lies far beyond the region where the measurements will be taken. When constructing the model, the outer air boundaries were set a fair distance away from the actual transformer tank, in order to get a more realistic view of the behavior of the wave as it impinges on the steel/air interface.
- The transformer tank walls were set to be absorptive, and reflective. This was implemented using the Neumann boundary condition, with the variable q > g. This condition specifies that some incident energy will be transmitted through the boundary, and some energy will be reflected.
- The boundaries of the iron core were set to be attenuating with the Neumann condition. Again, the variable q was set to be greater than g, in order to allow for the transmission of energy across the boundary.
- The point source, was specified to emit an acoustic wave, of constant magnitude of 100 N/m^2 for all time.

The following are the subdomain settings that were utilized:

- Speed of sound in the outer air region: 333.33 m/s
- Speed of sound in the steel tank wall: 3200 m/s
- Speed of sound in the transformer oil: 1400m/s
- Speed of sound in the iron core: 5800 m/s

The next step was to design a mesh, which will model the propagation of the acoustic wave realistically, and accurately. This was implemented by using a mesh of maximum node size of 11.3/15. For acoustic waves this is a recommended choice[21].

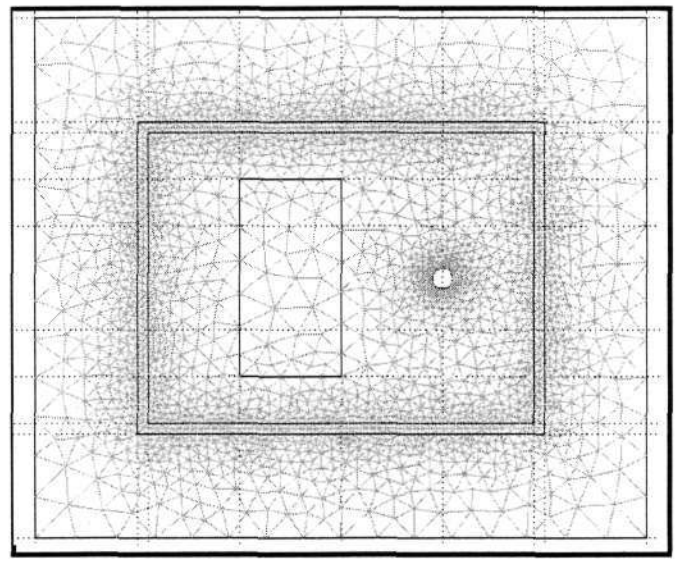

Figure (10.5) - Mesh design

Figure (10.5.), depicts the meshed model. Note that the nodes are tightly packed, which subsequently increases the accuracy of the simulation.

The model was then simulated using an iterative solver, for 5 milliseconds, in steps of 1 microsecond. Figure (10.6), shows the propagation of the acoustic wave through the iron core. Note, that due to the fact that the speed of sound in the iron core is very much larger in magnitude, than the speed of sound in transformer oil, the wave can be seen to propagate much faster through the iron core. Also note the reflections that begin to occur on the transformer tank wall (right hand side).

See overleaf for figure (10.6).....

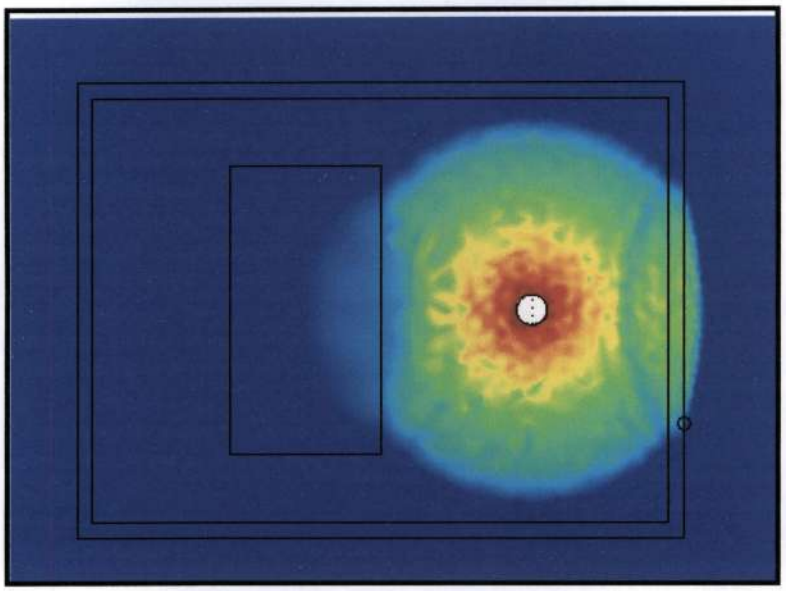

Figure (10.6) - Illustration of the acoustic wave propagating in the iron core, as well as the occurrence of reflections on the inner steel tank wall (right hand side)

Please refer to **Appendix A** for illustrations of the simulation at various times.

Sensor Positions for the simulation:

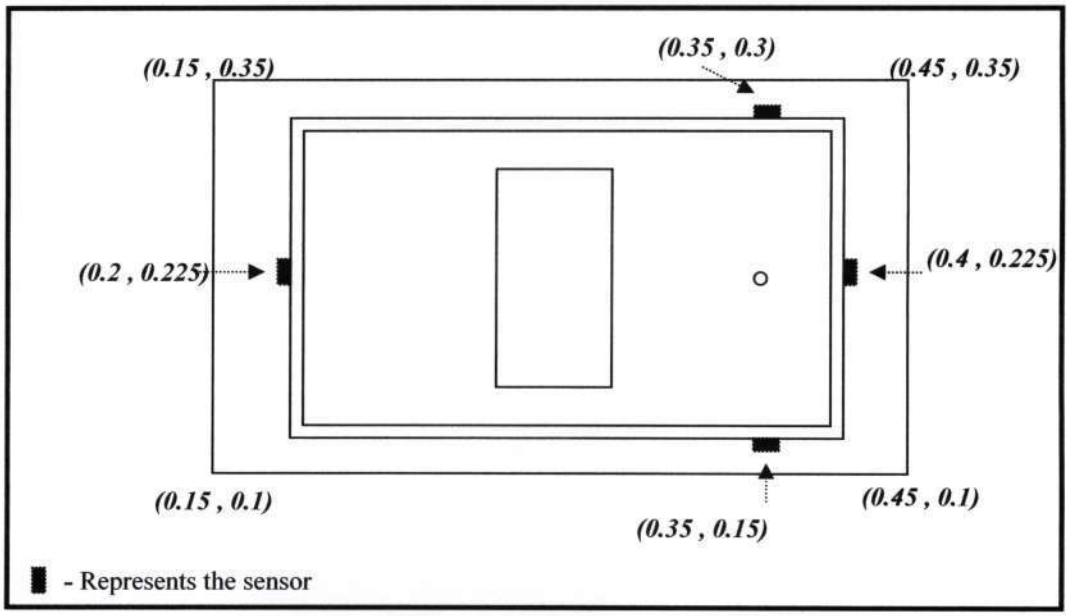

Figure (10.7): Sensor positions

Sensors were placed at various positions on the tank wall, and cross-sectional plots of the intensity of the acoustic signal at these positions were taken. The sensor was placed at the following positions:

- (0.4 , 0.225)
- (0.2 , 0.225)
- (0.35 , 0.3)
- (0.35 , 0.15)

Discussion of results:

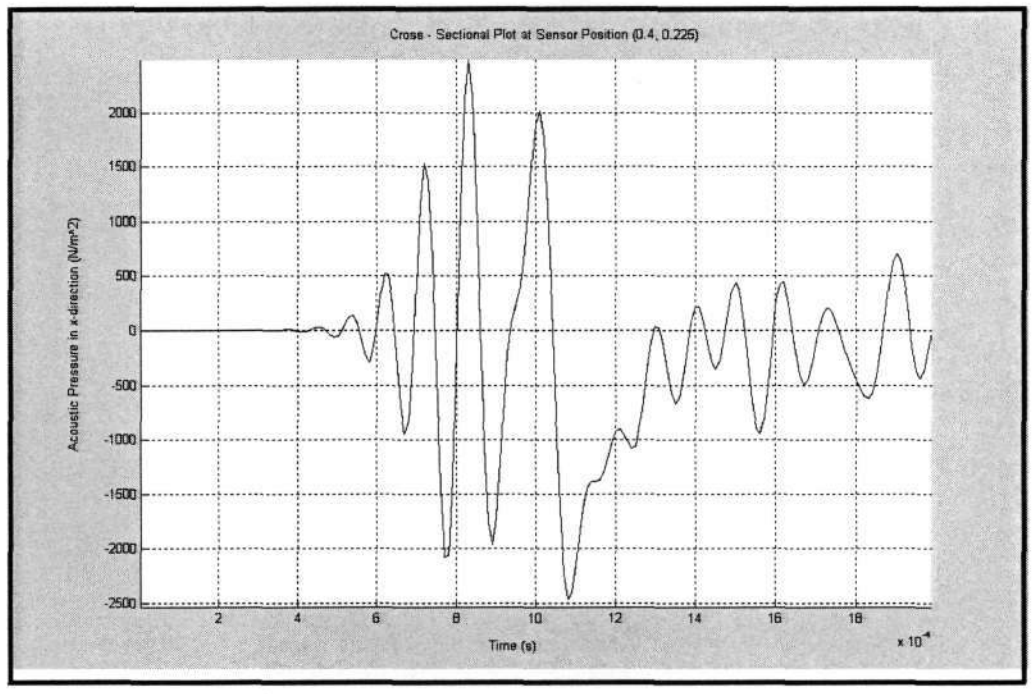

Figure (10.8) – Cross–sectional plot at sensor position (0.4 , 0.225)

The relative time of arrival of the acoustic wave at the sensor at position (0.4, 0.225) was 420 μs. The maximum amplitude of this cross-sectional plot is 2500 N/m^2.

Please turn over for figure (10.9).....

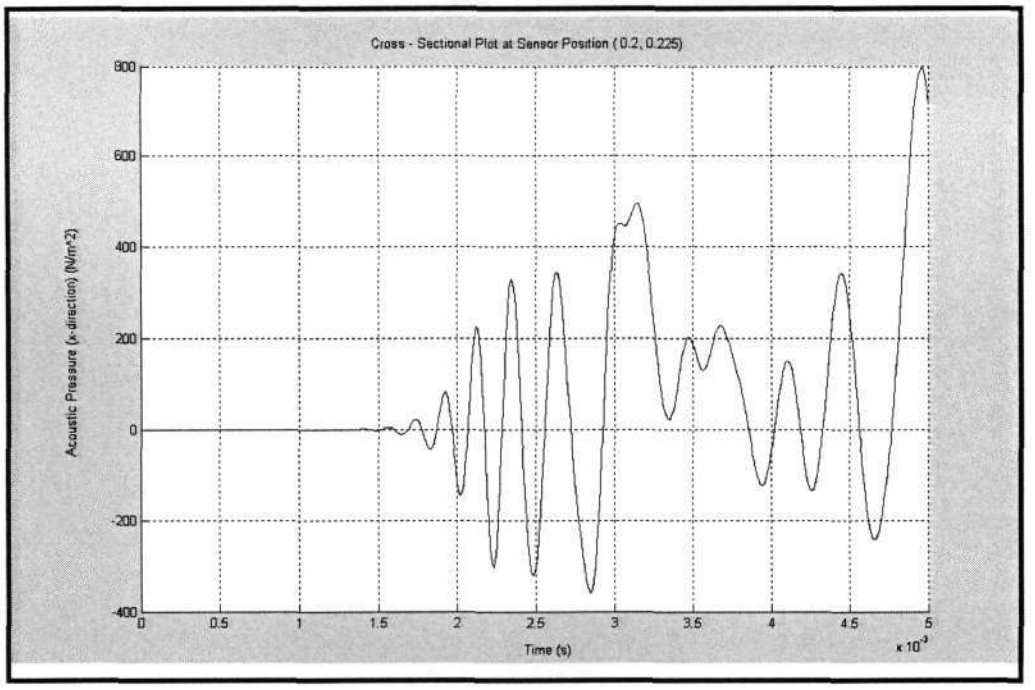

Figure (10.9) – Cross– sectional plot at sensor position (0.2 ,0.225)

From figure (10.9), the relative time of arrival of the acoustic wave at the sensor position (0.2, 0.225) was 1600 μs. This signal was heavily attenuated, with a maximum amplitude of 800 N/m^2.

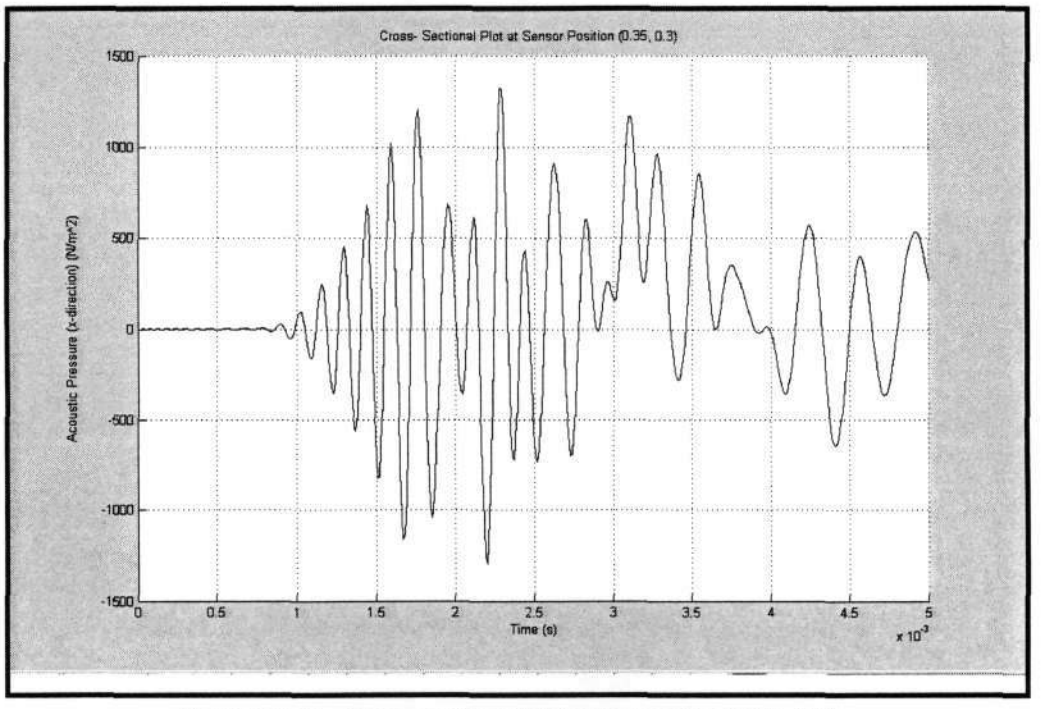

Figure (10.10) – Cross– sectional plot at sensor position (0.35 , 0.3)

The time of arrival of the acoustic wave at the sensor at position (0.35 , 0.3) was 600 μs. The maximum amplitude of this characteristic was 1323 N/m^2.

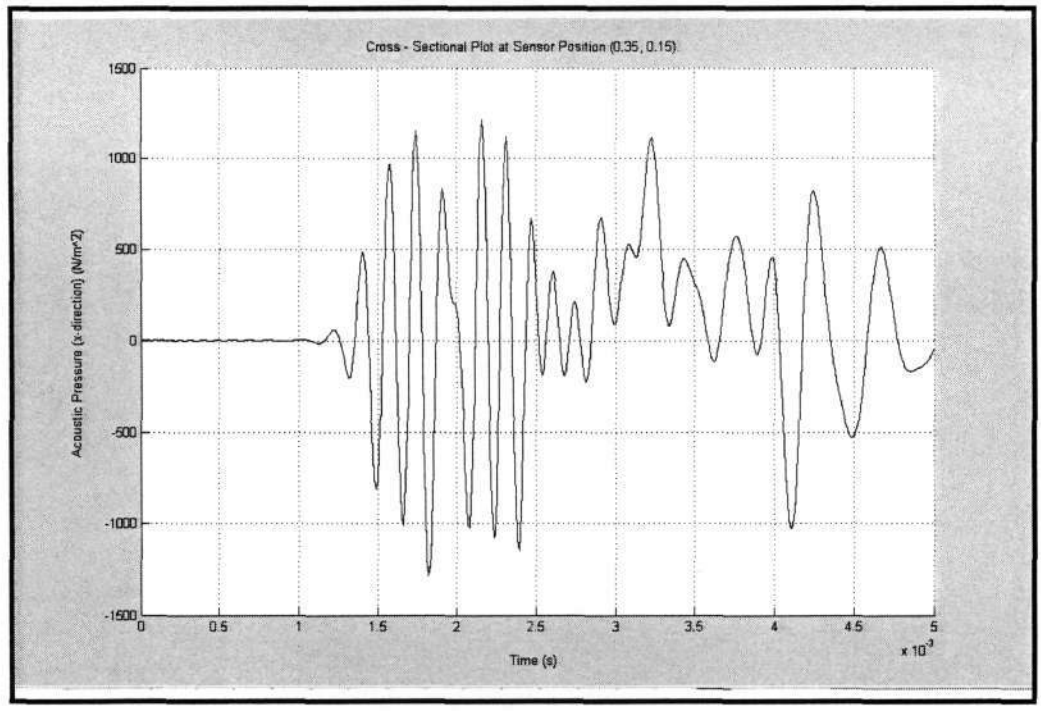

Figure (10.11) – Cross–sectional plot at sensor position (0.35 , 0.15)

The time of arrival of the acoustic wave at the sensor at position (0.35 , 0.15), is 700 μs. The maximum amplitude of the characteristic is 1210 N/m^2.

Localisation Calculations:

The three sensor positions (0.4 , 0.225), (0.35 , 0.3) and (0.35 , 0.15) produced characteristics, that are the least attenuated of all possible positions on the tank, due to their proximity to the point source, and also due to the fact that there are no obstructions in the path from the source to that particular sensor. The signal at position (0.2 , 0.225), is highly attenuated due to the iron core, which obstructs and attenuates the acoustic wave which propagates in that direction. It has therefore been omitted from the localization calculations. As mentioned in previous sections, the inner geometry of the transformer must be known in order to accurately locate the source of the partial discharge. The following calculations describe the procedure that was used to locate the source of the partial discharge in this simulation.

Calculation of the effect of the steel tank wall on the propagating signal:

Speed of sound through steel tank wall = **3200 m/s**

Thickness of wall = **0.005 m**

Time taken for wave to propagate through tank wall is calculated as:
= (Distance / Speed)
= [(0.005 *10) / 3200])
= **15.63 μs**

Therefore, to remove the effect of the steel tank wall, the time taken by the signal to propagate only through the tank wall will be subtracted from the total time taken for the acoustic signal to reach the sensor.

For the sensor at position (0.4 , 0.225):

(a). For propagation of the acoustic wave through the transformer oil:

Distance = Speed x time = [(1400 m/s) x (420 μs –15.63 μs)/10] = **0.0566 m**

For the sensor at position (0.35 , 0.3):

(a). For propagation of the acoustic wave through the transformer oil:

Distance = Speed x time = [(1400 m/s) x (600 μs -15.63 μs)/10] = **0.0818 m**

For the sensor at position (0.35 , 0.15):

(a). For propagation of the acoustic wave through the transformer oil:

Distance = Speed x time = [(1400 m/s) x (700 μs - 15.63 μs)/10] = **0.096 m**

Calculation of the position (x,y)

The sensor at (0.4 , 0.225) on a horizontal plane which is perpendicular to the partial discharge. This is where the received wave, will be the strongest. Therefore the x co-ordinate is given by (0.4 – 0.0566) = **0.343**.

The sensors at (0.35,0.3) and (0.35, 0.15) lie on a vertical plane which is perpendicular to the partial discharge. In this case the y co-ordinate is given by (0.3 – 0.0818) < y < (0.15 + 0.096). Therefore the y co-ordinate lies in the range **(0.220 < y < 0.246)**

Therefore, the prediction made, is that the sensor lies at position:
(x,y) = (0.343, 0.220 < y <0.246)

The actual position of the partial discharge is : **(x,y) = (0.350 , 0.225)**. The predicted location is a good approximation of the actual position.

10.4.4 Model 4:

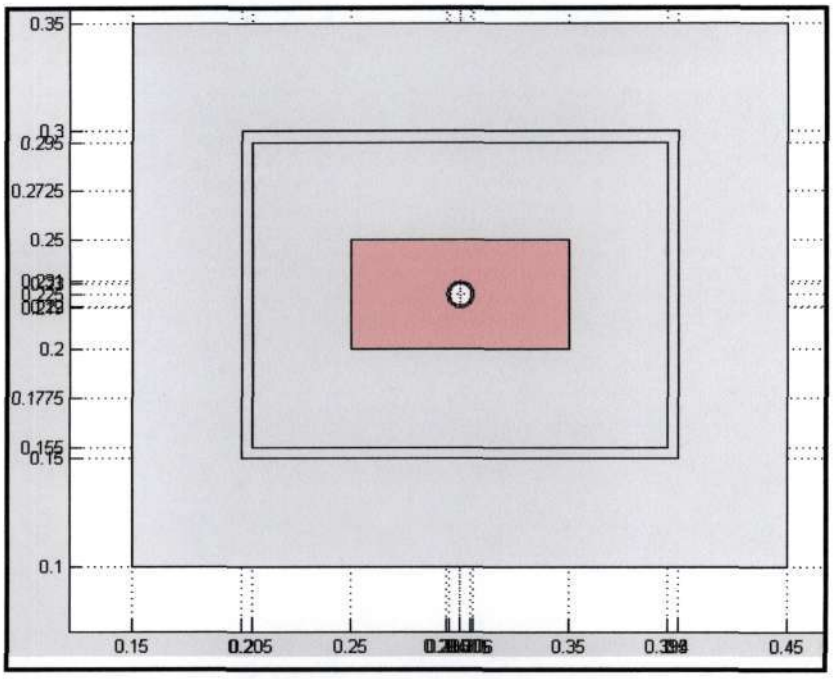

Figure (10.12) – Geometrical layout of model

Figure (10.12), depicts the geometrical layout of model 4. For this simulation, the point source for the partial discharge was placed inside the iron core. This model consists of the following regions:

- Outer air region
- Steel tank wall of transformer
- Inner transformer oil medium
- Inner iron core region
- Partial discharge source placed inside the iron core.

The boundary settings are unchanged from model 3. The point source was specified to emit an acoustic wave, of constant magnitude of 100 N/m^2 for all time. The speeds of sound in the various media were also unchanged from model 3.

The mesh was again using a mesh of maximum node size of 11.3/15, in order to achieve accurate results. Figure (10.13), depicts the meshed model.

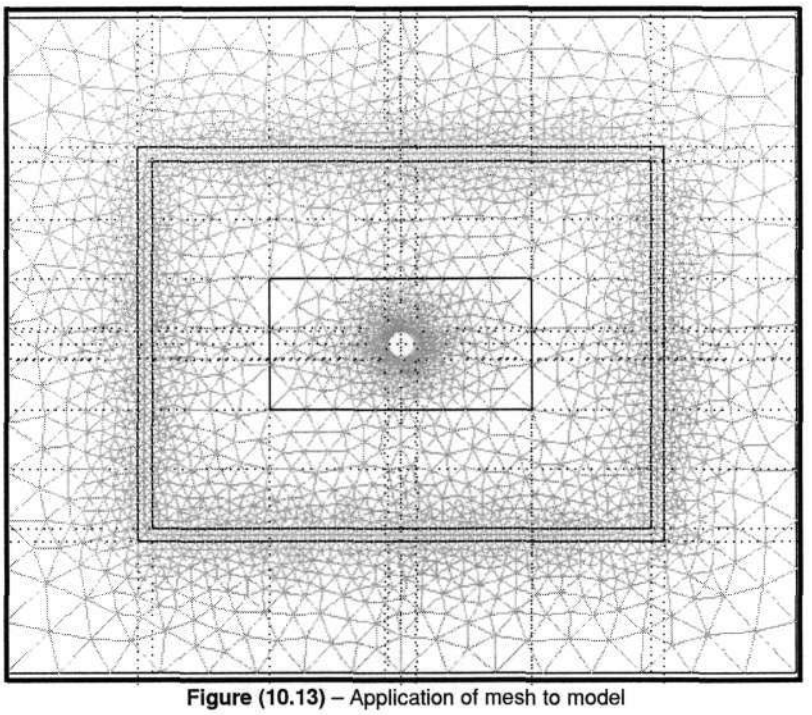

Figure (10.13) – Application of mesh to model

Sensors were placed on the tank at 4 positions. These positions are depicted below.

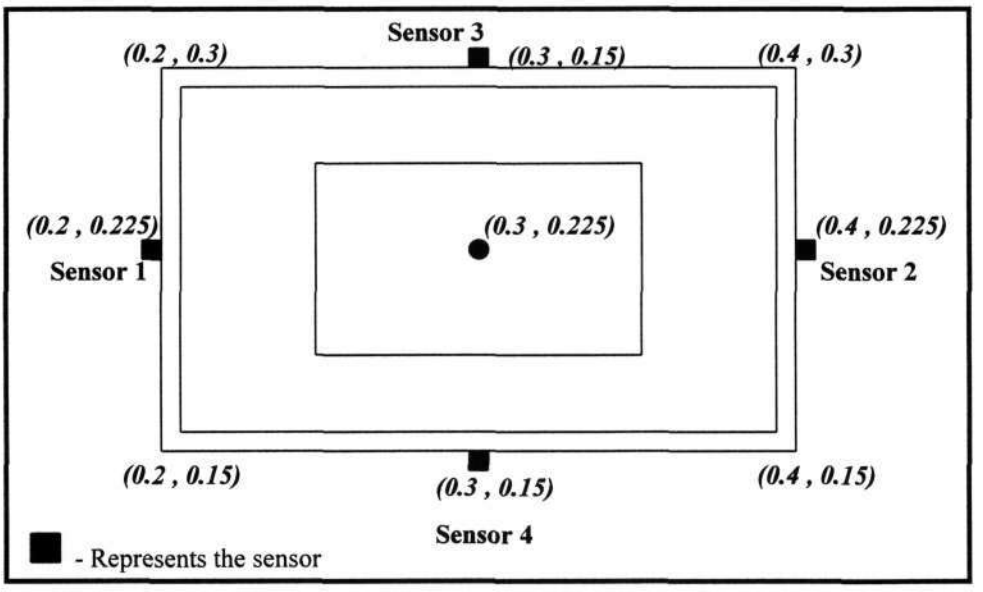

Figure (10.14) – Positions of sensors

The model was then simulated for 5 milliseconds, with a step size of 10 microseconds, using an iterative solver. Please refer to **Appendix B** for illustrations of the simulation at various times.

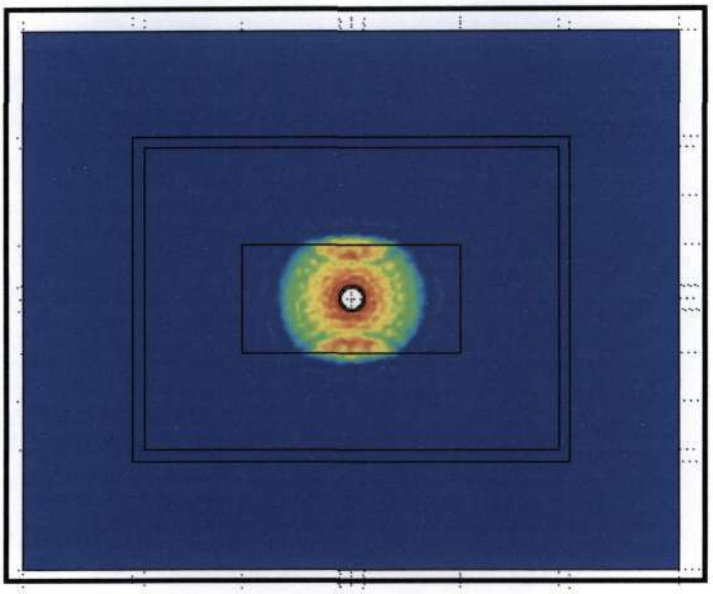

Figure (10.15) – *Simulation at time = 360 μs*

Figure (10.15), illustrates the acoustic wave as it impinges onto the boundary of the iron core. Some of the incident energy is reflected, while most of the energy is transmitted through into the transformer oil medium. The point source continues to emit a wave of constant intensity of $100N/m^2$.

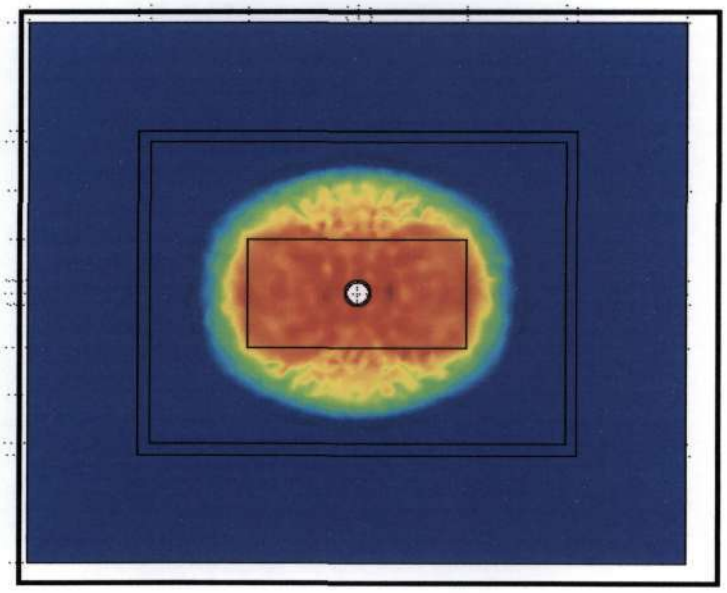

Figure (10.16) – Simulation at time = 1.12 ms

Figure (10.16), depicts the acoustic wave as it impinges onto the tank wall. Sensors are placed onto the tank wall, in order to measure the intensity of these acoustic waves.

Cross- sectional plots (shown below) were then taken at each of the sensor positions.

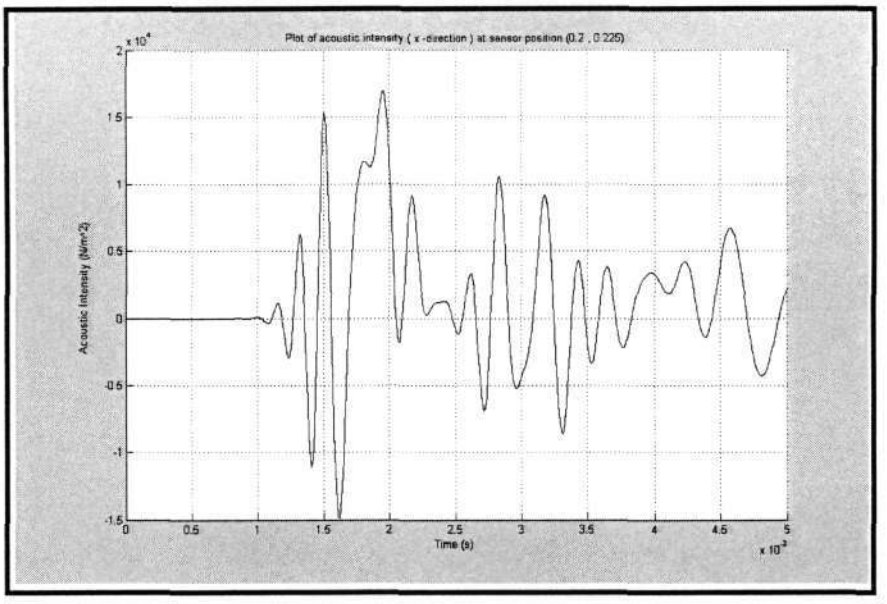

Figure (10.17) – Cross –sectional plot at sensor position (0.2 , 0.225)

A closer inspection of the waveform was performed, in order to clearly see the time of arrival of the acoustic wave at the sensor.

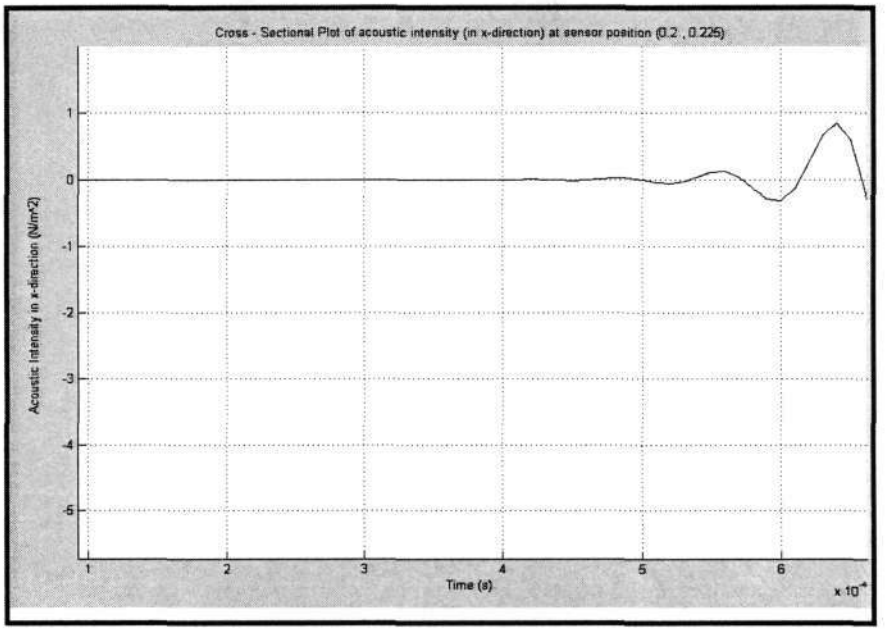

Figure (10.18) – Closer examination in order to determine time of arrival of waveform

It can be noted from Figure (10.18), that the signal arrives at the sensor at approximately 410 μs.

Figure (10.19), shows the acoustic intensity as measured by the sensor at position (0.4,0.225).

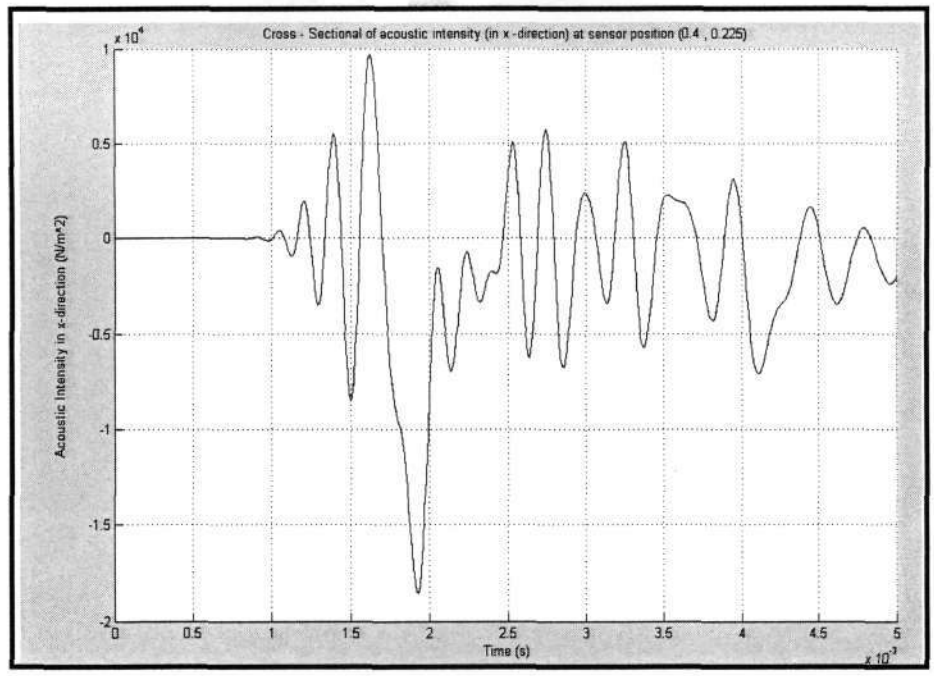

Figure (10.19) – Cross –sectional plot at sensor position (0.4 , 0.225)

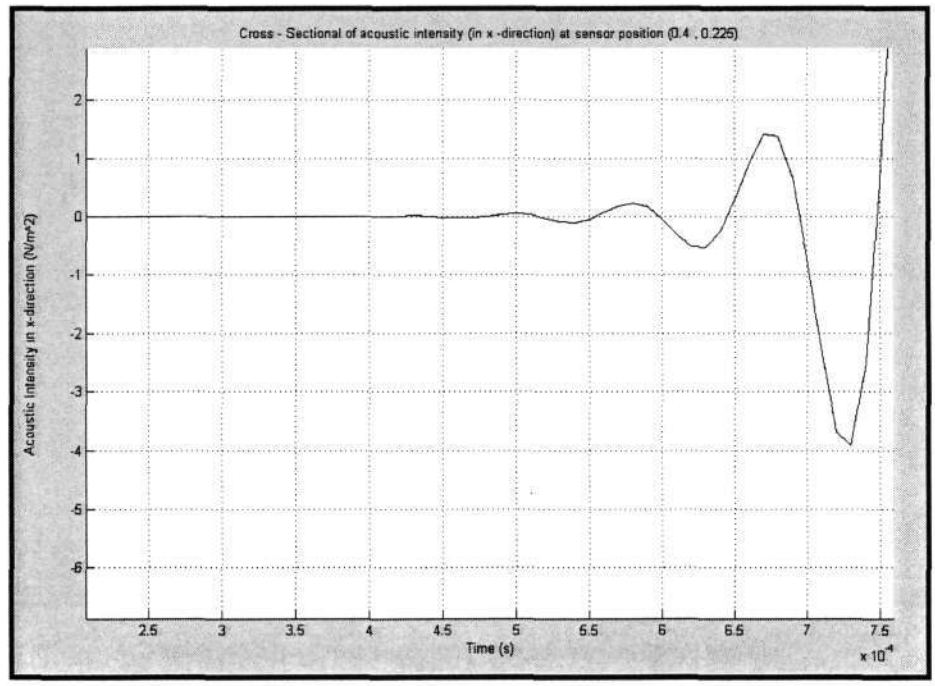

Figure (10.20) – Closer examination of figure (9.19)

It can be noted from Figure (10.20), that the signal arrives at the sensor at approximately 425 μs.

Figure (10.21), shows the acoustic intensity as measured by the sensor at position (0.3,0.3).

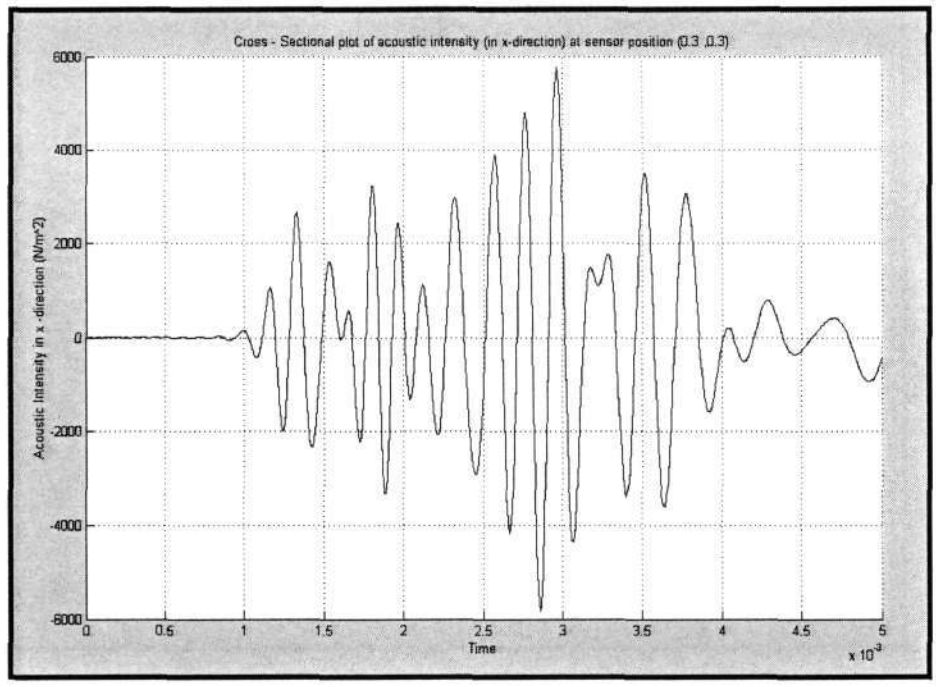

Figure (10.21) – Cross sectional plot at sensor position (0.3 ,0.3)

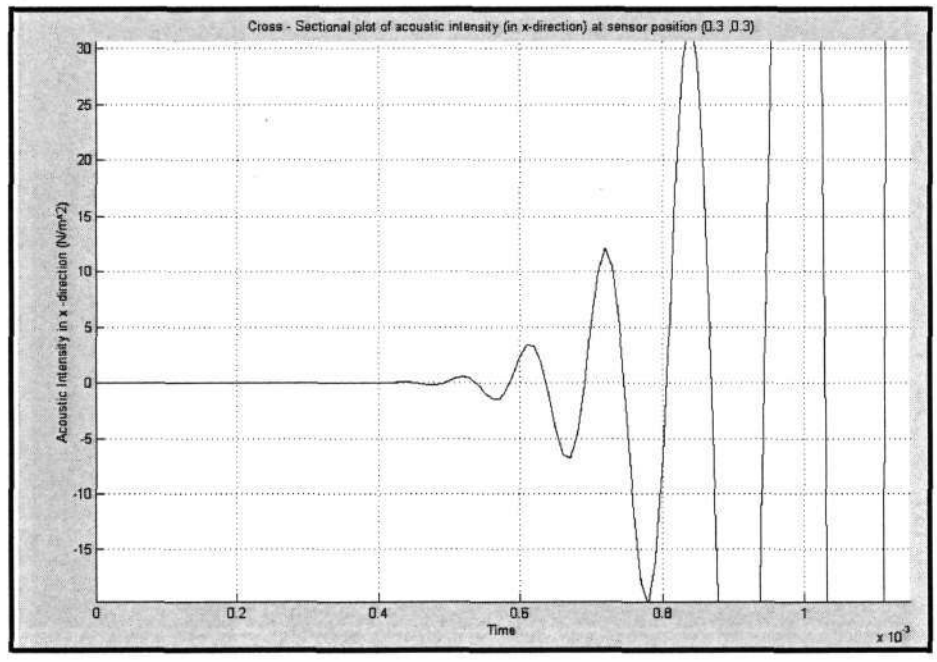

Figure (10.22) – Closer examination of figure (15.21)

From Figure (10.22), it can be noted that the signal arrives at the sensor at approximately 410 μs.

Figure (10.23), shows the acoustic intensity as measured by the sensor at position (0.3,0.15).

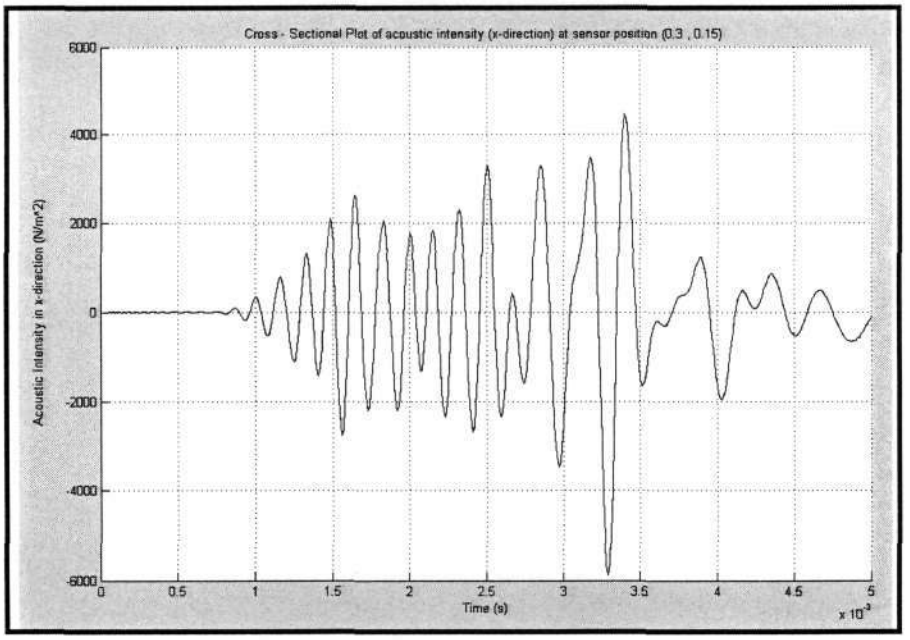

Figure (10.23) – Cross-sectional plot at sensor position (0.3 , 0.15)

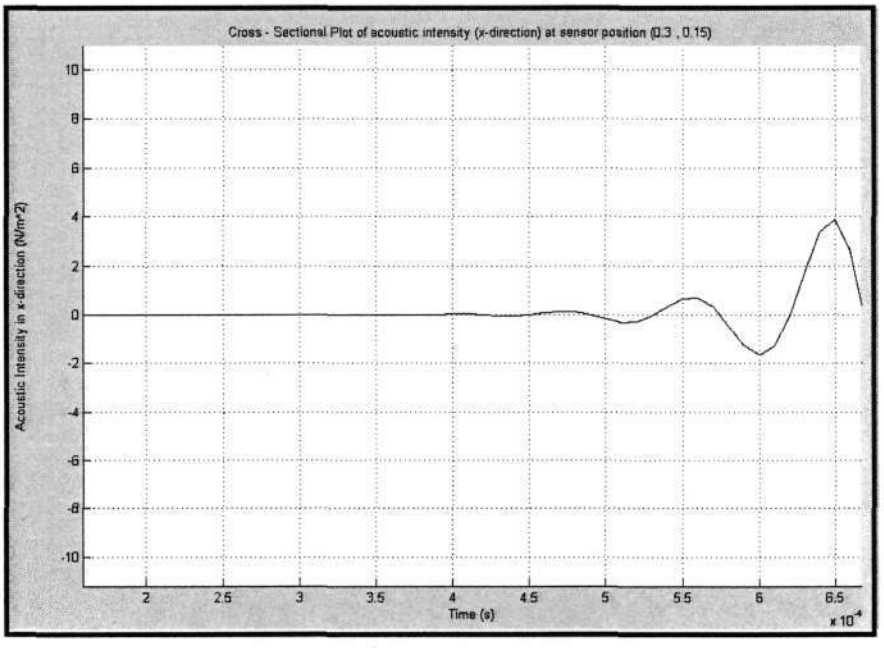

Figure (10.24) – Closer examination of figure (15.23)

From figure (10.24), it can be noted that the signal arrives at the sensor at 390 μs.

Localization Calculations for model 4:

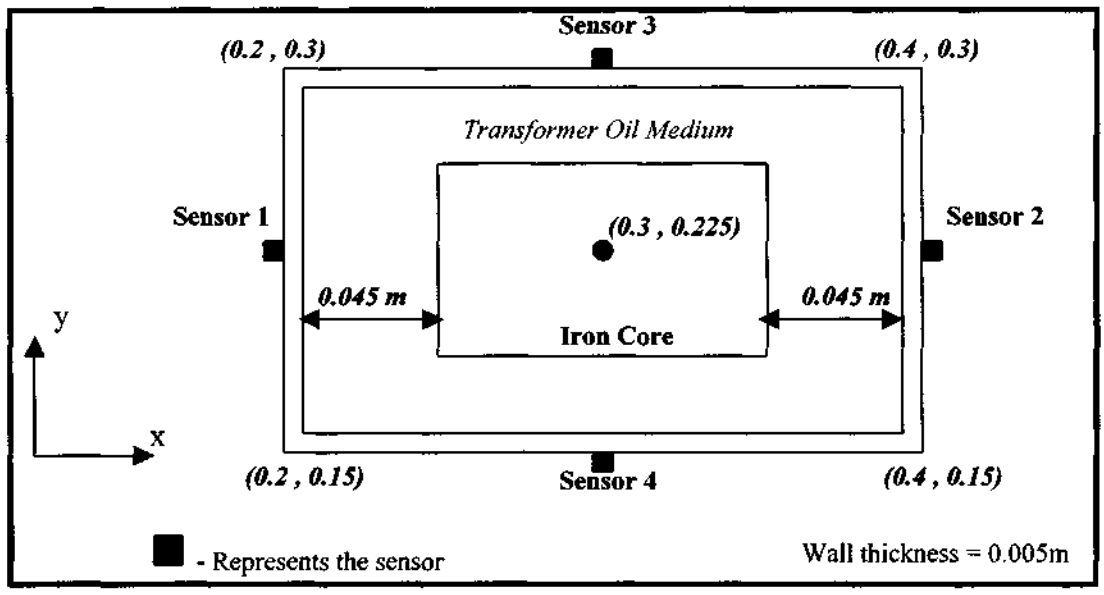

Figure (10.25) – Geometrical layout of model 4

The time taken for the signal to propagate through the transformer oil, to the left and right of the iron core, can be calculated using the formula

$$t_{oil} = \frac{dis\tan ce}{speed} = \frac{0.045 \times 10}{1400} = 321.43 \ \mu s$$

The time taken for the signal to travel through the steel tank wall is given by:

$$t_{wall} = \frac{dis\tan ce}{speed} = \frac{0.005 \times 10}{3200} = 15.625 \ \mu s$$

Note: The wall thickness is uniform.

Sensor 1:

From Figure (10.18), the signal takes 410 μs to reach sensor 1. The time taken for the signal to propagate through the iron core alone, is given by:

$t_{iron-core} = t_{total} - (t_{oil} + t_{wall})$

$= 410 \ \mu s - (321.43 \ \mu s + 15.625 \ \mu s)$

$= \mathbf{72.945 \ \mu s}$

The speed of sound in the iron core is 5800 m/s (from literature). Therefore, since the time taken for the signal to travel through the iron core is known, the distance traveled within the core can be calculated by:

Distance traveled in core = *speed x time*

= [(5800 m/s x 72.945 μs)/10]

= **0.0423 m**

This distance can be quoted in terms of the co-ordinate system, by using the x co-ordinate of sensor 1, as the reference point:
i.e. **predicted x-co-ordinate of p.d. source** = (0.2m + 0.005m + 0.045m + 0.0423m)
= **0.2923m**

Sensor 2:

From Figure (10.20), the signal takes 425 μs to reach sensor 2. The time taken for the signal to propagate through the iron core alone, is given by :

$t_{iron-core} = t_{total} - (t_{oil} + t_{wall})$
$= 425\ \mu s - (321.43\ \mu s + 15.625\ \mu s)$
$= \mathbf{87.945\ \mu s}$

Distance traveled in core = *speed x time*
= [(5800 m/s x 87.945 μs)/10]
= 0.051 m

This distance can be quoted in terms of the co-ordinate system, by using the x co-ordinate of sensor 2, as the reference point:

i.e. **predicted x-co-ordinate of p.d. source** = *(0.4m - 0.005m - 0.045m - 0.051m)*
= ***0.299m***

Therefore, the predicted range of the location of the p.d. in the x direction is:

0.2923 < x < 0.299

Note: The actual position of the p.d. is at x = 0.3 m

Sensor 3:

The time taken for the signal to propagate through the transformer oil, above and below the iron core, can be calculated using the formula

$$t_{oil} = \frac{distance}{speed} = \frac{0.045 \times 10}{1400} = 321.43\ \mu s$$

The time taken for the signal to travel through the steel tank wall is given by:

$$t_{wall} = \frac{distance}{speed} = \frac{0.005 \times 10}{3200} = 15.625\ \mu s$$

From figure (10.22), the signal takes 410 μs to reach sensor 3. The time taken for the signal to propagate through the iron core alone, is given by:

$t_{iron-core} = t_{total} - (t_{oil} + t_{wall})$
$= 410\ \mu s - (321.43\ \mu s + 15.625\ \mu s)$
$= \mathbf{72.945\ \mu s}$

Distance traveled in core = *speed x time*
= [(5800 m/s x 72.945 μs)/10]
= 0.0423 m

This distance can be quoted in terms of the co-ordinate system, by using the y co-ordinate of sensor 3, as the reference point:

i.e. **predicted y-co-ordinate of p.d. source** = (0.3m - 0.005m - 0.045m - 0.0423m)
= **0.2077m**

Sensor 4:

From figure (10.24), the signal takes 390 μs to reach sensor 4. The time taken for the signal to propagate through the iron core alone, is given by:

$$t_{iron-core} = t_{total} - (t_{oil} + t_{wall})$$
$$= 390\ \mu s - (321.43\ \mu s + 15.625\ \mu s)$$
$$= \mathbf{52.945\ \mu s}$$

Distance traveled in core = *speed x time*
= [(5800 m/s x 52.945 μs)/10]
= **0.0307 m**

This distance can be quoted in terms of the co-ordinate system, by using the y co-ordinate of sensor 4, as the reference point:

i.e. **predicted y-co-ordinate of p.d. source** = (0.15m + 0.005m + 0.045m + 0.0307m)
= **0.2307m**

Therefore, the predicted range of the location of the p.d. in the y direction is:

0.2077 < y < **0.2307**

Note: The actual position of the p.d. is at y = 0.225 m

Summary of Results:

The predicted location of the p.d., both on the x and y axes are:
(x,y) = (0.2923 < x < **0.299 , 0.2077** < y < **0.2307)**

The actual position of the partial discharge in the model is at **(x,y) = (0.3 , 0.225)**

The acoustic method therefore provides an accurate means of determining the location of the partial discharge, provided the internal geometry of the transformer is known.

10.4.5 Model 5

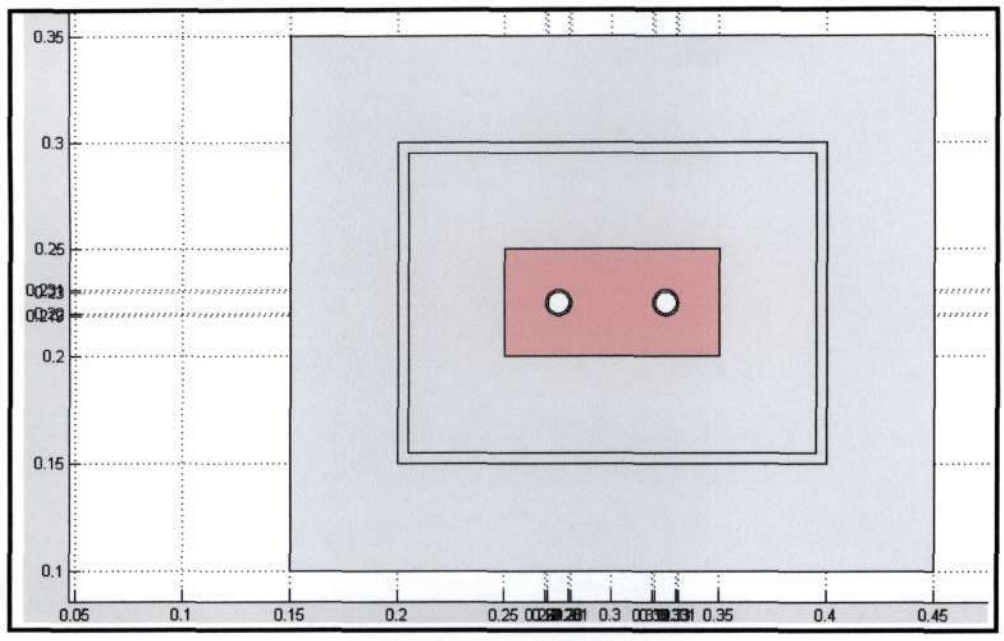

Figure (10.26)- Geometrical layout of model 5

Figure (10.26), depicts the geometrical layout of model 5. This model introduced two partial discharge sources into the windings surrounding the iron core, in order to investigate the effect on the accuracy of the detection and localization procedures.

This model comprises of the following sub domains:

- Outer air region
- Steel tank wall of transformer
- Inner transformer oil medium
- Inner iron core region
- Two partial discharge sources placed in the windings surrounding the iron core.

The following boundary conditions were imposed on the model:

- The value of the function was specified to be zero on the outer extremities of the air boundary, using the Dirichlet boundary condition. This was done, because this region lies far beyond the region where the measurements will be taken. During the construction phase of the model, this outer boundary was constructed a fair distance away from the actual transformer tank, in order to achieve a more realistic view of the behavior of the acoustic wave as it impinges onto the steel/air interface.
- The transformer tank wall was specified to be absorptive as well as reflective. This was implemented using the Neumann boundary condition, with the variable $q > g$. This condition specifies that some incident energy will be transmitted through the boundary, and some energy will be reflected.
- The outer boundaries of the iron core were set to be attenuating with the Neumann boundary condition. Again, the variable q was specified to be greater than g, in order to allow for the transmission of energy across the boundary.
- Both point sources were specified to emit an acoustic wave, of constant magnitude of 100 N/m^2 for all time. This was specified with the Dirichlet boundary condition.

The speed of the acoustic wave in the different media were specified in the sub domain settings as:

- Speed of sound in the outer air region: 333.33 m/s

- Speed of sound in the steel tank wall: 3200 m/s
- Speed of sound in the transformer oil: 1400 m/s
- Speed of sound in the iron core : 5800 m/s

The model was then meshed using a mesh of maximum node size of 11.3/15. This is a recommended choice for acoustic wave simulations.[21]

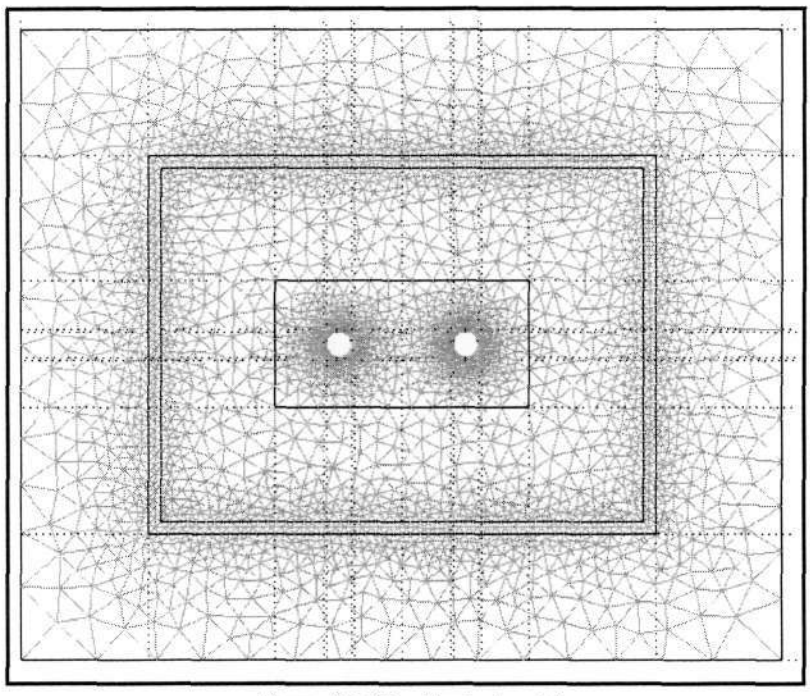

Figure (10.27) – Meshed model

The model was then simulated using an iterative solver, for 10 milliseconds, with a stepsize of 1 microsecond. The results are discussed overleaf.

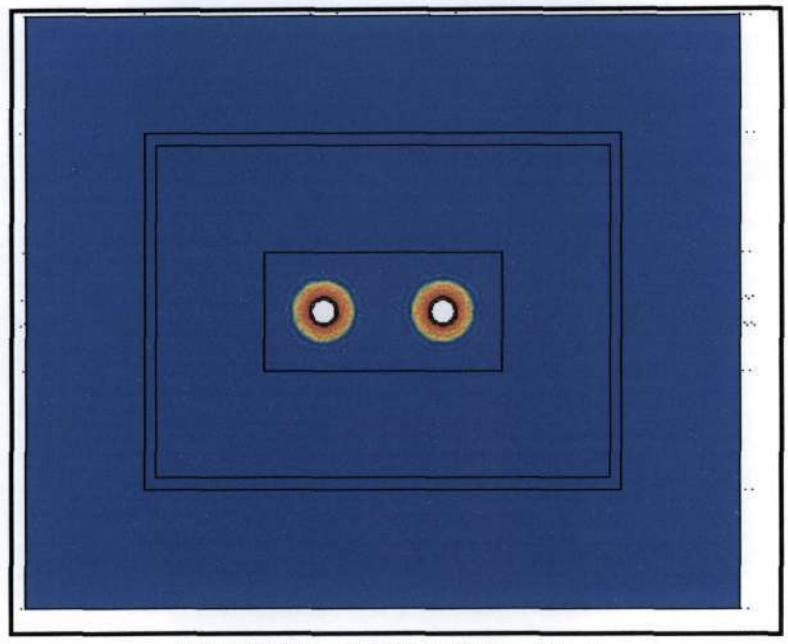

Figure (10.28) – Simulation at time = 100 μs

Figure (10.28), depicts the propagation of the acoustic waves from both p.d. sources at 100μs. Note that the p.d. sources are emitting an acoustic wave of constant magnitude of $100N/m^2$, for all time.

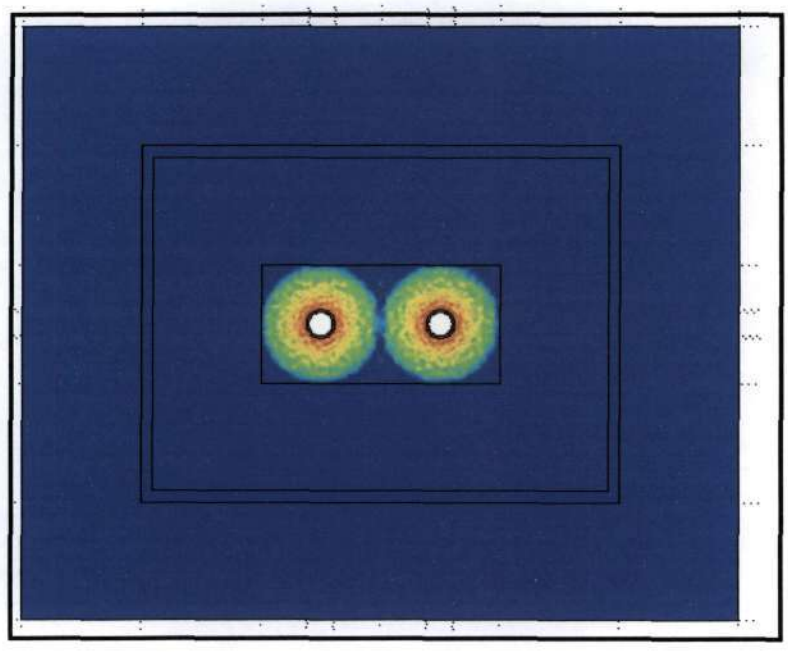

Figure (10.29)- Simulation at time = 250 μs

Figure (10.29), depicts the acoustic wave emitted by the two p.d. sources, about to impinge on the iron/transformer oil interface. In addition, the interference that starts to occur between the two waves (i.e. in the middle of the iron core) becomes evident.

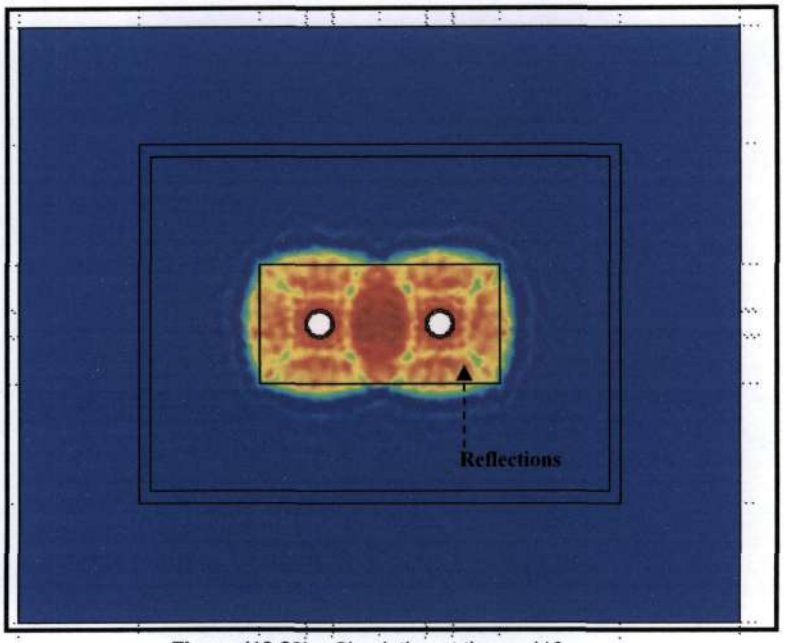

Figure (10.30) – Simulation at time = 410 μs

Figure (10.30), depicts the propagation of the acoustic wave in the transformer oil medium. Note the slower propagation of the wave in the transformer oil due to the relatively slower speed of sound in transformer oil. This figure also depicts the reflections that occur of the boundary of the iron core.

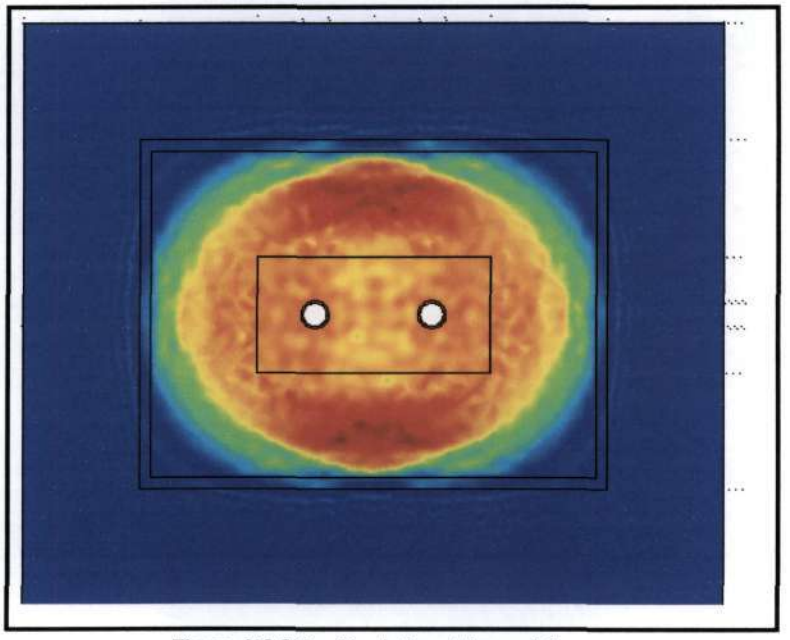

Figure (10.31) – Simulation at time = 1.5 ms

Figure (10.31), depicts the acoustic wave as it impinges onto the steel tank wall of the transformer. The acoustic sensors placed on the tank wall measure the effective intensity of this signal.

Sensors were placed at various positions on the tank wall, in order to measure the time of arrival of the acoustic wave on the outer steel tank wall. These sensor positions are depicted below:

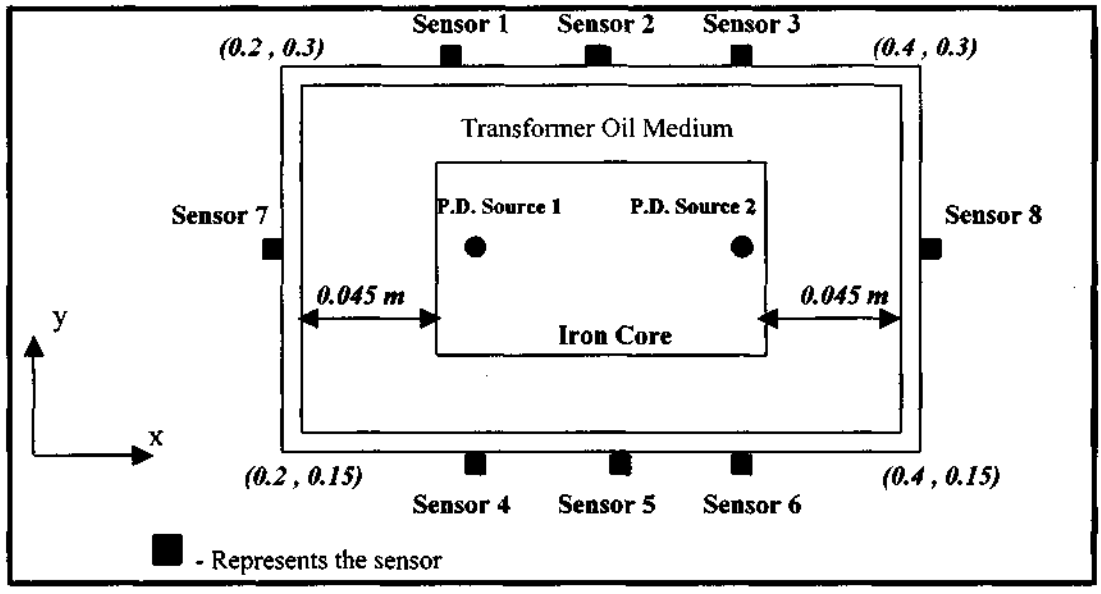

Figure (10.32) – Sensor Positions

Cross-sectional plots of the acoustic intensity (in the direction perpendicular to the tank wall) were then taken at each of the sensor positions. The acoustic waveforms are discussed overleaf.

The following are the actual geometrical positions of the p.d. sources:

- Partial Discharge source 1: **(0.275 , 0.225)**
- Partial Discharge source 2: **(0.325 , 0.225)**

Simulation Results:

Sensors on top of tank (waveforms have been enlarged to obtain the arrival time):

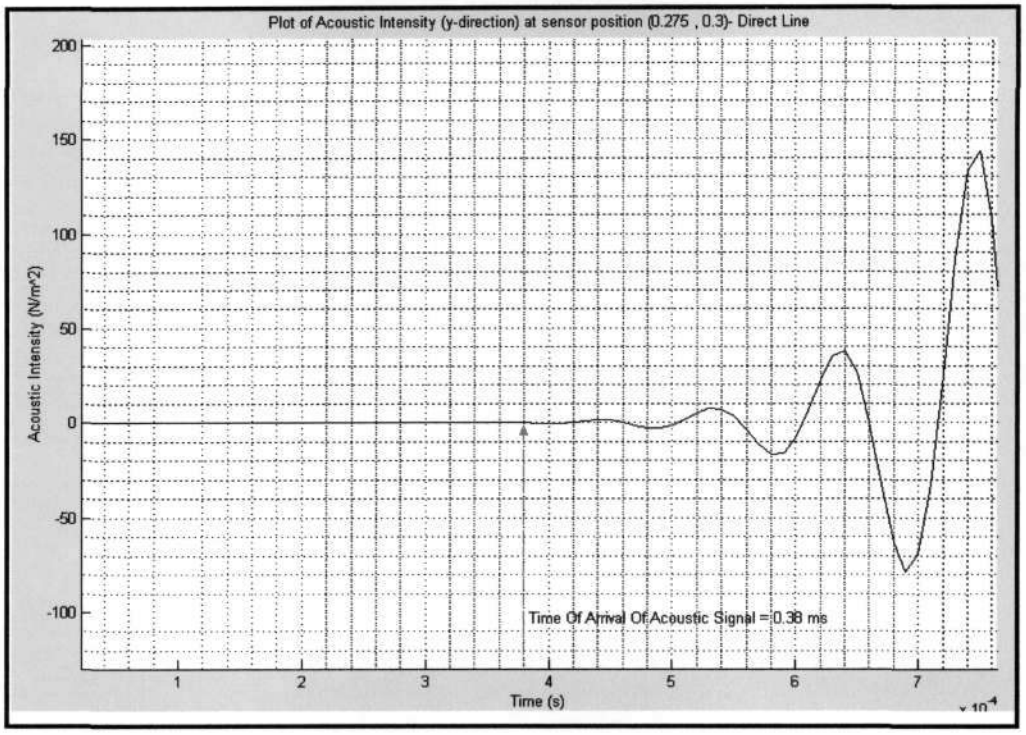

Figure (10.33) – Acoustic intensity as measured by sensor at position (0.275 , 0.3)

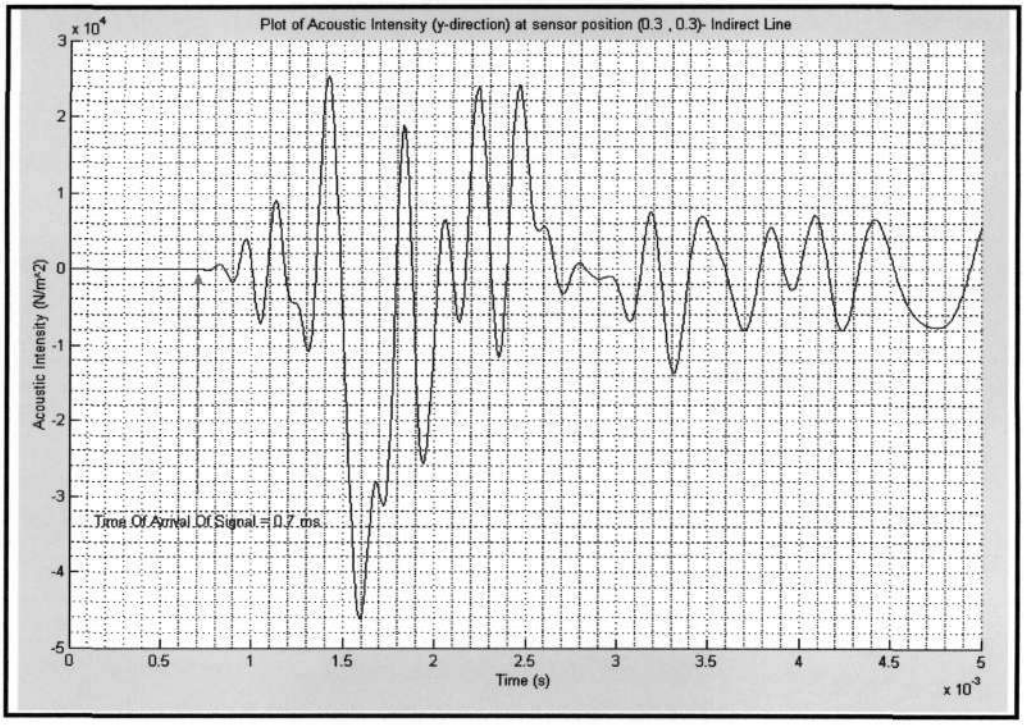

Figure (10.34) – Acoustic intensity as measured by sensor at position (0.3 , 0.3)

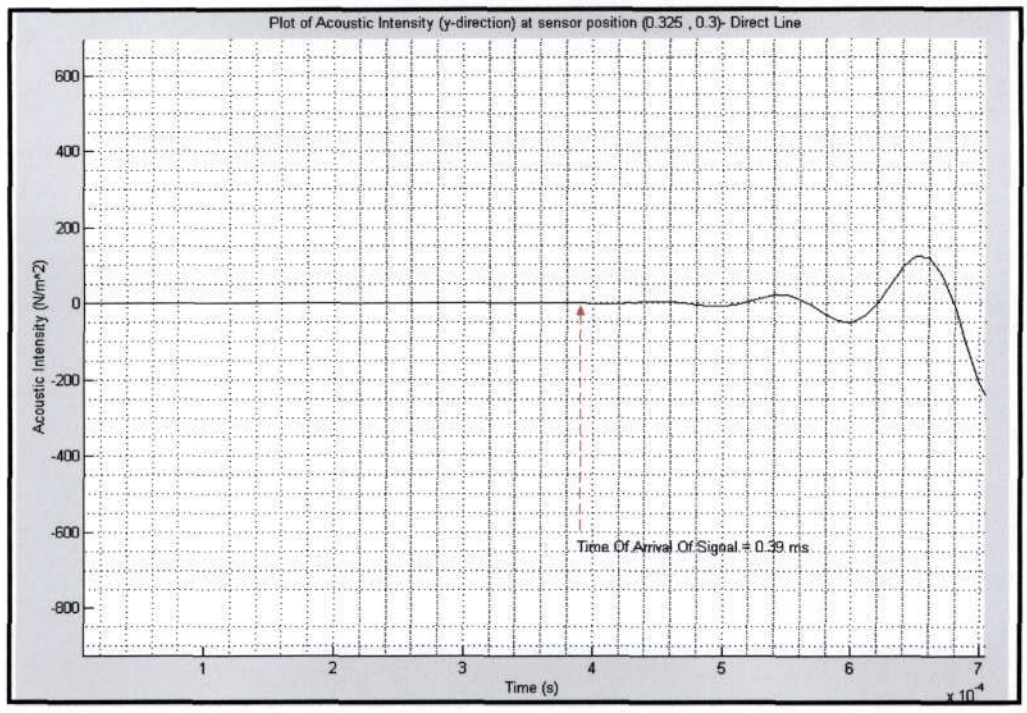

Figure (10.35) – Acoustic intensity as measured by sensor at position (0.325 , 0.3)

Analysis of waveforms obtained by sensors on tank top:

Note, from the waveforms obtained from the sensors which are located on the tank top, the sensors which lie in the direct line above the partial discharge source show the fastest arrival times. The sensors that lie directly above the source (i.e. in the direct path) were used in the localization calculations, due to accuracy purposes. Figure (10.34), depicts the waveform obtained from the sensor which was placed in the indirect line at position (0.3 , 0.3). The time of arrival of the signal at this position was noted to be significantly lower than in the case of the sensor that was placed in the direct line of the acoustic signal. This significantly lower arrival time can be attributed to the interference patterns, which occur in the areas outside the direct paths. These interference patterns can be clearly seen in figures (10.30) and figure (10.31). The following localization calculations (shown overleaf) are based on the waveforms obtained in figure (10.33) and figure (10.35).

Localization calculations based on sensor 1 and sensor 3

Time taken for signal to propagate through steel wall (uniform thickness):

The steel tank wall of the transformer has a uniform thickness of 0.005 m. From literature, it is known that acoustic waves propagate through transformer steel at a speed of 3200 m/s. The time taken for an acoustic wave to propagate through the wall can thus be calculated as:

$$s = \frac{dis\tan ce}{time}$$

$$\Rightarrow t_{wall} = \frac{d}{speed} = \frac{10 \times 0.005}{3200} = 15.63\ \mu s$$

Time taken for signal to propagate through the transformer oil:

The transformer oil section that lies in the direct line above the partial discharge in the model has a length of 0.045m. The sensor at position (0.275 , 0.3) , lies in the direct line above the partial discharge source. From literature it is known that the speed of propagation of acoustic waves in the transformer oil medium is approximately 1400 m/s. Using this information, the time taken for the acoustic wave to propagate through the transformer oil section can be ascertained from the following calculations:

$$t_{oil} = \frac{dis\tan ce}{speed} = \frac{0.045 \times 10}{1400} = 321.4\ \mu s$$

Calculation of the predicted position of the partial discharge from sensor 1 (0.275 , 0.3):

The total time taken for the acoustic signal to propagate through the different media, and final impinge on the outer tank wall is 0.38 ms (from figure (10.33). This information can now be used to ascertain the estimated location of the partial discharge within the spatial geometry of the transformer. This can be calculated as follows:

$$t_{core} = t_{total} - t_{wall} - t_{oil}$$

$$t_{core} = 0.38ms - 15.63\mu s - 321.4\mu s$$

$$t_{core} = 42.97\mu s$$

$$d_{core} = \frac{speed \times time}{10} = \frac{5800ms^{-1} \times 42.97\mu s}{10}$$

$$d_{core} = 0.025m$$

This distance represents the distance traveled by the acoustic signal in the iron core. This distance can now be quoted in terms of the co-ordinate arrangement utilized in this model.

Predicted y-coordinate of p.d. source 1 (from sensor 1):

Y co-ordinate of iron core – distance traveled by signal in core = 0.25 – 0.025 = **0.225 m**

Note: Actual y co-ordinate of p.d source 1 = 0.225. Therefore error = 0 %.

Calculation of the estimated position of p.d. source 2 from sensor 3 (0.325 , 0.3):

The transformer tank is symmetrical, therefore the time taken for the signal to propagate through the steel tank wall and the transformer oil medium (above p.d. source 2), will be same as calculated previously.

The total time taken for the acoustic signal to impinge on the outer tank wall is 0.39 ms (from figure 10.35). This information can now be used to ascertain the estimated location of the partial discharge within the spatial geometry of the transformer. This can be calculated as follows:

$$t_{core} = t_{total} - t_{wall} - t_{oil}$$
$$t_{core} = 0.39ms - 15.63\mu s - 321.4\mu s$$
$$t_{core} = 52.97\mu s$$

$$d_{core} = \frac{speed \times time}{10} = \frac{5800ms^{-1} \times 52.97\mu s}{10}$$
$$d_{core} = 0.031m$$

This distance represents the distance traveled by the acoustic signal in the iron core. This distance can now be quoted in terms of the co-ordinate arrangement utilized in this model.

Predicted y-coordinate of p.d. source 2 (from sensor 3):

Y co-ordinate of iron core – distance traveled by signal in core = 0.25 – 0.031 = **0.22 m**

Note: Actual y co-ordinate of p.d source 2 = 0.225. Therefore error = 2 %.

Sensors on tank bottom:

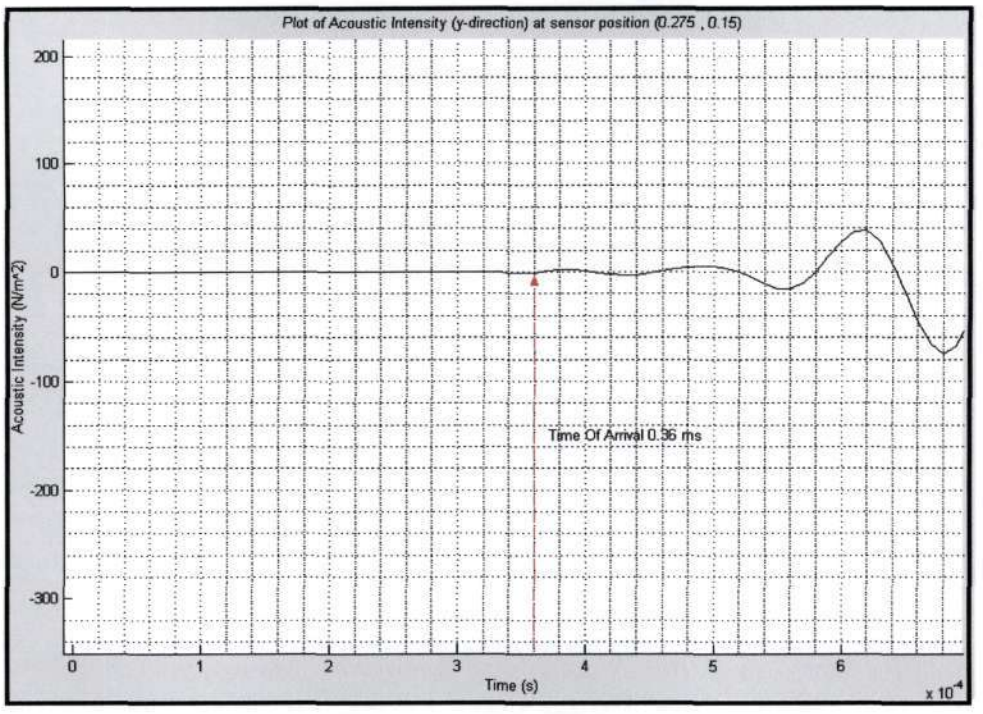

Figure (10.36) – Acoustic intensity as measured by sensor at position (0.275 , 0.15)

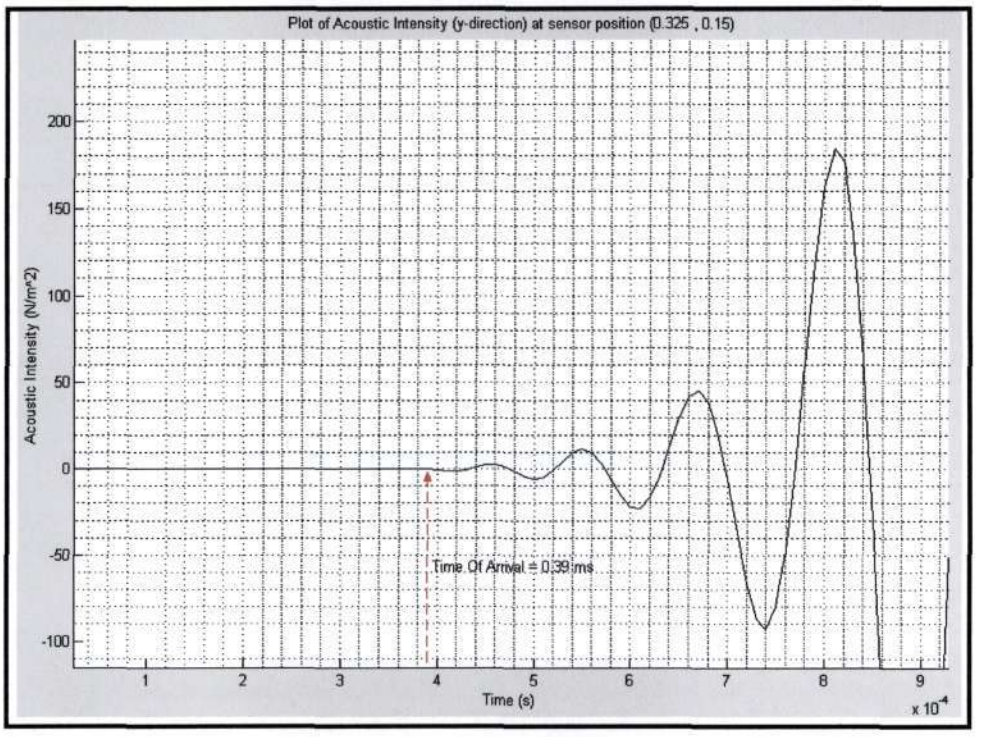

Figure (10.37) – Acoustic intensity as measured by sensor at position (0.325 , 0.15)

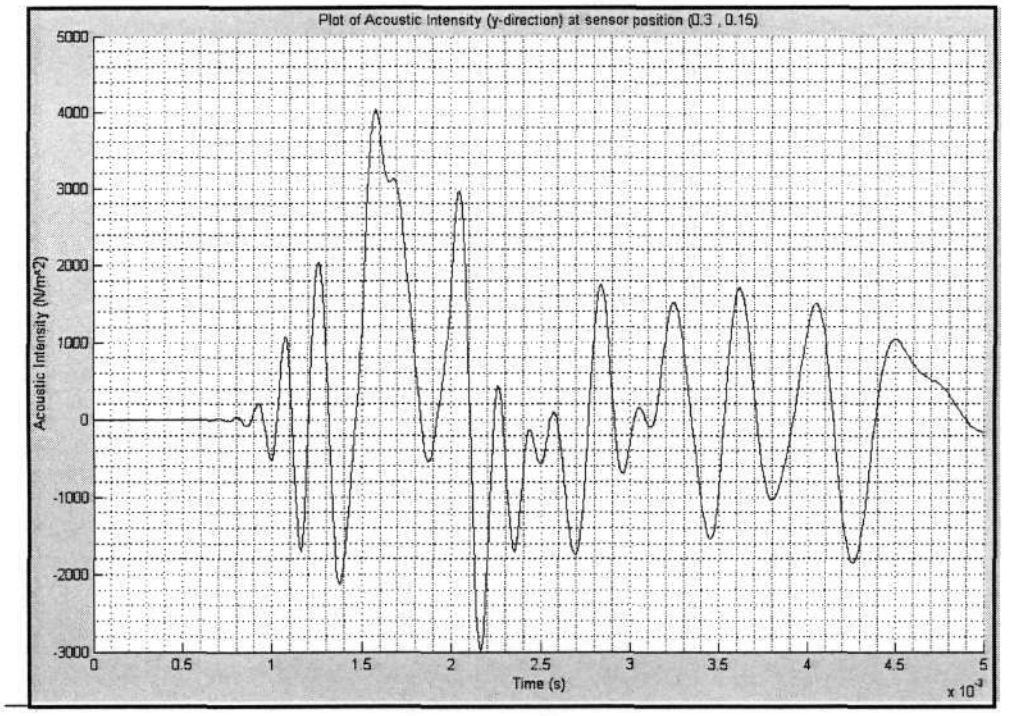

Figure (10.38) – Acoustic intensity as measured by sensor at position (0.3 , 0.15)

Analysis of waveforms obtained by sensors at the bottom of transformer tank

Sensor 4:

From figure (10.36), the time taken for the acoustic signal to arrive at sensor 4, is 0.36 ms. Using this value, the time taken for the signal to propagate through the iron core can be calculated as:

$$t_{Iron-Core} = t_{total} - (t_{oil} + t_{wall})$$

$$= 360\ \mu s - (321.43\ \mu s + 15.625\ \mu s)$$
$$= \mathbf{32.945\ \mu s}$$

The speed of sound in the iron core is known (from literature) to be 5800 m/s. Therefore, since the time taken for the acoustic signal to travel through the iron core is known, the distance of the p.d. source 1, within the core may be ascertained.

Therefore Distance traveled in core = speed x time
= [(5800 m/s x 22.945 μs)/10]
= 0.0191 m

This distance may now be quoted in terms of the co-ordinate system, by using the y co-ordinate of sensor 1, as the reference point:

Therefore, the second predicted y co-ordinate of p.d. source 1

= (0.15m + 0.005m + 0.045m + 0.0133m)
= **0.2191 m**

Combining the information received by sensor 1 and sensor 4, the predicted y co-ordinate of the partial discharge lies in the range **(0.2191 < y < 0.225).**

Sensor 6:

From figure (10.37), the time taken for the acoustic signal to arrive at sensor 4, is 0.39 ms. Using this value, the time taken for the signal to propagate through the iron core can be calculated as:

$$t_{Iron-Core} = t_{total} - (t_{oil} + t_{wall})$$

$$= 390\ \mu s - (321.43\ \mu s + 15.625\ \mu s)$$
$$= \mathbf{52.945\ \mu s}$$

The speed of sound in the iron core is known (from literature) to be 5800 m/s. Therefore, since the time taken for the acoustic signal to travel through the iron core is known, the distance of the p.d. source 1, within the core may be ascertained.

Therefore Distance traveled in core = speed x time
= [(5800 m/s x 22.945 μs)/10]
= 0.0307 m

This distance may now be quoted in terms of the co-ordinate system, by using the y co-ordinate of sensor 6, as the reference point:

Therefore, the second predicted y co-ordinate of p.d. source 1

= (0.15m + 0.005m + 0.045m + 0.0307m)
= **0.237 m**

Combining the information received by sensor 1 and sensor 4, the predicted y co-ordinate of the partial discharge lies in the range **(0.225 < y < 0.237).**

Sensors on tank sides

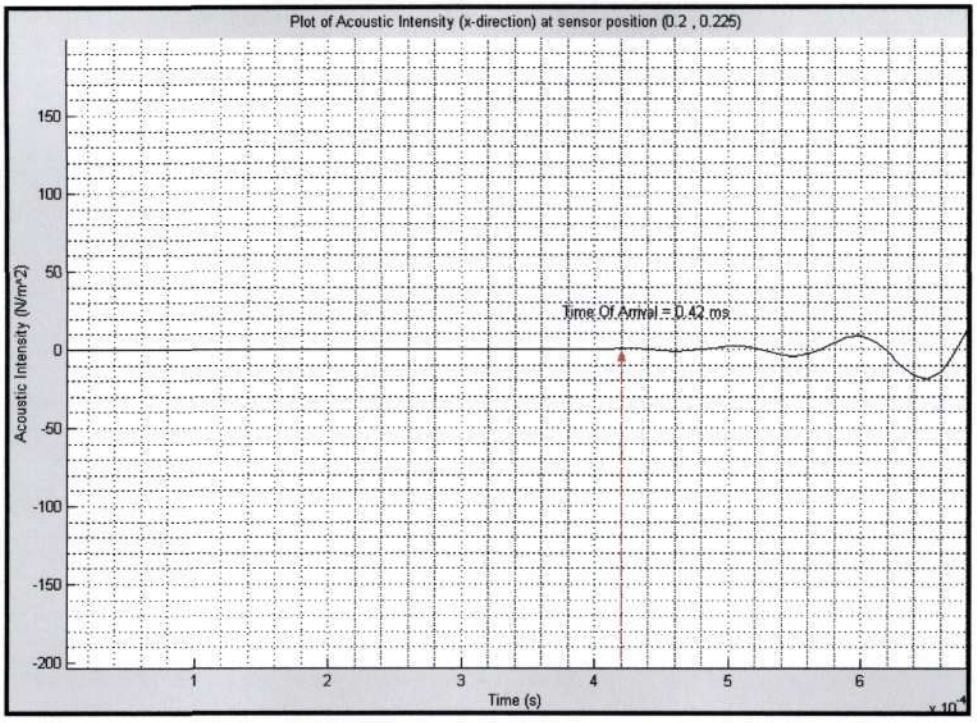

Figure (10.39) – Acoustic intensity as measured by sensor at position (0.2 , 0.225)

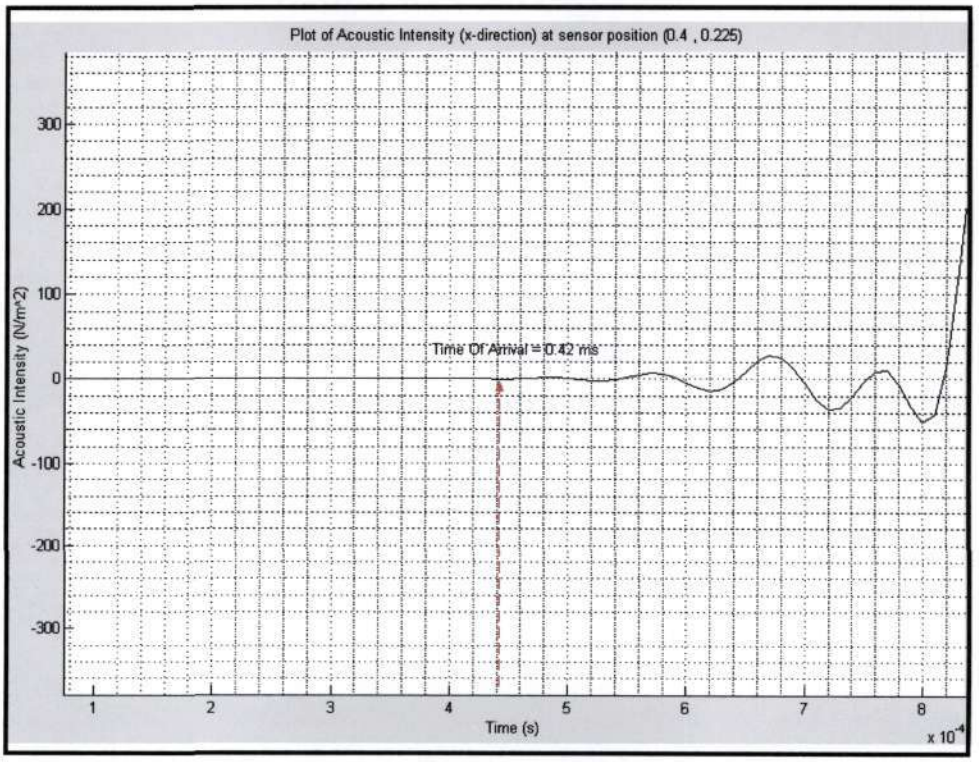

Figure (10.40) – Acoustic intensity as measured by sensor at position (0.4 , 0.225)

Analysis of waveforms obtained by acoustic sensors on tank sides

Sensor 7:

The time taken for the signal to propagate through the transformer oil, to the left p.d. source 1 can be calculated as:

$$t_{oil} = \frac{dis\tan ce}{speed} = \frac{0.045 \times 10}{1400} = 321.43 \ \mu s$$

The time taken for the acoustic signal to propagate through the steel wall is given by:

$$t_{Wall} = \frac{dis\tan ce}{speed} = \frac{0.005 \times 10}{3200} = 15.625 \ \mu s$$

From figure (10.39), the time taken for the acoustic signal to arrive at sensor 7, is 0.42 ms. Using this value, the time taken for the signal to propagate through the iron core can be calculated as:

$$t_{Iron-Core} = t_{total} - (t_{oil} + t_{wall})$$

$$= 420\ \mu s - (321.43\ \mu s + 15.625\ \mu s)$$
$$= \mathbf{82.945\ \mu s}$$

The speed of sound in the iron core is known (from literature) to be 5800 m/s. Therefore, since the time taken for the acoustic signal to travel through the iron core is known, the distance of the p.d. source 1, within the core may be ascertained.

Therefore Distance traveled in core = speed x time
= [(5800 m/s x 82.945 μs)/10]
= 0.0481 m

This distance may now be quoted in terms of the co-ordinate system, by using the x co-ordinate of sensor 7 (horizontal plane), as the reference point:

Therefore, predicted x co-ordinate of p.d. source 1

= (0.2m + 0.005m + 0.045m + 0.0481m)
= **0.298 m**

Therefore the predicted spatial location of partial discharge source 1 is :
(0.298 , 0.2191 < y < 0.225)

Note: The actual location of Partial Discharge source 1 : **(0.275 , 0.225)**.
The predicted spatial location is therefore a good approximation of the actual location.

Sensor 8:

The time taken for the signal to propagate through the transformer oil, to the right of p.d. source 2 can be calculated as:

$$t_{oil} = \frac{dis\tan ce}{speed} = \frac{0.045 \times 10}{1400} = 321.43 \ \mu s$$

The time taken for the acoustic signal to propagate through the steel wall is given by:

$$t_{Wall} = \frac{dis\tan ce}{speed} = \frac{0.005 \times 10}{3200} = 15.625 \ \mu s$$

From figure (10.40), the time taken for the acoustic signal to arrive at sensor 8, is 0.42ms. Using this value, the time taken for the signal to propagate through the iron core can be calculated as:

$$t_{Iron-Core} = t_{total} - (t_{oil} + t_{wall})$$

$$= 420\ \mu s - (321.43\ \mu s + 15.625\ \mu s)$$
$$= \mathbf{82.945\ \mu s}$$

The speed of sound in the iron core is known (from literature) to be 5800 m/s. Therefore, since the time taken for the acoustic signal to travel through the iron core is known, the distance of the p.d. source 2, within the core may be ascertained.

Therefore Distance traveled in core = speed x time
= [(5800 m/s x 82.945 μs)/10]
= 0.0481 m

This distance may now be quoted in terms of the co-ordinate system, by using the x co-ordinate of sensor 7 (horizontal plane), as the reference point:

Therefore, predicted x co-ordinate of p.d. source 1

= (0.4m - 0.005m - 0.045m - 0.0481m)
= 0.301 m

Therefore the predicted spatial location of partial discharge source 2 is :
(0.301 , 0.225 < y < 0.237)

Note: The actual location of Partial Discharge source 2 : **(0.325 , 0.225)**.

The predicted spatial location is therefore a good approximation of the actual location.

10.5 Three-Dimensional Simulations

10.5.1 Model 6

The first three dimensional model which was constructed was aimed at understanding the mechanisms underlying 3-D simulations in Femlab. The transformer was modeled as a square three-dimensional figure, and the iron cores as well as the steel wall (of finite thickness) were not considered. The geometry is depicted below:

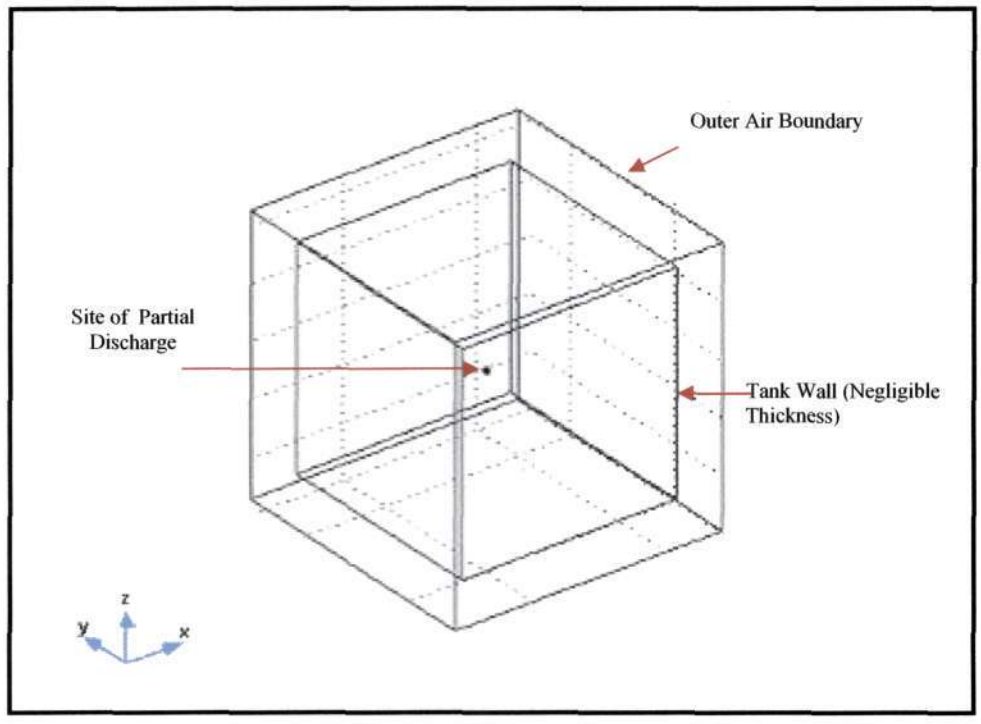

Figure (10.41) – Three Dimensional Model

This model comprised of the following sub domain regions:

- Inner Transformer Oil Region
- Outer Air Region

The following Boundary Conditions were imposed on the model:

- The value of the function was specified to be zero on the outer extremities of the air boundary, using the Dirichlet boundary condition. This was done, because this region lies far beyond the region where the measurements will be taken (i.e. on the tank wall). During the construction phase of the model, this outer boundary was constructed a fair distance away from the actual transformer tank, in order to achieve a more realistic view of the behavior of the acoustic wave as it impinges onto the steel/air interface.
- The transformer tank wall was specified to be absorptive as well as reflective. This was implemented using the Neumann boundary condition, with the variable $q > g$. This condition specifies that some incident energy will be transmitted through the boundary, and some energy will be reflected.
- The partial discharge (i.e. point source), was specified to emit an acoustic wave, of constant magnitude of 100 N/m^2 for all time. This was specified with the Dirichlet boundary condition.

The speed of the acoustic wave in the different media were specified in the sub domain settings as:

- Speed of sound in the outer air region: 333.33 m/s

- Speed of sound in the transformer oil: 1400 m/s

Figure (10.42), depicts the dimensional specifications and the sensor positions of the model:

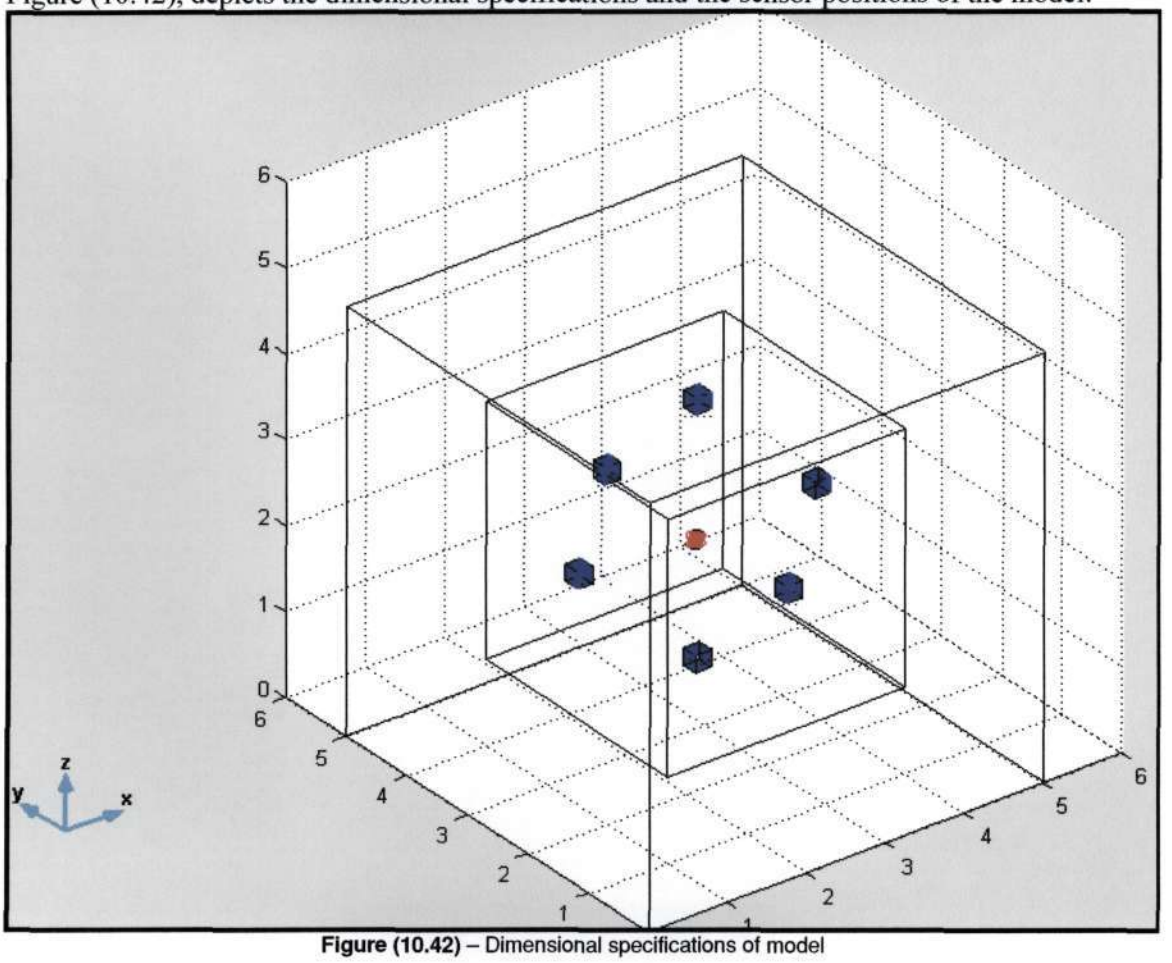

Figure (10.42) – Dimensional specifications of model

The point source was geometrically represented as a cylinder. The model was simulated for a duration of 10 milliseconds with a step-size of 20 microseconds, using an iterative solver. The following diagrams (shown overleaf) depict the propagation of the acoustic wave through the geometry, at various times during the simulation.

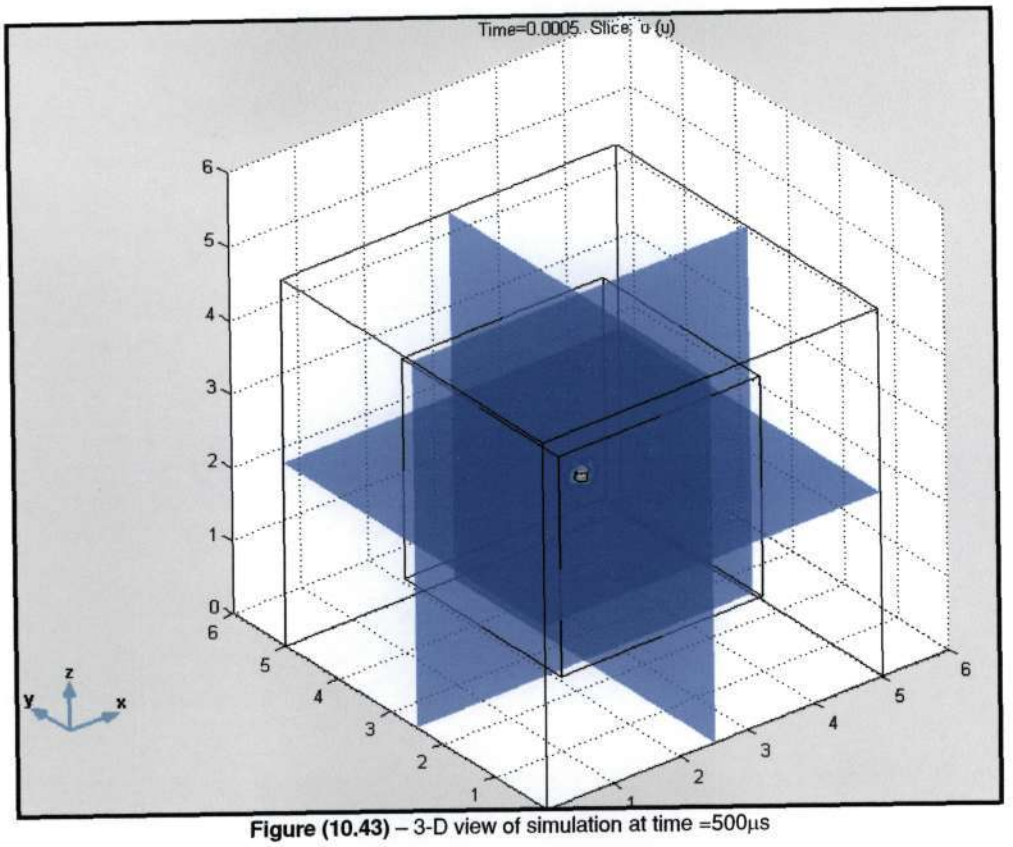

Figure (10.43) – 3-D view of simulation at time =500μs

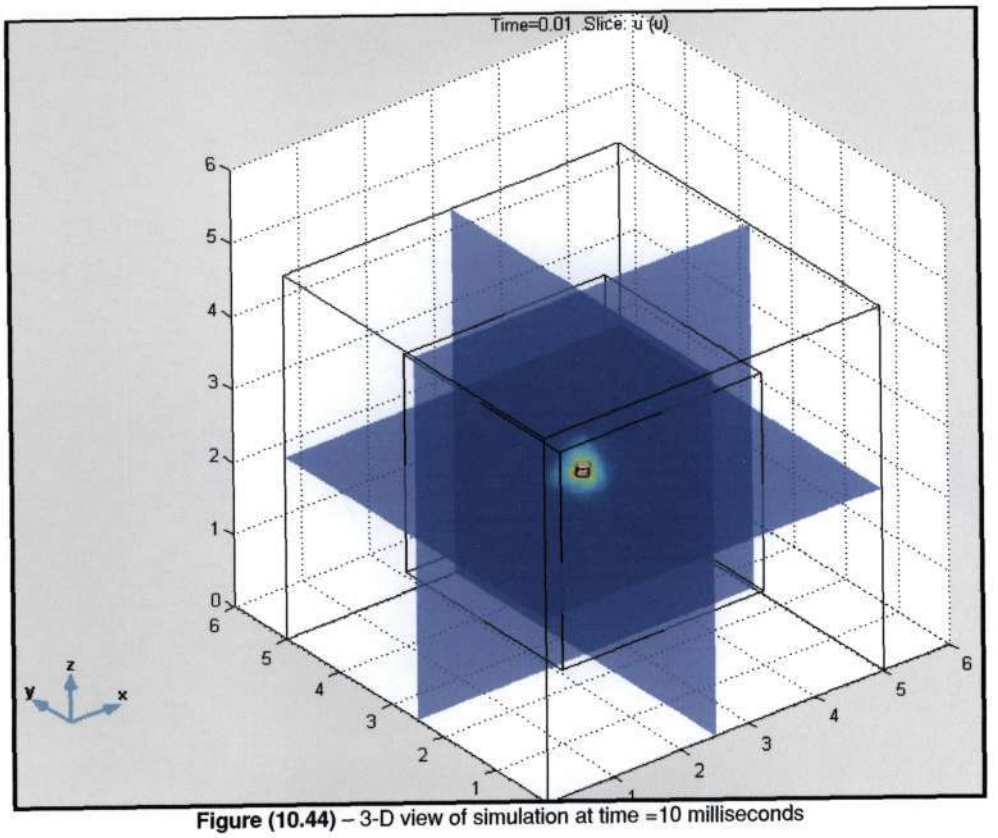

Figure (10.44) – 3-D view of simulation at time =10 milliseconds

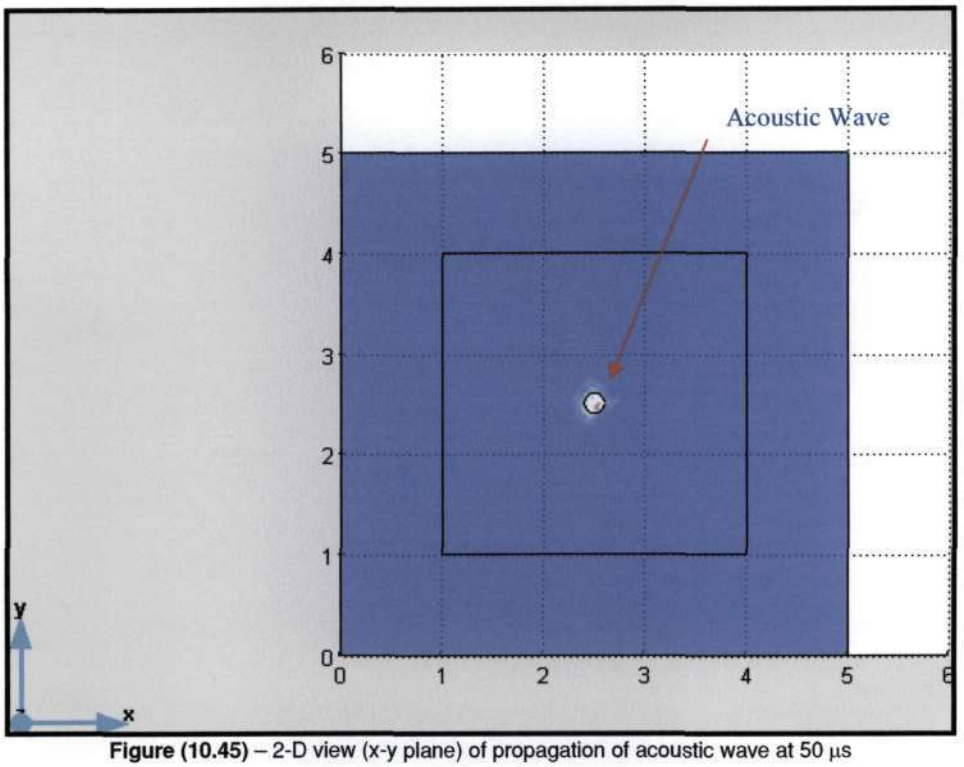

Figure (10.45) – 2-D view (x-y plane) of propagation of acoustic wave at 50 μs

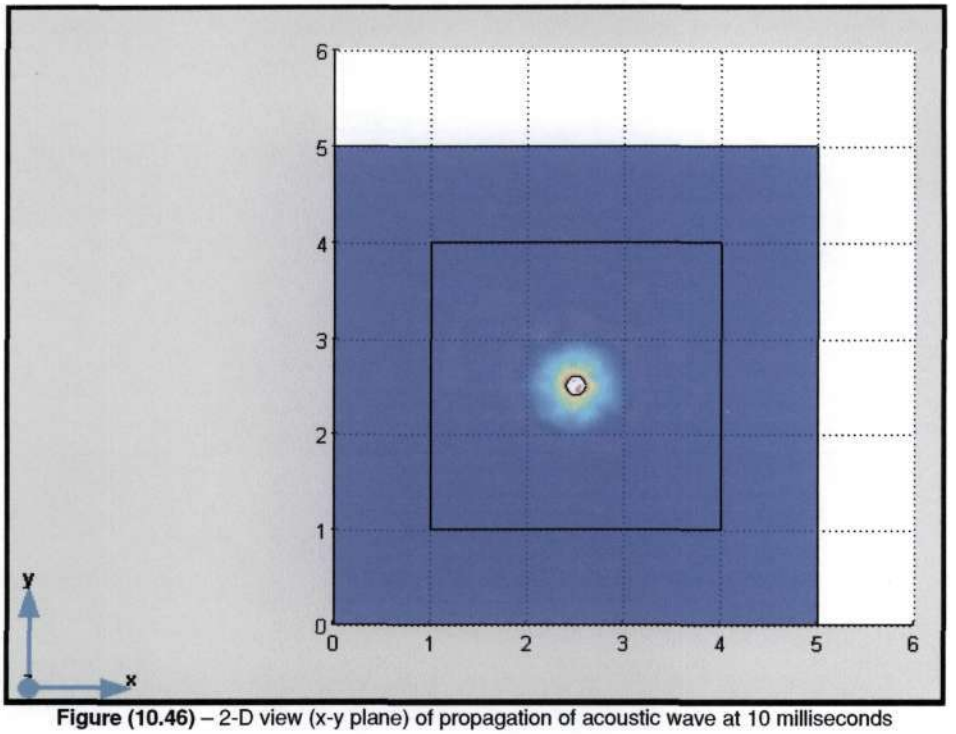

Figure (10.46) – 2-D view (x-y plane) of propagation of acoustic wave at 10 milliseconds

Waveforms obtained from cross-sectional plots at each of the sensor positions:

The following two plots were taken on the **x-plane**:

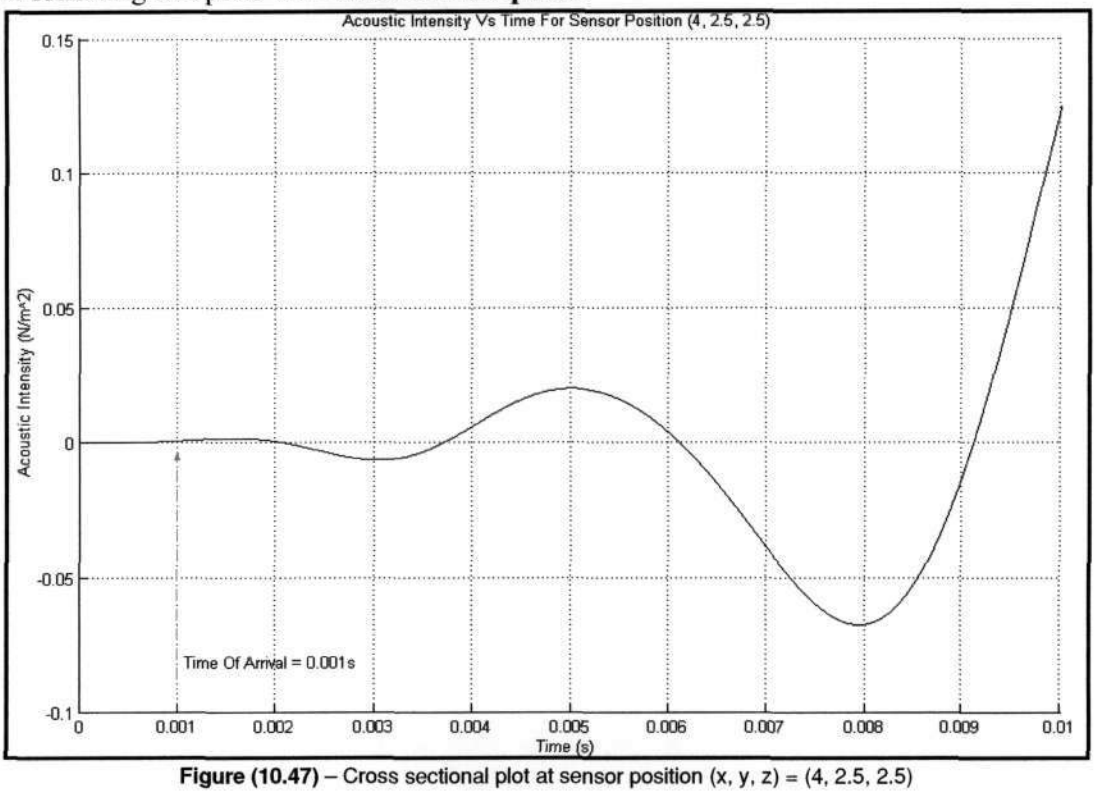

Figure (10.47) – Cross sectional plot at sensor position (x, y, z) = (4, 2.5, 2.5)

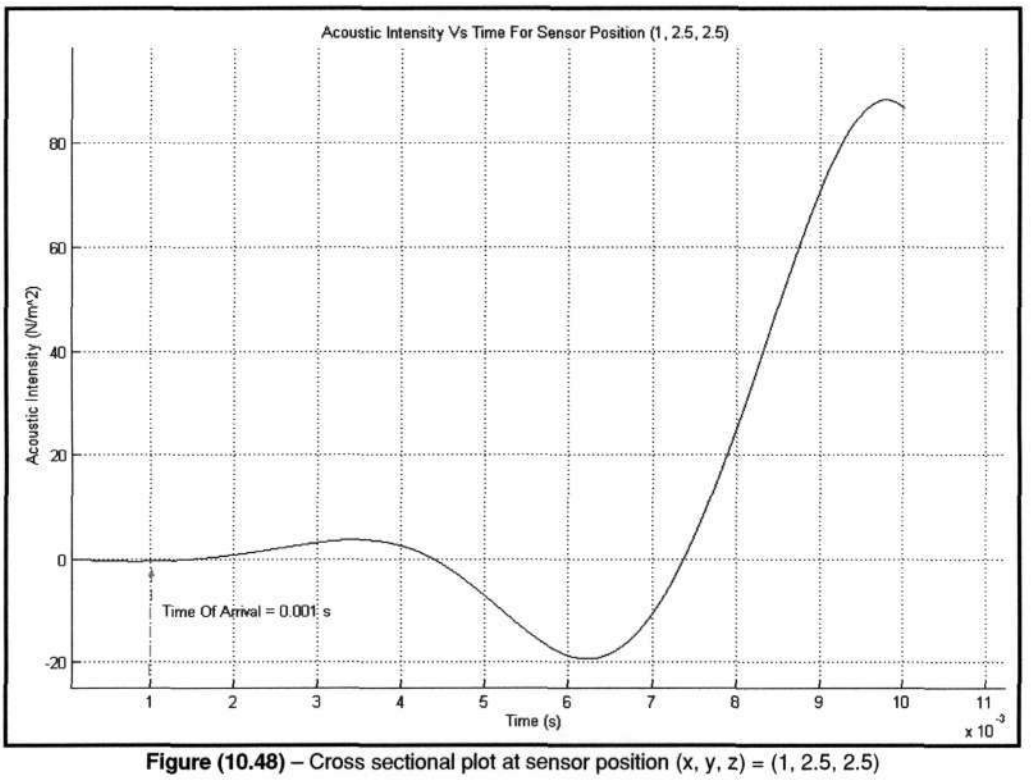

Figure (10.48) – Cross sectional plot at sensor position (x, y, z) = (1, 2.5, 2.5)

Analysis Of Results Obtained on the x-plane: Localisation Calculations

From figure (10.47), the time taken for the acoustic wave to arrive at sensor position 1, is 1ms. From literature, the speed of sound in transformer oil is known to be 1400 m/s. Using the relationship between speed and distance the predicted location of the p.d. source can be ascertained as follows:

$$distance = speed \times time = 1400m/s \times 1ms = 1.4m$$

This implies that the acoustic signal has traveled 1.4metres prior to impinging on the tank wall. In terms of the co-ordinate system used, the x co-ordinate (using the sensor x coordinate as the reference) is: (4 – 1.4) = **2.6**

The first predicted x-coordinate of the p.d. source is **x = 2.6 units.**

From figure (10.48), the time taken for the acoustic wave to arrive at sensor position 2, is 1ms. Using the relationship between speed and distance the predicted location of the p.d. source can be ascertained as follows:

$$distance = speed \times time = 1400m/s \times 1ms = 1.4m$$

This implies that the acoustic signal has traveled 1.4 metres prior to impinging on the tank wall. In terms of the co-ordinate system used, the x co-ordinate (using the sensor x coordinate as the reference) is: (1 + 1.4) = **2.4.**

The second predicted x-coordinate of the p.d. source is **x = 2.4 units.**

Therefore the predicted range (x plane), in which the p.d. source exists is **(2.4 < x < 2.6)**.

From the geometrical layout the p.d. source actually lies at x = 2.5. The predicted range is therefore a very good approximation of the actual position.

The following two plots were taken on the **y-plane**:

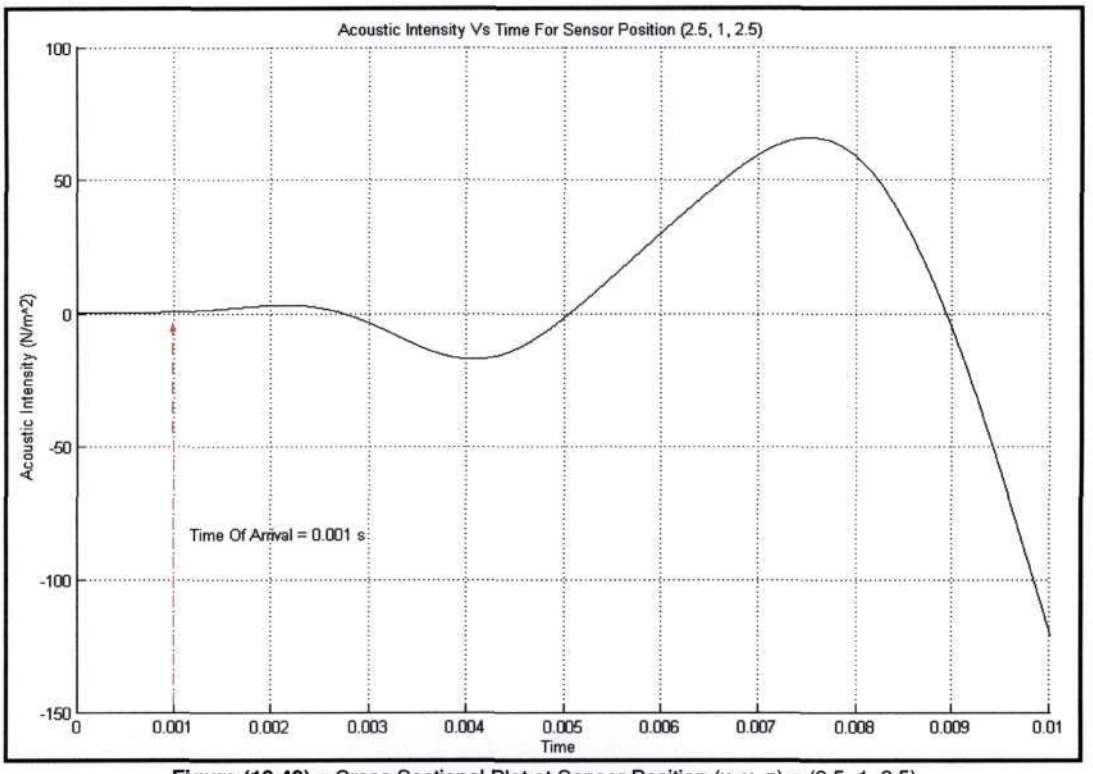

Figure (10.49) – Cross Sectional Plot at Sensor Position (x, y, z) = (2.5, 1, 2.5)

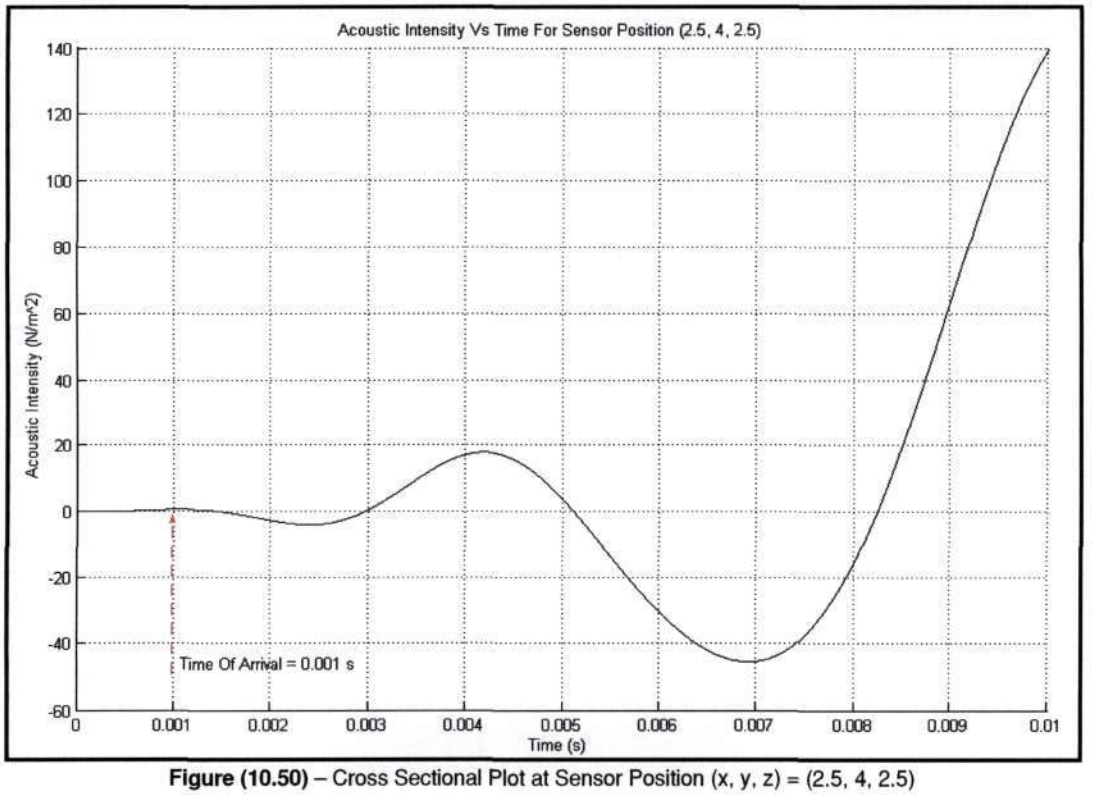

Figure (10.50) – Cross Sectional Plot at Sensor Position (x, y, z) = (2.5, 4, 2.5)

Analysis Of Results Obtained on the y-plane – Localisation Calculations

From figure (10.49), the time taken for the acoustic wave to arrive at sensor position 3, is 1ms. Using the relationship between speed and distance the predicted location of the p.d. source can be ascertained as follows:

$$distance = speed \times time = 1400m/s \times 1ms = 1.4m$$

This implies that the acoustic signal has traveled 1.4metres prior to impinging on the tank wall. In terms of the co-ordinate system used, the y co-ordinate (using the sensor y coordinate as the reference) is: (4 – 1.4) = **2.6**

The first predicted y-coordinate of the p.d. source is **y = 2.6 units.**

From figure (10.50), the time taken for the acoustic wave to arrive at sensor position 4, is 1ms. Using the relationship between speed and distance the predicted location of the p.d. source can be ascertained as follows:

$$distance = speed \times time = 1400m/s \times 1ms = 1.4m$$

This implies that the acoustic signal has traveled 1.4 metres prior to impinging on the tank wall. In terms of the co-ordinate system used, the y co-ordinate (using the sensor y coordinate as the reference) is: (1 + 1.4) = **2.4.**

The second predicted y-coordinate of the p.d. source is **y = 2.4 units.**

Therefore the predicted range (y plane) in which the p.d. source exists is **(2.4 < y < 2.6)**.

From the geometrical layout the p.d. source actually lies at y = 2.5. The predicted range is therefore a very good approximation of the actual position.

The following two plots were taken on the **z-plane**:

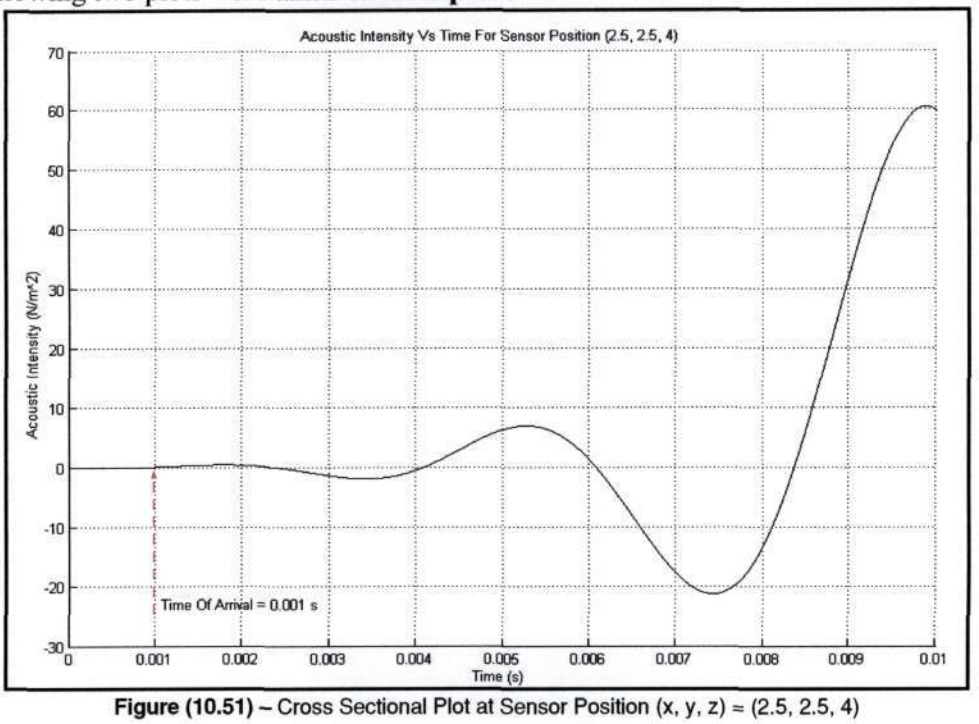

Figure (10.51) – Cross Sectional Plot at Sensor Position (x, y, z) = (2.5, 2.5, 4)

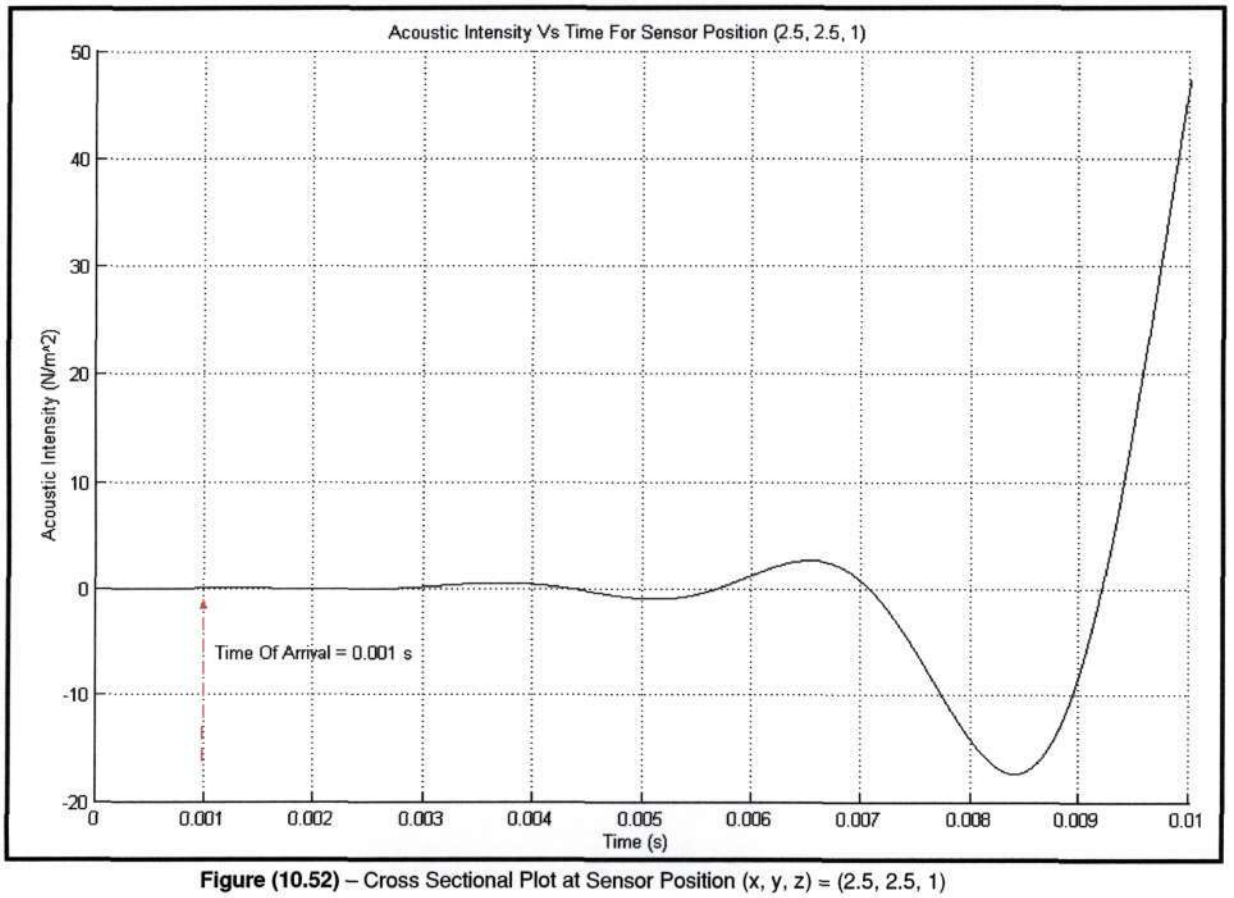

Figure (10.52) – Cross Sectional Plot at Sensor Position (x, y, z) = (2.5, 2.5, 1)

Analysis Of Results Obtained on the z-plane – Localisation Calculations

From figure (10.51), the time taken for the acoustic wave to arrive at sensor position 5, is 1ms. Using the relationship between speed and distance the predicted location of the p.d. source can be ascertained as follows:

$$distance = speed \times time = 1400m/s \times 1ms = 1.4m$$

This implies that the acoustic signal has traveled 1.4metres prior to impinging on the tank wall. In terms of the co-ordinate system used, the z co-ordinate (using the sensor z coordinate as the reference) is: (4 – 1.4) = **2.6**

The first predicted z-coordinate of the p.d. source is **z = 2.6 units.**

From figure (10.52), the time taken for the acoustic wave to arrive at sensor position 6, is 1ms. Using the relationship between speed and distance the predicted location of the p.d. source can be ascertained as follows:

$$distance = speed \times time = 1400m/s \times 1ms = 1.4m$$

This implies that the acoustic signal has traveled 1.4 metres prior to impinging on the tank wall. In terms of the co-ordinate system used, the z co-ordinate (using the sensor z coordinate as the reference) is: (1 + 1.4) = **2.4.**

The second predicted z-coordinate of the p.d. source is **z = 2.4 units.**

Therefore the predicted range (z plane), in which the p.d. source exists is **(2.4 < z < 2.6)**.

From the geometrical layout the p.d. source actually lies at z = 2.5. The predicted range is therefore a very good approximation of the actual position.

Summary Of Model 6:

The actual spatial position of the p.d. source is (x, y, z) = (2.5, 2.5, 2.5).

The following results were obtained from each of the sensor positions:
Sensor 1: x = 2.4
Sensor 2: x = 2.6
Sensor 3: y = 2.4
Sensor 4: y = 2.6
Sensor 5: z = 2.4
Sensor 6: z = 2.6

Therefore, the predicted spatial location of the p.d. source (in terms of the co-ordinate) system used is
x = (2.4 < x < 2.6)
y = (2.4 < y < 2.6)
z = (2.4 < z < 2.6)

The predicted position of the p.d. source obtained from the simulations is therefore a very good approximation of the actual position.

10.5.2 Model 7 – Inclusion of iron core with windings

This three dimensional model was modeled as a rectangular tank (dimensions similar to distribution transformer on which experimental testing will be performed). An iron core was included inside the transformer tank. It was assumed that the windings around this iron core contained a partial discharge, which acted as a point source for the acoustic emissions. The geometry of this model is depicted below:

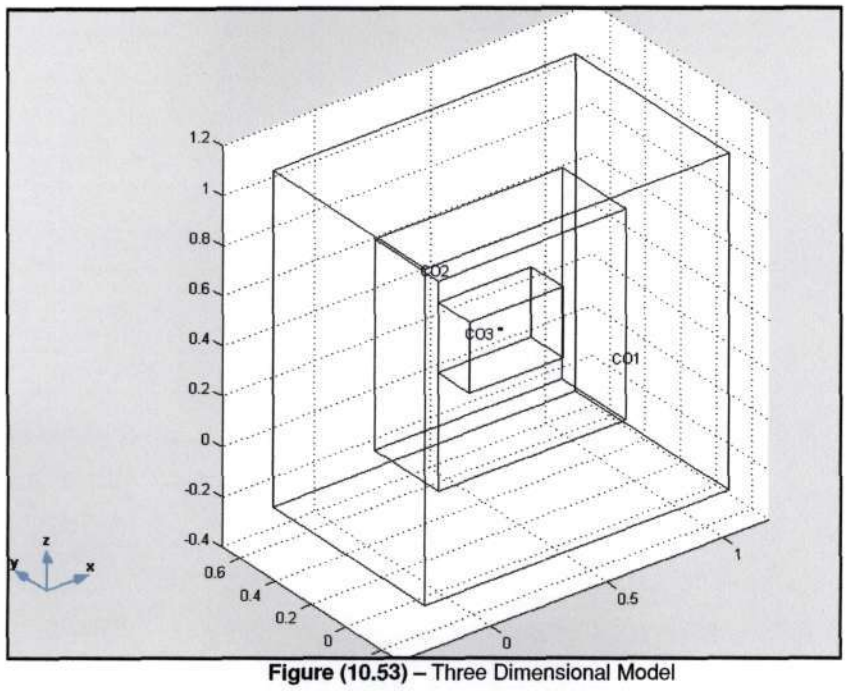

Figure (10.53) – Three Dimensional Model

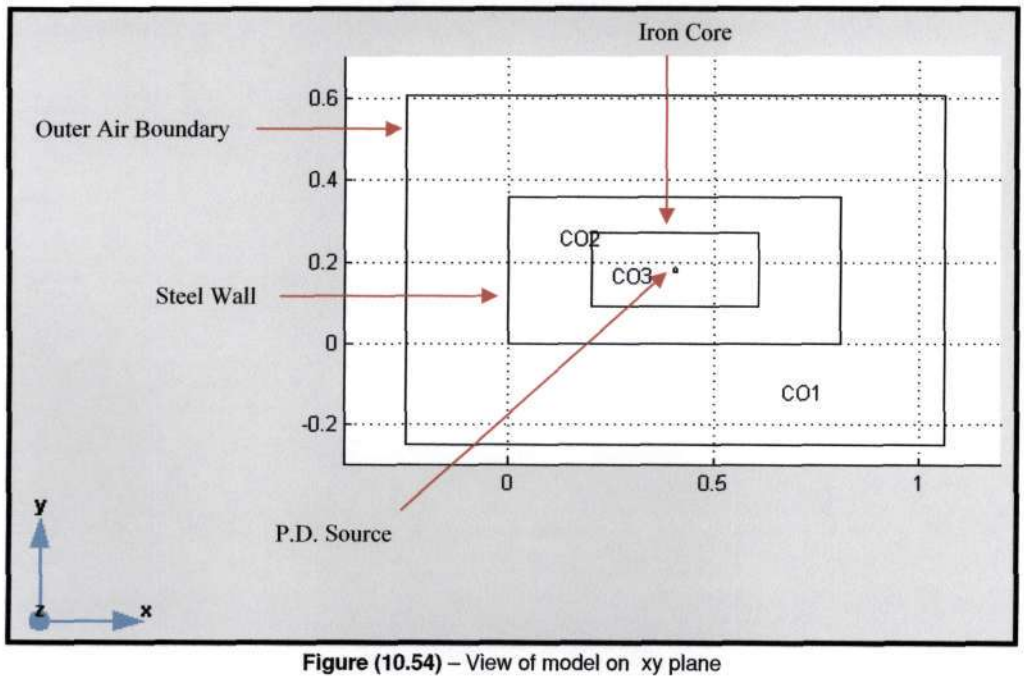

Figure (10.54) – View of model on xy plane

This model contained the following sub-domain regions:

- Iron Core Region.
- Transformer Oil Region.
- Outer Air Region.

The following boundary conditions were imposed on the model:

- The value of the function was specified to be zero on the outer extremities of the air boundary, using the Dirichlet boundary condition. This was done, because this region lies far beyond the region where the measurements will be taken (i.e. on the tank wall). During the construction phase of the model, this outer boundary was constructed a fair distance away from the actual transformer tank, in order to achieve a more realistic view of the behavior of the acoustic wave as it impinges onto the steel/air interface.
- The boundaries of the iron core, were set to be attenuating using the Neumann condition. The variable q was set to be greater than g, in order to allow for the transmission of energy across the boundary.
- The transformer tank wall was specified to be absorptive as well as reflective. This was implemented using the Neumann boundary condition, with the variable $q > g$. This condition specifies that some incident energy will be transmitted through the boundary, and some energy will be reflected.
- The partial discharge (i.e. point source), was specified to emit an acoustic wave, of constant magnitude of 100 N/m^2 for all time. This was specified with the Dirichlet boundary condition.

The speed of the acoustic wave in the different media were specified in the sub domain settings as:

- Speed of sound in the outer air region: 333.33 m/s
- Speed of sound in the transformer oil: 1400 m/s
- Speed of sound in the iron core region: 5800 m/s

Actual Position of Partial Discharge Source:
(x, y, z) = (0.405, 0.18, 0.42)

As in the previous model, the point source was geometrically represented as a cylinder. This model was simulated for 10 milliseconds with a step-size of 20 microseconds, using an iterative solver. The diagrams that follow depict the propagation of the acoustic wave through the different media of the transformer, at various times during the simulation.

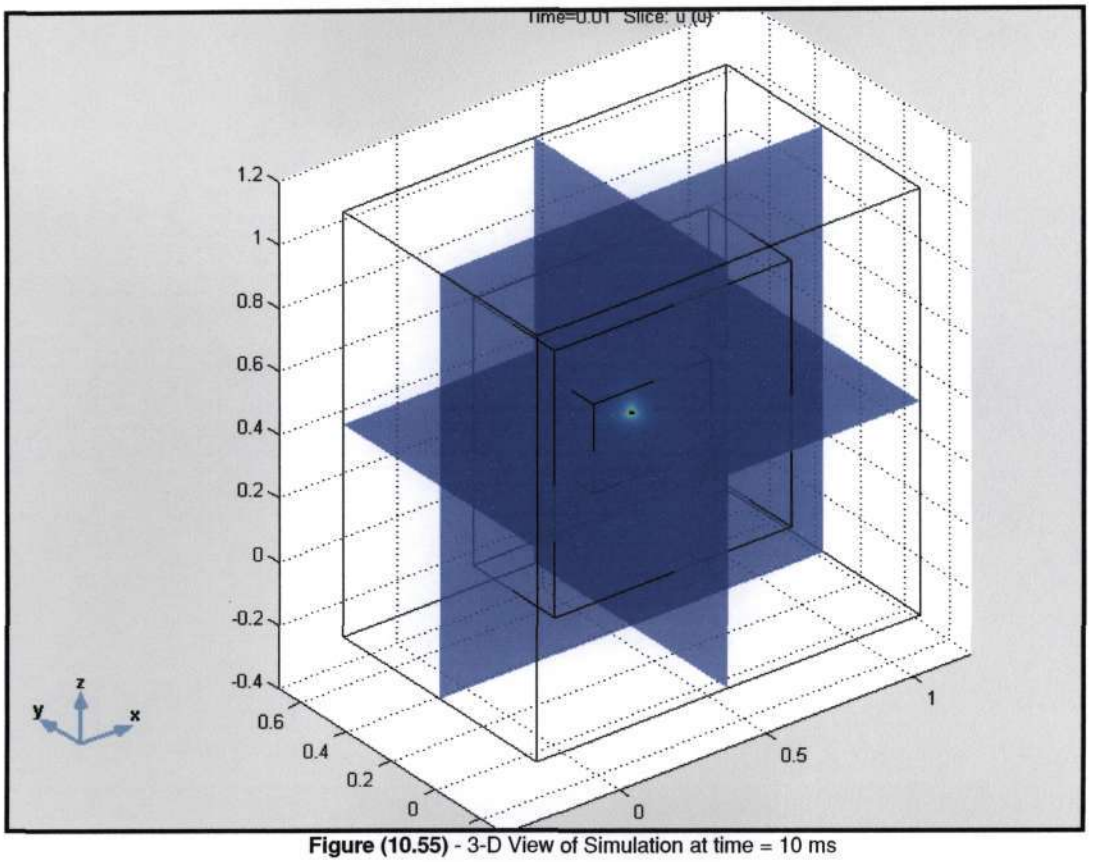

Figure (10.55) - 3-D View of Simulation at time = 10 ms

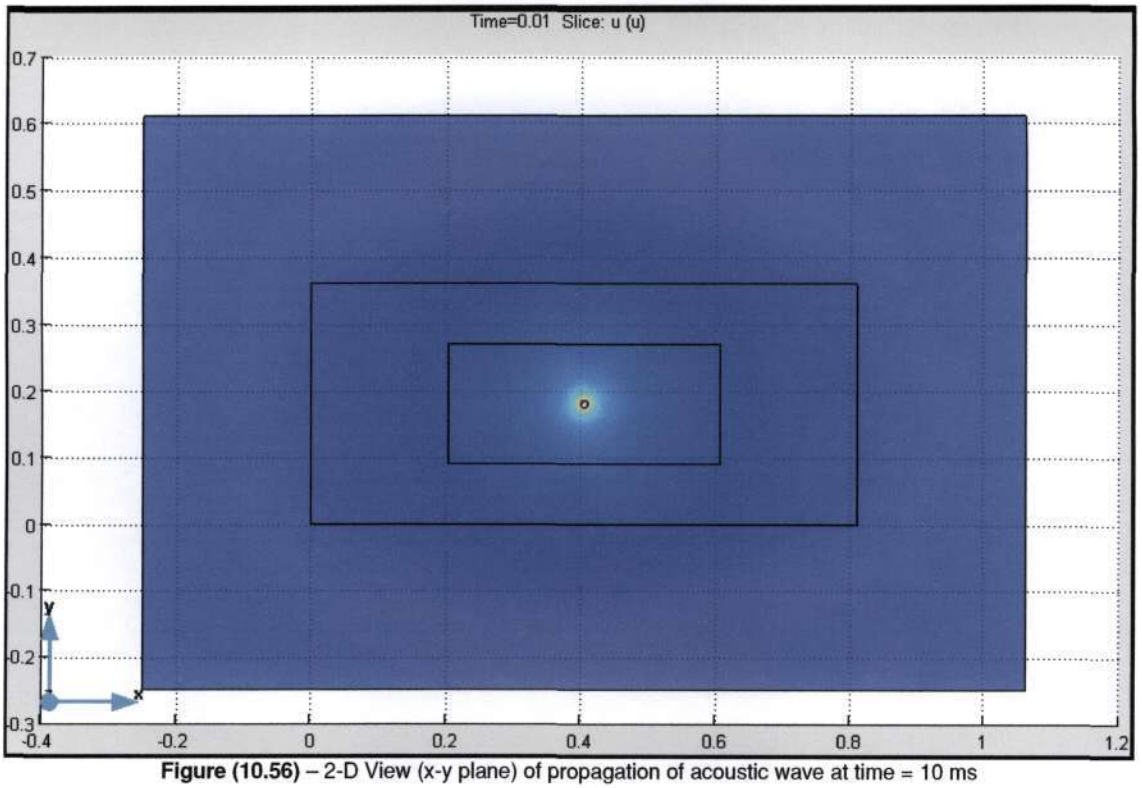

Figure (10.56) – 2-D View (x-y plane) of propagation of acoustic wave at time = 10 ms

Waveforms obtained from cross-sectional plots at each of the sensor positions:
The following plots were taken on the y-plane (sensor 1 and sensor 2):

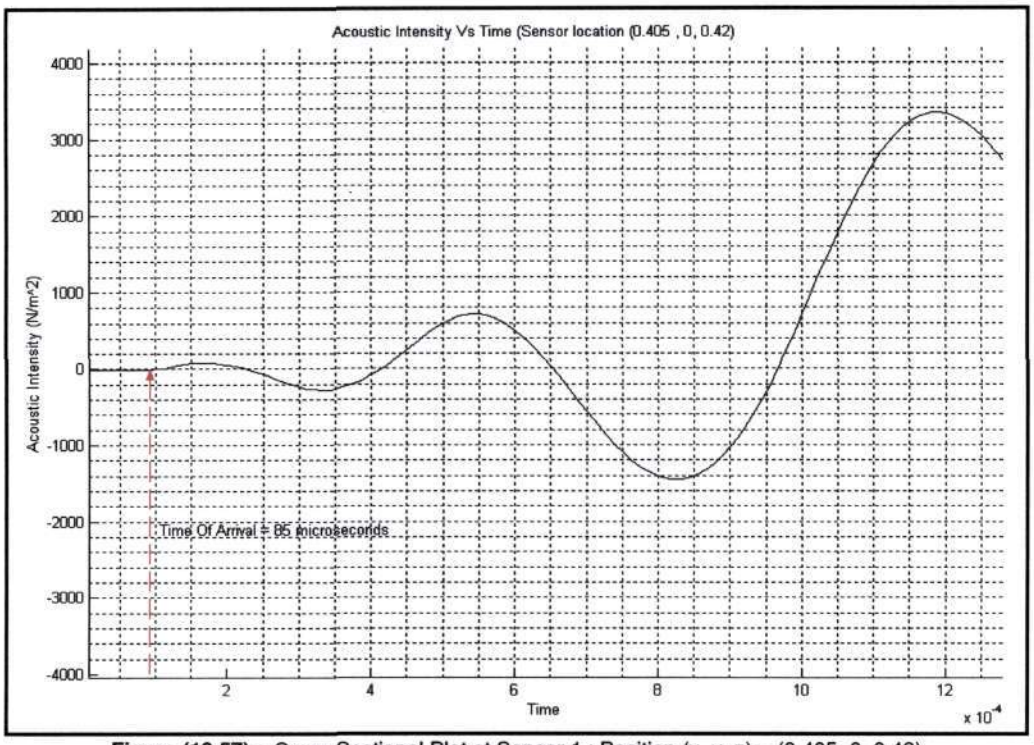

Figure (10.57) – Cross Sectional Plot at Sensor 1 : Position (x, y, z) = (0.405, 0, 0.42)

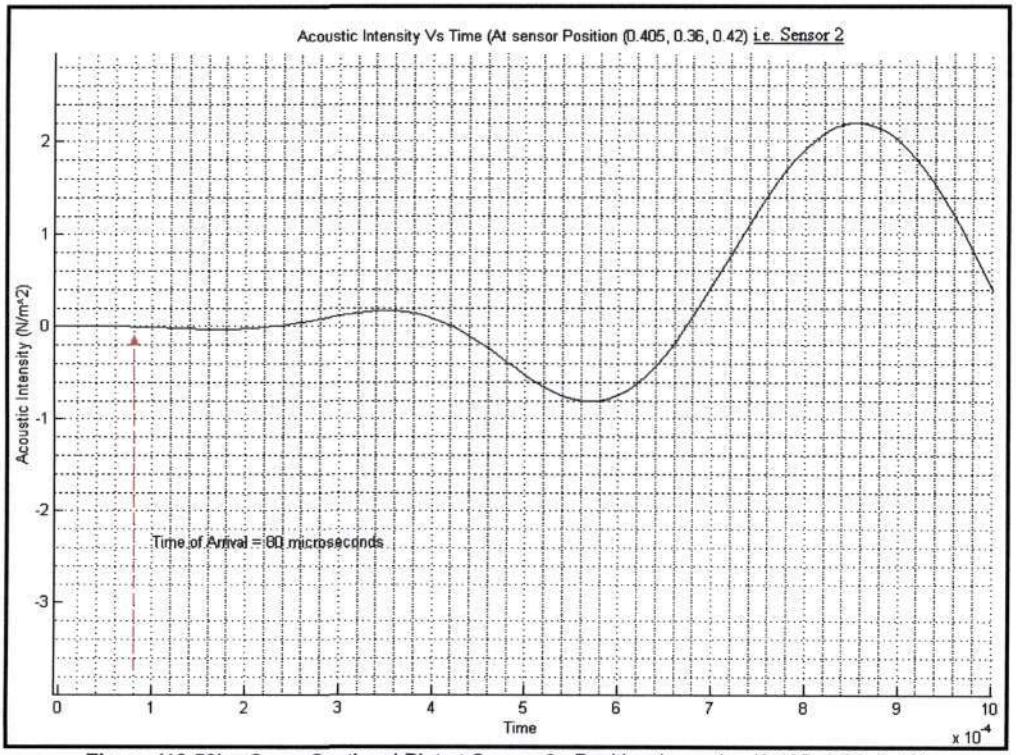

Figure (10.58) – Cross Sectional Plot at Sensor 2 : Position (x, y, z) = (0.405, 0.36, 0.42)

Analysis Of Results Obtained on the y-plane: Localisation Calculations

Figure (10.57), depicts that the time taken for the acoustic signal to reach sensor 1, is 85μs. The speed of sound in transformer oil is 1400 m/s and the speed of sound in the iron core is 5800 m/s (from literature). The following calculations are aimed at attaining the predicted location of the partial discharge source on the y-plane:

Time taken for signal to propagate through the transformer oil region:

Note: As discussed previously, the distance of the transformer oil region below the iron core is known to be 0.09 m (known from construction of model).

$$t_{oil} = \frac{dis\tan ce_{oil}}{speed_{oil}} = \frac{0.09m}{1400m/s} = 64.29\mu s$$

Now, that the time taken for the signal to travel only through the transformer oil is known, this implies that the time for the signal to propagate through the iron core may be calculated as:

$$t_{iron-core} = t_{total} - t_{oil} = 85\mu s - 64.29\mu s = \mathbf{20.71\mu s}$$

Now, that the time taken for the acoustic signal to propagate through the iron-core is known, the distance traveled in the core may be ascertained from:

$$dis\tan ce_{core} = speed_{core} \times t_{iorn-core} = 5800m/s \times 20.71\mu s = \mathbf{0.12m}$$

To quote this distance in terms of the reference frame, the predicted location of the partial discharge source in the y-plane is (y co-ordinate of iron-core) + (distance traveled in core) = (0.09m + 0.12m)
= 0.21 m

Now, to consider the information received from sensor 2. Figure (10.58), depicts that the time taken for the acoustic signal to reach sensor 2, is 80μs. The following calculations are aimed at attaining the second predicted location of the partial discharge source on the y-plane
(**Note**: The use of more than 1 sensor is aimed at improving the accuracy of the localization technique):

Time taken for signal to propagate through the transformer oil region:

Note: As discussed previously, the distance of the transformer oil region above the iron core is known to be 0.09 m (known from construction of model).

$$t_{oil} = \frac{dis\tan ce_{oil}}{speed_{oil}} = \frac{0.09m}{1400m/s} = 64.29\mu s$$

Now, that the time taken for the signal to travel only through the transformer oil is known, this implies that the time for the signal to propagate through the iron core may be calculated as:

$$t_{iron-core} = t_{total} - t_{oil} = 80\mu s - 64.29\mu s = \mathbf{15.71\mu s}$$

Now, that the time taken for the acoustic signal to propagate through the iron-core is known, the distance traveled in the core may be ascertained from:

$$dis\tan ce_{core} = speed_{core} \times t_{iorn-core} = 5800m/s \times 15.71\mu s = \mathbf{0.09m}$$

To quote this distance in terms of the reference frame, the second predicted location of the partial discharge source in the y-plane is (y co-ordinate of iron-core) – (distance traveled in core) = (0.27m – 0.09m)
= **0.18 m**

Combination of results of sensor 1 and sensor 2:

The predicted range within which the partial discharge exists is: **(0.21m < y < 0.18m)**.

The actual location of the partial discharge source in the y-plane is **y = 0.18**.

Summary: The predicted location of the partial discharge source in the y-plane correlates well with the actual location.

The following plots were taken on the x-plane (sensor 3 and sensor 4):

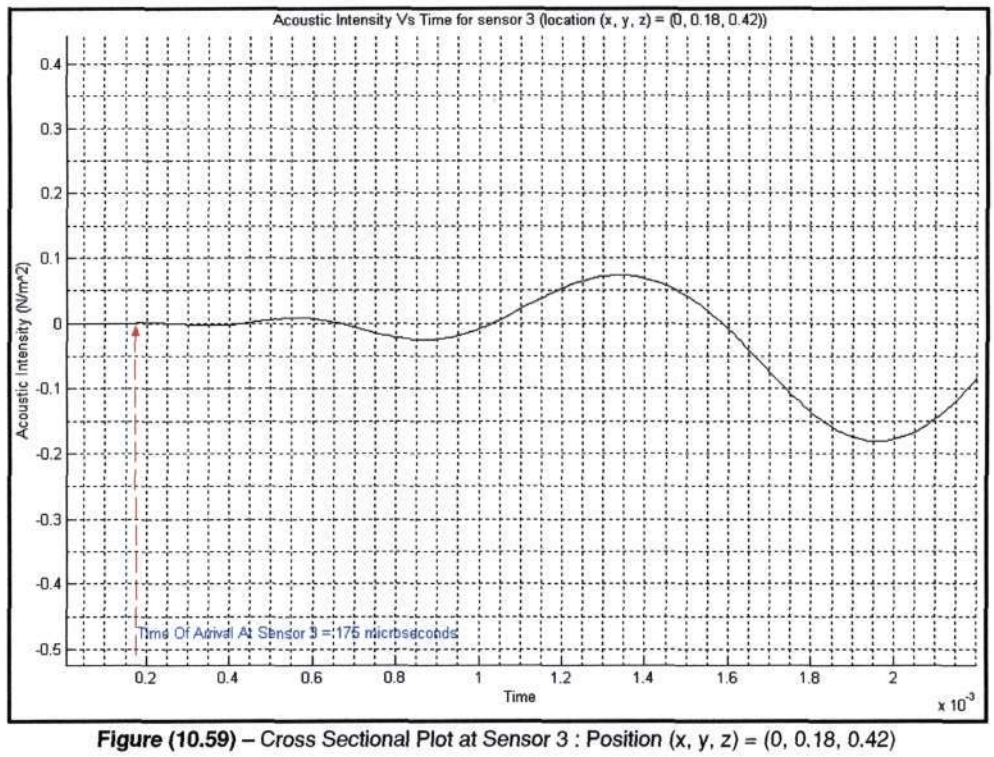

***Figure* (10.59)** – *Cross Sectional Plot at Sensor 3 : Position (x, y, z) = (0, 0.18, 0.42)*

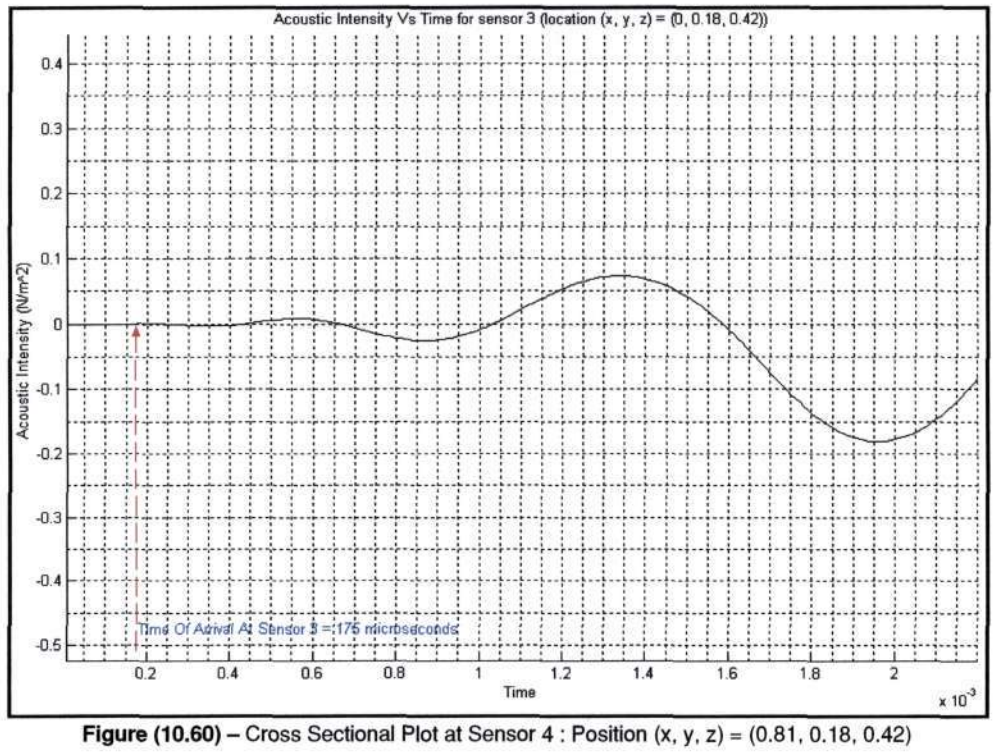

Figure (10.60) – Cross Sectional Plot at Sensor 4 : Position (x, y, z) = (0.81, 0.18, 0.42)

Analysis Of Results Obtained on the x-plane – Localisation Calculations

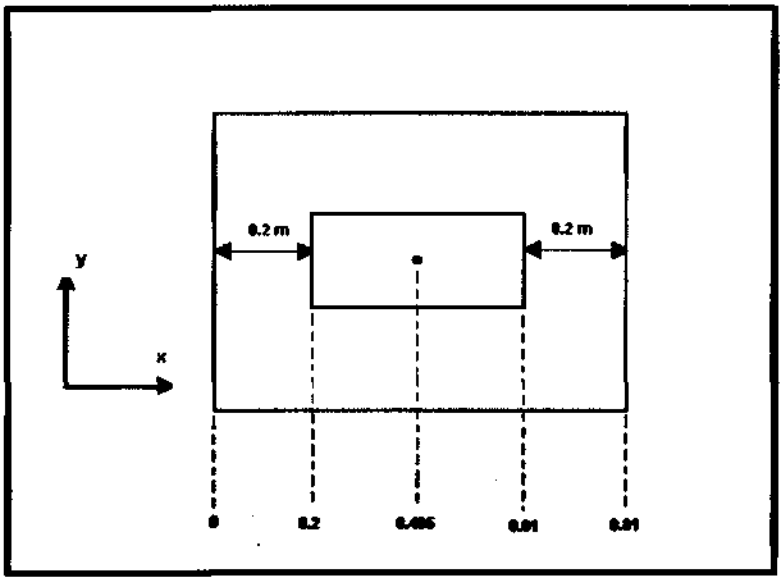

Figure (10.61) – View of Geometry on XY plane

Figure (10.59), depicts that the time taken for the acoustic signal to reach sensor 3, is 175μs. The following calculations are aimed at attaining the predicted location of the partial discharge source on the x-plane:

Time taken for signal to propagate through the transformer oil region:

Note: As discussed previously, the distance of the transformer oil region to the left the iron core is known to be 0.2 m (see figure 10.61).

$$t_{oil} = \frac{dis\tan ce_{oil}}{speed_{oil}} = \frac{0.2m}{1400m/s} = 142.86\mu s$$

Now, that the time taken for the signal to travel only through the transformer oil is known, this implies that the time for the signal to propagate through the iron core may be calculated as:

$$t_{iron-core} = t_{total} - t_{oil} = 175\mu s - 142.86\mu s = \mathbf{32.14\mu s}$$

Now, that the time taken for the acoustic signal to propagate through the iron-core is known, the distance traveled in the core may be ascertained from:

$$dis\tan ce_{core} = speed_{core} \times t_{iom-core} = 5800m/s \times 32.14\mu s = \mathbf{0.186m}$$

To quote this distance in terms of the reference frame, the predicted location of the partial discharge source in the x-plane is (x co-ordinate of iron-core) + (distance traveled in core) = (0.2m + 0.186m)
= 0.386 m

Now, to consider the information received from sensor 4. Figure (10.60), depicts that the time taken for the acoustic signal to reach sensor 4, is 170μs. The following calculations are aimed at attaining the second predicted location of the partial discharge source on the x-plane.

Time taken for signal to propagate through the transformer oil region:

Note: As discussed previously, the distance of the transformer oil region to the right of the iron core is known to be 0.2 m (known from construction of model).

$$t_{oil} = \frac{dis\tan ce_{oil}}{speed_{oil}} = \frac{0.2m}{1400m/s} = 142.86\mu s$$

Now, that the time taken for the signal to travel only through the transformer oil is known, this implies that the time for the signal to propagate through the iron core may be calculated as:

$$t_{iron-core} = t_{total} - t_{oil} = 170\mu s - 142.86\mu s = \mathbf{27.14\mu s}$$

Now, that the time taken for the acoustic signal to propagate through the iron-core is known, the distance traveled in the core may be ascertained from:

$$dis\tan ce_{core} = speed_{core} \times t_{iorn-core} = 5800m/s \times 27.14\mu s = \mathbf{0.157m}$$

To quote this distance in terms of the reference frame, the second predicted location of the partial discharge source in the x-plane is:
= (x co-ordinate of iron-core) – (distance traveled in core)
= (0.61m – 0.157m)
= **0.453 m**

Combination of results of sensor 3 and sensor 4:

The predicted range within which the partial discharge exists is: **(0.386m < x < 0.453m)**.

The actual location of the partial discharge source in the x-plane is **x = 0.405 m**

Summary: The predicted location of the partial discharge source in the x-plane correlates well with the actual location.

The following plots were taken on the z-plane (sensor 5 and sensor 6):

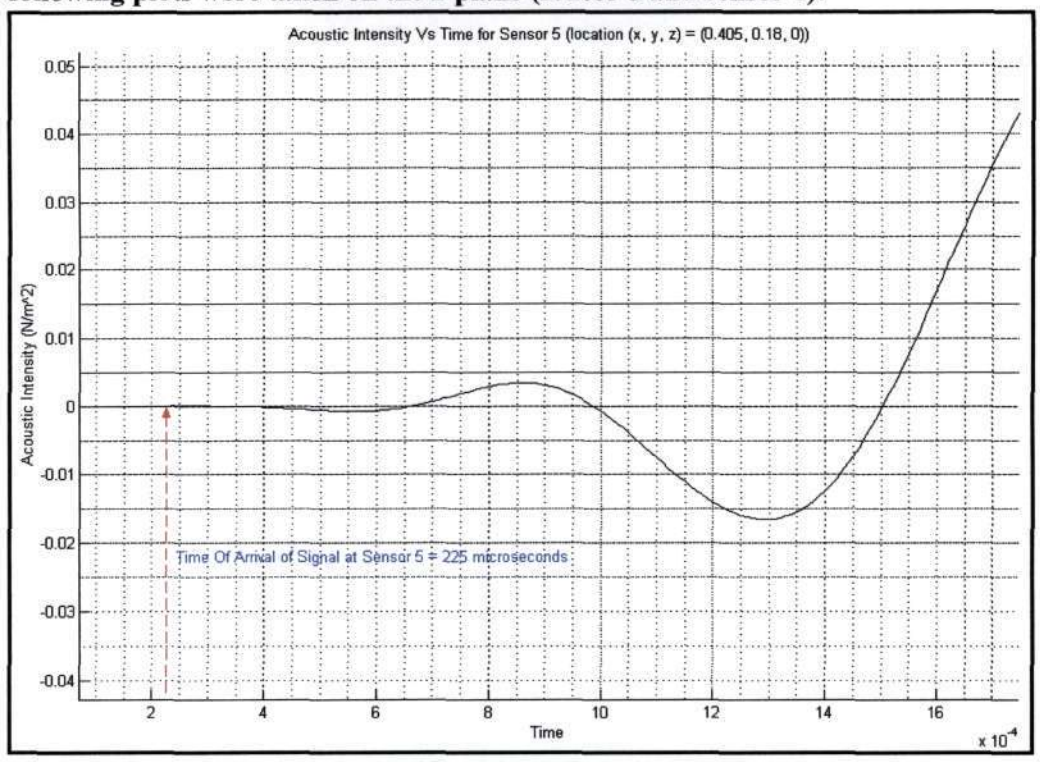

Figure (10.62)- Cross Sectional Plot at Sensor 5 : Position (x, y, z) = (0.405, 0.18, 0)

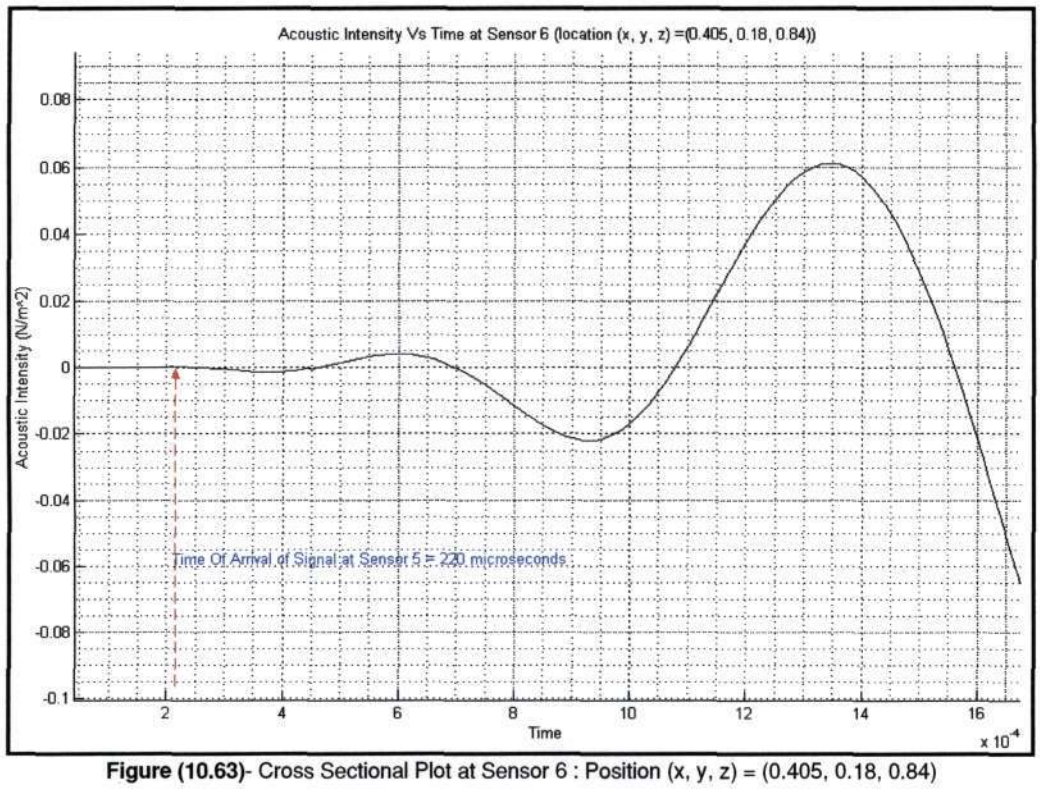

Figure (10.63)- Cross Sectional Plot at Sensor 6 : Position (x, y, z) = (0.405, 0.18, 0.84)

Analysis Of Results Obtained on the z-plane – Localisation Calculations

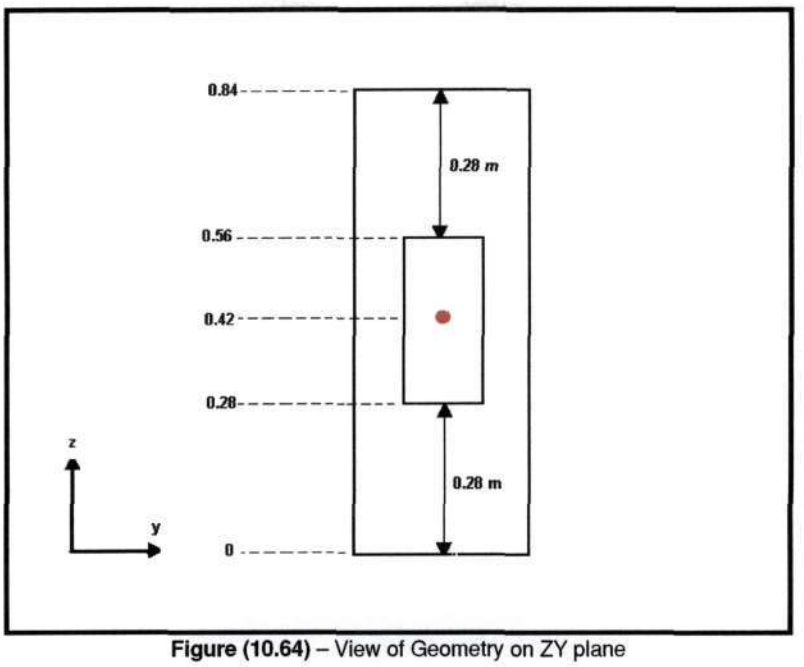

Figure (10.64) – View of Geometry on ZY plane

Figure (10.62), depicts that the time taken for the acoustic signal to reach sensor 5, is 225μs. The following calculations are aimed at attaining the predicted location of the partial discharge source on the z-plane:

Time taken for signal to propagate through the transformer oil region:

Note: As discussed previously, the distance of the transformer oil region below the iron core is known to be 0.28 m (see figure 10.64).

$$t_{oil} = \frac{dis\tan ce_{oil}}{speed_{oil}} = \frac{0.28m}{1400m/s} = 200\mu s$$

Now, that the time taken for the signal to travel only through the transformer oil is known, this implies that the time for the signal to propagate through the iron core may be calculated as:

$$t_{iron-core} = t_{total} - t_{oil} = 225\mu s - 200\mu s = \mathbf{25\mu s}$$

Now, that the time taken for the acoustic signal to propagate through the iron-core is known, the distance traveled in the core may be ascertained from:

$$dis\tan ce_{core} = speed_{core} \times t_{iorn-core} = 5800m/s \times 25\mu s = \mathbf{0.14m}$$

To quote this distance in terms of the reference frame, the predicted location of the partial discharge source in the x-plane is:
= (x co-ordinate of iron-core) + (distance traveled in core)
= (0.28m + 0.14m)
= **0.42 m**

Now, to consider the information received from sensor 6. Figure (10.63), depicts that the time taken for the acoustic signal to reach sensor 6, is 220μs. The following calculations are aimed at attaining the second predicted location of the partial discharge source on the z-plane.

Time taken for signal to propagate through the transformer oil region:

Note: As discussed previously, the distance of the transformer oil region above the iron core is known to be 0.28 m (known from construction of model).

$$t_{oil} = \frac{dis\tan ce_{oil}}{speed_{oil}} = \frac{0.28m}{1400m/s} = 200\mu s$$

Now, that the time taken for the signal to travel only through the transformer oil is known, this implies that the time for the signal to propagate through the iron core may be calculated as:

$$t_{iron-core} = t_{total} - t_{oil} = 220\mu s - 200\mu s = \mathbf{20\mu s}$$

Now, that the time taken for the acoustic signal to propagate through the iron-core is known, the distance traveled in the core may be ascertained from:

$$dis\tan ce_{core} = speed_{core} \times t_{iorn-core} = 5800m/s \times 20\mu s = \mathbf{0.116m}$$

To quote this distance in terms of the reference frame, the second predicted location of the partial discharge source in the x-plane is:
= (x co-ordinate of iron-core) – (distance traveled in core)
= (0.56m – 0.116m)
= **0.44 m**

Combination of results of sensor 5 and sensor 6:

The predicted range within which the partial discharge exists is: **(0.42m < z < 0.44m)**.

The actual location of the partial discharge source in the x-plane is **z = 0.42 m**

Summary: The predicted location of the partial discharge source in the z-plane correlates well with the actual location.

Summary Of Model 7:

The actual spatial position of the p.d. source is (x, y, z) = (0.405, 0.18, 0.42).

The following results were obtained from each of the sensor positions:
Sensor 1: y = 0.21
Sensor 2: y = 0.18
Sensor 3: x = 0.386
Sensor 4: x = 0.453
Sensor 5: z = 0.42
Sensor 6: z = 0.44

The predicted spatial location of the p.d. source (in terms of the co-ordinate) system used is:

x = (0.386 < x < 0.453)
y = (0.18 < y < 0.21)
z = (0.42 < z < 0.44)

The predicted spatial location of the partial discharge is a good approximation of the actual position.

10.5.3 Model 8 - Transformer Geometry Identical To Distribution Transformer

Model 8 was constructed to closely resemble one of the distribution transformers located in the H.V. laboratory. This distribution transformer is investigated further in section C (Experimental testing). The geometrical construction of model 8 is depicted below:

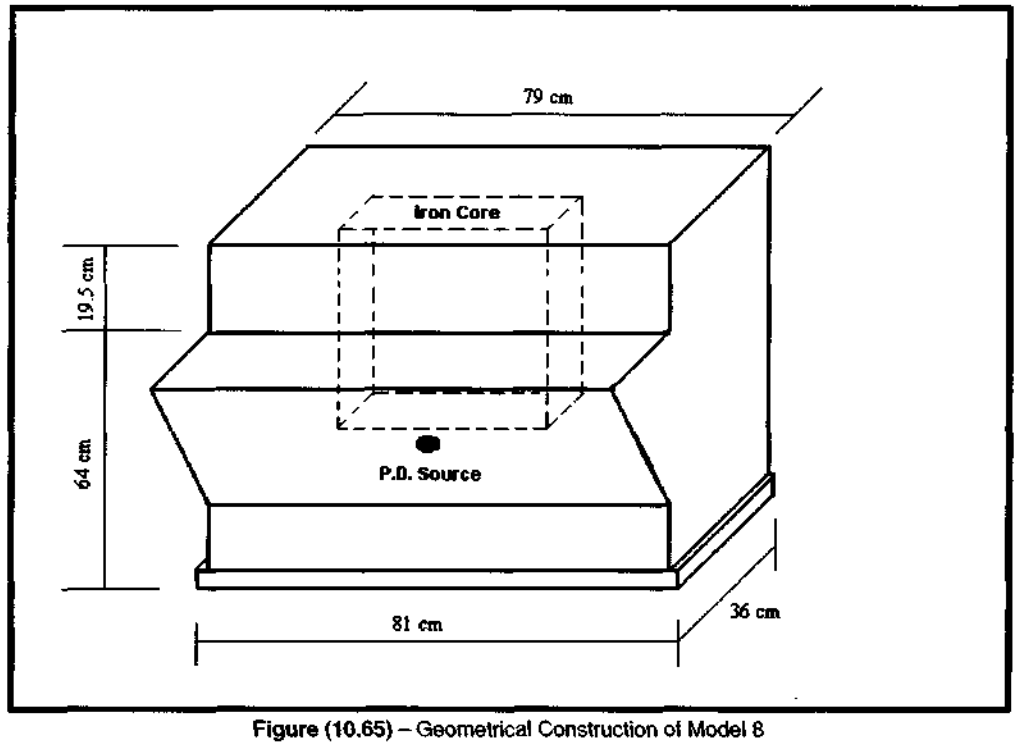

Figure (10.65) – Geometrical Construction of Model 8

An iron core was included in the model. Note, the position of the partial discharge source is approximately located in the region where the point-to-sphere gap configuration is present in the test transformer. The dimensions of the model were obtained from the actual test transformer.

This model consists of the following subdomain regions:

- Outer air region.
- Transformer Oil region.
- Iron Core region.

The boundary conditions, which were specified, had to cater for the fact that the iron core and the steel wall attenuate the signal (both reflective and absorptive media). In order to set the necessary conditions, the following boundary conditions were utilized:

- The value of the function was specified to be zero on the outer extremities of the air boundary, using the Dirichlet boundary condition. This was done, because this region lies far beyond the region where the measurements will be taken (i.e. on the tank wall). During the construction phase of the model, this outer boundary was constructed a fair distance away from the actual transformer tank, in order to achieve a more realistic view of the behavior of the acoustic wave as it impinges onto the steel/air interface.
- The boundaries of the iron core, were set to be attenuating using the Neumann condition. The variable q was set to be greater than g, in order to allow for the transmission of energy across the boundary.
- The transformer tank wall was specified to be absorptive as well as reflective. This was implemented using the Neumann boundary condition, with the variable $q > g$. This condition specifies that some incident energy will be transmitted through the boundary, and some energy will be reflected.

- The partial discharge (i.e. point source), was specified to emit an acoustic wave, of constant magnitude of 100 N/m^2 for all time. This was specified with the Dirichlet boundary condition.

The speed of sound in the different media (from literature) was specified in the subdomain settings as:

- Speed of sound in the outer air region : 333.33 m/s
- Speed of sound in transformer oil region: 1400 m/s
- Speed of sound in iron core region : 5800 m/s

The model was meshed using the most accurate mesh, which could be solved on the system. The simulation was executed utilizing an iterative solver, with a step size of 10μs and a total simulation time of 20 milliseconds. All significant stages in the simulation process are depicted below:

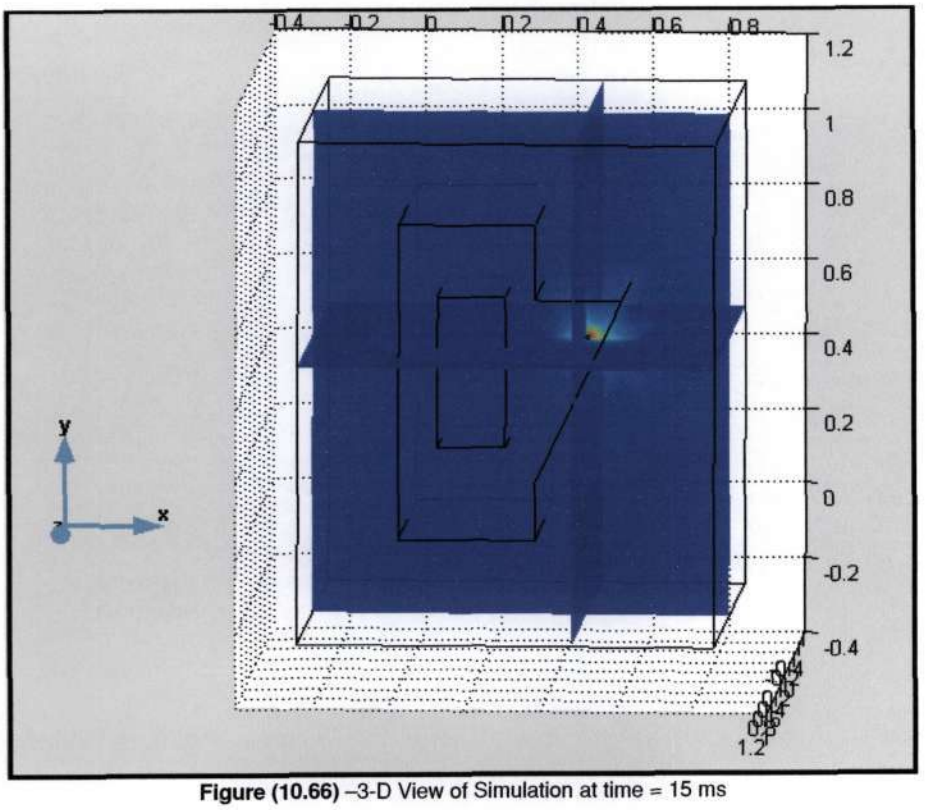

Figure (10.66) –3-D View of Simulation at time = 15 ms

View on the xy Plane

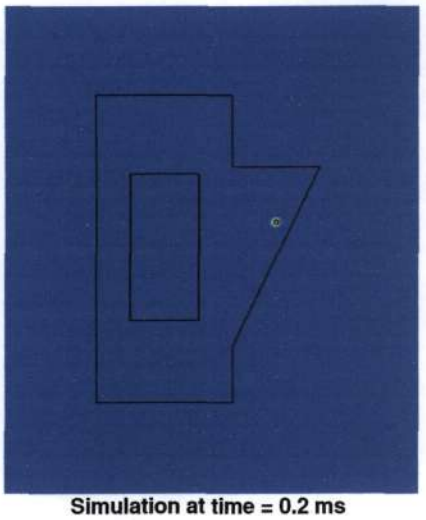

Simulation at time = 0.2 ms

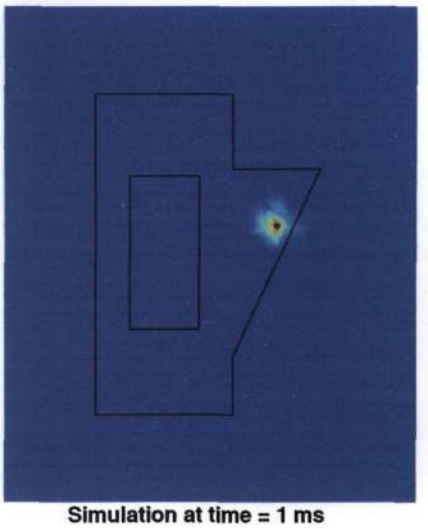

Simulation at time = 1 ms

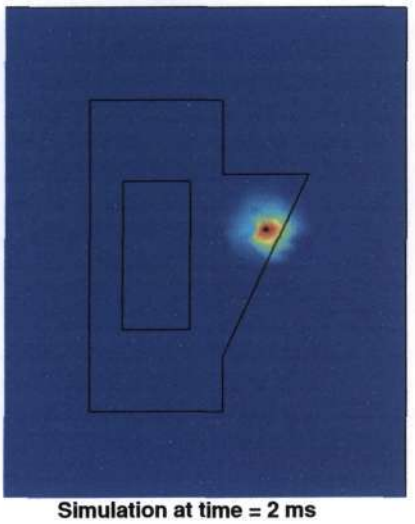

Simulation at time = 2 ms

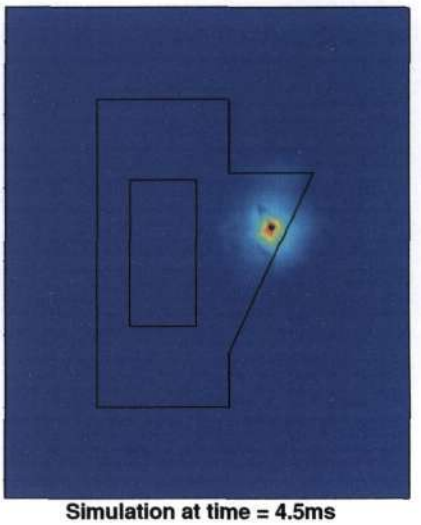

Simulation at time = 4.5ms

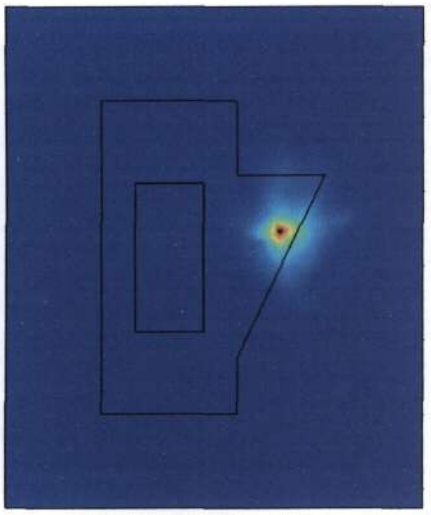

Simulation at time = 10 ms

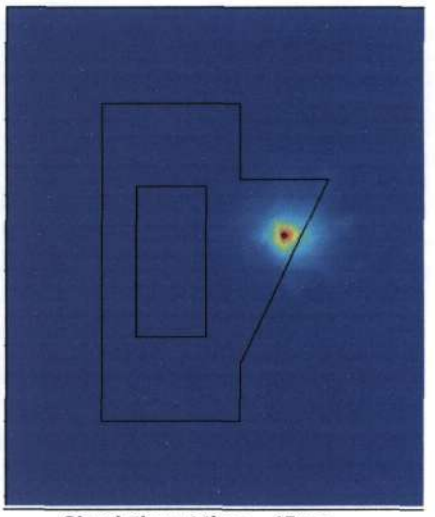

Simulation at time = 15 ms

Sensor Placement:

In order to implement the acoustic method of p.d. detection and localization, acoustic sensors were placed at various locations around the tank in order to triangulate and determine the spatial position of the p.d. source. Note, the sensors were placed in the direct line between the p.d. source and the steel wall, in order to achieve a high degree of accuracy in the triangulation technique. In practice, the user would not know immediately where the direct line is, so the sensor position would have to be varied until the shortest arrival time of the acoustic signal is attained. This position of the sensor would almost certainly have to be the direct line between the p.d. source and the tank wall (shortest distance traveled by signal therefore shortest time).

Analysis Of Waveforms Obtained from Cross-sectional Plots at Sensor Locations

X-Plane

The following sections deal with sensor 1 and sensor 2, which are utilized in order to determine the predicted x-coordinate of the partial discharge. The following diagram depicts the layout of the model in the XY plane. The co-ordinates shown below are used in the localization method.

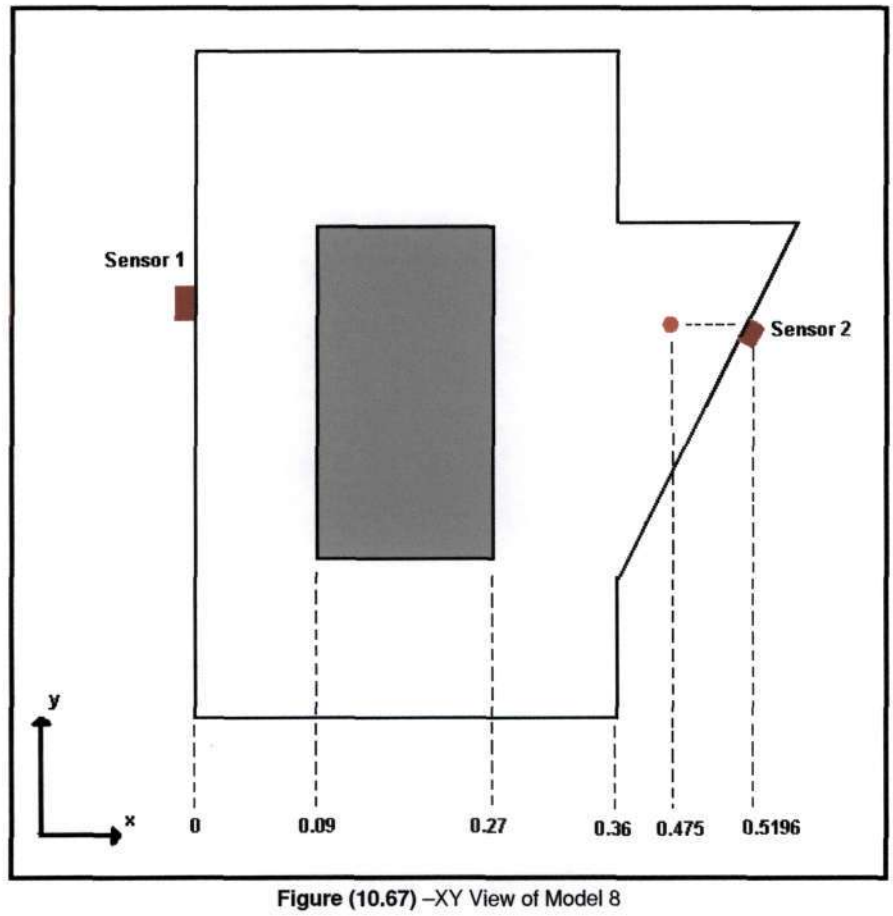

Figure (10.67) –XY View of Model 8

Sensor 1:

The following plot at sensor position 1, was attained:

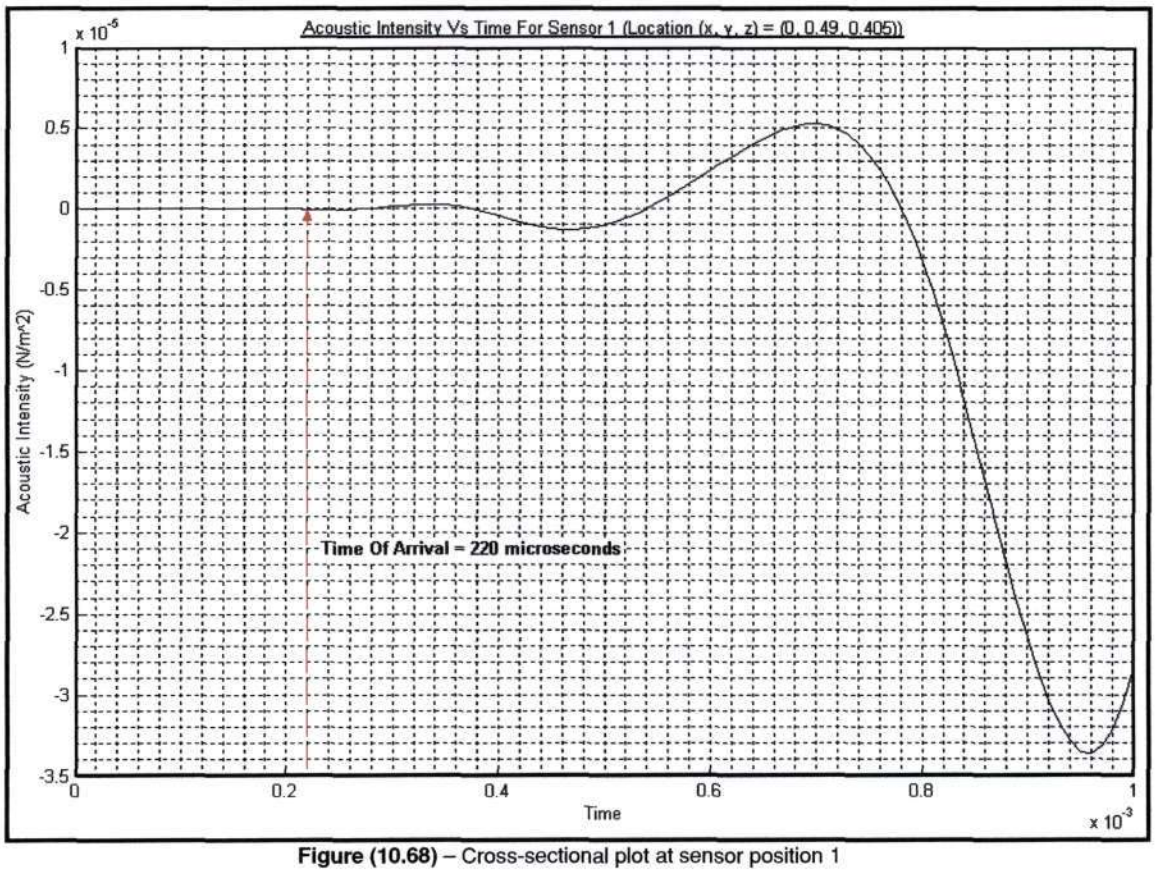

Figure (10.68) – Cross-sectional plot at sensor position 1

Localization Calculations:

As noted from figure (10.68), the acoustic signal reaches sensor 1 (location (x, y, z) = (0,0.49,0.405)), after 220 μs. Note, that the sensor has been placed in the direct line between the p.d. source and the tank wall. Practically, the direct line can be found by moving the sensor along the tank wall, until the position where the signal takes the shortest time to reach the sensor is found. This position lies in the direct line.

The following calculations are aimed at attaining the predicted location of the p.d. source on the x-plane:

- The time taken for an acoustic signal to propagate through the oil region which lies to the left of the iron core is:

$$t_{oil\_left} = \frac{dis\tan ce_{oil\_left}}{speed_{oil}} = \frac{0.09m}{1400m/s} = 64.29\mu s$$

Note, that the time taken for an acoustic signal to propagate through the oil region to the left of the iron core is 64.29 μs. The total time taken for the signal to propagate to sensor 1, is 220 μs (from figure 10.68). This time is greater than 64.29 μs, therefore it can be concluded that the source lies beyond this left oil region.

- The time taken for an acoustic signal to propagate through the iron core region is:

$$t_{iron\_core} = \frac{dis\tan ce_{iron\_core}}{speed_{iron\_core}} = \frac{0.18m}{5800m/s} = 31.03\mu s$$

The combined time for an acoustic signal to propagate through the oil region to the left of the iron core as well as the iron core itself is: 64.29μs + 31.03μs =**95.32μs**. This total time remains however, still lower than the total time detected by sensor 1 (i.e. 220 μs). Therefore it can be concluded that the source lies beyond this iron core region as well. The remaining time that has to be accounted for is 220 μs - 95.32μs = **124.68μs**.

- It is known that only an oil region exists to the right of the iron core. Therefore the p.d. source has to lie in this oil region. This distance/ spatial location of the discharge source in this oil region can be calculated as:

$$dis\tan ce = speed_{oil} \times time = 1400 \times 124.68\mu s = 0.175$$

Using the position of sensor 1 as the reference point, the x-coordinate of the p.d. source can be ascertained as:
0 + 0.09 + 0.18 + 0.175 = **0.445 m**

Summary of Calculations for Sensor 1:

The predicted x-coordinate of the p.d. source using the information attained from sensor 1 is **x = 0.445 m** (using the reference point shown in figure 10.67).

Sensor 2:

The following plot at sensor position 2, was attained:

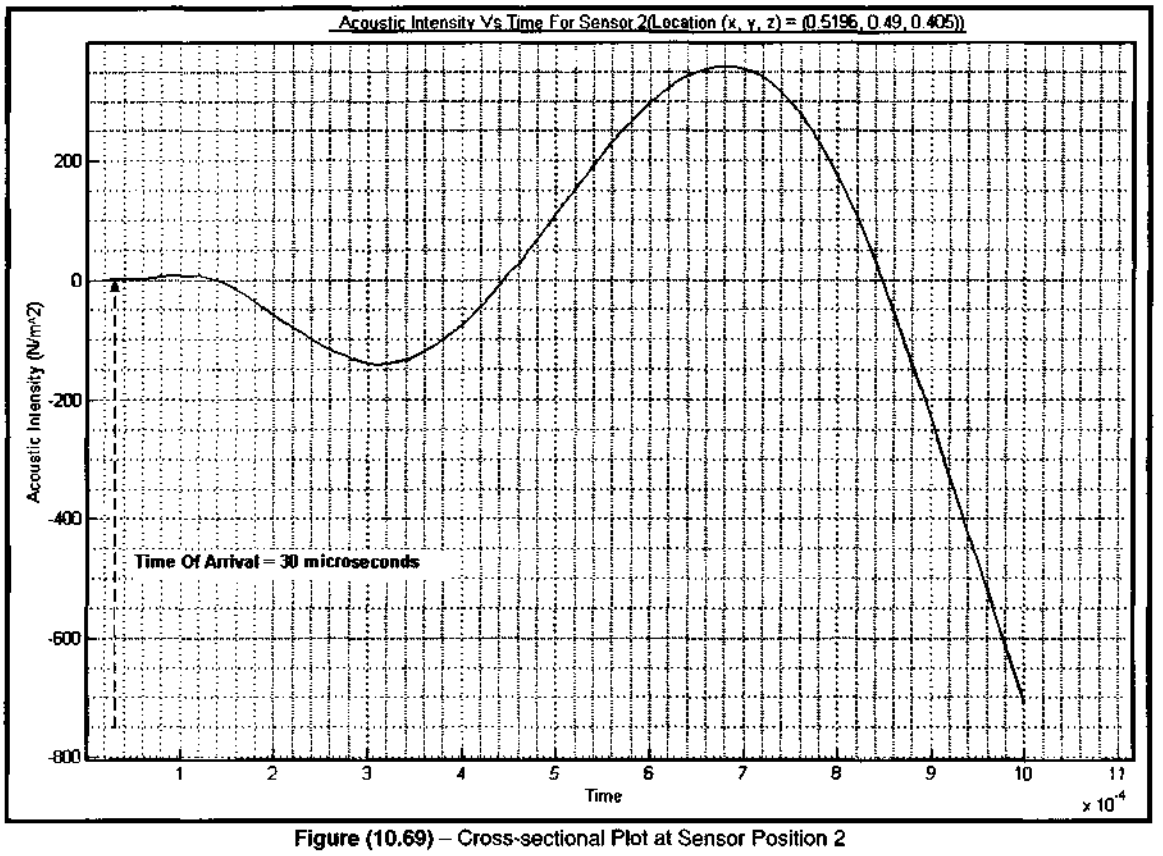

Figure (10.69) – Cross-sectional Plot at Sensor Position 2

Localization Calculations:

As noted from figure (10.69), the acoustic signal reaches sensor 2 (location (x, y, z) = (0.5196, 0.49, 0.405)), after 30 μs. Note, that the sensor has been placed in the direct line between the p.d. source and the tank wall.

The following calculations are aimed at attaining the second predicted location of the p.d. source on the x-plane. This second prediction is aimed at improving the accuracy of the localization method.

- The placement of sensor 2 is to the right of the iron core (as depicted in figure (10.67)). The time taken for an acoustic signal to propagate through the oil region to the right of the iron core is calculated as:

$$t_{oil\_right} = \frac{dis\tan ce_{oil\_right}}{speed_{oil}} = \frac{(0.5196m - 0.27m)}{1400m/s} = 178.29\mu s$$

Therefore, note the time taken for an acoustic signal to propagate through the oil region to the right of the iron core is larger than the time of arrival of the acoustic signal at the sensor. Therefore, it can be concluded that the p.d. source has to lie inside this oil region (to the right of the iron core).

The distance/ spatial location of the discharge source in this oil region can be calculated as:

$$dis\tan ce = speed_{oil} \times time \ = 1400 \times 35\mu s = 0.042$$

Using the position of sensor 2 as the reference point, the x-coordinate of the p.d. source can be ascertained as:

0.5196 – 0.042 = **0.4776 m**

Summary of Calculations for Sensor 2:

The second predicted x-coordinate of the p.d. source using the information attained from sensor 2 is **x = 0.4776 m** (using the reference point shown in figure 10.67).

Summary Of Results for the X-Plane:

The predicted spatial location of the partial discharge on the x-plane is (using the information obtained from sensor 1 and sensor 2) :

$$\mathbf{0.445 < x < 0.4776}$$

Note, the actual x co-ordinate of the partial discharge (as seen in figure (10.67)) is: **x=0.475**. The predicted location correlates well with the actual location.

Y-Plane

The following sections deal with sensor 3 and sensor 4, which are utilized in order to determine the predicted y-coordinate of the partial discharge. The following diagram depicts the layout of the model in the XY plane. The co-ordinates shown below are used in the localization method.

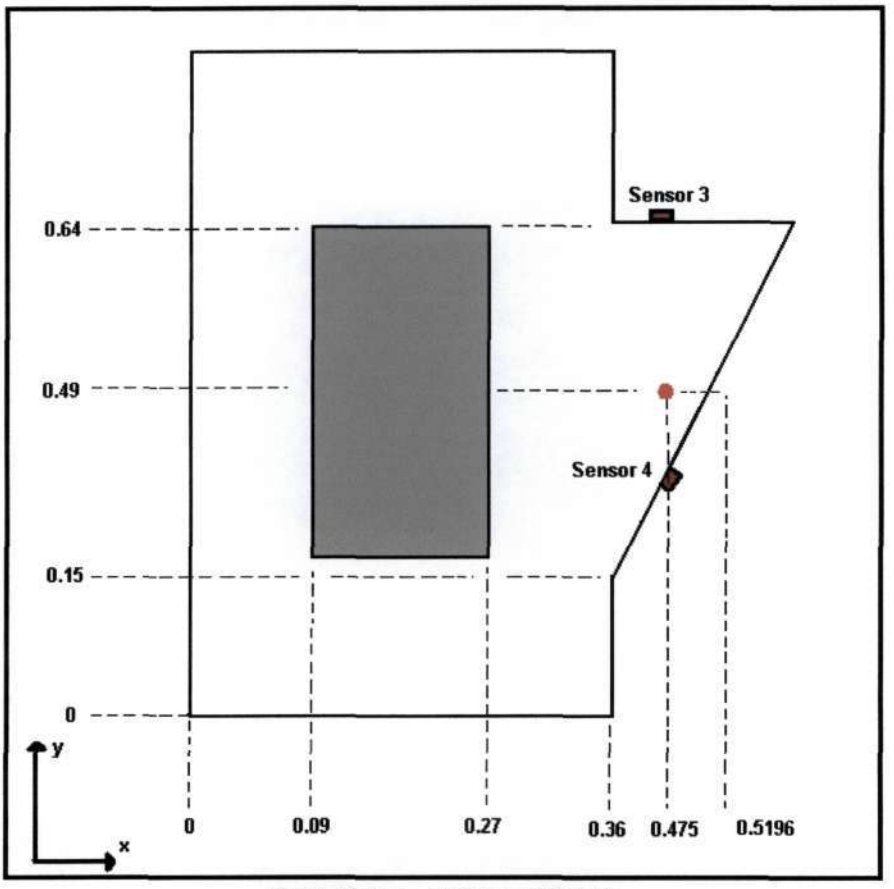

Figure (10.70) – XY view of Model 8

Please see overleaf for the waveform obtained from sensor 3.....

Sensor 3:

The following plot at sensor position 3, was attained:

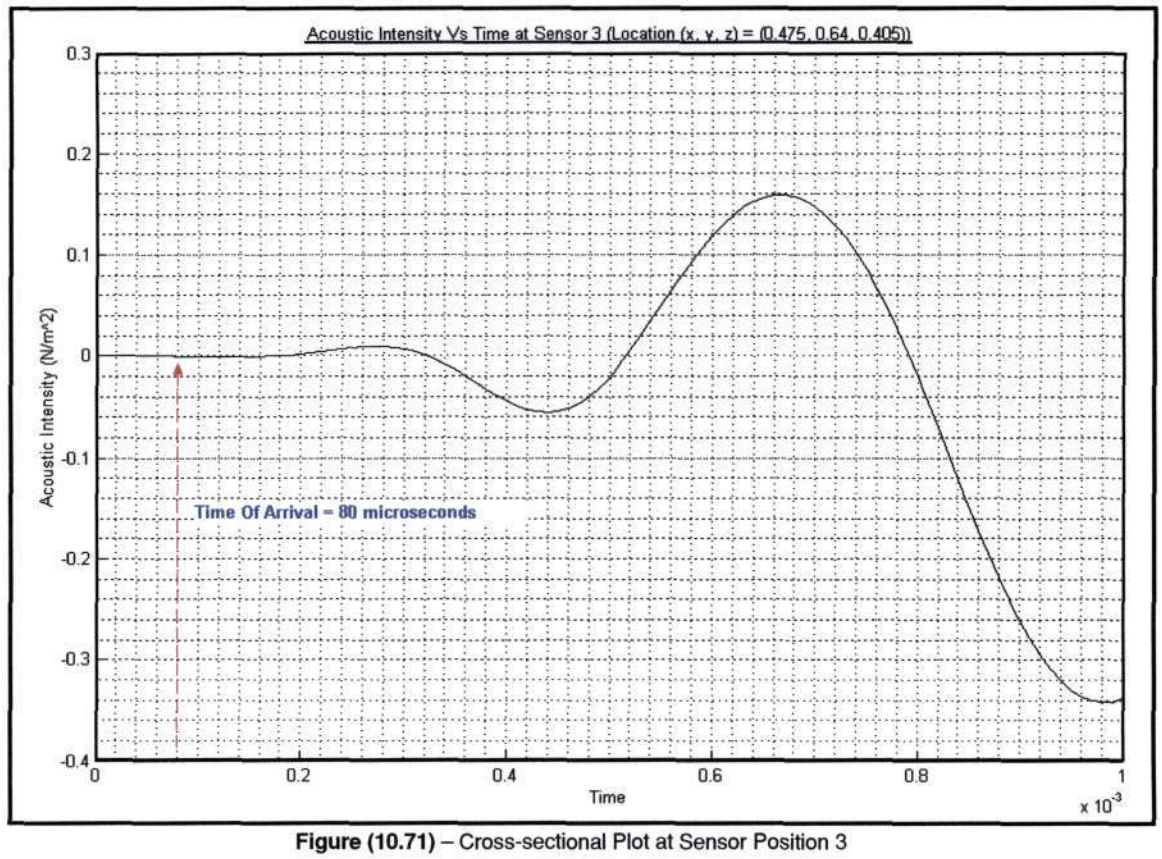

Figure (10.71) – Cross-sectional Plot at Sensor Position 3

Localization Calculations:

As noted from figure (10.71), the acoustic signal reaches sensor 3 (location (x, y, z) = (0.475, 0.64, 0.405)), after 80 μs. Note, that the sensor has been placed in the direct line between the p.d. source and the tank wall.

The following calculations are aimed at attaining the predicted location of the p.d. source on the y-plane.

- Sensor 3 has been placed at an x co-ordinate value of 0.475. This value lies in the predicted range as calculated in the previous calculations for the x-plane. Therefore in practice, once the x co-ordinate range has been ascertained the sensor should be placed within this x-range (preferably in the position in this range where the shortest arrival time is attained i.e. direct line), in order to determine the y co-ordinate range.

- From the geometry (figure 10.70), it is known that for the predicted x co-ordinate range, there is only an oil region present (below sensor 3). Therefore the distance of the p.d. source from sensor 3 can be ascertained as:

  $dis\tan ce = speed_{oil} \times time = 1400m/s \times 80\mu s = 0.113m$

  Using the y co-ordinate of sensor 3 as the reference, the predicted y co-ordinate of the p.d source is:

  0.64 m - 0.113m = **0.527 m**

Summary of Calculations for Sensor 3:

The predicted y-coordinate of the p.d. source using the information attained from sensor 3 is **y = 0.527 m** (using the reference point shown in figure 10.70).

Sensor 4:

The following plot at sensor position 4, was attained:

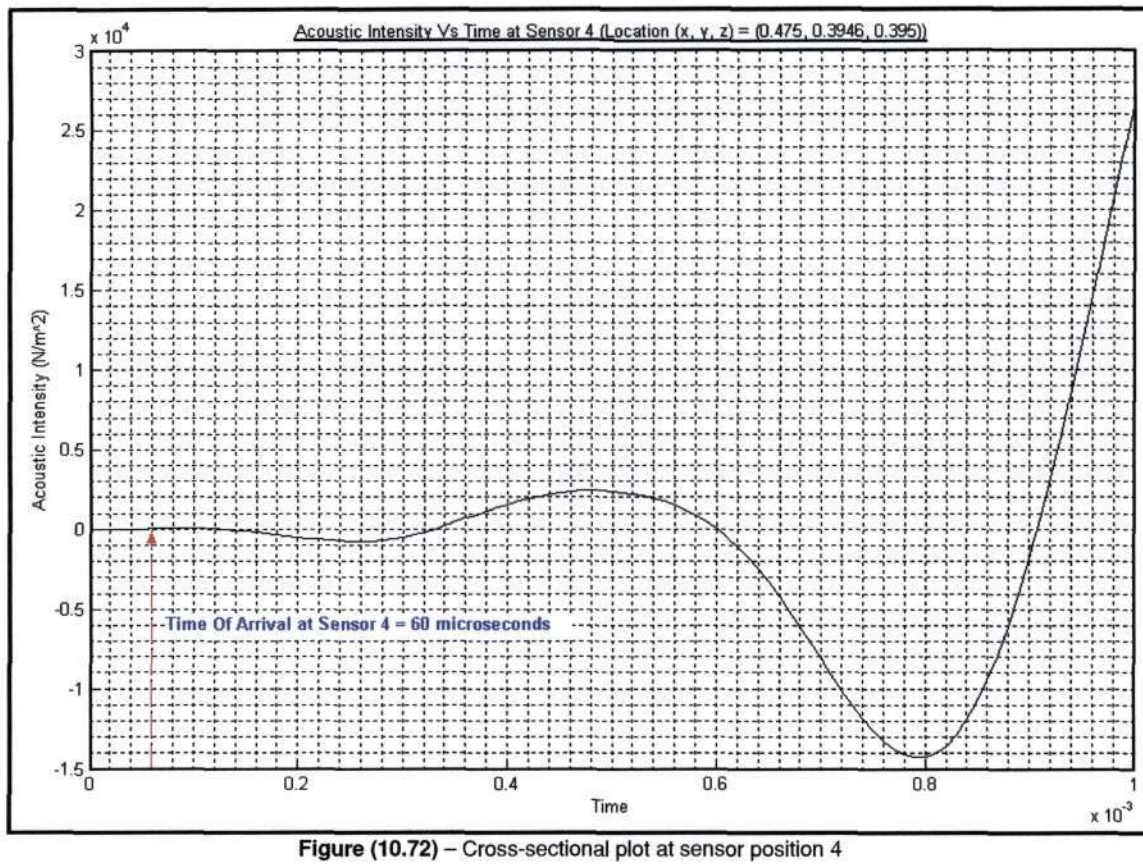

Figure (10.72) – Cross-sectional plot at sensor position 4

Localization Calculations:

As noted from figure (10.72), the acoustic signal reaches sensor 4 (location (x, y, z) = (0.475, 0.3946, 0.405)), after 60 μs. Note, that the sensor has been placed in the direct line between the p.d. source and the tank wall.

The following calculations are aimed at attaining the second predicted location of the p.d. source on the y-plane.

- Sensor 4 has been placed at an x co-ordinate value of 0.475. This value lies in the predicted range as calculated in the previous calculations for the x-plane. The corresponding y co-ordinate for this x co-ordinate which lies on the tank wall of the transformer is y = 0.3946.

- From the geometry (figure 10.70), it is known that for the predicted x co-ordinate range, there is only an oil region present (above sensor 4). Therefore the distance of the p.d. source from sensor 4 can be ascertained as:

  $dis\tan ce = speed_{oil} \times time = 1400m/s \times 60\mu s = 0.084m$

  Using the y co-ordinate of sensor 4 as the reference, the predicted y co-ordinate of the p.d source is:

  0.3946 m + 0.084m = **0.479 m**

Summary of Calculations for Sensor 4:

The second predicted y-coordinate of the p.d. source using the information attained from sensor 4 is **y = 0.479 m** (using the reference point shown in figure 10.70).

Summary Of Results for the Y-Plane:

The predicted spatial location of the partial discharge on the y-plane is (using the information obtained from sensor 3 and sensor 4):

$$\mathbf{0.479 < y < 0.527}$$

Note, the actual y co-ordinate of the partial discharge (as seen in figure (10.70)) is: **y=0.49m**. The predicted location correlates well with the actual location.

Z Plane:

The following sections deal with sensor 5 and sensor 6, which are utilized in order to determine the predicted z-coordinate of the partial discharge. The following diagram depicts the layout of the model in the XZ plane. The co-ordinates shown below are used in the localization method.

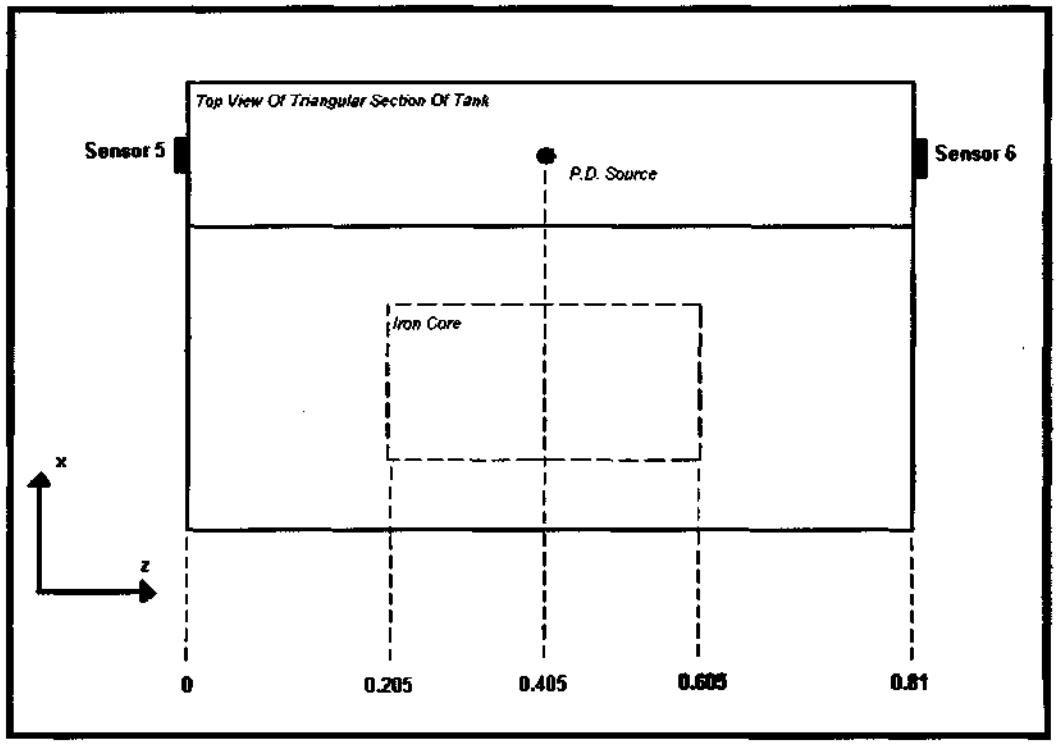

Figure (10.73) – View of Geometry on XZ plane

Note, from the previous sections, the predicted x co-ordinate as well as the predicted y co-ordinate of the p.d. source was calculated. Now, for determining the predicted z co-ordinate of the discharge source, the sensors should be placed along the calculated x and y planes.

Please see overleaf for waveforms obtained from the sensor locations.....

Sensor 5:

The following plot at sensor position 5, was attained:

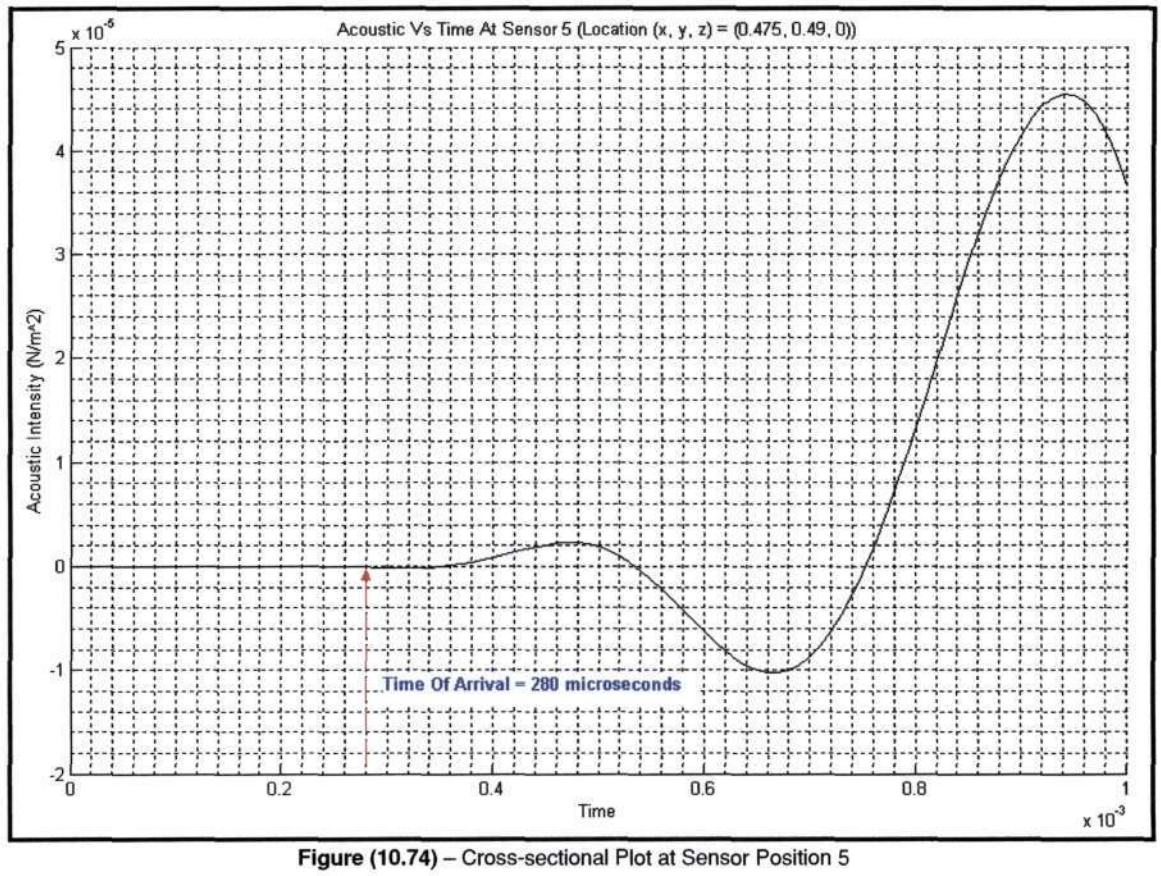

Figure (10.74) – Cross-sectional Plot at Sensor Position 5

Localization Calculations:

As noted from figure (10.74), the acoustic signal reaches sensor 5 (location (x, y, z) = (0.475, 0.49, 0)), after 280 μs. Note, that the sensor has been placed in the direct line between the p.d. source and the tank wall.

The following calculations are aimed at attaining the predicted location of the p.d. source on the z-plane.

- From the geometrical layout of the model (figure (10.73)), it is known that there is only an oil region present in the predicted x and y planes. Therefore, the predicted z co-ordinate of the p.d. source is calculated as follows:

  $dis\tan ce = speed_{oil} \times time = 1400m/s \times 280\mu s = 0.392m$

  Using the z co-ordinate of sensor 5 as the reference, the predicted z co-ordinate of the p.d source is:
  0 m + 0.392m = **0.392 m**

Summary of Calculations for Sensor 5:

The predicted z-coordinate of the p.d. source using the information attained from sensor 5 is **z = 0.392 m** (using the reference point shown in figure 10.73).

Sensor 6:

The following plot at sensor position 6, was attained:

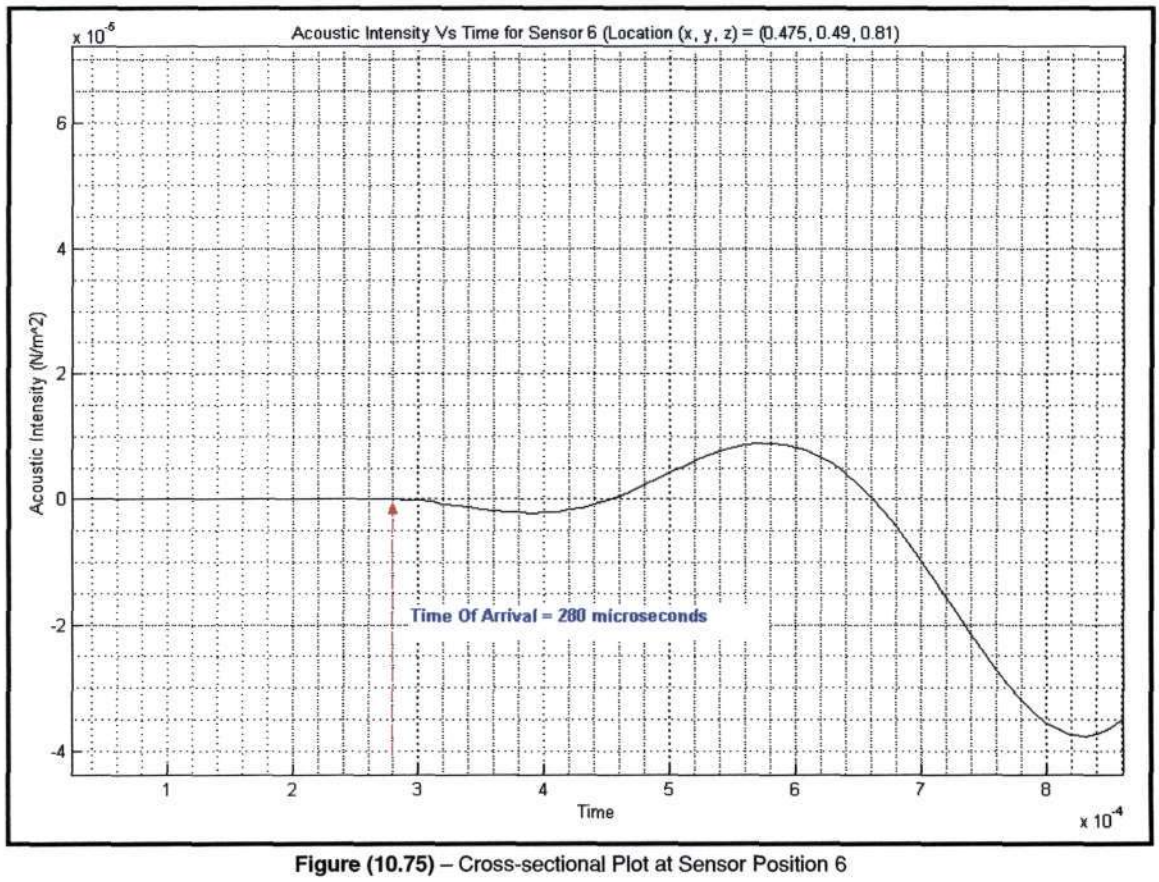

Figure (10.75) – Cross-sectional Plot at Sensor Position 6

Localization Calculations:

As noted from figure (10.75), the acoustic signal reaches sensor 6 (location (x, y, z) = (0.475, 0.49, 0.81)), after 280 μs. Note, that the sensor has been placed in the direct line between the p.d. source and the tank wall.

The following calculations are aimed at attaining the second predicted location of the p.d. source on the z-plane.

- From the geometrical layout of the model (figure (10.73)), it is known that there is also only an oil region present in the predicted x and y planes. Therefore, the predicted z co-ordinate of the p.d. source is calculated as follows:

  $dis\tan ce = speed_{oil} \times time = 1400m/s \times 280\mu s = 0.392m$

  Using the z co-ordinate of sensor 6 as the reference, the predicted z co-ordinate of the p.d source is:

  0.81 m - 0.392m = **0.418 m**

Summary of Calculations for Sensor 6:

The second predicted z-coordinate of the p.d. source using the information attained from sensor 6 is **z = 0.418 m** (using the reference point shown in figure 10.73).

Summary Of Results for the Z-Plane:

The predicted spatial location of the partial discharge on the z-plane is (using the information obtained from sensor 5 and sensor 6) :

$$\mathbf{0.392 < z < 0.418}$$

Note, the actual z co-ordinate of the partial discharge (as seen in figure (10.73)) is: **z=0.405m.** The predicted location correlates well with the actual location.

Summary Of Model 8:

The analysis of the waveforms obtained from each of the sensor positions on the transformer tank, revealed the following predicted spatial location of the p.d. site within the geometry of the transformer:

On the x-plane: **0.445 < x < 0.478** ***Actual Location: x = 0.475***
On the y-plane: **0.479 < y < 0.527** ***Actual Location: y = 0.490***
On the z-plane: **0.392 < z < 0.418** ***Actual Location: z = 0.405***

As shown above, the predicted spatial location of the partial discharge site, correlates well with the actual spatial location.

SECTION C
EXPERIMENTAL TESTING

CHAPTER 11
EXPERIMENTAL TESTING

11.1 Scope

This section describes the test apparatus and the experimental procedures, which were employed whilst experimentally evaluating the dielectric strength of transformer oil as a function of the electrode gap spacing without the presence of any filtering system.

11.2 Test cell design

The test cell design is depicted below:

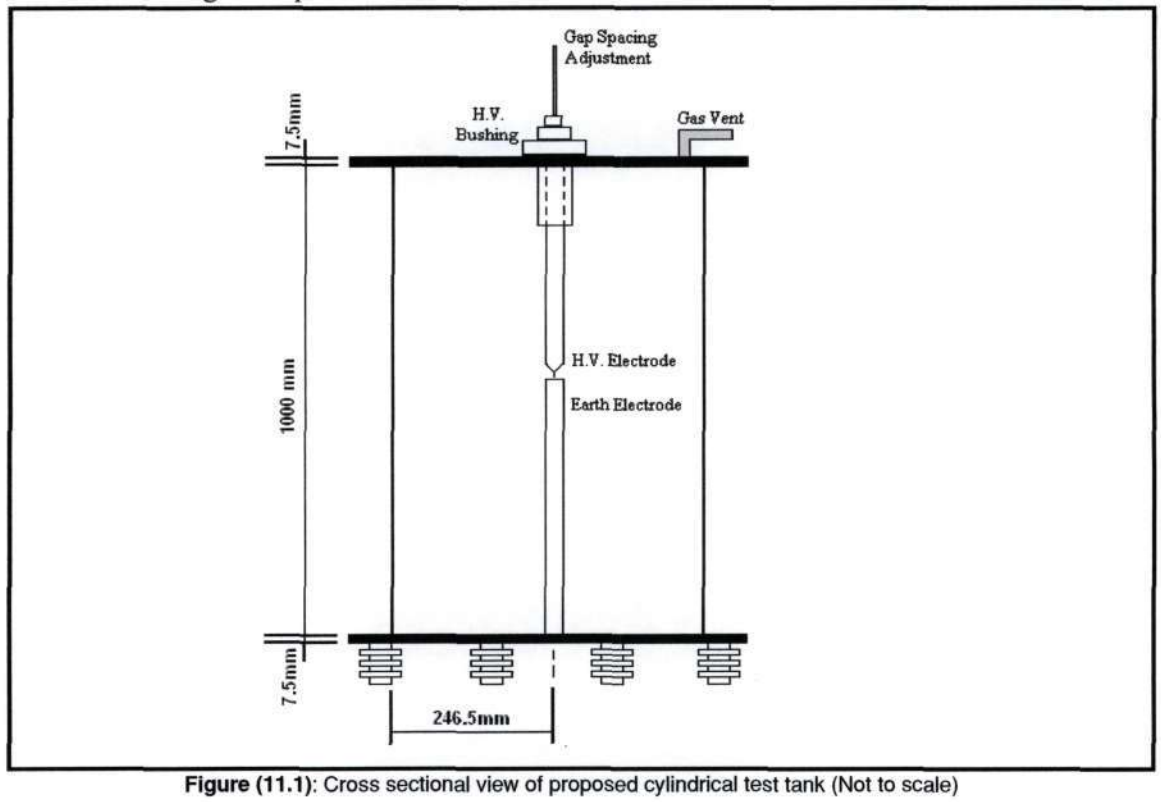

Figure (11.1): Cross sectional view of proposed cylindrical test tank (Not to scale)

11.2.1 Construction materials

The entire tank was constructed using Grade 316 Stainless Steel (4.5mm thickness). The top and bottom of the tank were sealed using various sealing agents and then bolted on. As prescribed in ASTM 3300-00, all materials that were used in the test cell are resistant to, and insoluble in, any of the dielectric test liquids and other cleaning solutions.

A gas vent was designed into the test cell in order to allow for the escape of evolved gas, which forms an inherent part of the electrical breakdown of dielectric liquids.

11.2.2 Test cell dimensions

The dimensions of the test cell have been chosen as follows, in order to ensure that breakdown is limited to the test gap:

	Measurement (mm)
Tank Diameter (excluding flanges)	493
Tank Diameter (including flanges)	563
Length of tank (excluding flanges)	1000
Length of tank (including flanges)	1015

Table (11.1): Test Cell Dimensions

11.2.3 Test electrodes

The electrode configuration utilised for the initial test was a point to plane configuration. This configuration was used so as to localise the discharge initiation near the point by using the field enhancement near the point to induce breakdown at modest voltages. The specifications of the electrodes used were:

- Point electrode: As recommended in ASTM 3300-00, the point electrode utilised was an ordinary steel phonograph needle (0.06mm ± 20% radius of curvature).
- Plane electrode: The plane electrode that was utilised was a polished brass electrode (in accordance with ASTM 3300-00).

The test cell design allowed for easy replacement of the electrodes.

11.3 Dielectric liquid

The test tank was completely filled with the following dielectric liquid (insulating oil) for electrical transformers:

- BP Energol, JS-A (SABS 555). Conforms to IEC 296 (1982) Class 1, British Standard Specification BBS 148 1985 and SABS 555-1985 and carries the mark.[47]

This insulating oil has the following properties[47]:

- High dielectric strength.
- High oxidation resistance.
- Low sludge formation.
- Long service life in condition of frequent spark quenching.
- Low viscosity combined with low volatility. The low viscosity allows for the oil to be circulated easily as well as allowing the oil to penetrate all spaces in the tank. The low volatility minimises the vapour loss.

The following are the typical characteristics[47] of this insulating oil:

			JS-A
Density @ 20°C	kg/l	IP261	0.858
Viscosity @ 20°C	cSt	ASTM D445	30
Viscosity @ -15°C	St	ASTM D445	800
Flash Point PMCC	°C	ASTM D93	160
Pour Point	°C	ASTM D97	-45
Acidity (NV)		IEC 296	0.03
Corrosive Sulphur		ASTM D1275	Non-corrosive
Water Content	mg/kg	Karl Fischer	10
Electrical Strength (Average BDV)	kV	BS 148	50
Loss Tangent (Tan Delta)		BS 148	0.003
Oxidation Stability			
Acidity after oxidation	mgKOH/g	SABS 555	0.2
Sludge after oxidation	%m/m		0.03

Table (11.2) – *Characteristics of BP Energol JS-A*

11.4 Test circuit

The following test circuit was utilized for the experimental testing:

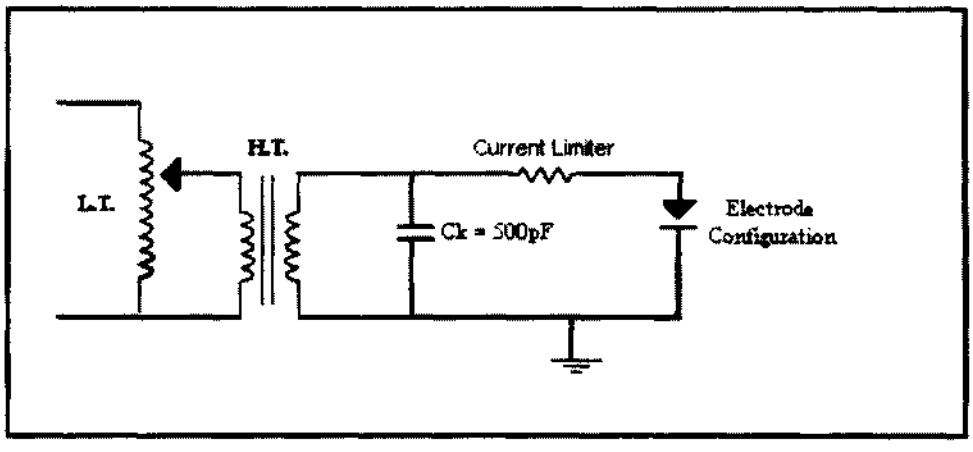

Figure (11.2): Test Circuit

11.5 Test procedure

The tests were conducted with the dielectric liquid at room temp.[46, 47] Variable or unsatisfactory results may be obtained if the test are conducted at temperatures that are lower than room temperature.

The following test procedure was followed during the experimental testing:

1) Visual inspection of the tank, electrodes and all connected equipment.
2) The test cell was then rinsed with a portion of the sample liquid, which was then discarded.
3) Whilst taking care that no air-bubbles are entrained, the test cell was slowly filled with the test liquid after which it was left undisturbed for a period of at least 2 minutes prior to the commencement of any testing.
4) The ambient temperature and barometric pressure as well as the temperature of the dielectric liquid were then recorded.
5) The top of the tank housing the H.V. bushing was then fitted on and secured to the tank.
6) The electrode gap spacing was then set to the predetermined/desired value. The point of contact was established electrically with an ohmmeter.
7) The following connections were then be made:
    - Connection of the fixed electrode to ground.
    - Connection of the movable electrode to the H.V. source.
8) Final inspection of the test tank and all connected equipment.
9) The AC wave was then applied to the H.V electrode. Three tests were conducted at each voltage level[46], with a minimum duration of 30 seconds between tests.
10) The applied voltage was increased until breakdown was observed. The crest voltage level was recorded at breakdown. Approximately three withstand levels were obtained prior to breakdown[46].
11) In order to prevent damage to the electrodes and decomposition of the test liquid, the voltage across the test cell was switched off as soon as possible after breakdown.
12) Steps (6), (8), (9) and (10) were then repeated for different gap spacings.

Five breakdown tests were conducted for each gap spacing.

11.6 Experimental results: Test 1

Please refer to Appendix C for the results obtained from these tests.

11.7 Discussion of experimental results: Test 1

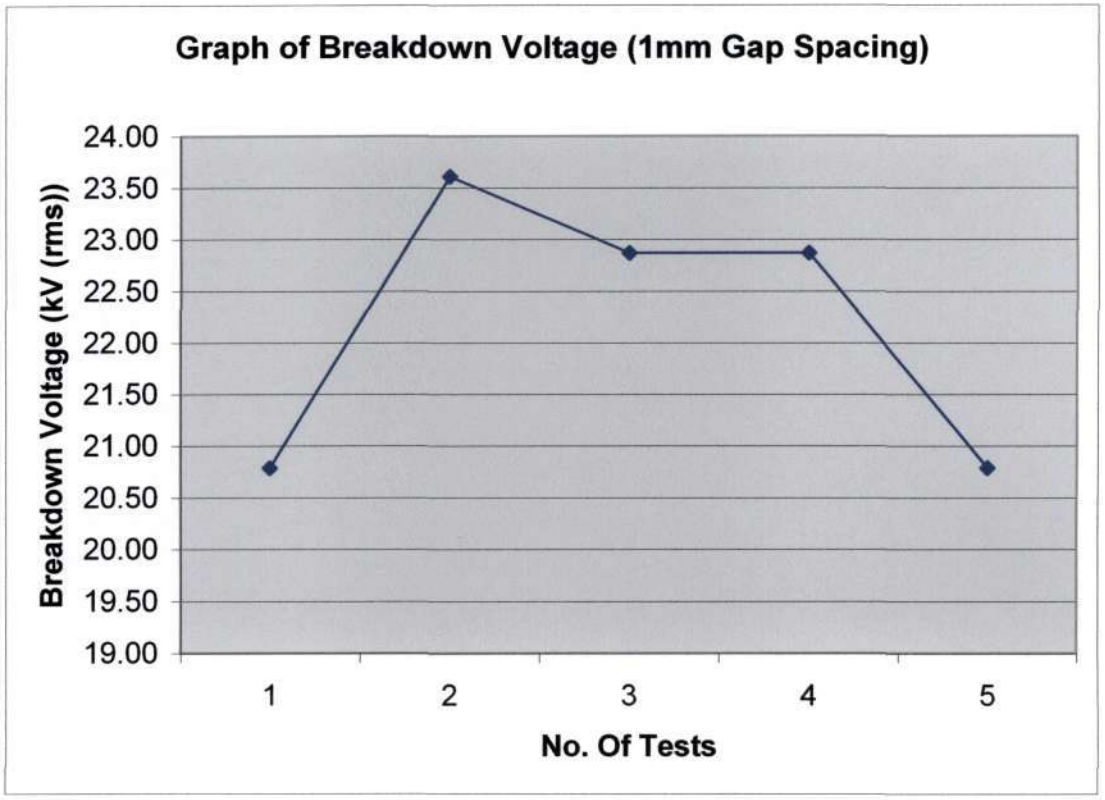

Graph (11.1): Graph of Breakdown Voltage(kV (rms)) for 5 breakdown tests: 1mm electrode gap spacing

Summary of experimental data (1mm electrode gap spacing):

Average breakdown voltage	22.18 kV rms
Highest breakdown voltage	23.61 kV rms
Lowest breakdown voltage	20.79 kV rms
Variation	13.5%
STD Deviation	1.31
Max. Deviation from mean value	6.43%

Table (11.2): Summary of Experimental data (2mm gap spacing)

Discussion

The experimental results obtained from the 1mm electrode gap testing depict an average breakdown voltage of 22.18 kV rms, with a standard deviation of 1.31. The data points deviate from the average value by a maximum of 6.43%, which is deemed to be acceptable according to ASTM D3300-00 (Maximum allowable deviation of 33.3%).

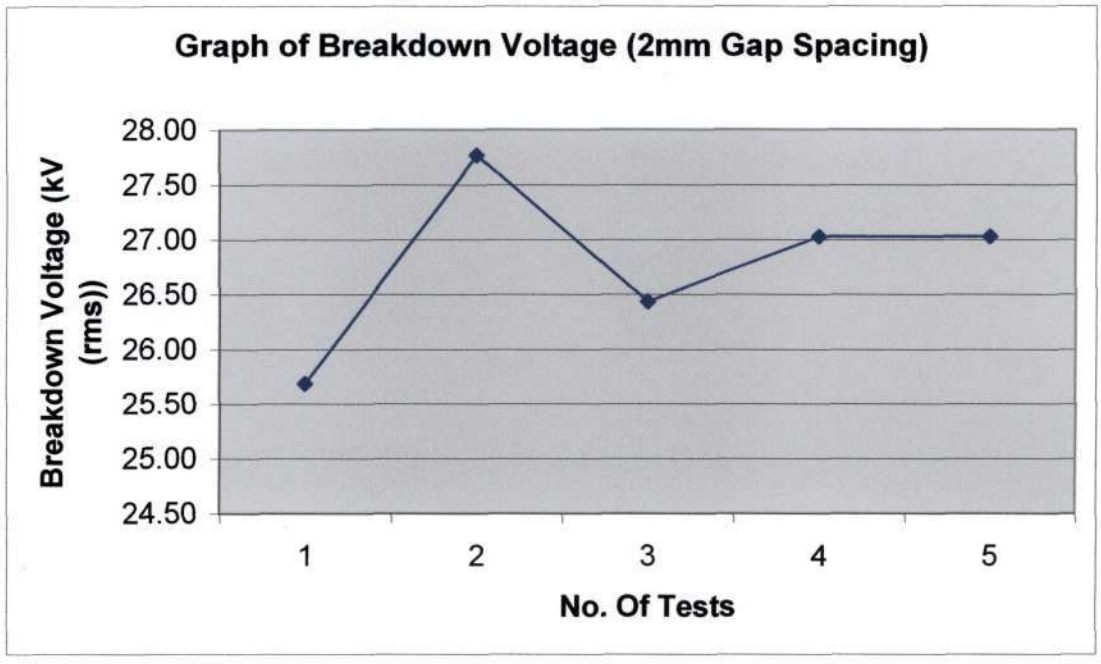

Graph (11.2) – Graph of Breakdown Voltage(kV (rms)) for 5 breakdown tests: 2 mm electrode gap spacing

Summary of experimental data (2mm electrode gap spacing):

Average breakdown voltage	26.79 kV rms
Highest breakdown voltage	27.77 kV rms
Lowest breakdown voltage	25.69 kV rms
Variation	8.1%
STD Deviation	0.78
Max. deviation from mean value	4.10%

Table (11.3): Summary of Experimental data (2mm gap spacing)

Discussion

The experimental results obtained from the 2mm electrode gap testing depict an average breakdown voltage of 26.79 kV rms, with a standard deviation of 0.78. The data points are more closely arranged than observed in the 1mm gap spacing tests, which suggests that breakdown was being achieved more consistently.

The data points deviate from the average value by a maximum of 4.10%.

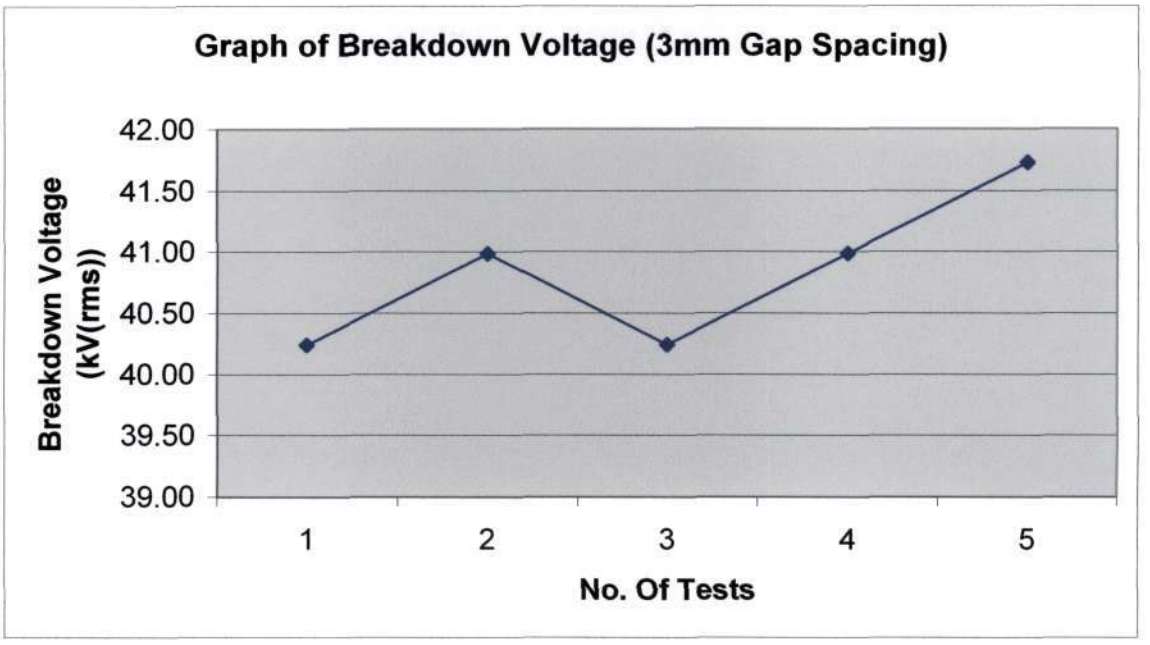

Graph (11.3) – Graph of Breakdown Voltage(kV (rms)) for 5 breakdown tests: 3 mm electrode gap spacing

Summary of experimental data (3mm electrode gap spacing):

Average breakdown voltage	40.84 kV rms
Highest breakdown voltage	41.73 kV rms
Lowest breakdown voltage	40.24 kV rms
Variation	3.6 %
STD Deviation	0.62
Max. deviation from mean value	2.18 %

Table (11.4): Summary of Experimental data (3mm gap spacing)

Discussion

Initial tests conducted using the 3mm electrode gap spacing, produced results with large variations. This test was conducted directly after the 1mm, and 2mm gap tests. The test cell was then opened and the condition of the electrodes were examined. The point electrode was cleaned of all carbon deposits and the system was then re-connected. The tests were then repeated.

The experimental results obtained from the 3mm electrode gap testing depict an average breakdown voltage of 40.84 kV rms, with a standard deviation of 0.62. The data points are more closely arranged than observed in the 1mm and 2mm gap spacing tests.

The data points deviate from the average value by a maximum of 2.18%.

11.8 Summary

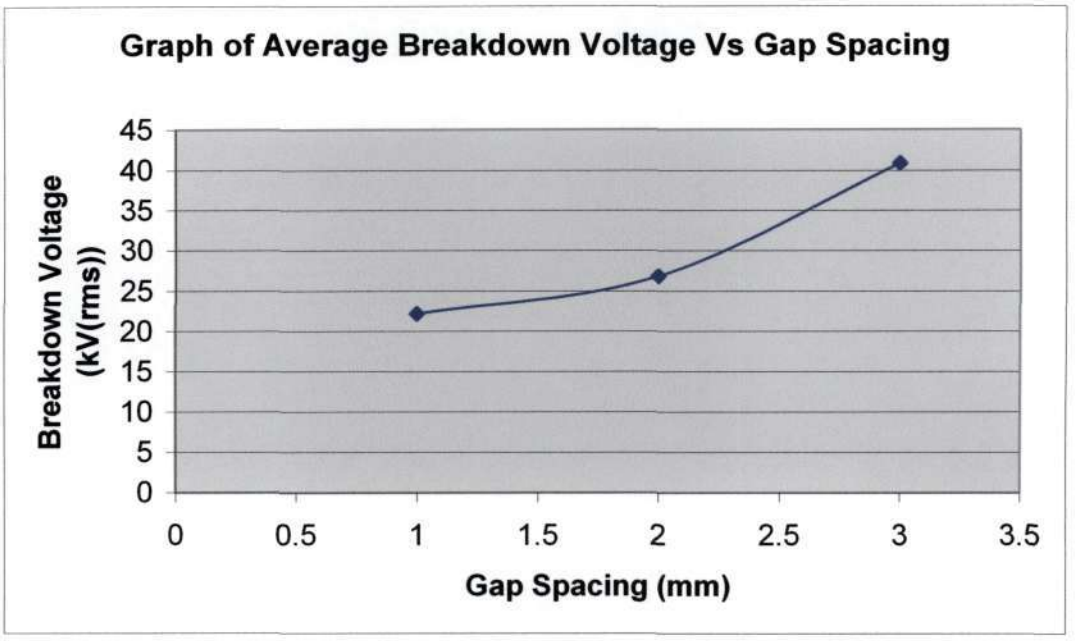

Graph (11.4) – Graph of average breakdown voltage(kV (rms)) vs electrode gap spacing

Summary of experimental data (1mm, 2mm and 3mm electrode gap spacings):

Average breakdown voltage (1mm)	22.18 kV rms
Average breakdown voltage (2mm)	26.79 kV rms
Average breakdown voltage (3mm)	40.84 kV rms

Table (11.5): Summary of Experimental data (1mm, 2mm and 3mm gap spacings)

Discussion

As depicted in graph (11.4), the average breakdown voltage increases nonlinearly with an increase in the electrode gap spacing. These tests were conducted with no filtering system is place, which implies that the dielectric liquid was contaminated after each breakdown. This could have had a significant effect on the results obtained. The following tests (Chapter 12) were conducted with a filtering system installed on the test cell.

11.9 Conclusion

The following conclusions were drawn based on the aforementioned results:

- It was noted that after successive tests, the average dielectric strength of the test liquid reached a stable or plateau with small variances. The conclusion drawn is in accordance with Reference [32]. This conclusion draws attention to the fact that the point electrode was removed from the system and cleaned prior to the commencement of testing. During the cleaning and drying process, it is exposed to air and other impurities (from the surrounding environment). When the electrode is replaced into the test chamber, it now contains absorbed gas as well as impurities. Therefore, the stabilization of the dielectric strength can be attributed to the gradual removal of this absorbed gas and impurities after successive breakdowns.

- The results obtained further highlight the fact that the breakdown voltage of transformer oil (under A.C. test conditions) increases non-linearly with an increase in the electrode gap spacing.

CHAPTER 12
EXPERIMENTAL TESTING: WITH FILTERING SYSTEM

12.1 Background

This phase of experimental testing involved the installation of a filtering system, to remove all impurities present in the dielectric liquid. Such impurities are already present in the oil or introduced into the dielectric liquid during electrical breakdown.

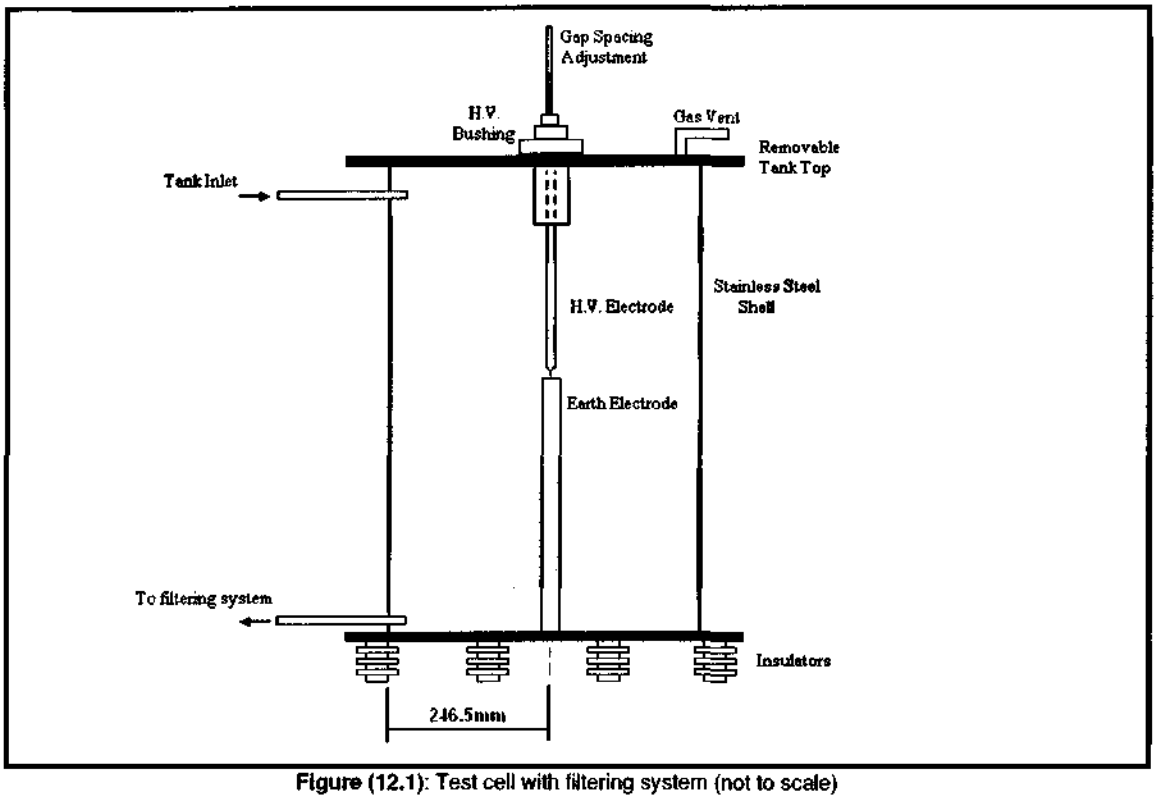

Figure (12.1): Test cell with filtering system (not to scale)

Specifications of filtering system:

Size of filtering pump	0.24 kW
Filter Manufacturer	PALL Filters
Filter Model	Ultipleat SRT Element, 8"
Filter Porosity	5μm

The test circuit utilized for this testing remained unchanged from Chapter 11 (depicted in Figure 11.2).

12.2 Test procedure

The tests were conducted with the specimen at room temp.[46, 47]

The following test procedure was followed during the experimental testing:

1. Visual inspection of the tank, electrodes and all connected equipment.
2. The test cell was then rinsed with a portion of the sample liquid, which was then discarded.
3. Whilst taking care that no air-bubbles are entrained, the test cell was slowly filled with the test liquid after which it was left undisturbed for a period of at least 2 minutes prior to the commencement of any testing.
4. The ambient temperature and barometric pressure as well as the temperature of the dielectric liquid were then recorded.
5. The top of the tank housing the H.V. bushing was then fitted on and secured to the tank.
6. The electrode gap spacing was then set to the predetermined/desired value. The point of contact was established electrically with an ohmmeter.
7. The following connections were then be made:
    - Connection of the fixed electrode to ground.
    - Connection of the movable electrode to the H.V. source.
8. Final inspection of the test tank and all connected equipment.
9. The filtering pump was switched on, and the dielectric liquid was filtered prior to the commencement of any testing.
10. The H.V. source was switched on and the AC wave was applied to the H.V. electrode.
11. The applied voltage was increased until breakdown was observed. The crest voltage level was recorded at breakdown. Approximately three withstand levels were obtained prior to breakdown[46].
12. In order to prevent damage to the electrodes and decomposition of the test liquid, the voltage across the test cell was switched off as soon as possible after breakdown.
13. Steps (6), (8), (9) and (10) were then repeated for different gap spacings. Five breakdown tests were conducted for each gap spacing.

12.3 Experimental results: Test 2

Please refer to Appendix D for the results obtained from these tests.

12.4 Discussion of experimental results

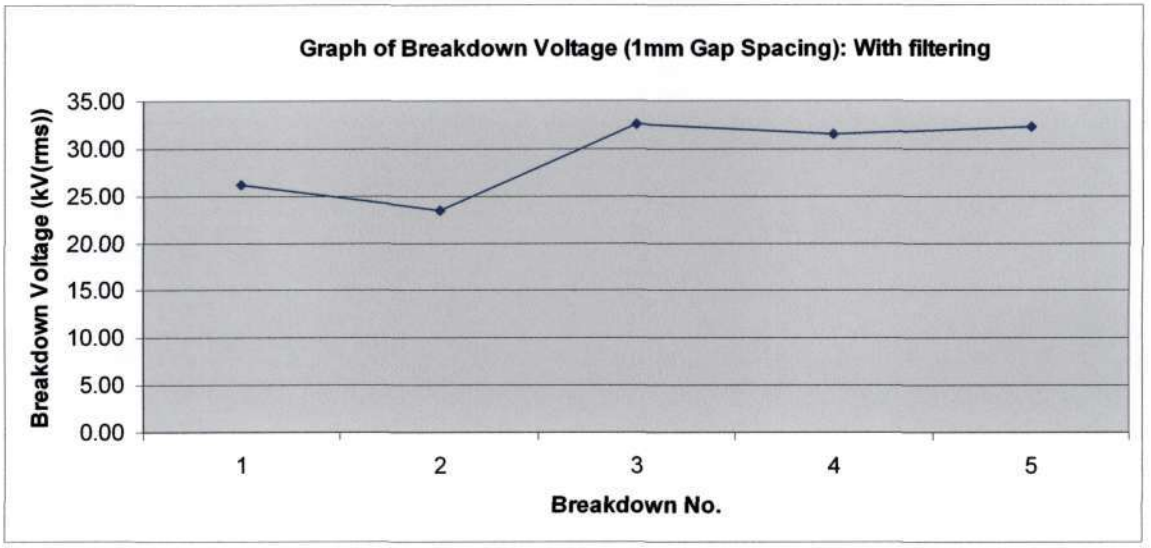

Graph (12.1): Graph of Breakdown Voltage(kV (rms)) for 5 breakdown tests: 1 mm electrode gap spacing

Summary of experimental data (1mm electrode gap spacing with filtering):

Average breakdown voltage	29.19 kV rms
Highest breakdown voltage	32.53 kV rms
Lowest breakdown voltage	23.45 kV rms
STD Deviation	4.13
Max. deviation from mean value	19.65 %

Table (12.1): Summary of Experimental data (1mm gap spacing)

Discussion

The experimental results obtained from the 1mm electrode gap testing, depict an average breakdown voltage of 29.19 kV rms, with a standard deviation of 4.13. The maximum deviation of the data values from the mean value is 19.65%. In comparison, the average breakdown voltage from the 1mm electrode gap test, without the filtering, revealed an average breakdown voltage of 22.18 kV rms. This indicates a **31.61%** increase in the breakdown voltage. These preliminary results indicate a significant influence of filtering on the breakdown voltage.

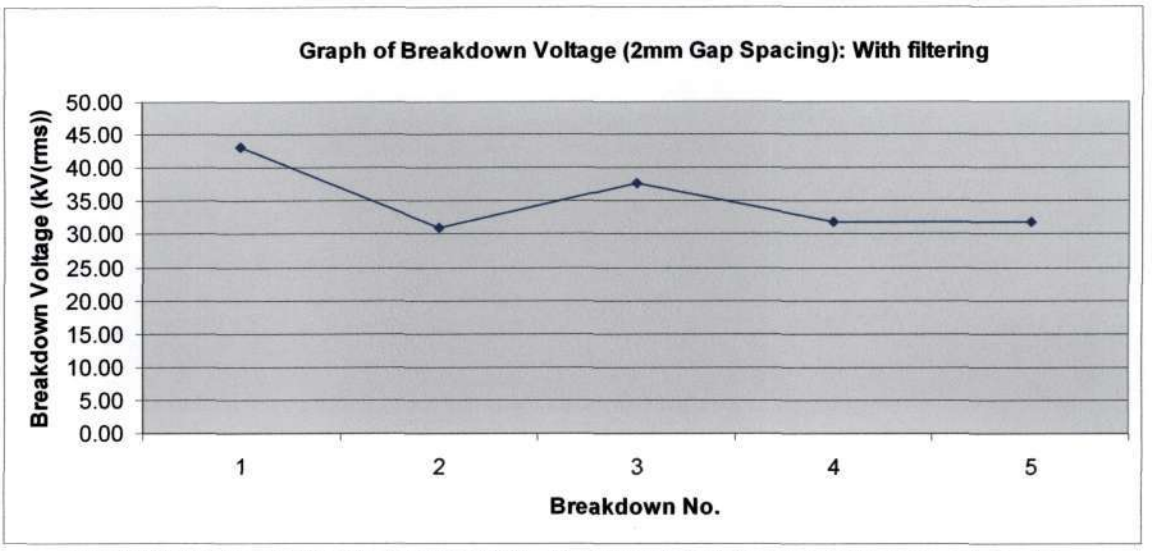

Graph (12.2): Graph of breakdown voltage(kV (rms)) for 5 breakdown tests: 2 mm electrode gap spacing

Summary of experimental data (2mm electrode gap spacing with filtering):

Average breakdown voltage	35.09 kV rms
Highest breakdown voltage	43.00 kV rms
Lowest breakdown voltage	31.03 kV rms
STD Deviation	5.13
Max. deviation from mean value	22.54 %

Table (12.2): Summary of Experimental data (2mm gap spacing)

Discussion

The experimental results obtained from the 2mm electrode gap testing, depict an average breakdown voltage of 35.09 kV rms, with a standard deviation of 5.13. The maximum deviation of the data values from the mean value is 22.54%. Comparatively, the average breakdown voltage from the 2mm electrode gap test, without the filtering, revealed an average breakdown volage of 26.79 kV rms. This indicates a **30.98%** increase in the breakdown voltage. These results, as with the 1mm gap spacing results, seem to indicate that filtering has a significant influence on the breakdown voltage.

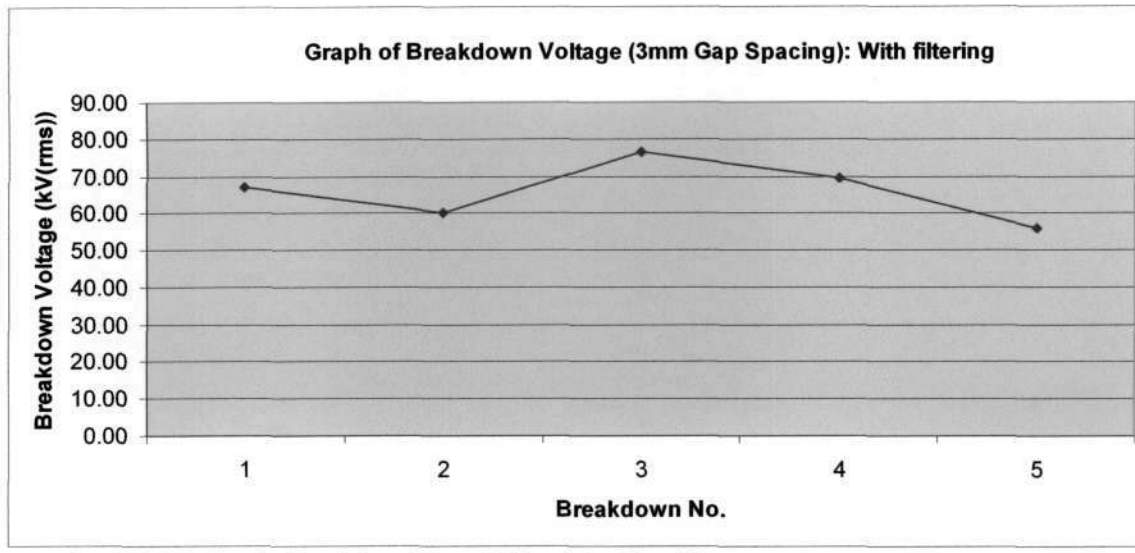

Graph (12.3): Graph of Breakdown Voltage(kV (rms)) for 5 breakdown tests: 3 mm electrode gap spacing

Summary of experimental data (3mm electrode gap spacing):

Average breakdown voltage	65.84 kV rms
Highest breakdown voltage	76.47 kV rms
Lowest breakdown voltage	55.68 kV rms
STD Deviation	8.10
Max. deviation from mean value	16.15 %

Table (12.3): Summary of Experimental data (3mm gap spacing)

Discussion

The experimental results obtained from the 3mm electrode gap testing, depict an average breakdown voltage of 65.84 kV rms, with a standard deviation of 8.10. In comparison, the average breakdown voltage from the 3mm electrode gap test, without the filtering, revealed an average breakdown voltage of 40.84 kV rms. This indicates a **61.21%** increase in the breakdown voltage. These results, as with the 1mm and 2mm gap spacing results, confirms that filtering has a significant influence on the breakdown voltage. The summary and conclusions drawn are explained overleaf.

12.5 Summary

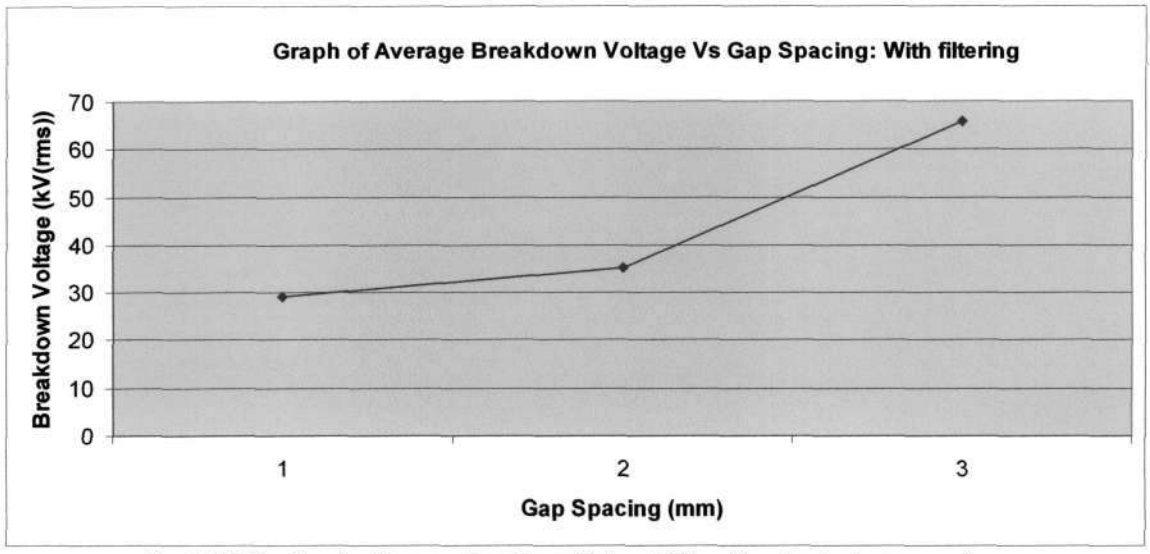

Graph (12.4) – Graph of Average Breakdown Voltage(kV (rms)) vs Electrode gap spacing

Summary of experimental data (1mm, 2mm and 3mm electrode gap spacings):

Average breakdown voltage (1mm)	29.19 kV rms
Average breakdown voltage (2mm)	35.09 kV rms
Average breakdown voltage (3mm)	65.84 kV rms

Table (12.4): Summary of Experimental data (1mm, 2mm, and 3mm gap spacings)

Comparisons of results for unfiltered and filtered tests:

	Unfiltered System	**Filtered System**	**% Increase**
Average breakdown voltage (1mm)	22.18 kV rms	29.19 kV rms	**31.61%**
Average breakdown voltage (2mm)	26.79 kV rms	35.09 kV rms	**30.98%**
Average breakdown voltage (3mm)	40.84 kV rms	65.84 kV rms	**61.21%**

Table (12.5): Comparison of filtered and unfiltered test results

Discussion

As depicted in Table (12.5), the filtering system resulted in a considerable increase in the breakdown voltage for each of the electrode gap spacings. This confirms that the average dielectric strength of the oil is significantly increased by circulation and filtering. Essentially, the act of circulation and filtering removes the impurities that may be present in the oil. These impurities (as mentioned in Chapter 4)[32], can be categorized into 4 groups:

1) Dust or fibre particles already present in the liquid.
2) Particles produced by previous discharges. These could be in the form of minute metallic particles, which are removed from the electrode surfaces during breakdown, or carbon particles that are formed due to the decomposition of the liquid.
3) Deliberately introduced additives. This is not applicable for this testing.
4) Water.

These impurities, which have a higher dielectric constant than that of the liquid, are attracted into regions of high electric stress and eventually form a bridge. This bridge will eventually result in breakdown.

As the liquid is filtered, the distribution of the particle sizes moves to smaller values and hence the formation of the particle bridges in the areas of high electric stress is impeded. Therefore, the act of decreasing the filter porosity will result in a decrease in the mean dielectric strength of the dielectric liquid.

In addition, the circulation of the oil also results in an increase in the mean dielectric strength of the oil. This is due to the fact that the motion of the oil delays the formation of the particle bridges across the electrodes i.e. the flow of the oil impedes the entry of impurities into the gap. The increase in the circulation speed of the oil will result in a change in the mean dielectric strength of the oil. However, the increase in the mean dielectric strength of the oil is not indefinite. As the circulation of the oil is increased, this will in turn cause an increasingly turbulent flow. This turbulent flow will result in a pressure difference in the oil, which will in turn reduce the dielectric strength of the oil.

12.6 Conclusion

The results obtained prove the following:

- The circulation and filtering of the oil increases the mean dielectric strength of the transformer oil. The percentage increase in the breakdown voltage, for each gap spacing, is depicted in Table (12.5).
- It can be concluded that a decrease in the filter porosity will result in an increase in the mean dielectric strength of the oil.
- It can also be concluded that an increase in the circulation flow of the oil will result in an increase in the mean dielectric strength of the oil. This increase is however not indefinite.
- Higher variances in the breakdown voltage were noted for each gap spacing when compared with the results obtained in Chapter 11. However, the data points were noted to be stabilizing towards the end of the testing. The higher variances could be attributed to gas absorption and impurities, which were introduced into the test cell during the installation of the filtering system. These impurities were being circulated through the system through the testing. The stabilization that was noted at the end of the testing was a result of the removal of the absorbed gas by successive breakdowns as well as the removal of impurities by the filtering system.

CHAPTER 13
ACOUSTIC TESTING: AREA OF DIRECT RECEPTION

EXPERIMENTAL TESTING: PHASE 3 – ACOUSTIC MONITORING: AREA OF DIRECT RECEPTION

13.1 Background

When measuring the time of arrival of the acoustic signal at each of the acoustic sensors mounted on the transformer tank wall, it is essential to have a zero reference point from which the time can be measured. It is for this reason that a combination of the acoustic as well as the electrical method is necessary. When the partial discharge occurs, it results in formation of a current impulse (principles of formation examined in Chapter (4)). The occurrence of this impulse should be taken as the zero reference point, from which the relative time of arrival of the acoustic wave at each of the sensors should be measured. This method was implemented in the laboratory testing.

13.2 Objective

This objective of this segment of the experimental testing is to investigate the acoustic emissions in the breakdown phase in liquid dielectrics. The test cell as depicted in figure (13.1), was used for this segment of the experimental testing. The acoustic sensors were placed in the line of direct reception, i.e. in the same horizontal plane as the electrode gap. The effect of placing of the acoustic sensors in the indirect line is examined Chapter 14. In order to reduce the effect of any external disturbance on the acoustic detection system, the circulation pump was not switched on for this test. The oil was however, filtered prior to the commencement of any testing. The effect of filtering on the acoustic method is examined in Chapter 14.

13.3 Positioning of acoustic sensors: Area of direct reception

The acoustic sensors were placed in the area of direct reception i.e. in the same horizontal plane as the electrode gap spacing. This is depicted below:

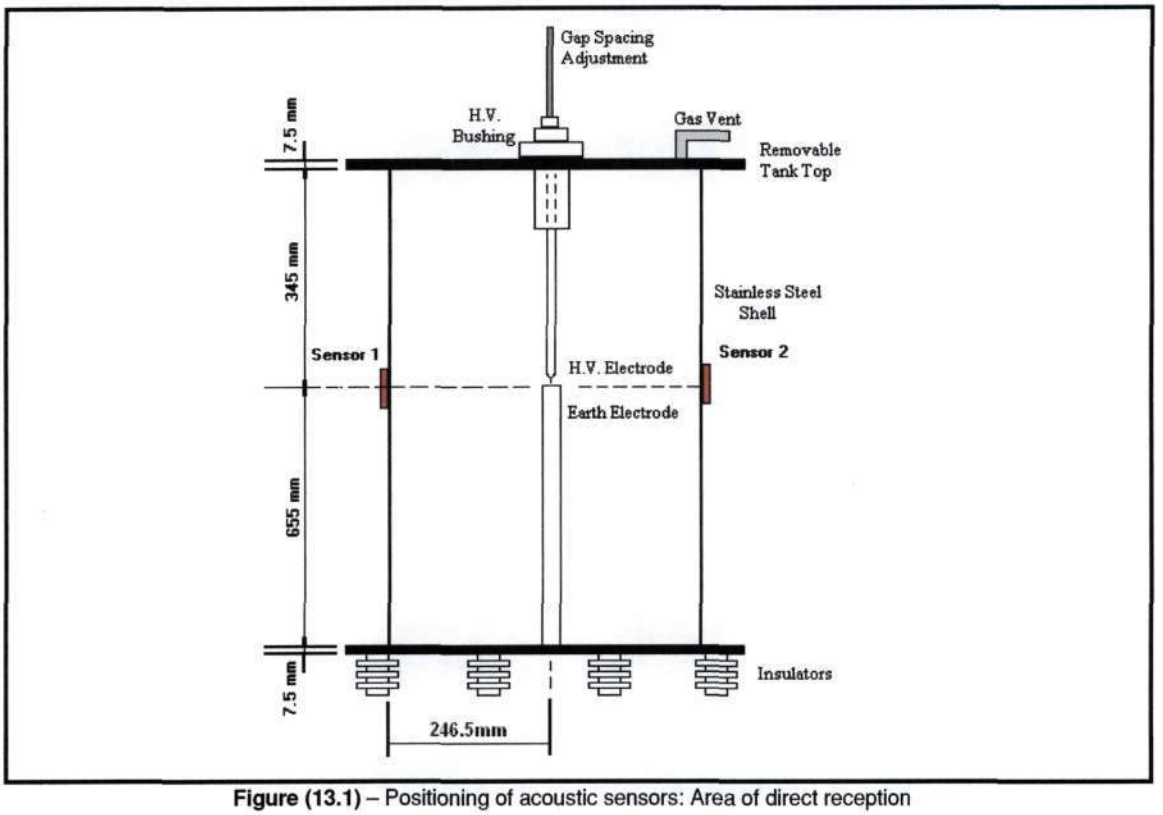

Figure (13.1) – Positioning of acoustic sensors: Area of direct reception

From Figure (13.1), it can be noted that the actual distance between the acoustic sensors and the p.d. site is approximately **246.5mm**.

13.4 Acoustic system

The following acoustic system was used for this segment of the testing:

Brand	**Physical Acoustics Corp.**
No. of input channels	**3**
No. of output channels	**3**
No. of sensors used	**2**
Input channels used	**1 & 2**
Output channels used	**1 & 2**

Table (13.1): Specifications of acoustic system

13.5 Test Procedure: Area of direct reception

The tests were conducted with the specimen at room temp.[46, 47]

The following test procedure was followed during the experimental testing:

1) The acoustic sensors were coated with a layer of silicon gel and were then positioned of the test cell shell wall in the area of direct reception i.e. in the same horizontal plane as the electrode gap spacing. It was ensured that there was proper contact between the surface of the acoustic sensor and the test cell wall.
2) The acoustic sensors were then connected to the signal-processing unit using coaxial cables.
3) A visual inspection of the tank, electrodes and all connected equipment was conducted.
4) The ambient temperature, barometric pressure, and humidity were recorded.
5) The electrode gap spacing was then set to the predetermined value (3mm). The point of contact was established electrically with an ohmmeter.
6) The following connections were then made:

- Connection of the fixed electrode to ground.
- Connection of the H.V electrode to the H.V. source.
- A current probe was installed on the earth path, in order to measure the instant of electrical breakdown. This is necessary so that a zero reference point can be established for the arrival of the acoustic wave.

7) Final inspection of the test tank and all connected equipment.
8) A tap test was performed to ensure the correct operation of the acoustic sensors as well as the signal-processing unit.
9) The AC wave was then applied.
10) The applied voltage was increased until breakdown was observed. The crest voltage level was recorded at breakdown. Approximately three withstand levels were obtained prior to breakdown[46].
11) In order to prevent damage to the electrodes and decomposition of the test liquid, the voltage across the test cell was switched off as soon as possible after breakdown.
12) The acoustic emissions, prior to breakdown as well as during breakdown, were recorded together.

Five breakdown tests were recorded from the sample. [46]

13.6 Test Results – Area of direct reception

13.6.1 Tap test

The acoustic sensors were positioned in the area of direct reception, (as illustrated in figure (13.1)), and a tap test was performed to ensure that the sensors were fully functionally. The results obtained confirmed that both sensors were in a proper working condition.

13.6.2 Testing without H.V. electrode

In order to ensure that partial discharges were not occurring at sites other than the electrode gap, the H.V. electrode was removed from the test cell, and the test voltage was applied to the bushing. The test voltage was increased up to 50 kV. No partial discharges were observed at voltages up to and including 50 kV. This confirmed that no partial discharges were occurring at sites other than the electrode gap, at voltages up to and including 50 kV.

13.6.3 Observation and measurement

The acoustic and electrical signals were observed simultaneously on the oscilloscope. These waveforms were examined for:

- Correlation between the electrical breakdown (noted by the current impulse on the earth lead), and the occurrence of the corresponding mechanical stress wave (acoustic wave).
- Relative time of arrival of the mechanical stress wave (acoustic wave), using the instant of the occurrence of the current impulse as the zero reference point.

The following waveforms were obtained, and are examined overleaf.

13.6.4 Environmental conditions during testing

The following environmental conditions were prevalent during the experimental testing:
Dry Bulb: 21 °C
Wet Bulb: 19.5 °C
Humidity: 18 g/m^3
Pressure: 100.1 kPa

13.6.5 Electrode gap spacing

The electrode gap spacing was set at 3mm, in order to initiate electrical breakdown at higher voltages. This gap spacing was maintained for the duration of the testing.

13.6.6 Filtering system

The oil circulating and filtering system was switched off during the testing, in order to eliminate any acoustic disturbances due to the circulation of the oil. This influence will be examined in later sections.

Please see experimental results overleaf.....

13.6.7 Plot 1: Acoustic sensor position 1

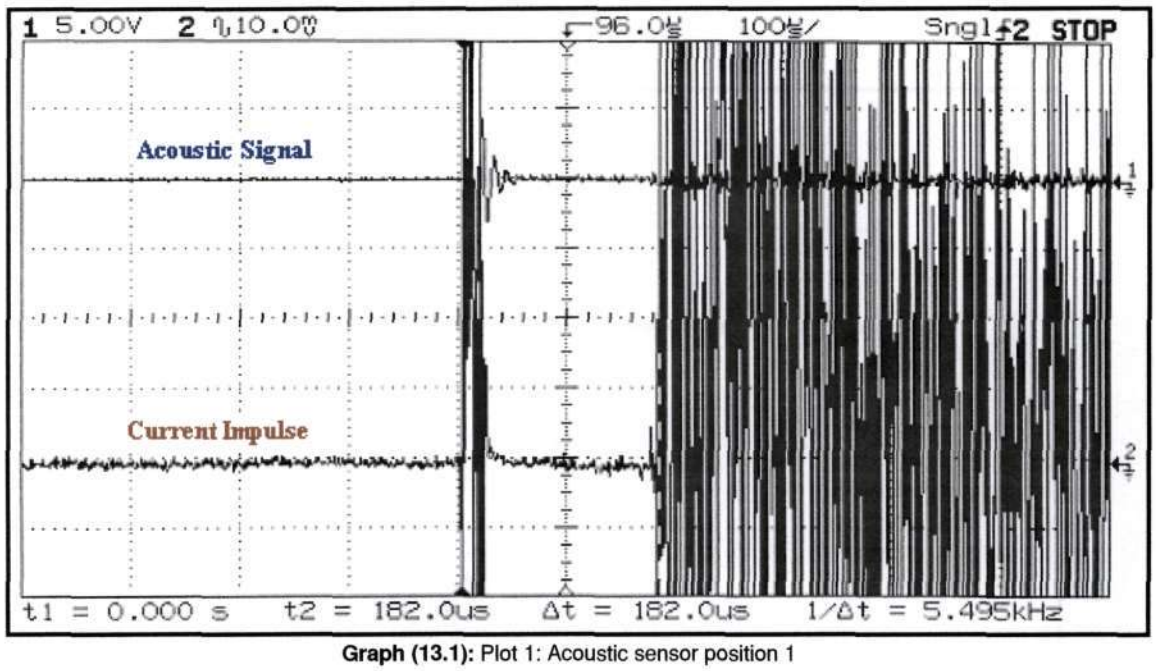

Graph (13.1): Plot 1: Acoustic sensor position 1

Graph (13.1), depicts the occurrence of complete electrical breakdown within the electrode gap spacing. Waveform (2) depicts the current waveform, whilst waveform (1), depicts the corresponding acoustic waveform as recorded at sensor position **1**. The current impulse is utilized as the zero reference point for the timing of the arrival of the acoustic signal. The acoustic signal was noted to arrive at the acoustic sensor, **182 µs** after the occurrence of the current impulse.

The internal structure of the test cell, between the partial discharge source and the acoustic sensor, contains two different types of media. These media are:

- A dielectric liquid region (transformer oil).
- The steel tank wall of the transformer.

As listed previously, the thickness of the steel tank wall is 4.5mm. From literature, it is known that the speed of sound through steel is approximately 3200 m/s. Therefore the time taken for the signal to propagate through the steel wall is calculated as:

$$time_{steel} = \frac{thickness_{wall}}{speed_{steel}} = \frac{4.5\times10^{-3}\,m}{3200m/s} = 1.406\mu s$$

Therefore, the time taken for the signal to propagate through the oil region is:

$$time_{oil} = time_{total} - time_{steel} = 182\mu s - 1.406\mu s = 180.594\mu s$$

Therefore, the distance of the occurrence of the partial discharge away from the sensor (taking into account that the sensor is in the direct line) is calculated as:

$$distance = speed_{oil} \times time_{oil} = 1400m/s \times 180.594\mu s = 252.83mm$$

Taking the thickness of the steel wall into account: 252.83mm + 4.5mm= **257.33mm**.

Therefore, the experimental result indicates that the p.d. source lies on a radius of **257.33mm** away from Sensor 1. This result can be depicted as:

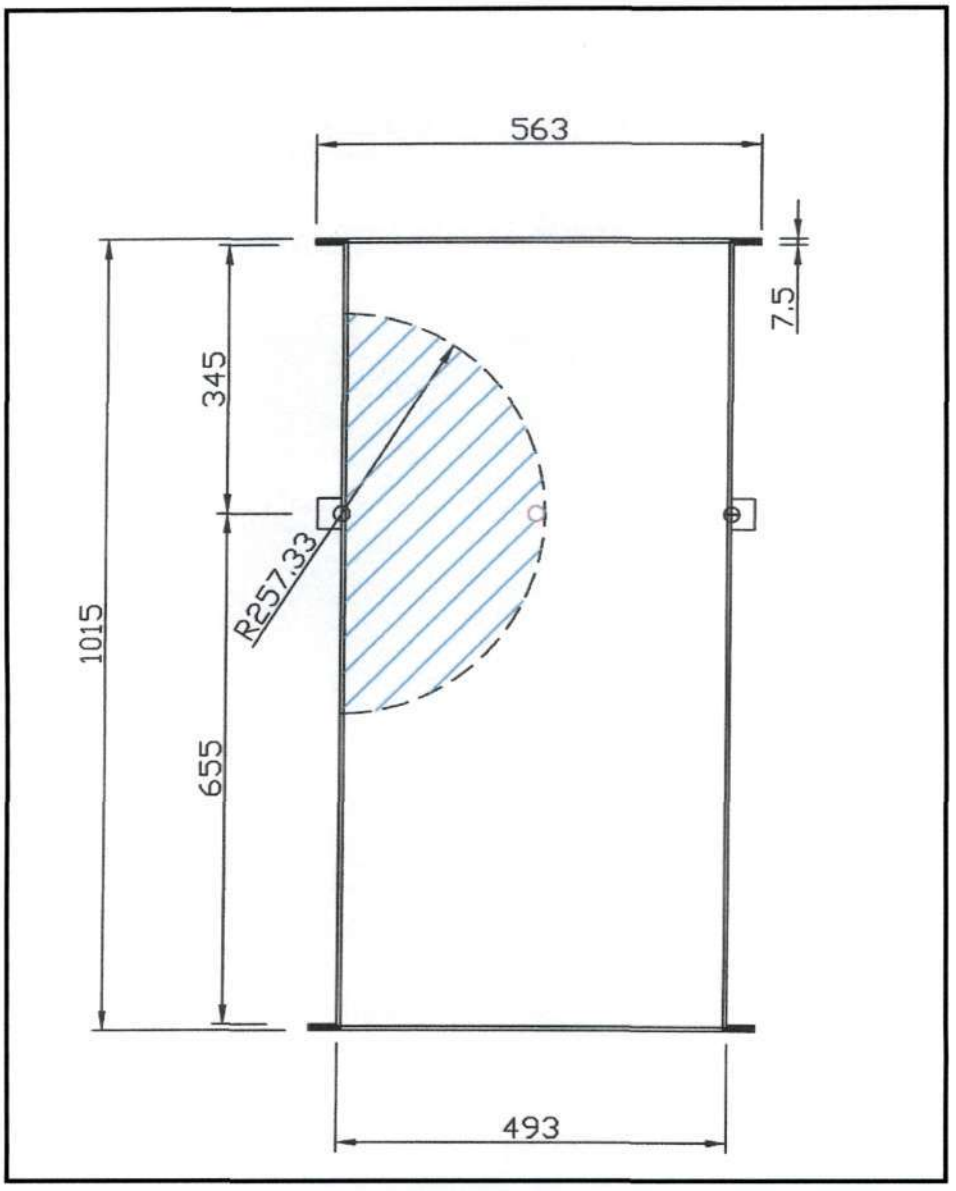

Figure (13.2) – Predicted p.d. area based on experimental results (Drawn to scale 1:10)

Figure (13.2) depicts the predicted p.d. site, as indicated by the hatched area, based on the data received from sensor 1. The actual p.d. site is depicted by the red circle. The result obtained from sensor 1 therefore accurately encloses the actual p.d. site. In the next experiment, sensor 2 will be used to reduce the predicted p.d. area.

13.6.8 Plot 2: Acoustic sensor position 2

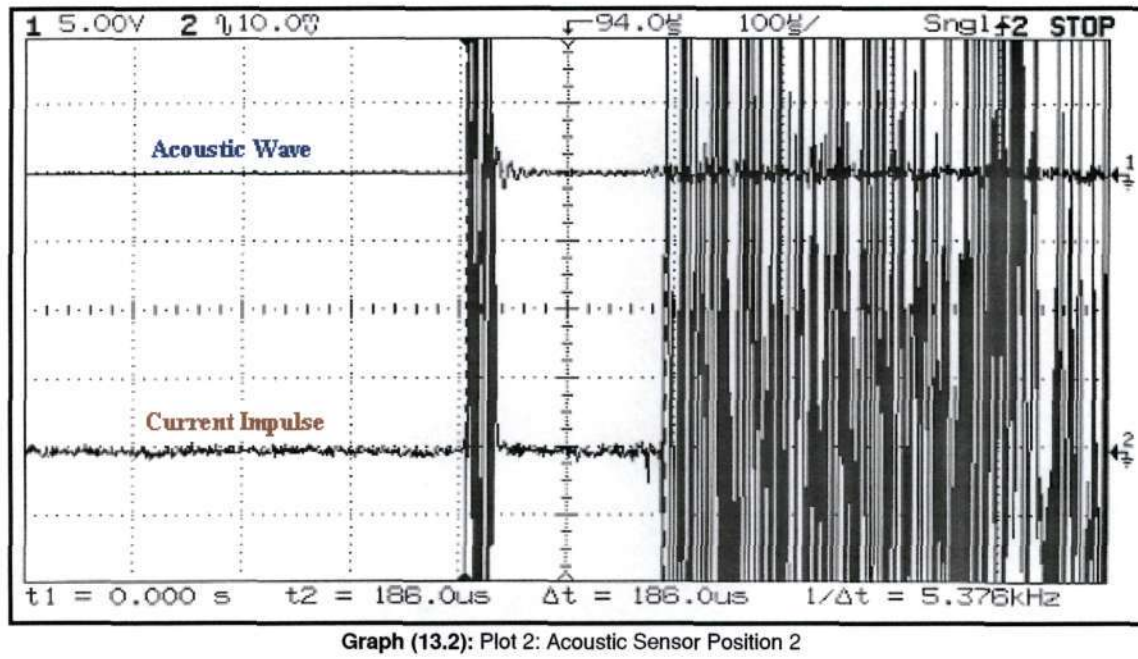

Graph (13.2): Plot 2: Acoustic Sensor Position 2

Graph (13.2), depicts the occurrence of a complete electrical breakdown within the electrode gap spacing. Waveform (2) depicts the current waveform, whilst waveform (1), depicts the corresponding acoustic waveform as recorded at sensor position **2**. Note, here the relative time of arrival of the acoustic signal at acoustic sensor 2, is **186 μs**.

As calculated in plot 1, the time taken for the acoustic signal to propagate through the outer steel wall is 1.406μs. This implies that the time taken for the signal to propagate through the oil region is given by:

$$time_{oil} = time_{total} - time_{steel} = 186\mu s - 1.406\mu s = 184.594\mu s$$

Therefore, the distance of the occurrence of the partial discharge away from the sensor (taking into account that the sensor is in the direct line) is calculated as:

$$dis\tan ce = speed_{oil} \times time_{oil} = 1400m/s \times 184.594\mu s = 258.43mm$$

Taking the thickness of the steel wall into account: 258.43mm + 4.5mm= **262.93mm**.

Therefore, the experimental result indicates that the p.d. source lies on a radius of **262.93mm** away from Sensor 2. This result, in combination with the result obtained from the sensor 1, can be depicted as (please see overleaf):

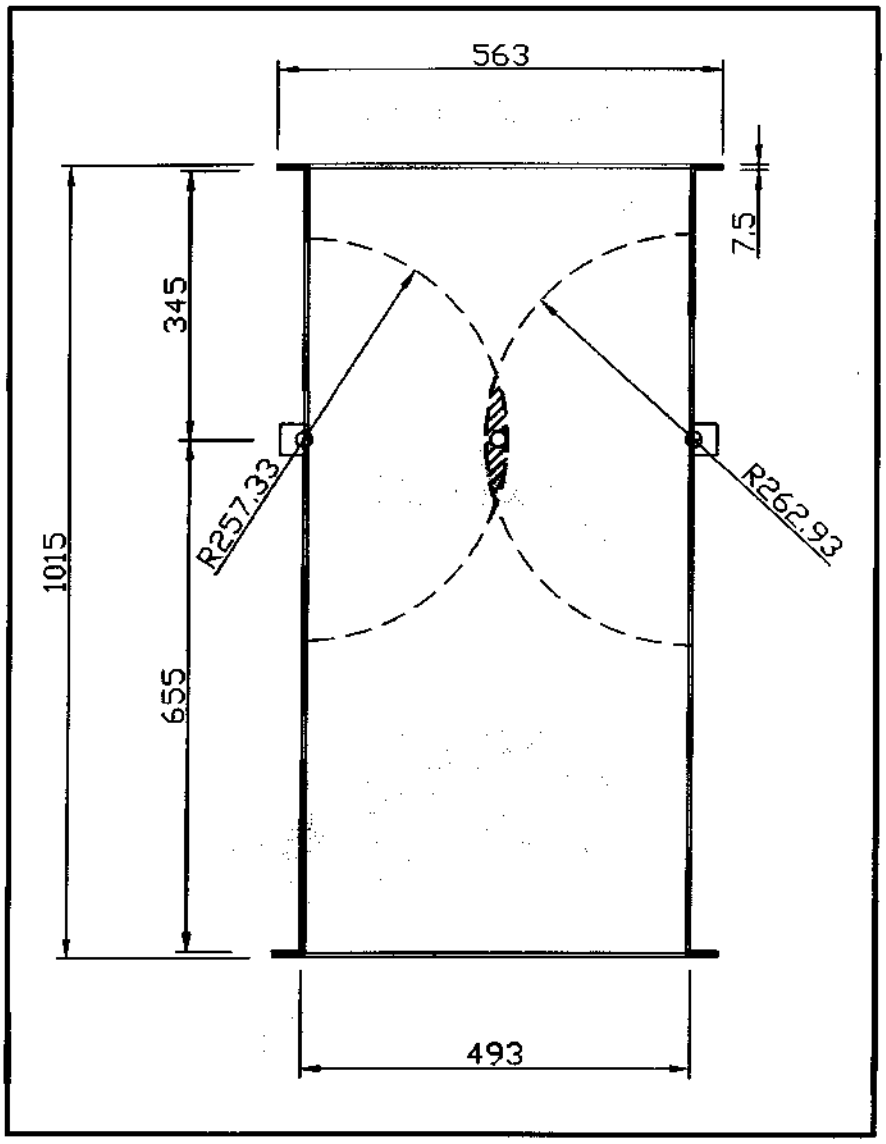

Figure (13.3): Summary of Results (Area of direct Reception)

Figure (13.3) depicts the predicted p.d. site, as indicated by the hatched area, based on the data received from sensor 1 and sensor 2. As can be noted, the predicted p.d. area is now significantly reduced, whilst retaining the accuracy. The actual p.d. site is depicted by the red circle. Therefore, combining the results obtained from sensor 1 and sensor 2 produces an accurate prediction of the p.d. site. In Chapter 14, the effect of more sensors in the area of indirect reception will be examined.

13.7 Conclusions: Acoustic testing – area of direct reception

The results obtained from the aforementioned acoustic experiments prove the following:

- The acoustic method can be used reliably to determine the existence of a p.d.
- The acoustic method can be used reliably to determine the spatial location of the p.d. site, when the acoustic sensors are placed in the direct line.
- It is necessary to have details of the internal geometry of the test transformer so that accurate calculations may be performed.
- The effect adding sensors in the area of indirect reception is evaluated in Chapter 14.

CHAPTER 14
ACOUSTIC TESTING: AREAS OF DIRECT AND INDIRECT RECEPTION

14.1 Objective

The objective of this phase of the experimental is to examine the influence of installing acoustic sensors into an area of indirect reception (i.e. areas which lie out of the direct path of the acoustic wave), whilst maintaining acoustic sensors in the area of direct reception. The original test cell was utilized for this phase of the testing.

14.2 Positioning of acoustic sensors

The acoustic sensors were placed in the areas of direct and indirect reception. This is depicted below:

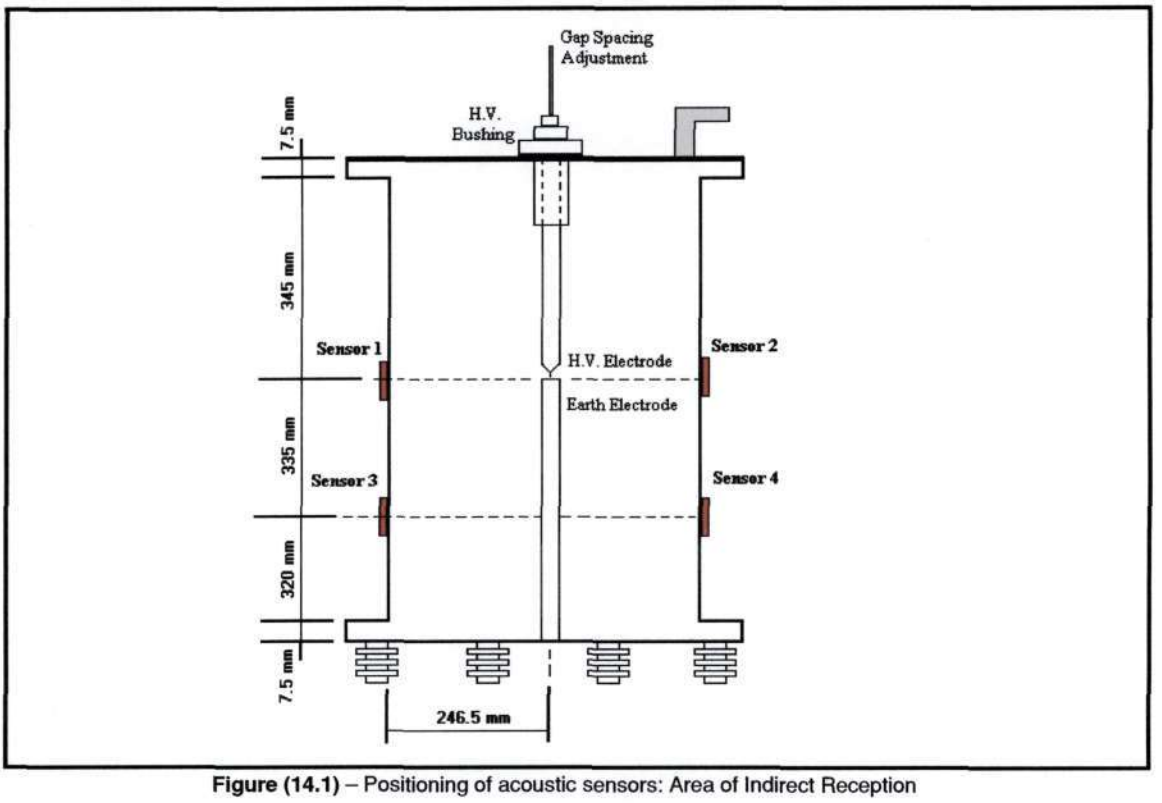

Figure (14.1) – Positioning of acoustic sensors: Area of Indirect Reception

The geometrical location of the actual p.d. site remains unchanged from Chapter 13. The distance between the p.d. site and sensors 3 and 4, are calculated overleaf.

14.3 Actual location of partial discharge source in relation to sensors

Geometrically, the distance between the sensors and the partial discharge source is calculated as:

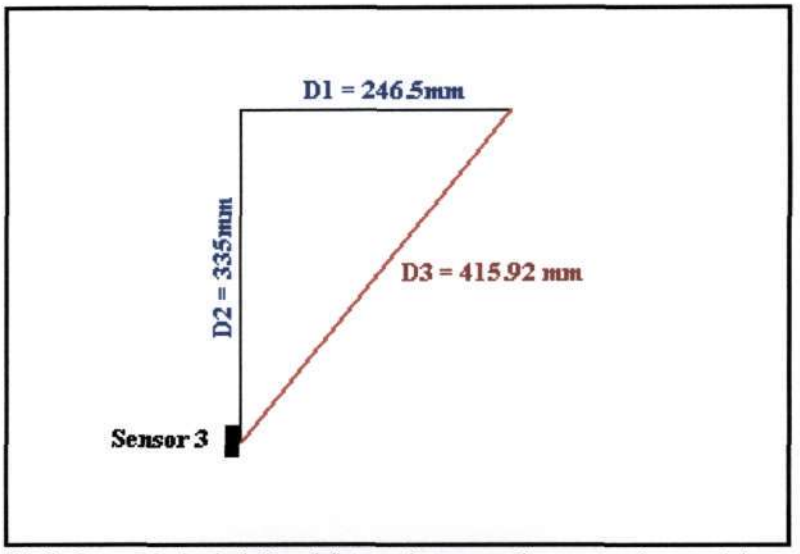

Figure (14.2): Geometrical calculation of distance between p.d. source and sensor 3 (not to scale)

As depicted in Figure (14.2), the straight line distance between the p.d. source and sensor 3 is **415.92mm**.

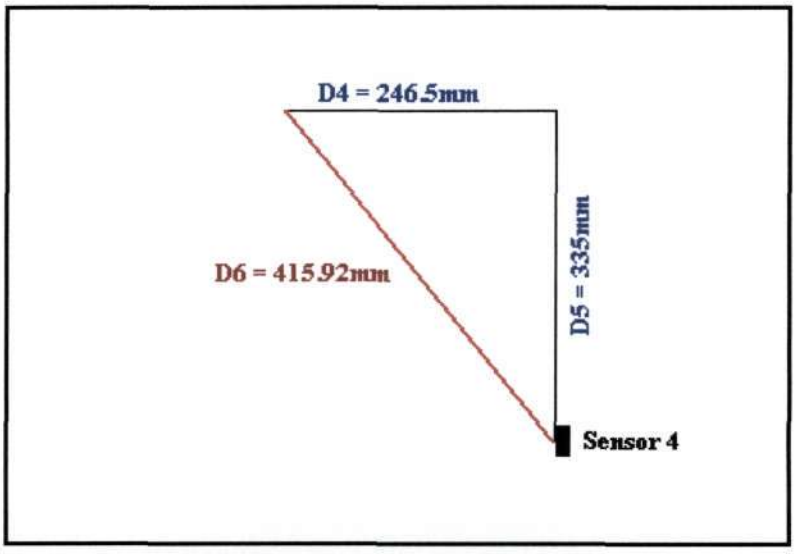

Figure (14.3): Geometrical calculation of distance between p.d. source and sensor 4 (not to scale)

The straight line distance between the p.d. source and sensor 4 is similarly calculated as **415.92mm**.

14.4 Test procedure: Area of indirect reception

The tests were conducted with the specimen at room temp.[46, 47]

The following test procedure was followed during the experimental testing:

1) The acoustic sensors were coated with a layer of silicon gel and were then positioned of the test cell shell wall in the area of indirect reception. It was ensured that there was proper contact between the surface of the acoustic sensor and the test cell wall.
2) The acoustic sensors were then connected to the signal-processing unit using coaxial cables.
3) A visual inspection of the tank, electrodes and all connected equipment was conducted.
4) The ambient temperature, barometric pressure, and humidity were recorded.
5) The electrode gap spacing was then set to the predetermined value (3mm). The point of contact was established electrically with an ohmmeter.
6) The following connections were then made:
7) Connection of the fixed electrode to ground.
8) Connection of the H.V electrode to the H.V source.
9) A current probe was installed on the earth path, in order to measure the instant of electrical breakdown. This is necessary so that a zero reference point can be established for the arrival of the acoustic wave.
10) Final inspection of the test tank and all connected equipment.
11) A tap test was performed to ensure the correct operation of the acoustic sensors as well as the signal-processing unit.
12) The AC wave was then applied.
13) The applied voltage was increased until breakdown was observed. The crest voltage level was recorded at breakdown. Approximately three withstand levels were obtained prior to breakdown[46].
14) In order to prevent damage to the electrodes and decomposition of the test liquid, the voltage across the test cell was switched off as soon as possible after breakdown.
15) The acoustic emissions, prior to breakdown as well as during breakdown, were recorded together.

Five tests were recorded with the sensor positions unchanged for the duration of the testing. [46]

14.5 Test results – Area of indirect reception

14.5.1 Tap test

A tap test was performed to ensure that the sensors were fully functionally. The results obtained confirmed that both sensors were in a proper working condition.

14.5.2 Testing without H.V. electrode

In order to ensure that partial discharges were not occurring at sites other than the electrode gap, the H.V. electrode was removed from the test cell, and the test voltage was applied to the bushing. The test voltage was increased up to 50 kV. No partial discharges were observed at voltages up to and including 50 kV. This confirmed that no partial discharges were occurring at sites other than the electrode gap, at voltages up to and including 50 kV.

14.5.4 Environmental conditions during testing

The following environmental conditions were prevalent during the experimental testing:

Dry Bulb: 20.5 °C
Wet Bulb: 18.5 °C
Humidity: 17 g/m^3
Pressure: 100.2 kPa

14.5.5 Electrode gap spacing

The electrode gap spacing was set at 3mm, in order to initiate electrical breakdown at higher voltages. This gap spacing was maintained for the duration of the testing.

14.5.6 Filtering system

The oil circulating and filtering system was switched off during the testing, in order to eliminate any acoustic disturbances due to the circulation of the oil. This influence will be examined in later sections.

14.5.7 Observation and measurement

The acoustic and electrical signals were observed simultaneously on the oscilloscope. These waveforms were examined for:

- Correlation between the electrical breakdown (noted by the current impulse on the earth lead), and the occurrence of the corresponding mechanical stress wave (acoustic wave).
- Relative time of arrival of the mechanical stress wave (acoustic wave), using the instant of the occurrence of the current impulse as the zero reference point.

The following waveforms were obtained, and are examined overleaf.

14.5.8 Plot 3: Acoustic sensor position 3

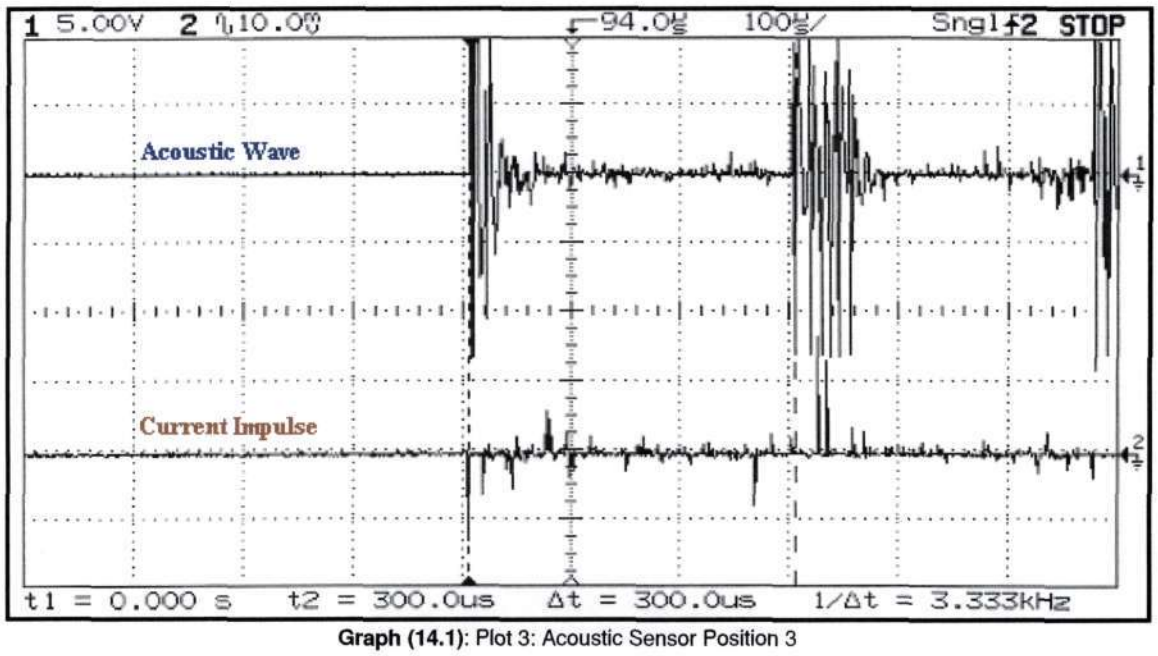

Graph (14.1): Plot 3: Acoustic Sensor Position 3

Graph (14.1), depicts the occurrence of complete electrical breakdown within the electrode gap spacing. Waveform (2) depicts the current waveform, whilst waveform (1), depicts the corresponding acoustic waveform as recorded at sensor position **3**. The acoustic signal was noted to occur **300 μs** after the occurrence of the current impulse. This is significantly longer than the times measured in Chapter 13 where the sensors were located in the area of direct reception. This longer time can be attributed to the longer distance traveled by the acoustic wave before reaching sensor 3.

As discussed in Chapter 13, the internal structure of the test cell, between the partial discharge source and the acoustic sensor, contains two different types of media. These media are:

- A dielectric liquid region (transformer oil).
- The steel tank wall of the transformer.

As listed previously, the thickness of the steel tank wall is 4.5mm. From literature, it is known that the speed of sound through steel is approximately 3200 m/s. Therefore the time taken for the signal to propagate through the steel wall is calculated as:

$$time_{steel} = \frac{thickness_{wall}}{speed_{steel}} = \frac{4.5 \times 10^{-3} m}{3200 m/s} = 1.406 \mu s$$

Therefore, the time taken for the signal to propagate through the oil region is:

$$time_{oil} = time_{total} - time_{steel} = 300 \mu s - 1.406 \mu s = 298.594 \mu s$$

Therefore, the distance of the occurrence of the partial discharge away from the sensor (taking into account that the sensor is in the direct line) is calculated as:

$$distance = speed_{oil} \times time_{oil} = 1400 m/s \times 298.594 \mu s = 418.03 mm$$

Taking the thickness of the steel wall into account: 418.03mm + 4.5mm= **422.53mm**.

Therefore, the experimental result indicates that the p.d. source lies on a radius of **422.53mm** away from Sensor 3. This result, in combination with the results obtained from the direct-line sensors (sensor 1 and sensor 2), can be depicted as:

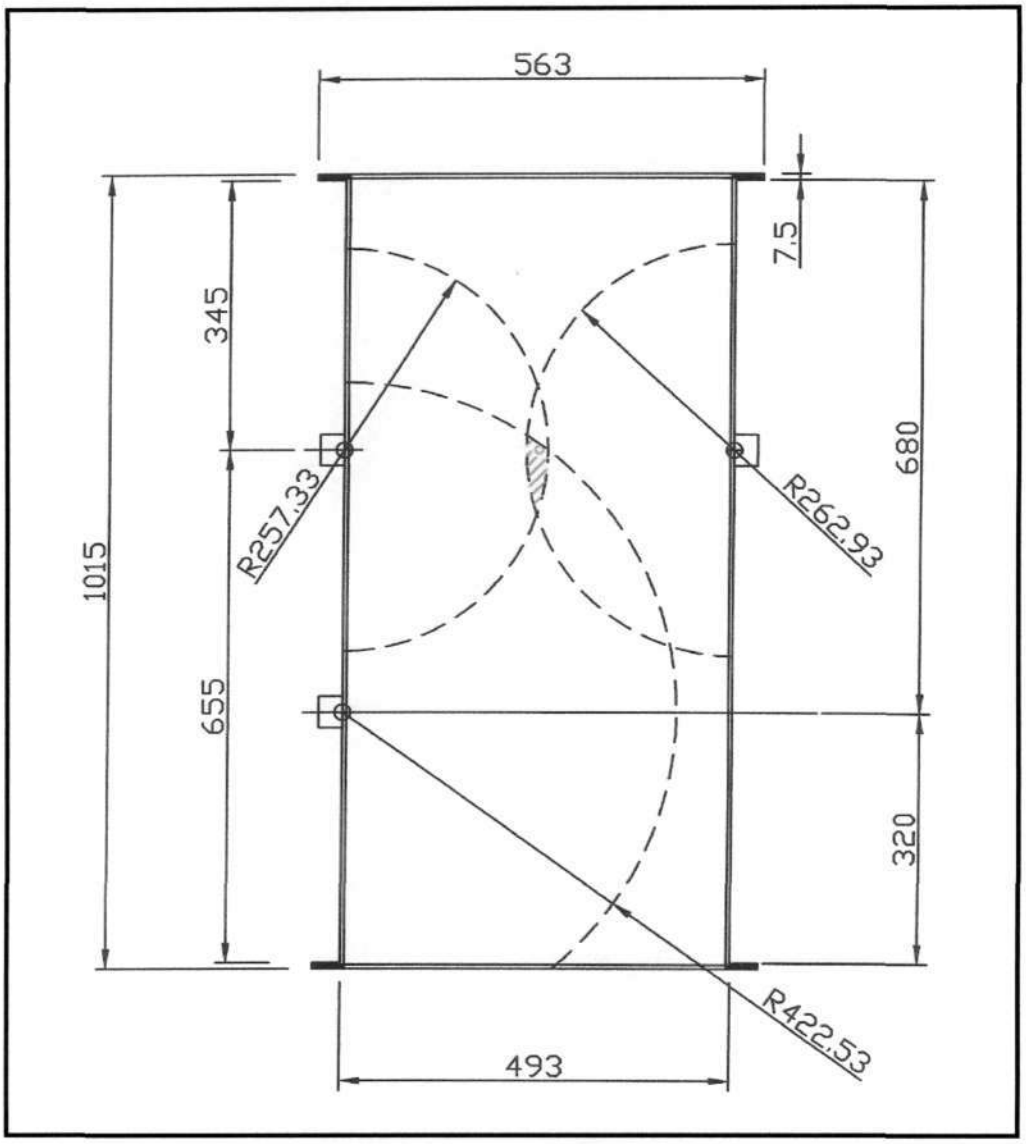

Figure (14.4): Predicted p.d. area based on experimental results (Drawn to scale)

As depicted in Figure (14.4), the results obtained from sensor 3 accurately reduces the predicted area of the p.d. site, when combined with the results obtained from sensor 1 and sensor 2. Theses preliminary results indicate that sensors placed in the area of indirect reception produce readings that are accurate and assist in reducing the predicted p.d. site area.

14.5.9 Plot 4: Acoustic sensor position 4

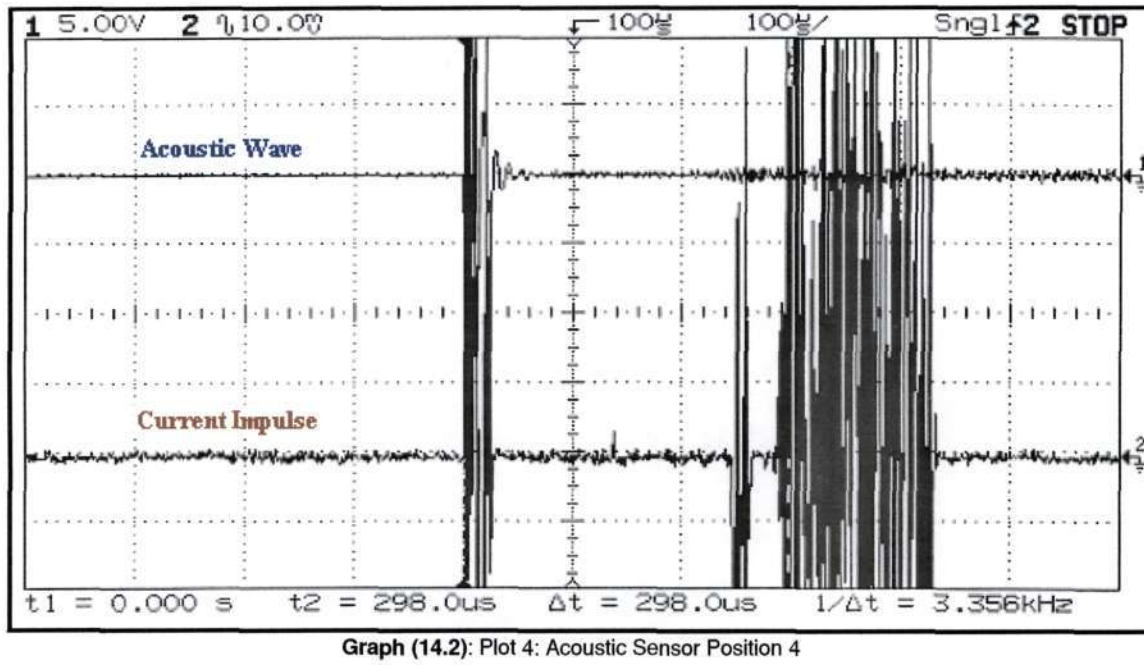

Graph (14.2): Plot 4: Acoustic Sensor Position 4

Graph (14.2), depicts the occurrence of a complete electrical breakdown within the electrode gap spacing. Waveform (2) depicts the current waveform, whilst waveform (1), depicts the corresponding acoustic waveform as recorded at sensor position **4**. Note, here the relative time of arrival of the acoustic signal at acoustic sensor 2, is **298 µs**. This is also significantly longer than the times measured in Chapter 13 where the sensors were located in the area of direct reception. This longer time can also be attributed to the longer distance traveled by the acoustic wave before reaching sensor 4.

As calculated in plot 3, the time taken for the acoustic signal to propagate through the outer steel wall is 1.406µs. This implies that the time taken for the signal to propagate through the oil region is given by:

$$time_{oil} = time_{total} - time_{steel} = 298\mu s - 1.406\mu s = 296.594\mu s$$

Therefore, the distance of the occurrence of the partial discharge away from the sensor (taking into account that the sensor is in the direct line) is calculated as:

$$dis\tan ce = speed_{oil} \times time_{oil} = 1400m/s \times 296.594\mu s = 415.23mm$$

Taking the thickness of the steel wall into account: 415.23mm + 4.5mm= **419.73mm**.

Therefore, the experimental result indicates that the p.d. source lies on a radius of **419.73mm** away from Sensor 4. This result, in combination with the results obtained from the direct-line sensors (sensor 1 and sensor 2) as well as sensor 3, can be depicted as:

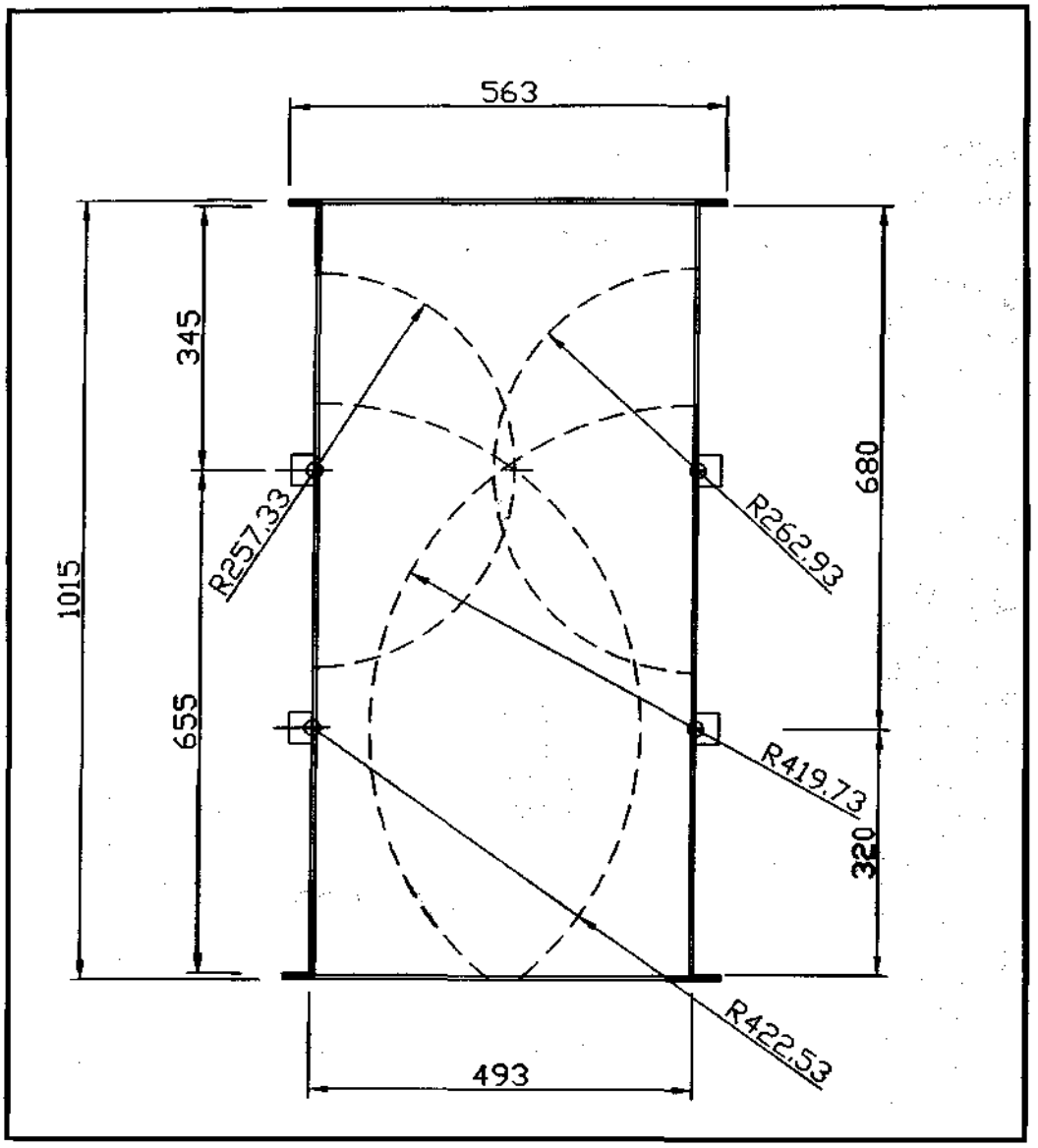

Figure (14.5): Predicted p.d. area based on experimental results (Drawn to scale)

14.6 Effect of filtering on the acoustic method

The acoustic tests were repeated with the filtering system switched on. The results obtained with the sensors in the area of direct reception, as well as with the sensors in the area of indirect reception were identical to the results obtained with the filtering system switched off (Sections (14.2) and (14.3)).

It was concluded that the flow rate in the test cell, induced by the filtering system, was not sufficient to induce significant acoustic disturbances into the test system. It is believed that the installation of larger circulation pumps with higher flow rates, will induce significant acoustic disturbances into the system which will have to be filtered out. In such instances, the noise levels with the active filtering system will have to be established prior to the commencement of testing. The acoustic monitoring system will then have to be adjusted so as to filter out the noise levels introduced by the filtering system. Thereafter, testing may proceed as specified in Section (14.2) and (14.3).

14.7 Conclusion

The aforementioned results together with the results obtained in Chapter 13, further confirm the accuracy and consistency of the acoustic method of p.d. detection and localization.

- Numerous tests were conducted and the results obtained were consistent and reliable in (1). Indicating the presence of a p.d., and (2). Determining the spatial location of the p.d. site.
- The addition of acoustic sensors increases the accuracy of the acoustic method i.e. the predicted area of the p.d. site is reduced.
- The effect of switching on the circulation and filtering system was negligible (as discussed in Section 14.6). It is however believed, that pumps with significantly higher flow rates will introduce acoustic disturbances into the system, which will then have to be isolated and filtered by the acoustic conditioning unit.

CHAPTER 15
ACOUSTIC TESTING – DISTRIBUTION TRANSFORMER GEOMETRY

15.1 Experimental setup

An 11kV distribution type transformer was used during this phase of testing. This transformer has been modified to include a point-to-sphere electrode configuration, which creates the partial discharge when the specified voltage is applied to the point electrode. The gap spacing (s), between the point and the sphere is manually adjustable through a lever that protrudes from the side of the transformer.

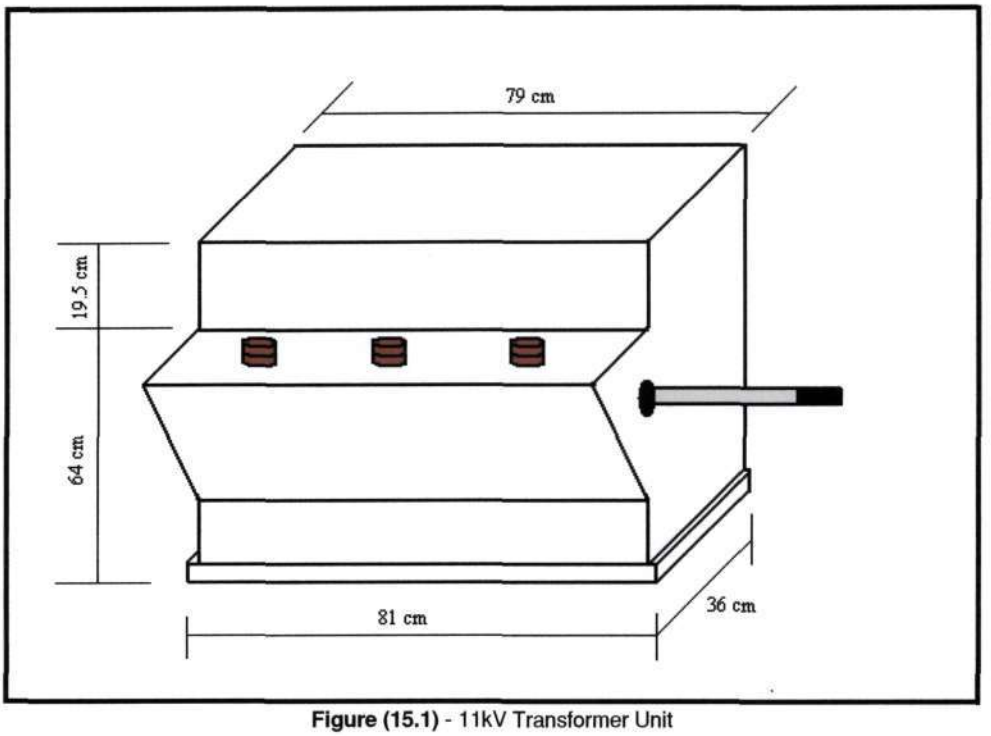

Figure (15.1) - 11kV Transformer Unit

The test circuit utilized for testing purposes is illustrated below.

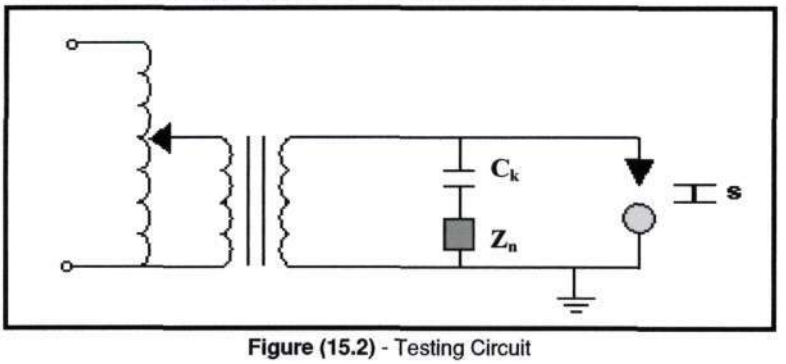

Figure (15.2) - Testing Circuit

The sensors were housed in magnetic holders, which facilitated their mounting onto the steel tank wall of the transformer. A thin layer of silicon grease was applied to the measuring surface of each of the sensors, in order to improve the contact by eliminating any air space between the sensor and the tank wall. The sensor output was observed on an oscilloscope. The current signal was obtained via a current transformer (10mA/ mV) with a bandwidth of 1 MHz to 1.2 GHz. This signal was observed simultaneously on the oscilloscope.

The results of the various tests, which were performed, are discussed in following sections.

15.2 Experimental results

15.2.1 Experiment 1:

Preliminary investigations of the electrical and acoustic waveforms seemed to indicate that partial discharges were occurring at sites other than at the point-to-sphere gap. It was for this reason that the decision to open the lid of the transformer tank and perform a further examination of the transformer was taken.

The upper lid of the transformer was opened, and the point-to-sphere gap was closely examined. In order to determine whether partial discharges were occurring at other areas in the transformer, the point electrode was removed from the tank, and the voltage was applied to the bushing that was previously attached to the point electrode. At voltages of approximately 18 kV partial discharges were noted on the observation unit. This occurrence confirmed the suspicion that partial discharges were in fact occurring in another area in the transformer. The most probable area where these partial discharges were occurring was the transformer bushing.

It was then decided that the point electrode would be re-installed into its previous position, and the gap distance (s) between the point and sphere would be decreased to such an extent, that the gap would flashover before the inception voltage of the other partial discharges would be reached. In this way, the partial discharges, which would be observed, would be only as a result of the flashover of the point-to-sphere gap. In order to facilitate in making the point-to-sphere gap flashover at low voltages, an artificial defect was introduced in the spacing between the point and sphere. This defect was made up of a Mylar® sandwich which consisted of 5 layers of Mylar® film (each layer = 50 μm thick). Therefore, the gap spacing between the point and sphere was reduced to 250μm.

The voltage was then applied to the point electrode, and partial discharges were observed to occur at voltages of approximately 15,6 kV. One acoustic sensor was used, and the position of the sensor on the tank is depicted overleaf:

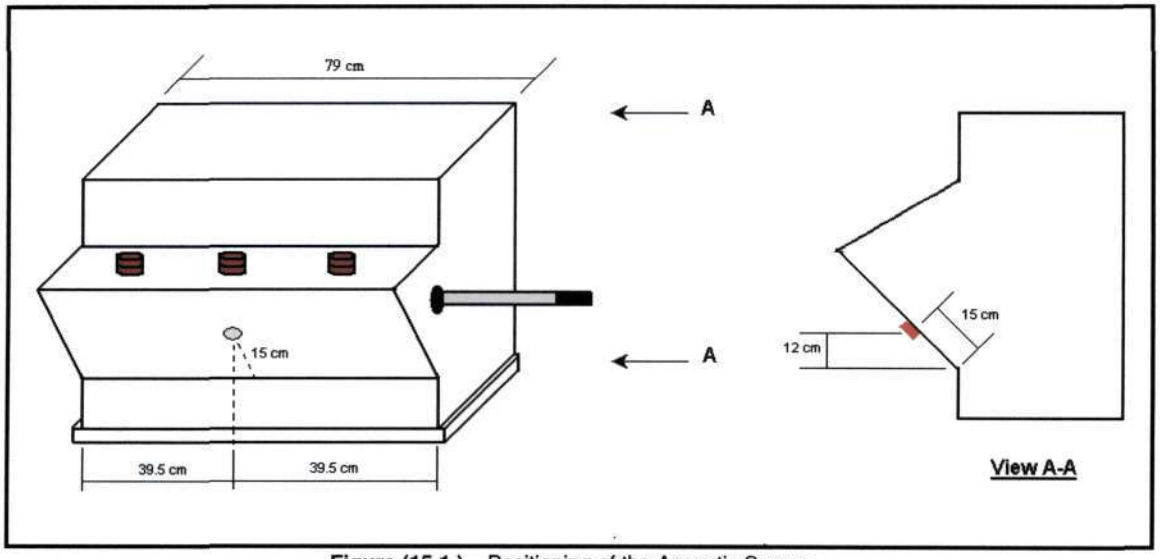

Figure (15.1.) – Positioning of the Acoustic Sensor

The acoustic and electrical waveforms were observed simultaneously on the observation unit. The waveforms were examined for the following:

- Correlation between the occurrence of a current impulse on the electrical signal, and the occurrence of the corresponding acoustic wave.

- Relative time of arrival of the acoustic wave using the instant of the occurrence of the current impulse as the zero reference point.

The following waveforms were obtained and are examined overleaf:
(**Note**: Localization with respect to the actual position of the partial discharge source is commenced in Experiment 2.)

Plot 1:

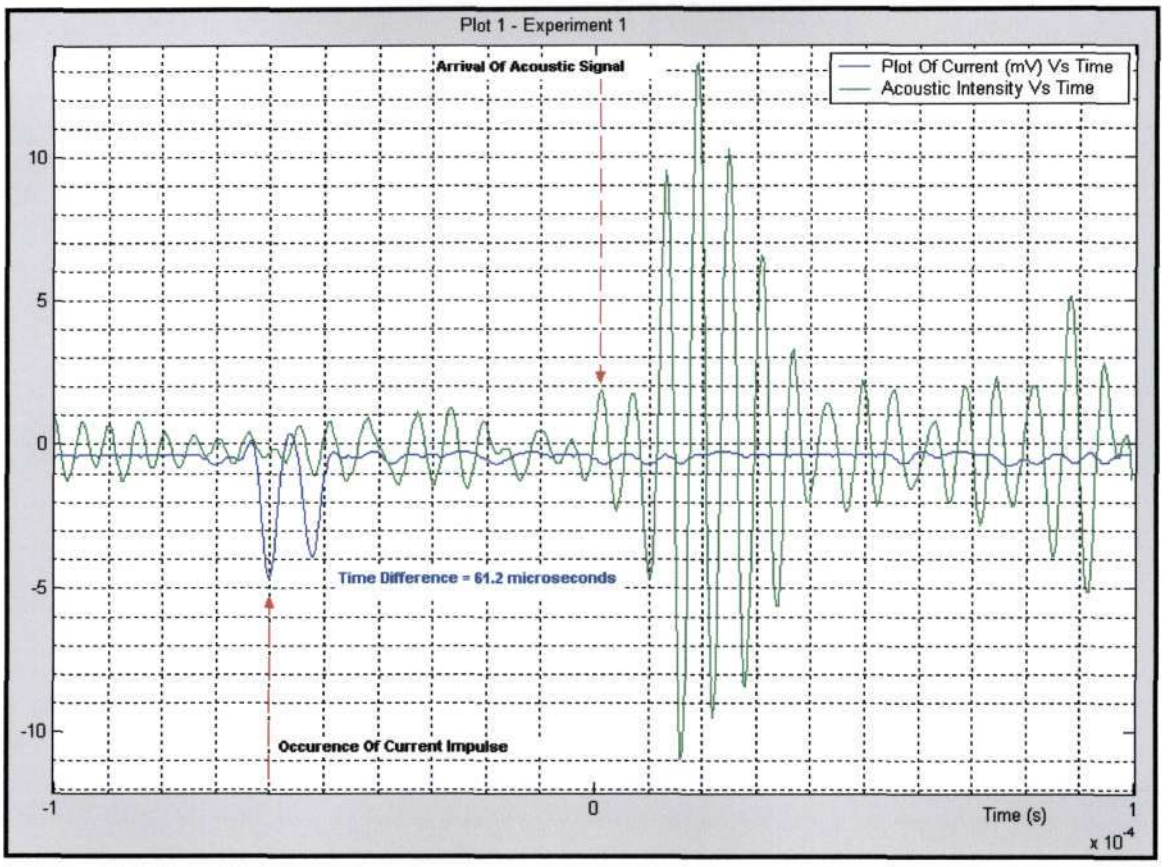

Figure (15.2.) – Plot 1: Experiment 1

Figure (15.2), depicts the occurrence of a partial discharge during experiment 1. The current impulse is shown. This current impulse is utilized as the zero reference point for timing the arrival of the acoustic signal. The acoustic signal was noted to occur 61.2 μs after the occurrence of the current impulse.

The internal structure of the transformer, between the partial discharge source and the sensor contains two different types of media (as observed). These media are:

- A transformer oil region
- The steel tank wall of the transformer

For calculation purposes the tank wall was taken to have a thickness of 2mm. From literature, it is known that the speed of sound through transformer steel is approximately 3200 m/s. Therefore the time taken for the signal to propagate through the steel wall is calculated as:

$$time_{steel} = \frac{thickness_{wall}}{speed_{steel}} = \frac{2\times10^{-3}\,m}{3200m/s} = 0.625\mu s$$

Therefore, the time taken for the signal to propagate through the oil region is:

$$time_{oil} = time_{total} - time_{steel} = 61.2\mu s - 0.625\mu s = 60.575\mu s$$

Therefore, the distance of the occurrence of the partial discharge away from the sensor (assuming the sensor is in the direct line) is calculated as:

$$dis\tan ce = speed_{oil} \times time_{oil} = 1400m/s \times 60.575\mu s = 8.481cm$$

Taking the thickness of the steel wall into account: 8.481cm + 0.2cm= **8.681 cm**.

Therefore, the partial discharge site lies **8.681 cm** away from the sensor (assuming the sensor location lies in the direct line between the p.d. site and the tank wall).

Plot 2:

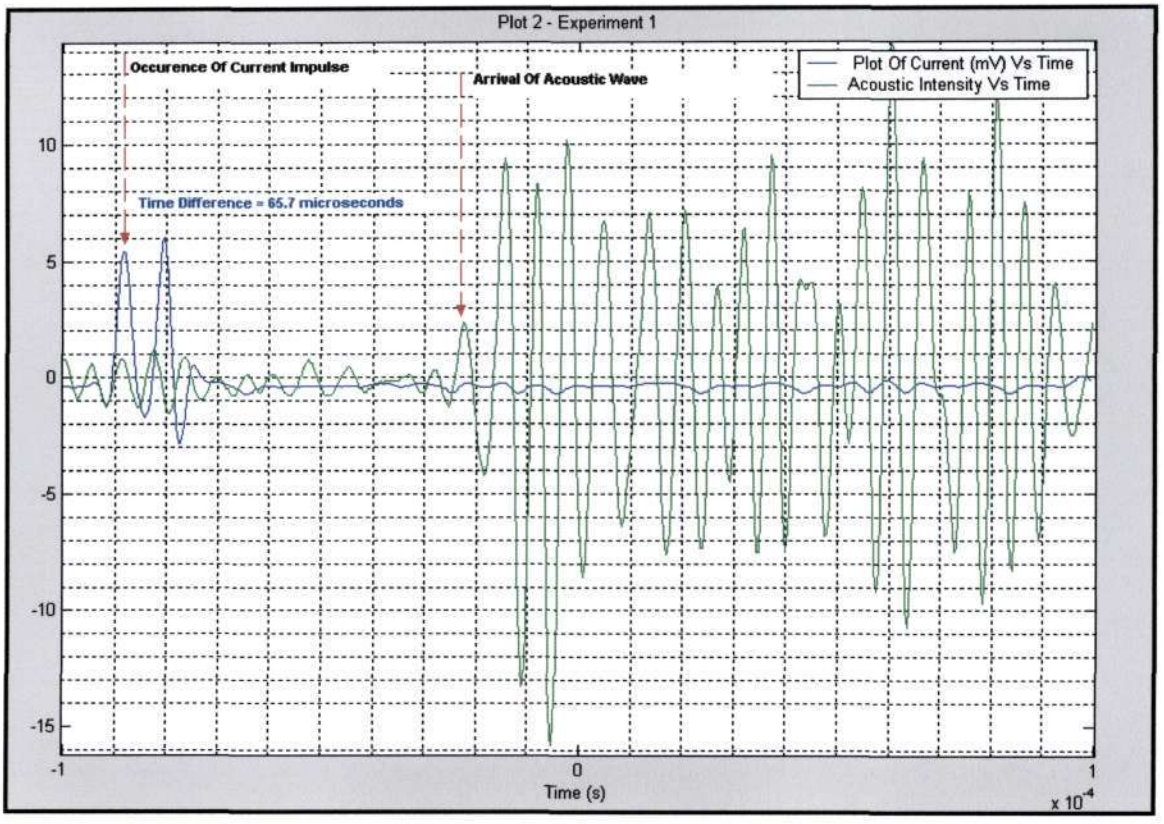

Figure (15.3.) – Plot 2

Figure (15.3), depicts the occurrence of the next p.d. which was observed on the oscilloscope. Note, here the relative time of arrival of the acoustic signal at the sensor is 65.7 μs.

As in calculated in plot 1, the time taken for the acoustic signal to propagate through the steel wall is 0.625 μs. This implies that the time taken for the signal to propagate through the oil region only, is given by:

$$time_{oil} = time_{total} - time_{steel} = 65.7\mu s - 0.625\mu s = 65.075\mu s$$

Therefore, the distance of the occurrence of the partial discharge away from the sensor (assuming the sensor is in the direct line) is calculated as:

$$distance = speed_{oil} \times time_{oil} = 1400m/s \times 65.075\mu s = 9.1105cm$$

Taking the thickness of the steel wall into account: 9.1105cm + 0.2= **9.3105 cm**.

Therefore, the partial discharge site lies **9.3105 cm** away from the sensor (assuming the sensor location lies in the direct line between the p.d. site and the tank wall).

Plot 3:

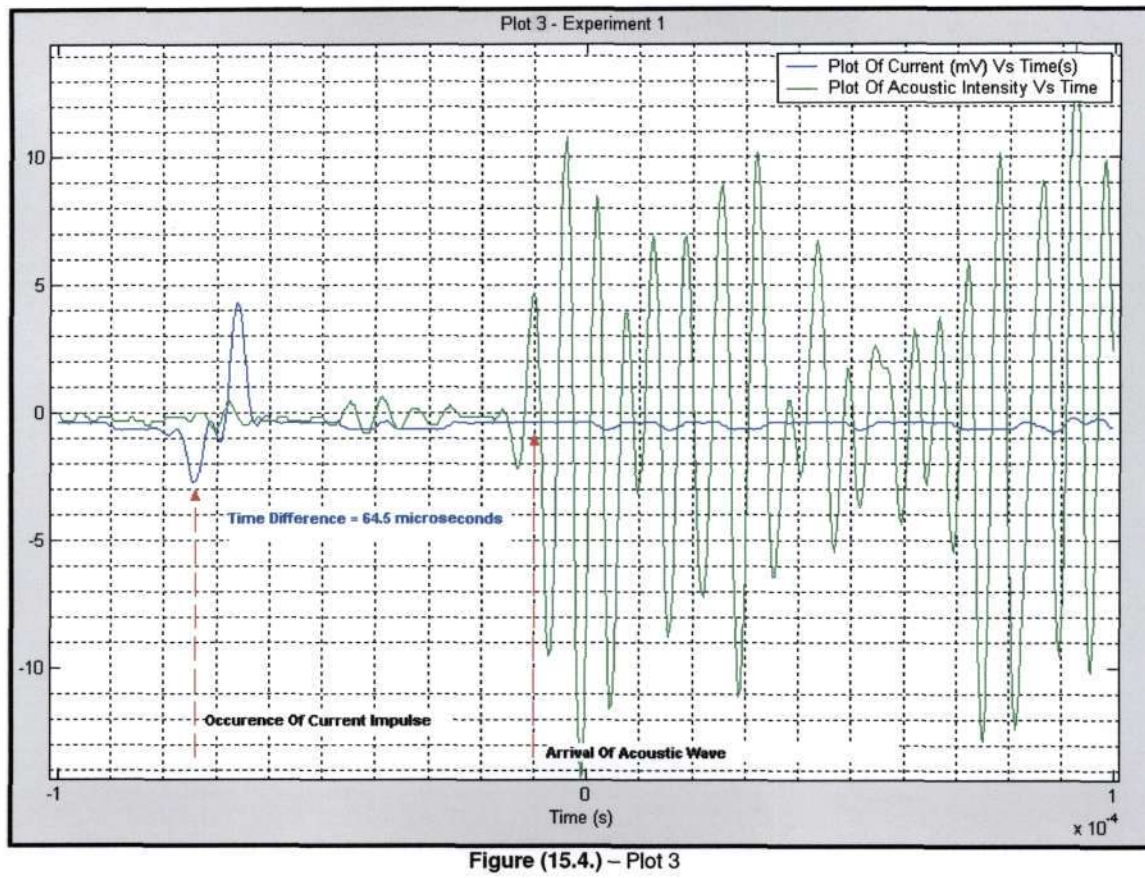

Figure (15.4.) – Plot 3

Figure (15.4), depicts the occurrence of the next p.d. which was observed on the oscilloscope. In this case the relative time of arrival of the acoustic signal at the sensor is 64.5 μs.

As in calculated in plot 1, the time taken for the acoustic signal to propagate through the steel wall is 0.625 μs. This implies that the time taken for the signal to propagate through the oil region only, is given by:

$$time_{oil} = time_{total} - time_{steel} = 64.5\mu s - 0.625\mu s = 63.875\mu s$$

Therefore, the distance of the occurrence of the partial discharge away from the sensor (assuming the sensor is in the direct line) is calculated as:

$$dis\tan ce = speed_{oil} \times time_{oil} = 1400m/s \times 63.875\mu s = 8.943cm$$

Taking the thickness of the steel wall into account: 8.943cm + 0.2 = **9.143 cm**.

Therefore, the partial discharge site lies **9.143 cm** away from the sensor (assuming the sensor location lies in the direct line between the p.d. site and the tank wall).

15.2.2 Experiment 2

The test circuit utilized for experiment 2, is depicted below:

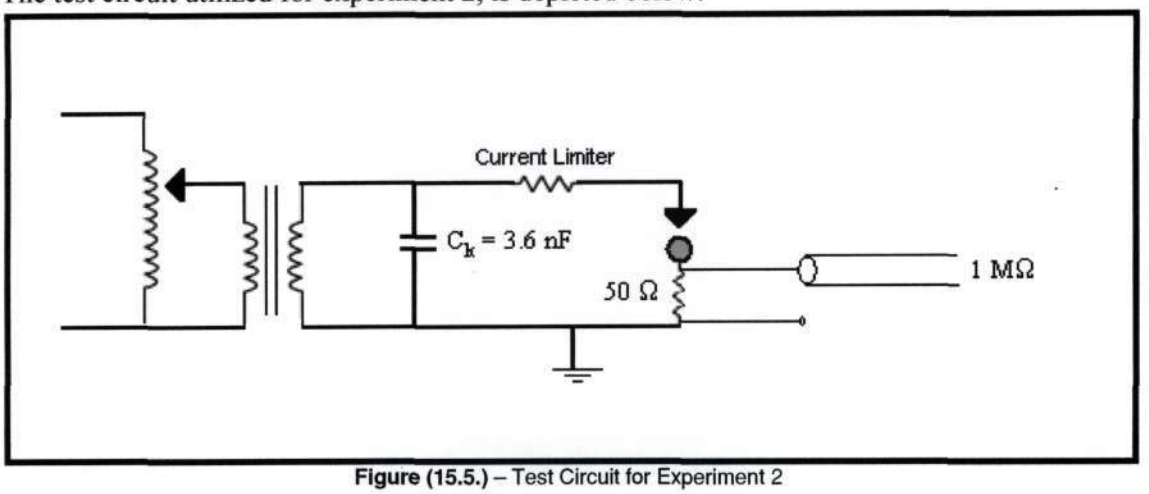

Figure (15.5.) – Test Circuit for Experiment 2

The size of the Mylar® sandwich which was introduced into the gap between the point and sphere electrodes was increased to 8 layers, which in turn equates to a total gap distance of approximately (50 μm × 8 layers) 400 μm. Initially one acoustic sensor was placed on the tank wall in the following position:

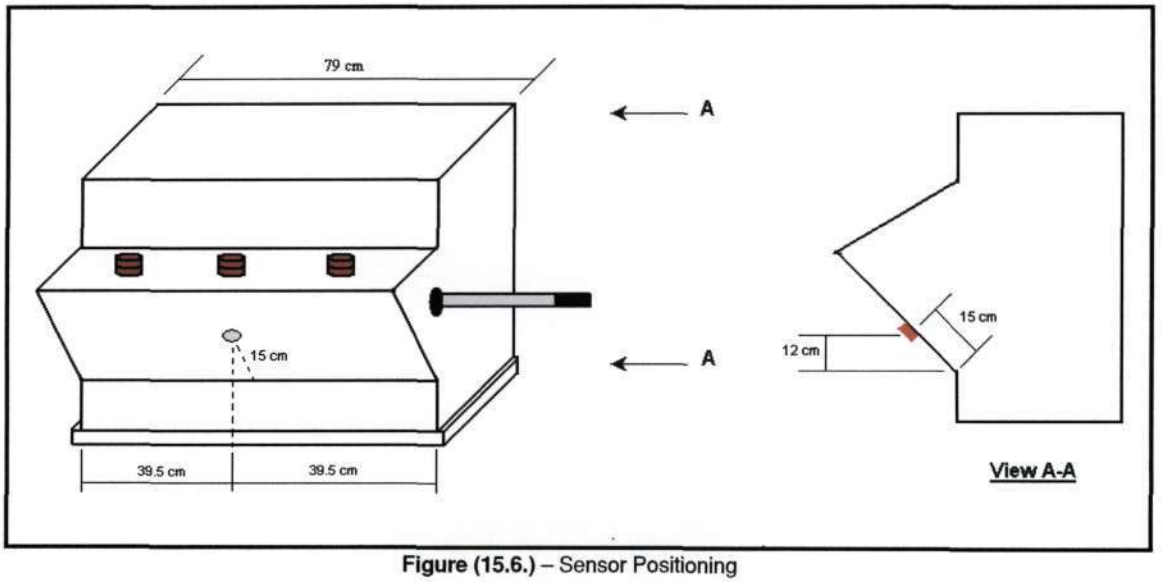

Figure (15.6.) – Sensor Positioning

The acoustic method was applied simultaneously with the electrical method. The applied voltage was raised to 7 kV and, both the acoustic signal and the electrical signal (current impulse) where observed simultaneously on the oscilloscope. The waveforms obtained are depicted overleaf:

The actual location of the partial discharge source is depicted overleaf.

Actual location of partial discharge source in transformer tank

The following diagram illustrates the sensor position in relation to the p.d. source:

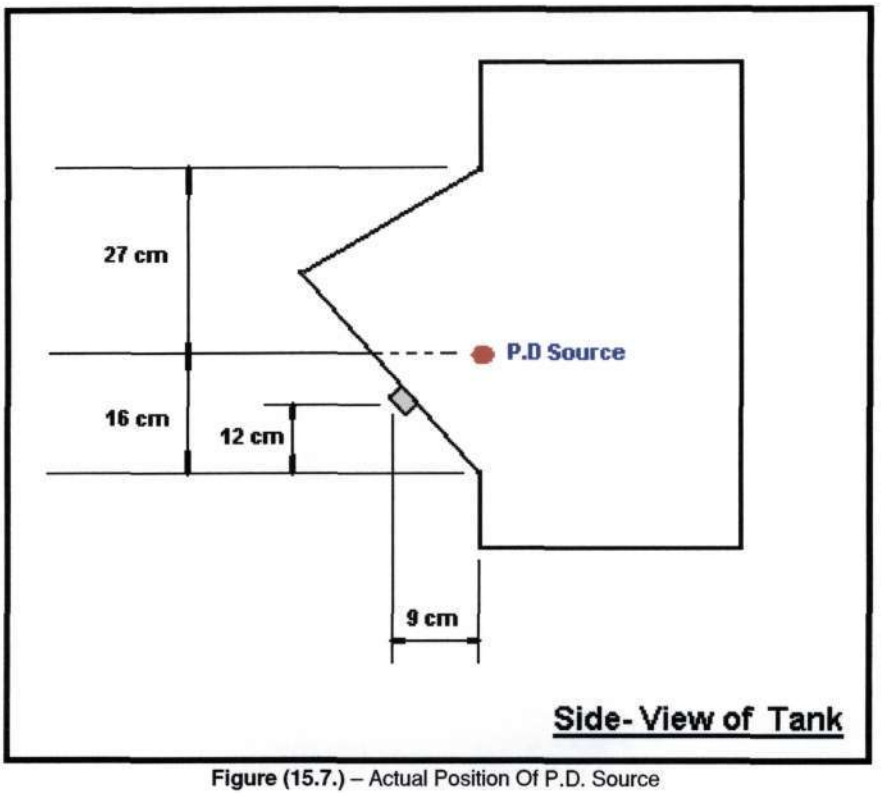

Figure (15.7.) – Actual Position Of P.D. Source

Geometrically, the distance between the sensor and the partial discharge source is calculated as:

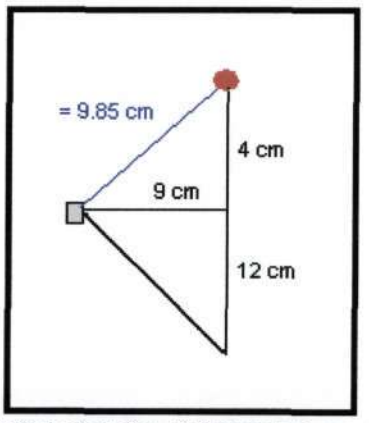

Figure (15.8.) – Geometrical calculation of distance between sensor and p.d. source

Plot 1:

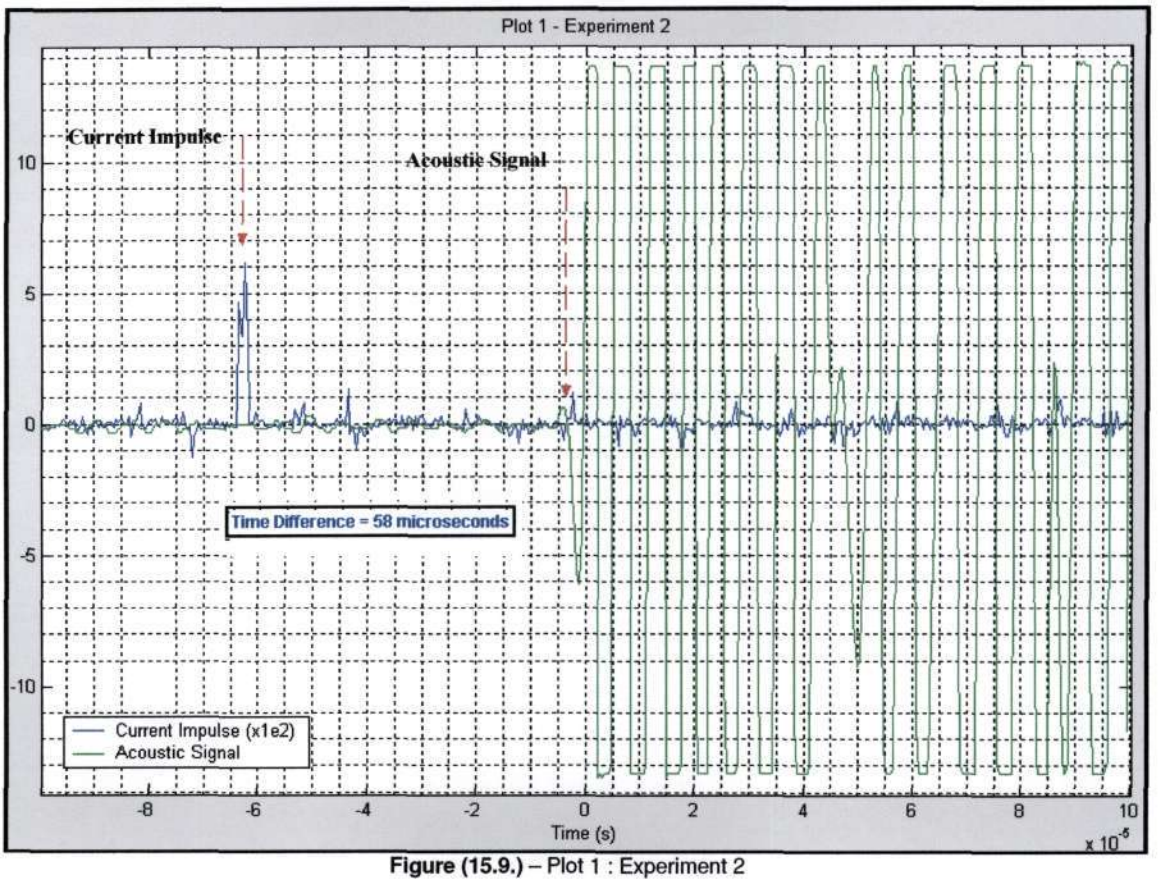

Figure (15.9.) – Plot 1 : Experiment 2

Figure (15.9), depicts the occurrence of a partial discharge during experiment 2. The current impulse is shown. This current impulse is utilized as the zero reference point for timing the arrival of the acoustic signal. The acoustic signal was noted to occur 58 μs after the occurrence of the current impulse.

The internal structure of the transformer, between the partial discharge source and the sensor contains two different types of media (as observed). These media are:

- A transformer oil region
- The steel tank wall of the transformer

For calculation purposes the tank wall was taken to have a thickness of 2mm. From literature, it is known that the speed of sound through transformer steel is approximately 3200 m/s. Therefore the time taken for the signal to propagate through the steel wall is calculated as:

$$time_{steel} = \frac{thickness_{wall}}{speed_{steel}} = \frac{2\times10^{-3}m}{3200m/s} = 0.625\mu s$$

Therefore, the time taken for the signal to propagate through the oil region is:

$$time_{oil} = time_{total} - time_{steel} = 58\mu s - 0.625\mu s = 57.375\mu s$$

Therefore, the calculated distance of the site of the partial discharge away from the sensor is calculated as:

$$dis\tan ce = speed_{oil} \times time_{oil} = 1400m/s \times 57.375\mu s = 8.0325cm$$

Taking the thickness of the steel wall into account: 8.0325cm + 2×10^{-3} = **8.0345 cm**.

Therefore, the predicted location of the partial discharge site lies in the region which is **8.0345 cm** away from the sensor.

The sensor was not specially positioned to lie in the direct line of the acoustic wave, therefore the predicted range in which the partial discharge lies is actually in a circle of radius = 8.0345 cm around the acoustic sensor. This can be diagrammatically depicted as:

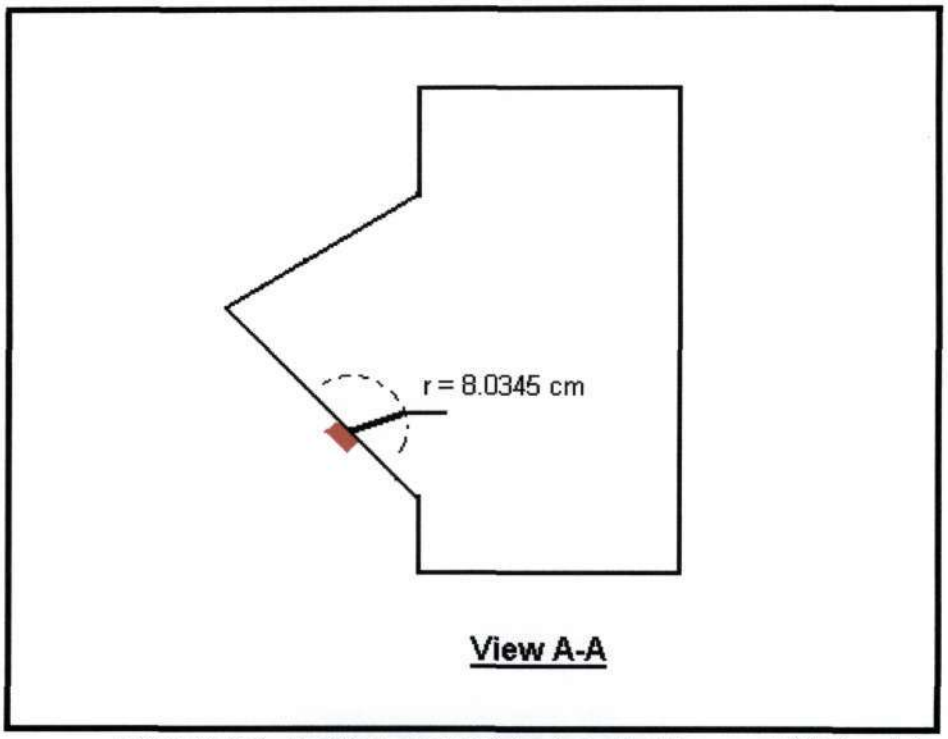

Figure (15.10.) – Predicted range in which p.d. site should be present (Not to scale)

The actual distance between the sensor and the p.d. source is 9.85 cm (as calculated previously). The margin of error can be attributed to the associated experimental errors.

Plot 2:

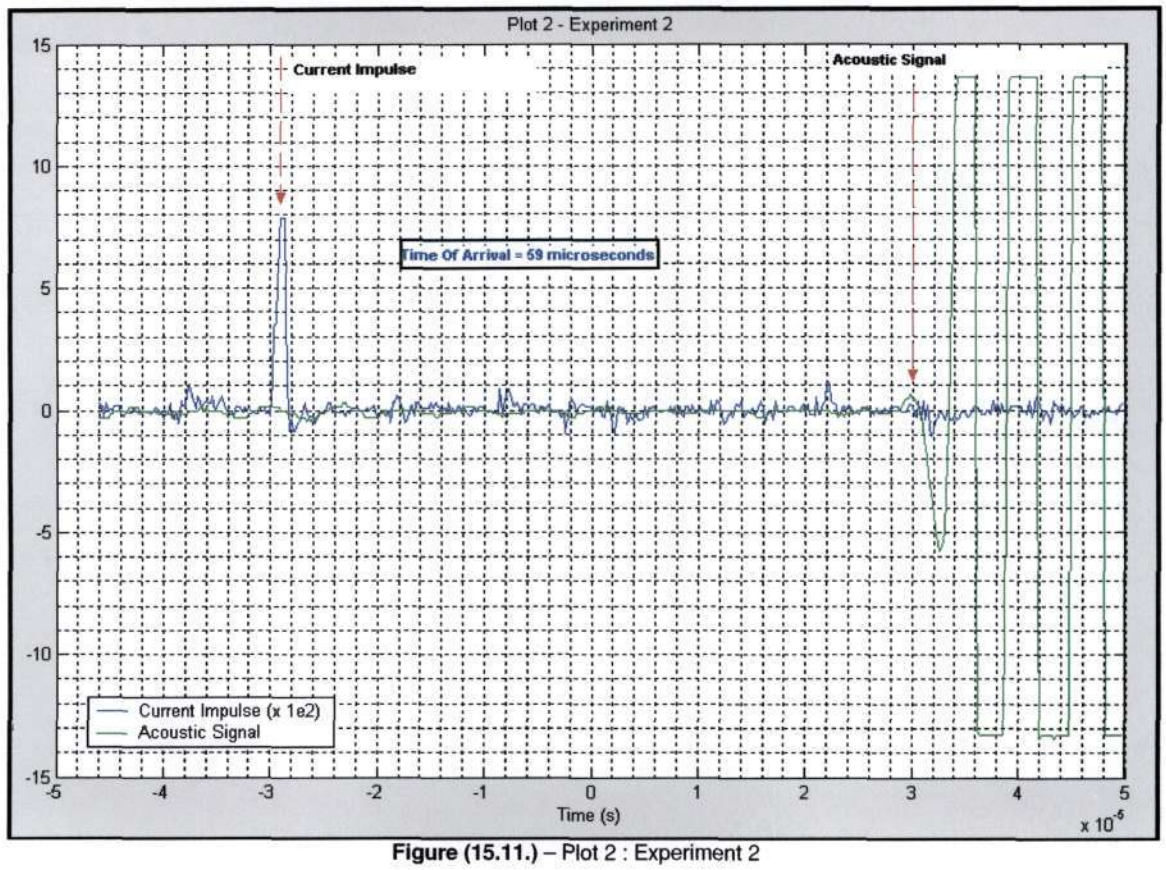

Figure (15.11.) – Plot 2 : Experiment 2

Figure (15.11), depicts the occurrence of another partial discharge during experiment 2. The acoustic sensor position remained unchanged from the previous location. The current impulse and the corresponding arrival of the acoustic signal are shown. The acoustic signal was noted to occur 59 μs after the occurrence of the current impulse.

The time taken for the signal to propagate through the steel wall is calculated as (using previous information from plot 1 i.e. thickness of wall = 2mm):

$$time_{steel} = \frac{thickness_{wall}}{speed_{steel}} = \frac{2\times10^{-3}\,m}{3200m/s} = 0.625\mu s$$

Therefore, the time taken for the signal to propagate through the oil region is:

$$time_{oil} = time_{total} - time_{steel} = 59\mu s - 0.625\mu s = 58.375\mu s$$

Therefore, the calculated distance of the site of the partial discharge away from the sensor is calculated as:

$$dis\tan ce = speed_{oil} \times time_{oil} = 1400m/s \times 58.375\mu s = 8.1725cm$$

Taking the thickness of the steel wall into account: 8.1725cm + 2×10^{-3} = **8.1745 cm**.

Therefore, the predicted location of the partial discharge site lies in the region that is **8.1745 cm** away from the sensor.

The sensor was not specially positioned to lie in the direct line of the acoustic wave, therefore the predicted range in which the partial discharge lies is actually in a circle of radius = 8.1745 cm around the acoustic sensor. This can be diagrammatically depicted as:

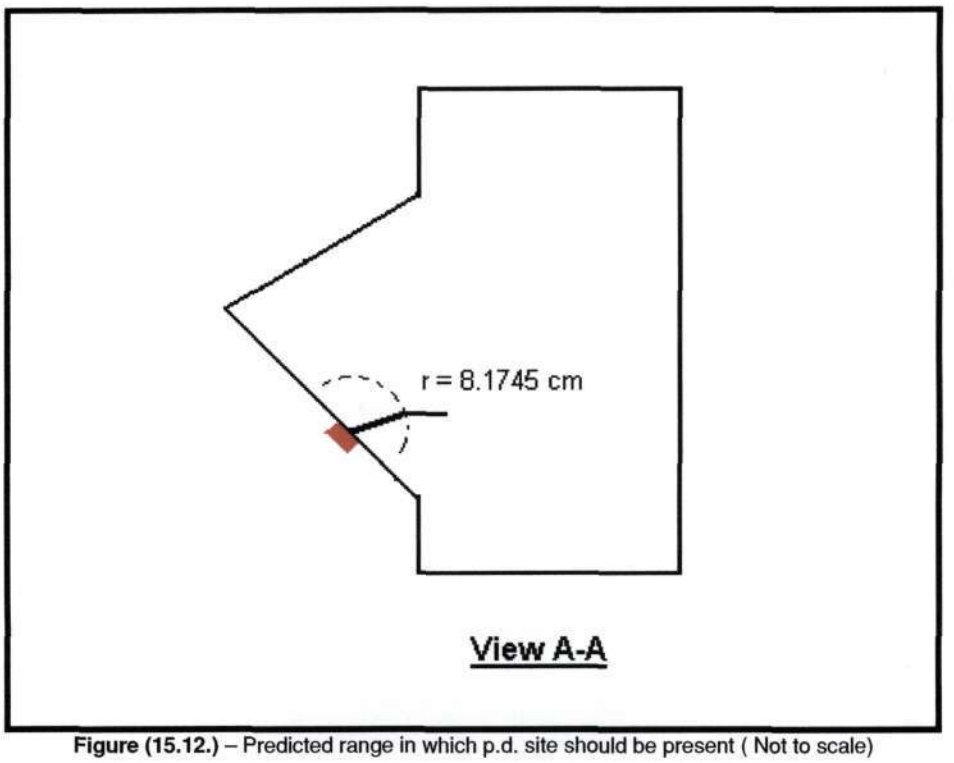

Figure (15.12.) – Predicted range in which p.d. site should be present (Not to scale)

Plot 3:

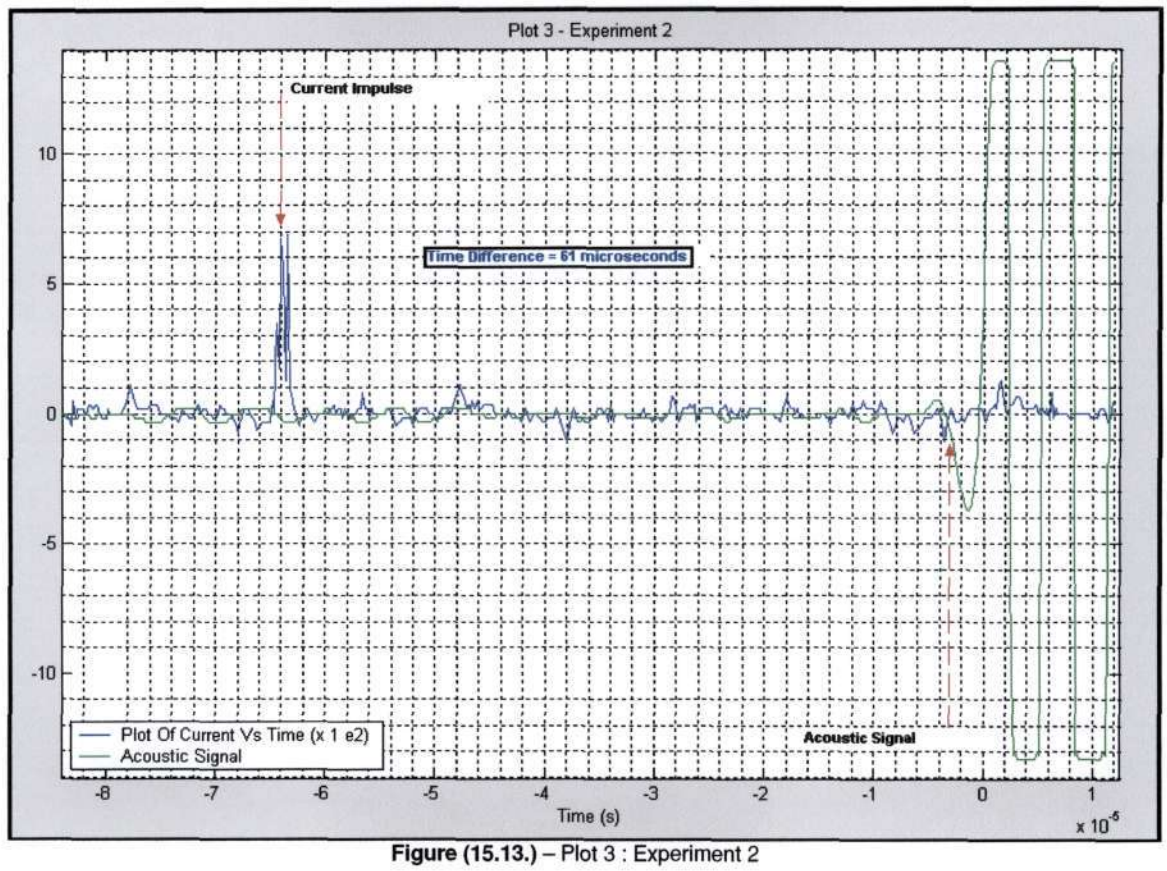

Figure (15.13.) – Plot 3 : Experiment 2

Figure (15.13), depicts the occurrence of another partial discharge during experiment 2. The acoustic sensor position remained unchanged from the previous location. The current impulse and the corresponding arrival of the acoustic signal are shown. The acoustic signal was noted to occur 61 μs after the occurrence of the current impulse.

The time taken for the signal to propagate through the steel wall is calculated as (using previous information from plot 1 i.e. thickness of wall = 2mm):

$$time_{steel} = \frac{thickness_{wall}}{speed_{steel}} = \frac{2\times10^{-3}\,m}{3200m/s} = 0.625\mu s$$

Therefore, the time taken for the signal to propagate through the oil region is:

$$time_{oil} = time_{total} - time_{steel} = 61\mu s - 0.625\mu s = 60.375\mu s$$

Therefore, the calculated distance of the site of the partial discharge away from the sensor is calculated as:

$$dis\tan ce = speed_{oil} \times time_{oil} = 1400m/s \times 60.375\mu s = 8.4525cm$$

Taking the thickness of the steel wall into account: 8.4525cm + 2×10^{-3} = **8.4545 cm**.

Therefore, the predicted location of the partial discharge site lies in the region which is **8.4545 cm** away from the sensor.

The sensor was not specially positioned to lie in the direct line of the acoustic wave, therefore the predicted range in which the partial discharge lies is actually in a circle of radius = 8.1745 cm around the acoustic sensor. This can be diagrammatically depicted as:

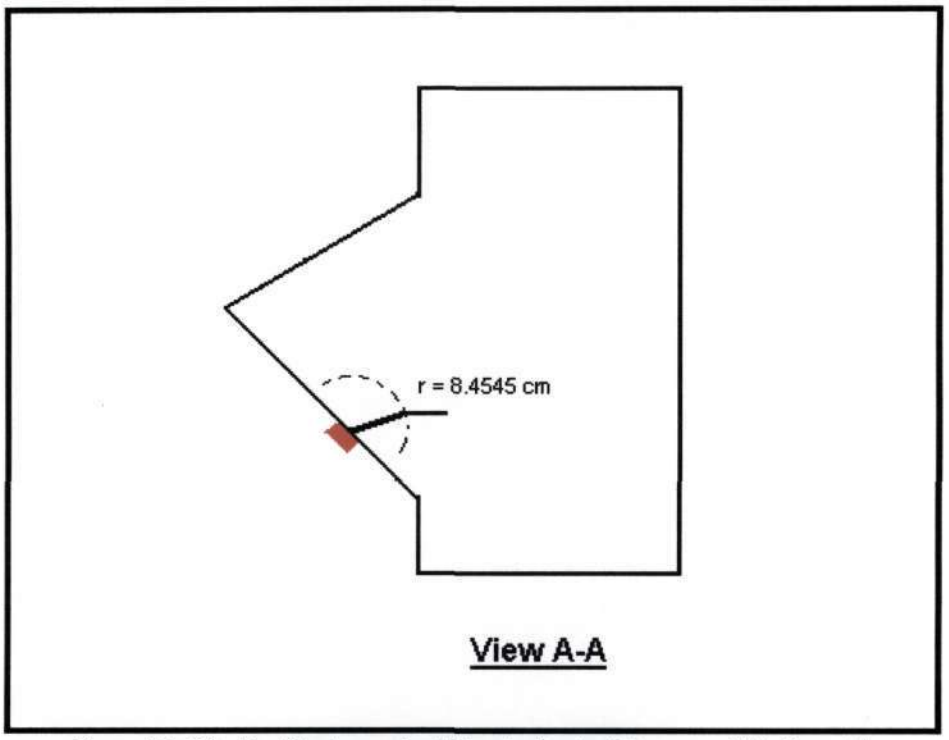

Figure (15.14.) – Predicted range in which p.d. site should be present (Not to scale)

Summary of experiment 2:

The results obtained for experiment 2, highlights the following:

- The strong correlation between the occurrence of the current impulse, and the arrival of the acoustic wave a certain time later.
- The accuracy achieved with the simultaneous use of the electrical method, and the acoustic method.
- The localization technique employed using the information obtained from the waveforms.

The predicted spatial location of the partial discharge site (performed using the experimental data) correlates well with the theoretically predicted location.

15.2.3 Experiment 3

The test circuit utilized for experiment 3 remained unchanged from experiment 2. The gap distance remained unchanged at 400 μm. The sensor position was the only parameter that was changed for experiment 3. The sensor was moved to the back of the transformer tank (approximately in the center). This setup is depicted below:

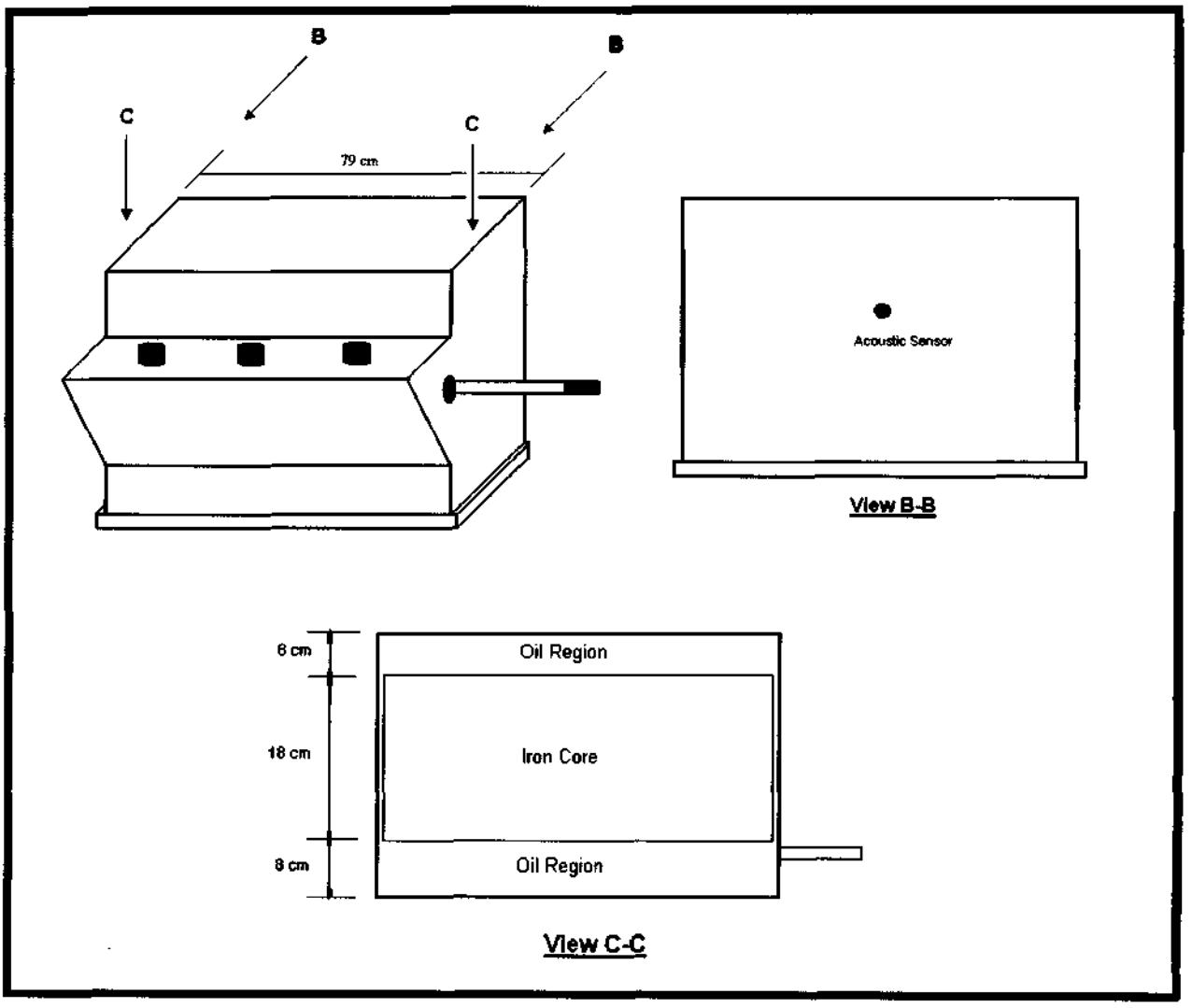

Figure (15.15.) – Positioning of Acoustic Sensor for Experiment 3

Note, the acoustic signal will propagate through the first **oil region** (at ± 1400 m/s), then through the **iron core** (at ± 5800 m/s) and lastly through the second oil region (at ± 1400 m/s), before it impinges upon the back steel wall of the transformer where the acoustic signal is positioned. Therefore, the time taken for the signal to reach the acoustic sensor in it's current position should typically be very much larger than the time taken in experiment 2.

The acoustic method was applied simultaneously with the electrical method. The applied voltage was raised to 7 kV and, both the acoustic signal and the electrical signal (current impulse) were observed simultaneously on the oscilloscope. The waveform obtained is depicted below:

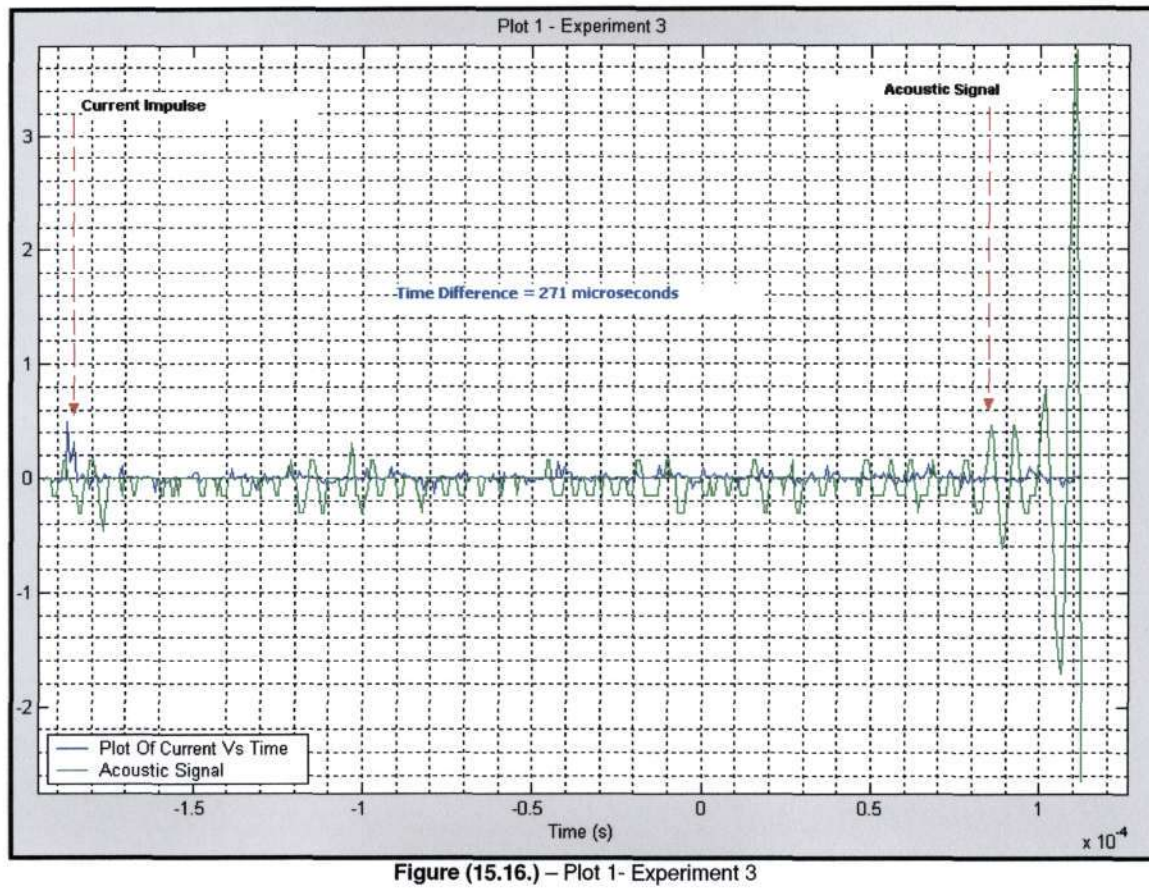

Figure (15.16.) – Plot 1- Experiment 3

The occurrence of the current impulse marks the zero reference frame from which the arrival of the acoustic signal at the sensor is measured. The acoustic signal takes 271 μs to arrive at the sensor. This relative time of arrival will now be used to locate the site of the partial discharge.

Localization calculations:

The localization calculations have been divided into the following steps:

(1). Time taken for an acoustic signal to propagate through oil region nearest to sensor:

$$time_{oil\_1} = \frac{dist_{oil\_region}}{speed_{oil}} = \frac{0.08m}{1400m/s} = 57.14\mu s$$

The time taken for an acoustic signal to travel through the first oil region is 57.14μs. This is shorter than the total time taken for the signal to reach the sensor, therefore it can be stated that the partial discharge site has to lie beyond this first oil region.

(2). Time taken for signal to propagate through iron core + copper region

Note, the region which contains the transformer windings, also has copper material contained in it. The speed of sound in copper is approximately 3500 m/s. Therefore, in order to determine the speed of sound through this winding region, an average of the speed of sound in iron (5800 m/s) and the speed of sound in copper (3500 m/s) was taken. Therefore, the speed of sound through the region is 4650 m/s.

$$time_{iron+copper} = \frac{dist_{iron+copper\_region}}{speed_{iron+copper}} = \frac{0.18m}{4650m/s} = 38.71\mu s$$

Therefore, the total time for a signal to propagate through the first oil region and this iron+copper region = 57.14μs + 38.71μs = 95.85μs.

This is still shorter than the total time taken for the signal to reach the sensor, therefore it can be stated that the partial discharge site has to lie beyond this combined first oil region and this transformer windings region.

(3). Calculation of location of P.D. source

Due to the fact that the inner geometry of this transformer is known, it is known that there are is only an oil region beyond this transformer windings region. Therefore to calculate the distance from which this acoustic signal is originating within this oil region, the following steps are followed:

$$time_{remaining} = time_{total} - (time_{oil} + time_{iron+copper}) = 175.15\mu s$$

$$distance = speed_{oil} \times time_{rem} = 1400m/s \times 175.15\mu s = 0.245m$$

Therefore, to quote this distance in terms of the geometry of the transformer, by using the sensor as the reference:

Distance of p.d. source from sensor = (distance of first oil region) + (iron and copper region) + (Distance to source from iron and copper region)
= (8cm + 18cm + 24.5cm) = **50.5 cm**

The following diagram quotes this distance in terms of the measured geometry of the transformer:

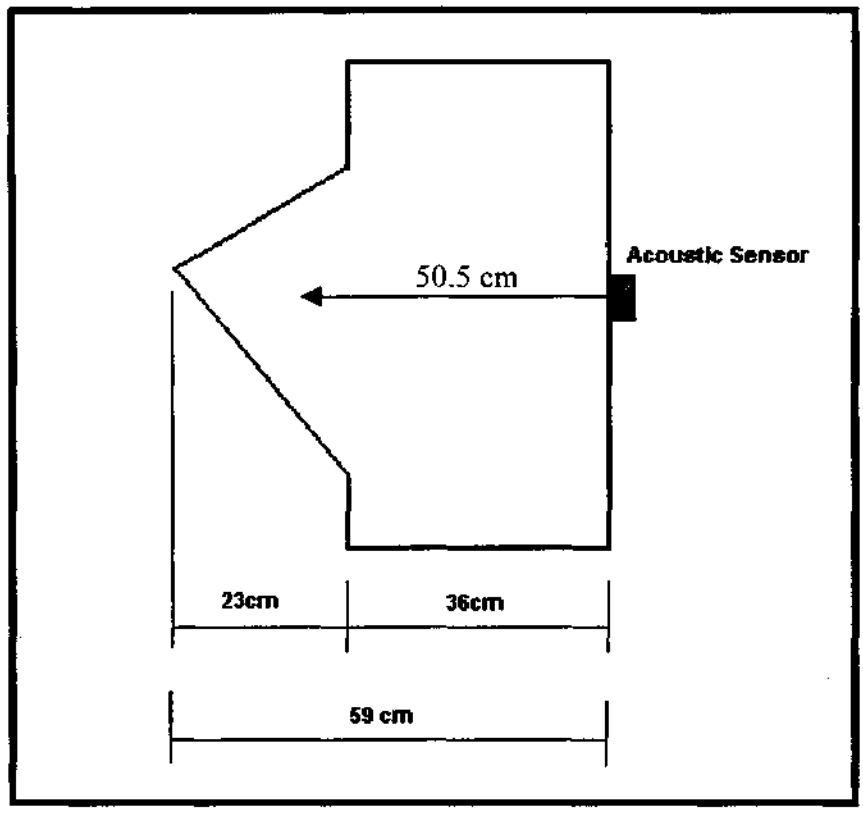

Figure (15.17.) – Illustration of result

Therefore, the prediction correlates well to the actual location of the partial discharge source i.e. point-to-sphere electrode gap.

15.2.4 Experiment 4

The tests performed in experiment 4, involved the utilization of two acoustic sensors simultaneously. The test circuit and the gap spacing remained unchanged from experiments 2 and 3. One acoustic sensor was placed at the front of the transformer tank (as in experiment 2), while the other acoustic sensor was placed at the back of the tank (approximately in the center, as in experiment 3). This setup is depicted below:

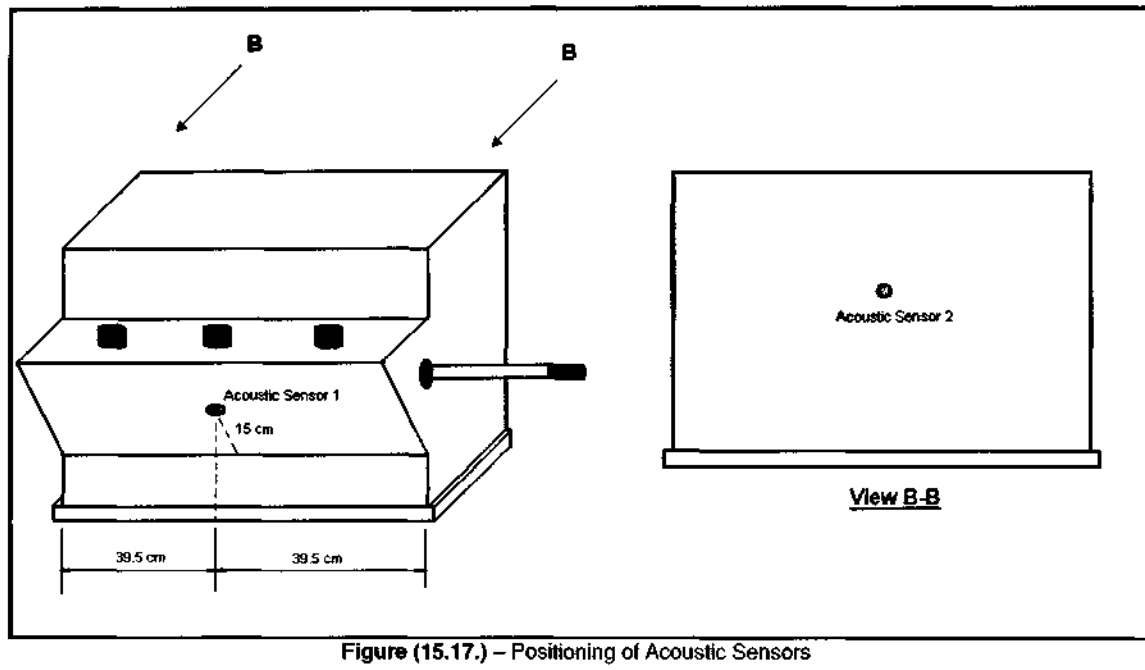

Figure (15.17.) – Positioning of Acoustic Sensors

The acoustic method was applied simultaneously with the electrical method. The applied voltage was raised to 7 kV and, both acoustic signals (from both sensors) and the electrical signal (current impulse) were observed simultaneously on the oscilloscope. The waveforms obtained are depicted overleaf:

Plot 1:

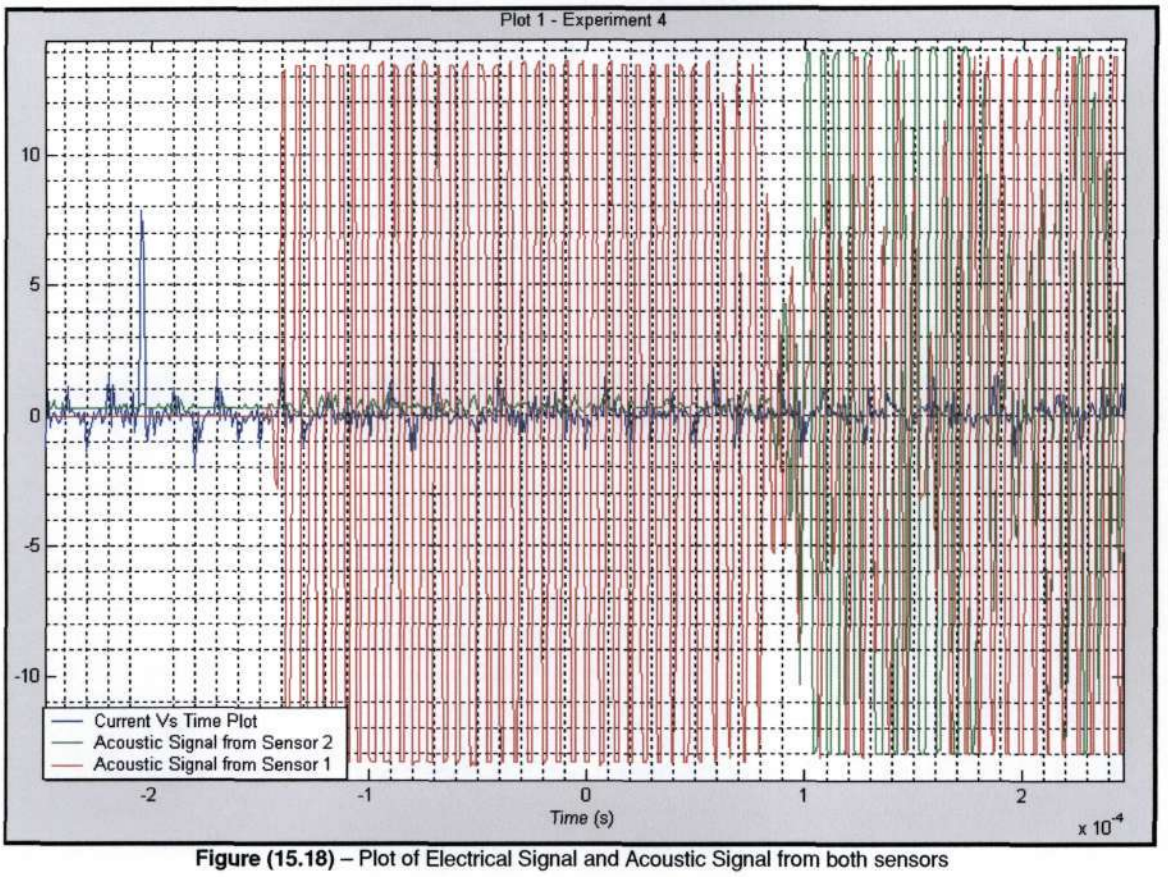

Figure (15.18) – Plot of Electrical Signal and Acoustic Signal from both sensors

In order to attain the arrival times of each of the acoustic signals with respect to the reference frame i.e. the current impulse, separate plots are done overleaf:

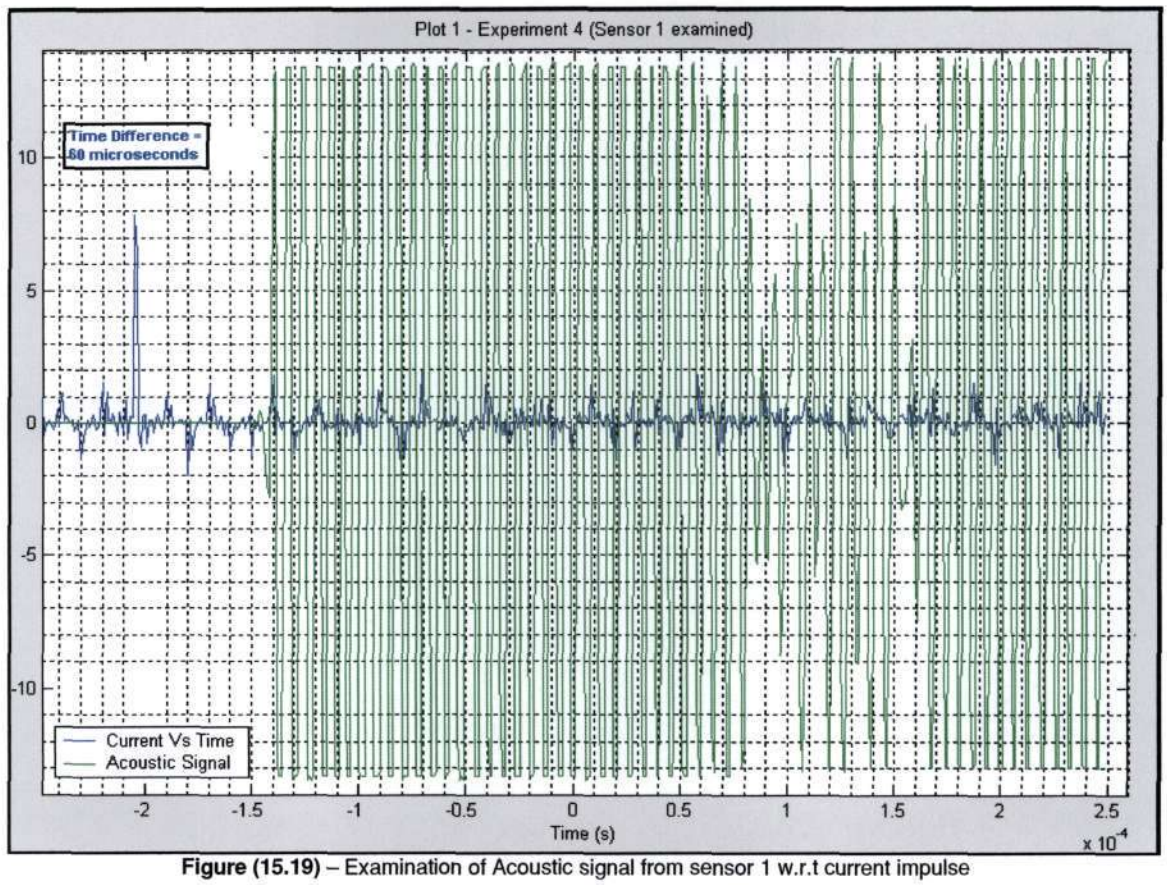

Figure (15.19) – Examination of Acoustic signal from sensor 1 w.r.t current impulse

Figure (15.19), depicts the acoustic signal received from sensor 1, showing the occurrence of a partial discharge. The acoustic signal was noted to occur 60 μs after the occurrence of the current impulse.

The steel wall will be considered. For calculation purposes the tank wall was taken to have a thickness of 2mm. From literature, it is known that the speed of sound through transformer steel is approximately 3200 m/s. Therefore the time taken for the signal to propagate through the steel wall is calculated as:

$$time_{steel} = \frac{thickness_{wall}}{speed_{steel}} = \frac{2 \times 10^{-3} m}{3200 m/s} = 0.625 \mu s$$

Therefore, the time taken for the signal to propagate through the transformer therefore is:

$$time_{transformer} = time_{total} - time_{steel} = 60 \mu s - 0.625 \mu s = 59.375 \mu s$$

The oil region nearest to the sensor (between the sensor and core) has a distance of 0.31m. Therefore, the time taken for an acoustic signal to propagate through this oil region is given by:

$$time_{oil} = \frac{dis\tan ce_{oil\_region}}{speed_{oil}} = \frac{0.31m}{1400 m/s} = 221 \mu s$$

But, the acoustic signal from the partial discharge site took a shorter time to reach the sensor (60 μs). Therefore, the partial discharge site must lie within this oil region.

Therefore, the calculated distance of the site of the partial discharge away from the sensor is calculated as:

$$dis\tan ce = speed_{oil} \times time_{oil} = 1400 m/s \times 59.375 \mu s = 8.3125 cm$$

Taking the thickness of the steel wall into account: 8.3125cm + 0.2 = **8.3145 cm**.

Therefore, the predicted location of the partial discharge site lies in the region that is **8.3145 cm** away from the sensor.

The sensor was not specially positioned to lie in the direct line of the acoustic wave, therefore the predicted range in which the partial discharge lies is actually in a circle of radius = 8.3145 cm around the acoustic sensor. This can be diagrammatically depicted as:

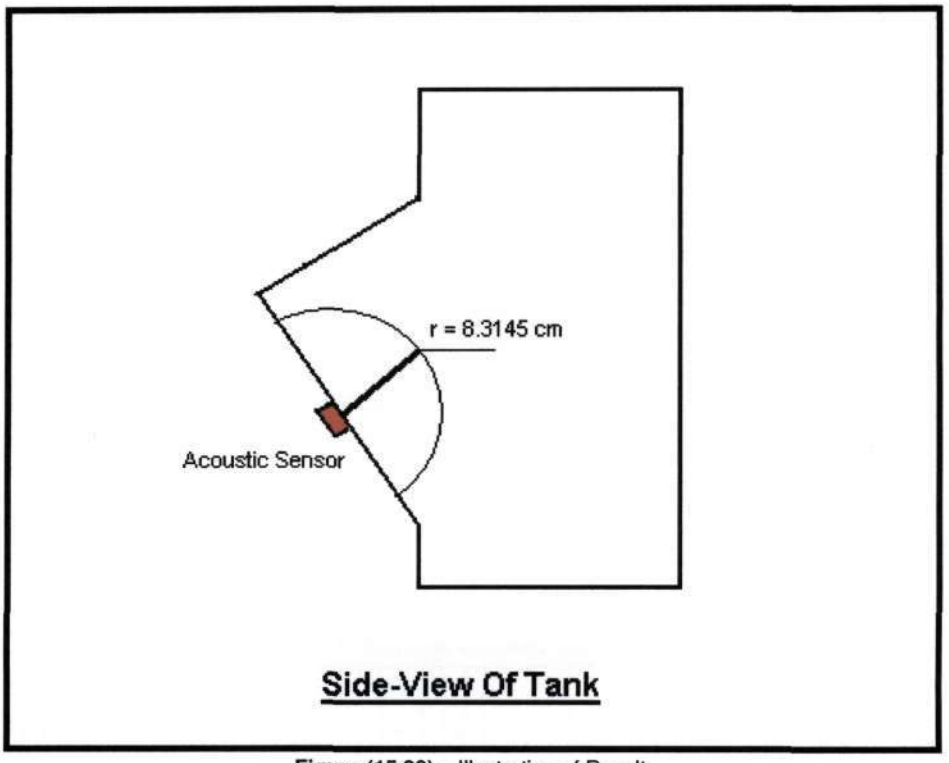

Figure (15.20) – Illustration of Result

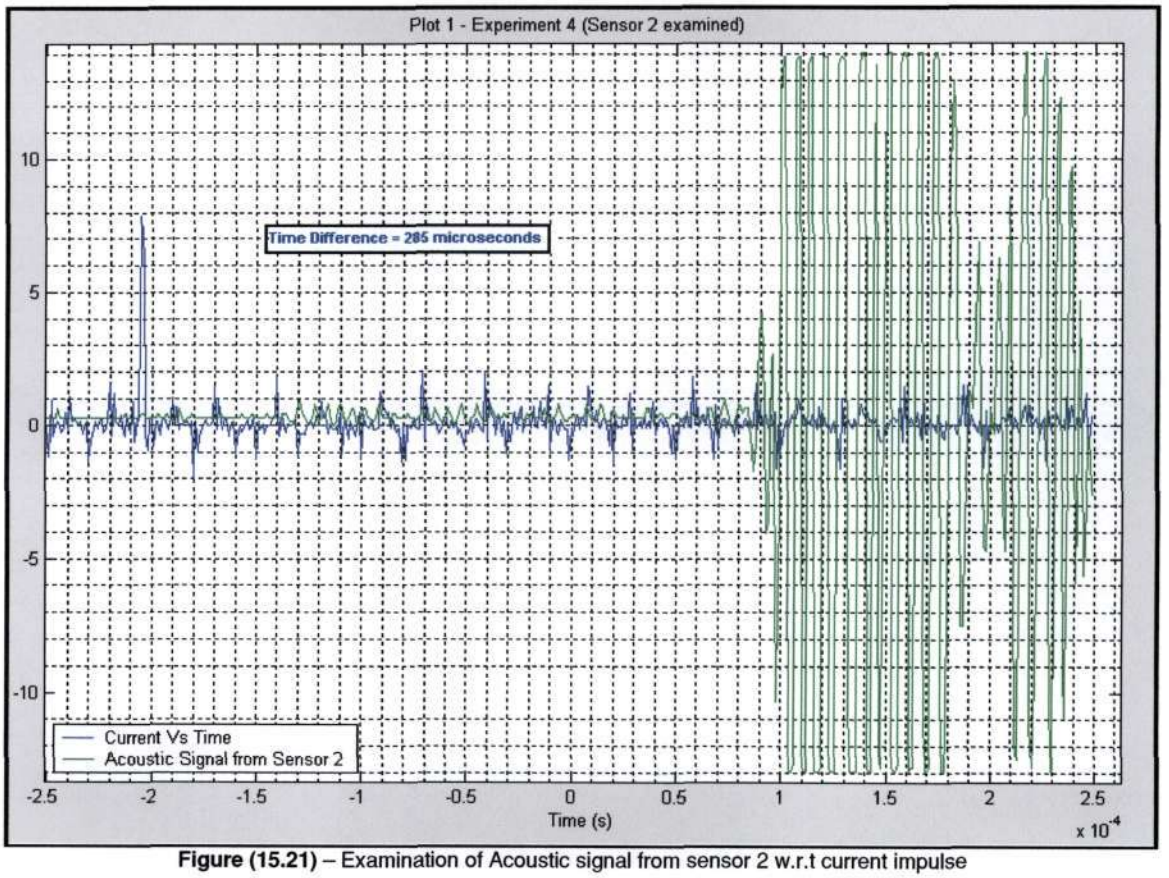

Figure (15.21) – Examination of Acoustic signal from sensor 2 w.r.t current impulse

Figure (15.21), depicts the acoustic signal received from sensor 2, showing the occurrence of the partial discharge. The acoustic signal was noted to occur 285 μs after the occurrence of the current impulse.

Localization calculations:

The localization calculations have been divided into the following steps:

(1). Time taken for acoustic signal to propagate through the steel wall

The time taken for the signal to propagate through the steel wall (taking steel wal to be 2mm thick) is calculated as:

$$time_{steel} = \frac{thickness_{wall}}{speed_{steel}} = \frac{2\times10^{-3}\,m}{3200m/s} = 0.625\mu s$$

Therefore, the time taken for the signal to propagate through the transformer therefore is:

$$time_{transformer} = time_{total} - time_{steel} = 285\mu s - 0.625\mu s = 284.375\mu s$$

(2). Time taken for an acoustic signal to propagate through oil region nearest to sensor:

$$time_{oil\_1} = \frac{dist_{oil\_region}}{speed_{oil}} = \frac{0.08m}{1400m/s} = 57.14\mu s$$

The time taken for an acoustic signal to travel through the first oil region is 57.14μs. This is shorter than the total time taken for the signal to reach the sensor, therefore it can be stated that the partial discharge site has to lie beyond this first oil region.

(3). Time taken for signal to propagate through iron core + copper region

Note, the region which contains the transformer windings, also has copper material contained in it. The speed of sound in copper is approximately 3500 m/s. Therefore, in order to determine the speed of sound through this winding region, an average of the speed of sound in iron (5800 m/s) and the speed of sound in copper (3500 m/s) was taken. Therefore, the speed of sound through the region is 4650 m/s.

$$time_{iron+copper} = \frac{dist_{iron+copper\_region}}{speed_{iron+copper}} = \frac{0.18m}{4650m/s} = 38.71\mu s$$

Therefore, the total time for a signal to propagate through the first oil region and this iron+copper region = 57.14μs + 38.71μs = 95.85μs.

This is still shorter than the total time taken for the signal to reach the sensor, therefore it can be stated that the partial discharge site has to lie beyond this combined first oil region and this transformer windings region.

(4). Calculation of location of P.D. source

Due to the fact that the inner geometry of this transformer is known, it is known that there are is only an oil region beyond this transformer windings region. Therefore to calculate the distance from which this acoustic signal is originating within this oil region, the following steps are followed:

$$time_{remaining} = time_{total} - (time_{steel\_wall} + time_{oil} + time_{iron+copper}) = 188.255\mu s$$

$$distance = speed_{oil} \times time_{rem} = 1400m/s \times 188.255\mu s = 0.263m$$

Therefore, to quote this distance in terms of the geometry of the transformer, by using the sensor as the reference:

Distance of p.d. source from sensor = (distance of steel wall)(distance of first oil region) + (iron and copper region) + (Distance to source from iron and copper region)
= (0.2cm + 8cm + 18cm + 26.3cm) = **52.3 cm**
The following diagram quotes this distance in terms of the measured geometry of the transformer:

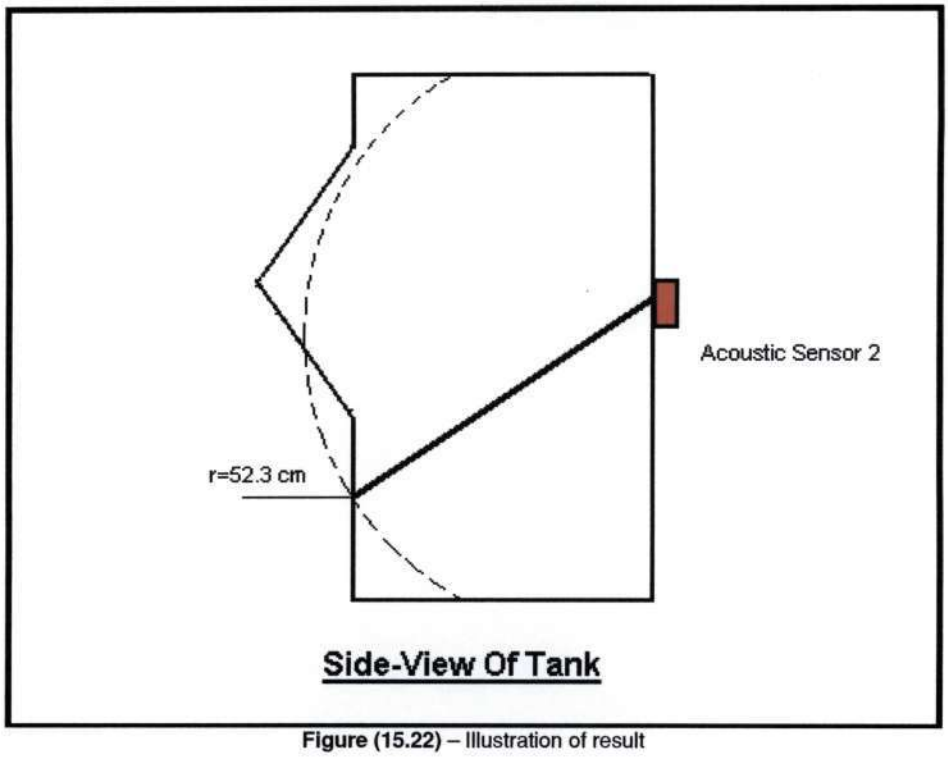

Figure (15.22) – Illustration of result

Combination of results of sensor 1 and sensor 2

The results of sensor 1 and sensor 2 are combined below. This greatly improves the accuracy of the prediction:

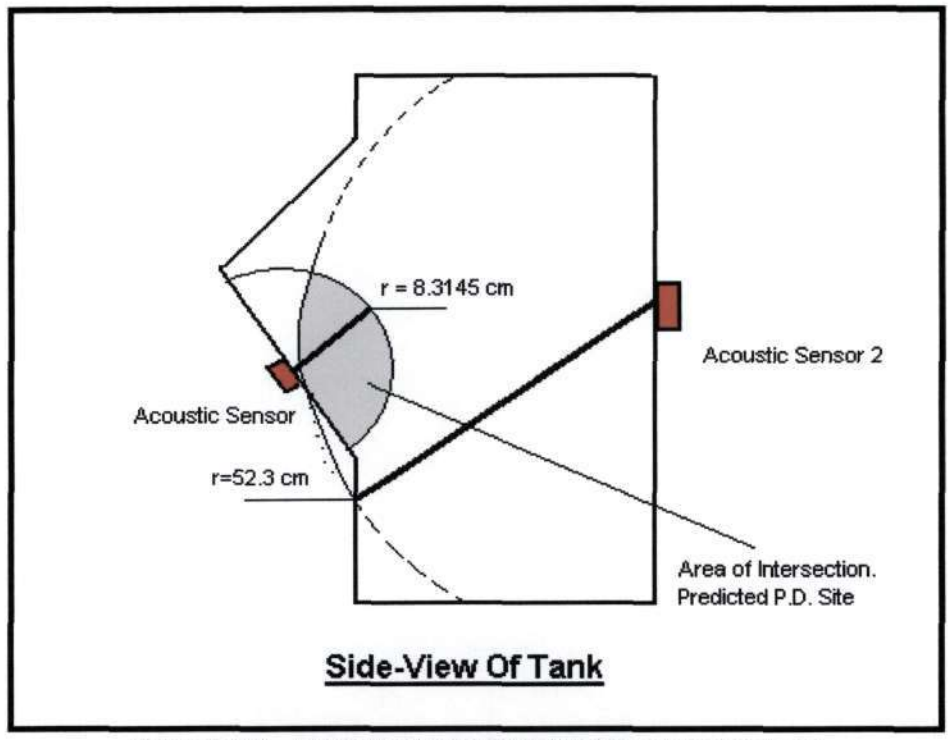

Figure (15.23) – *Illustration of Combined result of Sensor 1 and Sensor 2*

Conclusion

It can be concluded that the accuracy of the simultaneous application of the acoustic and electrical for partial discharge localization greatly increases with the addition of more sensors.

In addition, it can be noted from the above, that the acoustic/electrical method provides an accurate means of determining the location of a partial discharge.

CHAPTER 16
SUMMARY AND CONCLUSION

This chapter presents a summary of the study. It also provides conclusions regarding all outcomes of the study, based on the literature study, the finite element simulations and modeling, and the experimental testing.

16.1 Summary

The acoustic method of partial discharge detection and localization was necessitated by the limitations associated with the conventional methods e.g. the gas in-oil-analysis. Essentially, the acoustic method involves the examination of the acoustic emissions that emanate from high voltage transformer units. This allows several deductions about the condition of the transformer to be made.

The literature review (Section A) provided a detailed review of the following areas:

- Definition and classification of partial discharges
- Characteristics of liquid dielectrics
- Prebreakdown phenomena in liquid dielectrics
- The occurrence and characteristics of streamers
- Breakdown of transformer oil
- The effect of the electrode gap on breakdown in dielectric liquids
- Vapour bubble formation in dielectric liquids
- Fundamental concepts in acoustics
- Transformer insulation: characteristics and properties
- Partial discharge detection techniques
- The acoustic method of partial detection and localisation
- Localisation of the partial discharge site
- The electrical method of partial discharge detection

The finite element modeling (Section B) conclusively proved the following:

- The acoustic method is reliable and consistent in (1) determining the existence of a partial discharge, and (2) determining the spatial location of the partial discharge site.
- In addition, the modeling proved that the acoustic method can be employed successfully in cases where there is more than one partial discharge source present in the same transformer unit.
- Furthermore, the simulations proved that the acoustic method can be used successfully and reliably in complex transformer geometries.

The experimental testing on the specially designed test cell (Section C) conclusively proved the following:

- The breakdown voltage of transformer oil increases non-linearly with an increase in the electrode gap spacing under A.C. test conditions (point to plane electrode configuration).
- It was observed that after successive tests the average dielectric strength of the test liquid reached a stable or plateau with small variances.
- The circulation and filtering of the dielectric test liquid increases the mean dielectric strength of the liquid.
- A decrease in the filter porosity results in an increase in the mean dielectric strength of the dielectric test liquid.
- An increase in the circulation flow of the oil results in an increase in the mean dielectric strength of the test liquid. This increase is not indefinite.

Acoustic testing

- The acoustic method and the electrical method were simultaneously applied during the experimental testing.
- This combination resulted in a method, which had a greatly increased sensitivity and a higher immunity to false alarms. The electrical method was used to provide a zero reference point, from which the time of arrival of the acoustic signal was measured.
- The laboratory tests confirmed the consistency and accuracy of the combined acoustic/electrical for the detection and localization of partial discharges for (1) the case where the acoustic sensors were located in the area of direct reception and (2) the case where the acoustic sensors were located in the area of indirect reception.
- It was also proved that the accuracy of the acoustic method of partial discharge localization increases with an increase in the number of sensors used.
- For all tests a strong correlation between the experimental results and the theoretically predicted results was observed.
- The effect of circulation and filtering in the test cell did not influence the accuracy of the acoustic method. It is believed that pumps with significantly higher flow rates will introduce acoustic disturbances in the system. These disturbances will have to be isolated and filtered by the acoustic conditioning unit.
- It is however imperative that the internal geometry of the transformer is known. This enables accurate calculations of the partial discharge site to be performed.

16.2 Conclusion

The results obtained from this study confirm that acoustic emission sensing offers an excellent, real time solution for the detection as well as the localization of partial discharges. The acoustic sensing method when combined with the electrical method offers a solution that has a greatly increased sensitivity and a higher immunity to false alarms. In order to ensure the accuracy of the method, it is imperative that the internal geometry of the test unit is known. In addition, all sources of possible acoustic disturbances in the system should be isolated and filtered to ensure that the results produced are accurate.

CHAPTER 17: APPENDICES

Appendix: A – Illustrations of simulations for model 3

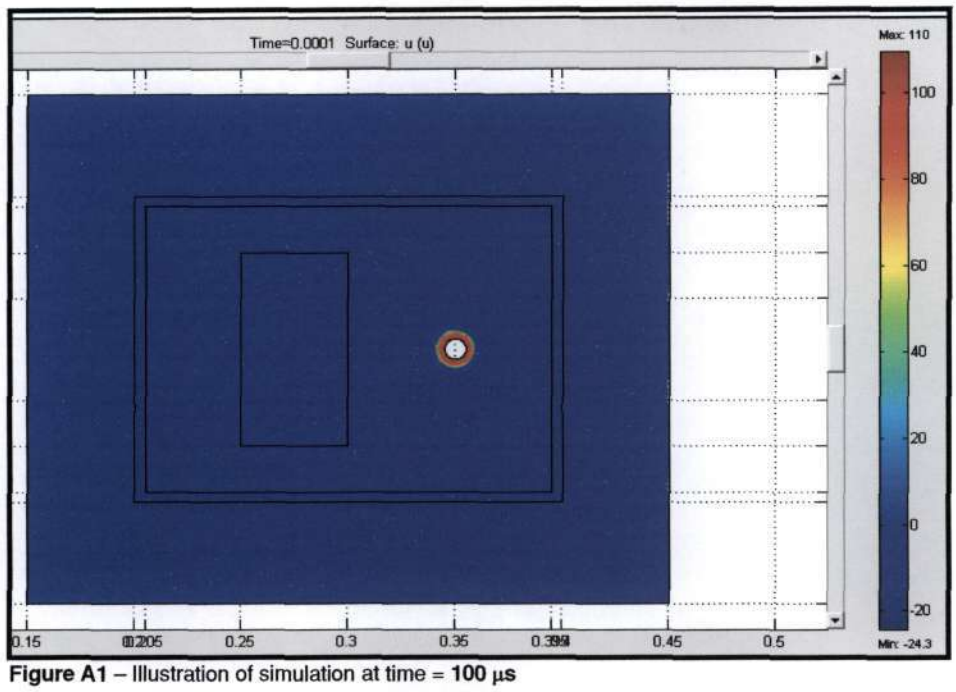

Figure A1 – Illustration of simulation at time = **100 μs**

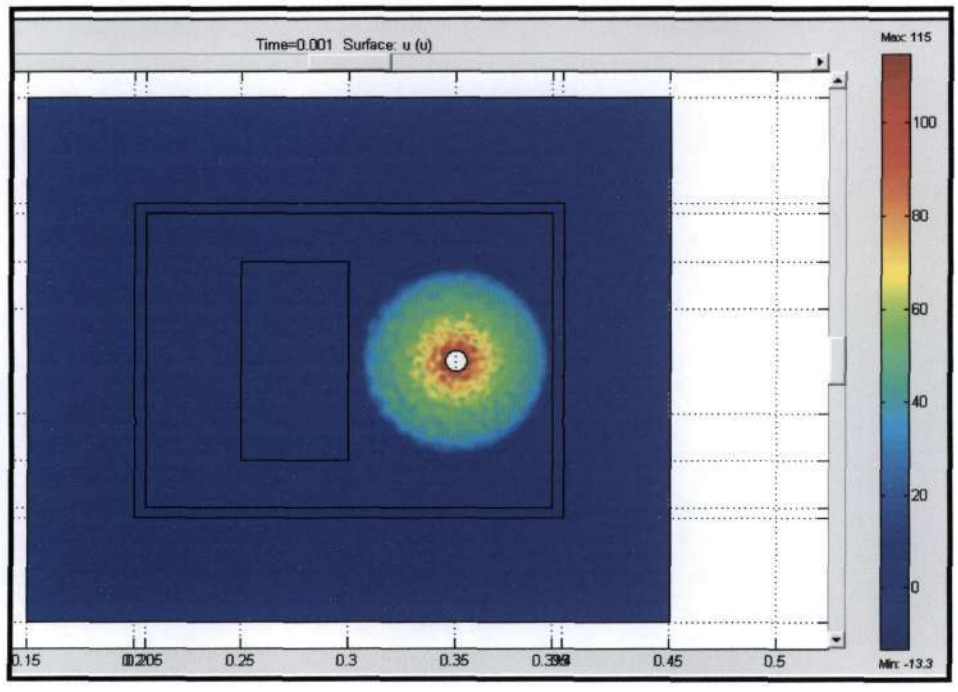

Figure A2 – Illustration of simulation at time = **1 ms**

Figure A1, depicts the initial propagation of the acoustic wave from the p.d. source. Figure A2, shows the wave as it impinges onto the boundaries of the iron core, and the transformer tank wall. Note, that the wave propagation speed increases as it enters the iron core due to the fact the speed of sound in the iron core is significantly larger than the speed of sound in the transformer oil medium.

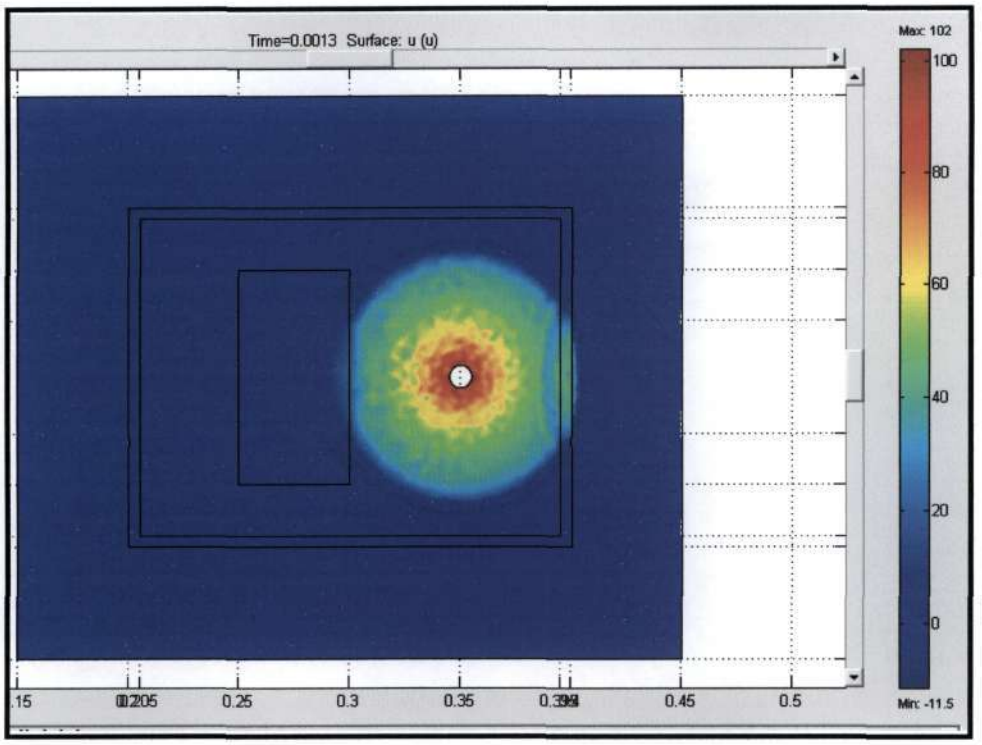

Figure A3 – Illustration of simulation at time = **1.3 ms**

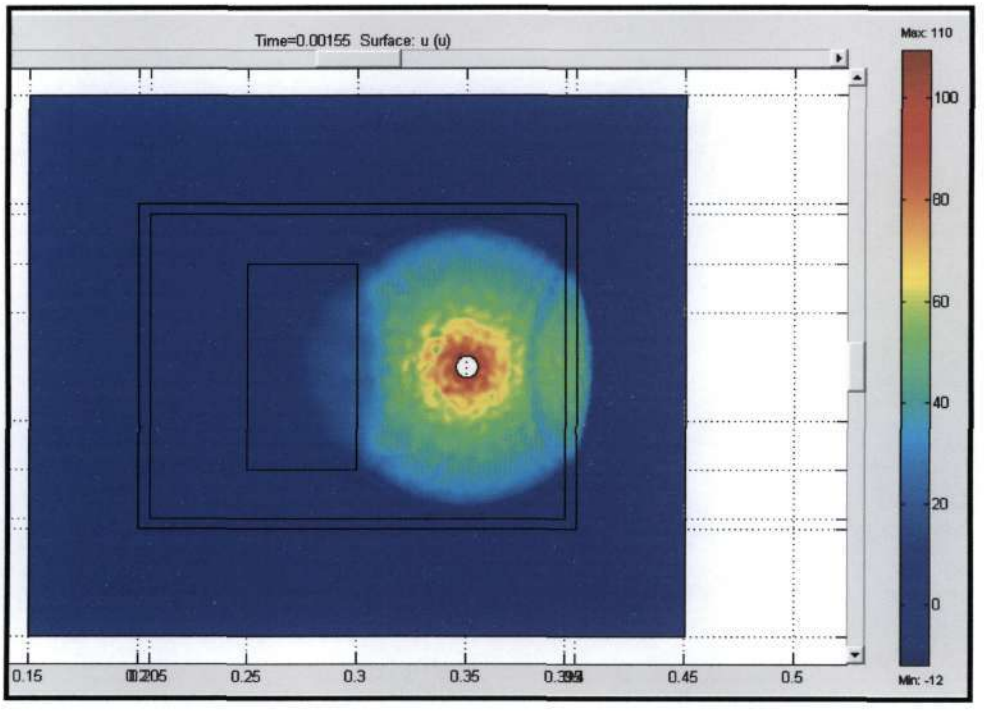

Figure A4 – Illustration of simulation at time = **1.55 ms**

Figure (A3) and figure (A4), illustrate the energy which is transmitted, and the energy which is reflected when the acoustic wave impinges onto the inner iron core, and the boundary of the steel tank wall.

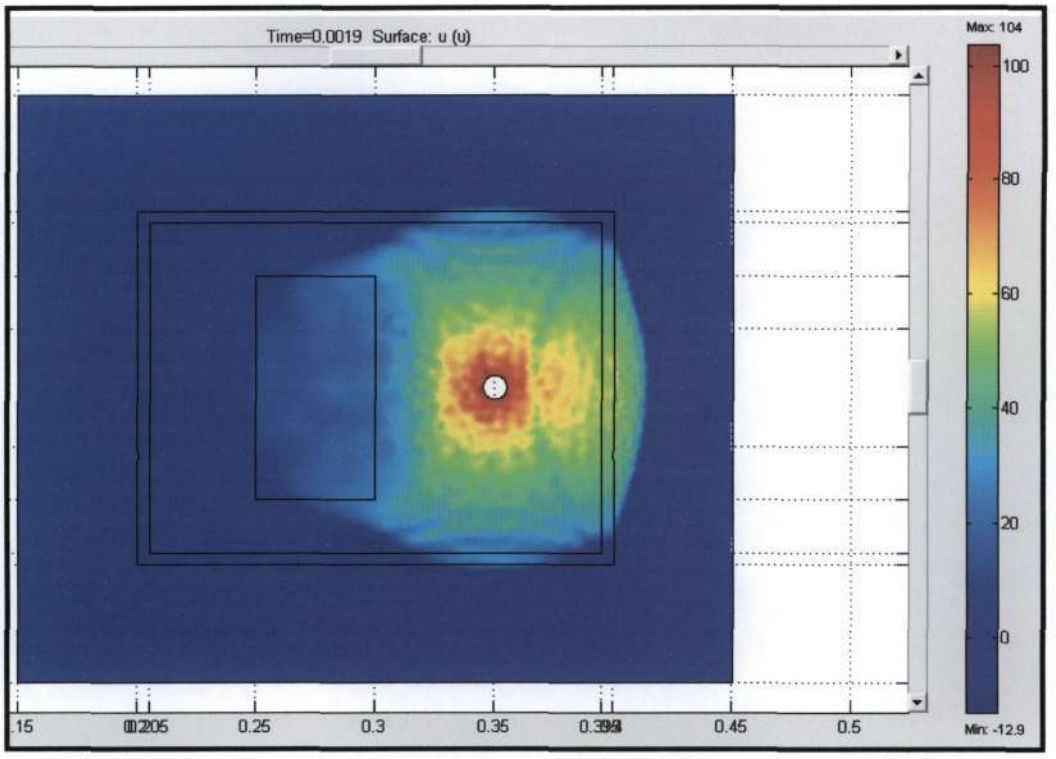

Figure A5 – Illustration of simulation at time = **1.9 ms**

Figure (A5), depicts the wave as it impinges onto the outer tank walls of the transformer. The acoustic sensors measure the intensity (in the x-direction), of the signal as it impinges onto the wall.

Appendix B - Illustrations of simulations for model 4

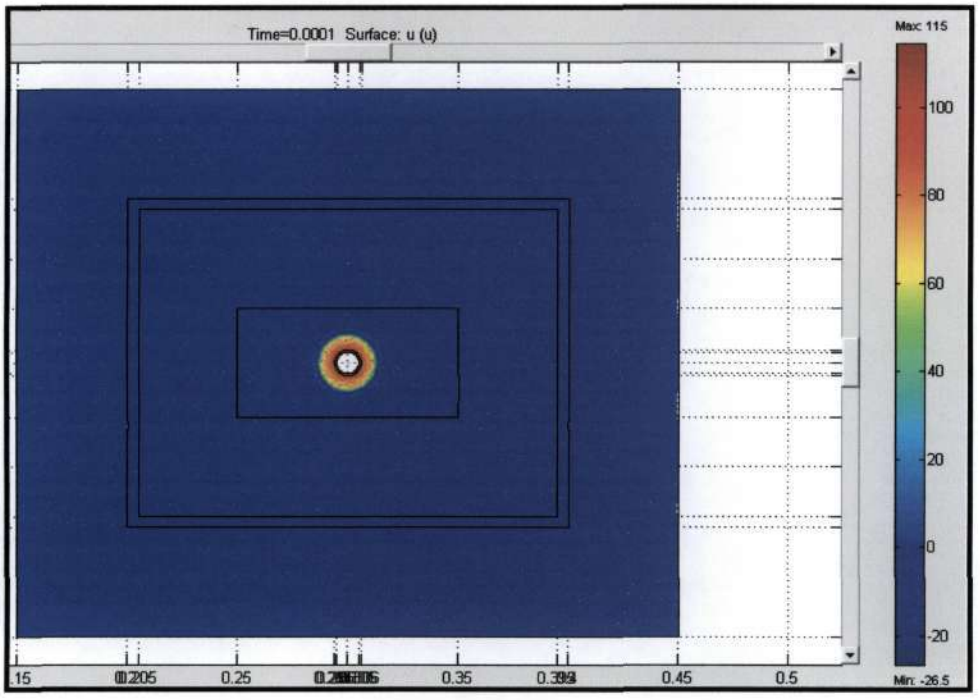

Figure B1 – Illustration of simulation at time = **100 μs**

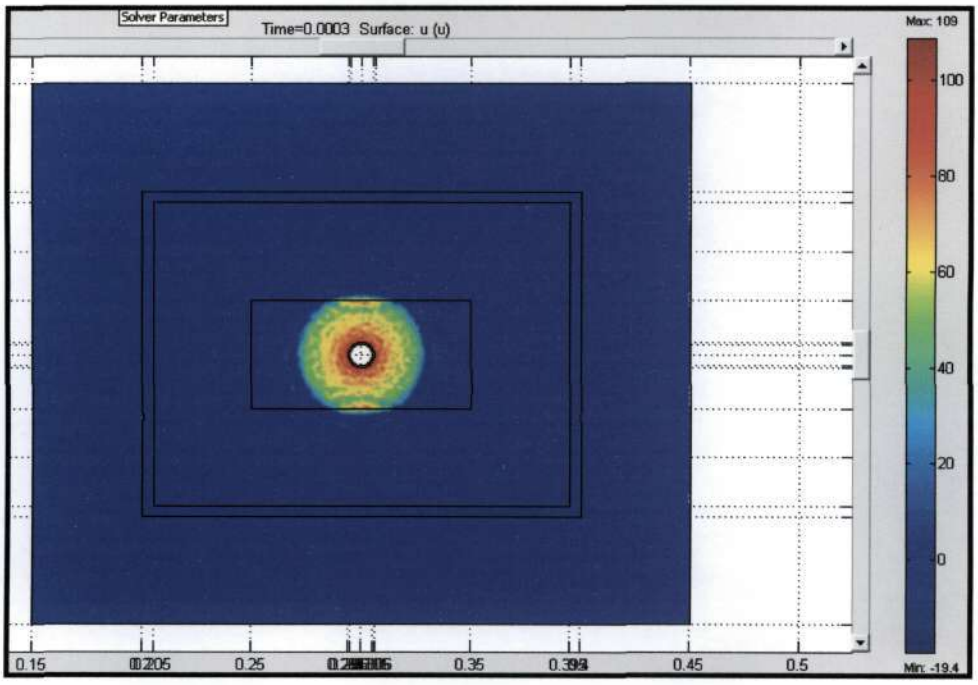

Figure B2 – Illustration of simulation at time = **300 μs**

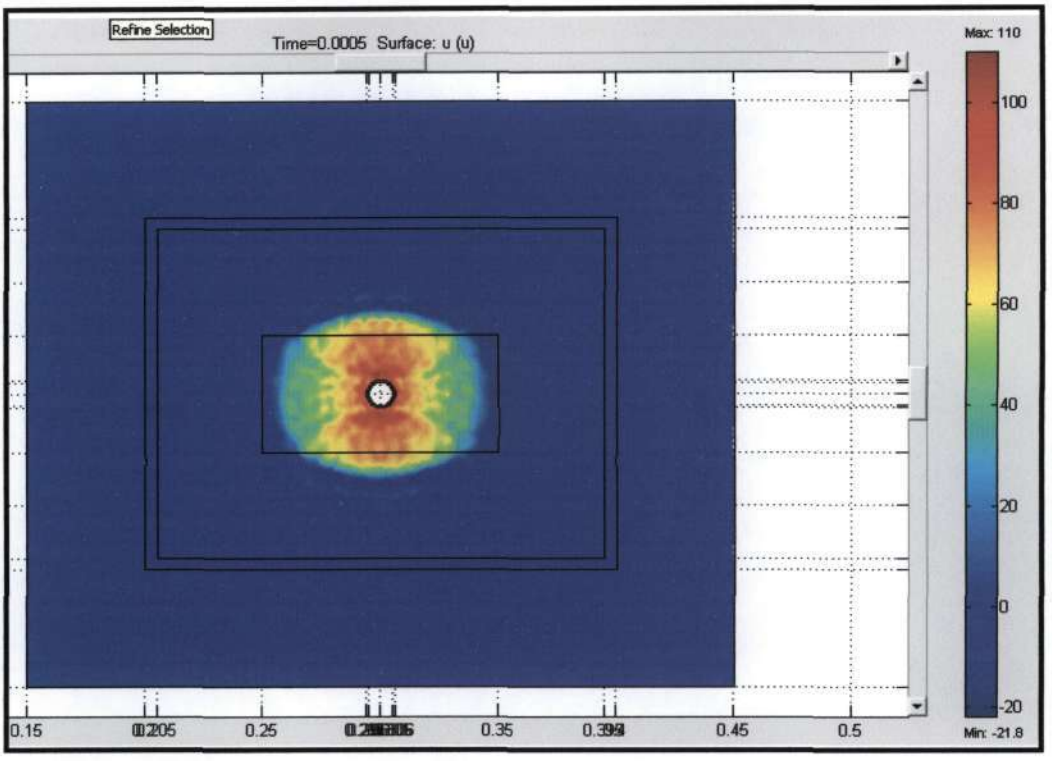

Figure B3 – Illustration of simulation at time = **500 μs**

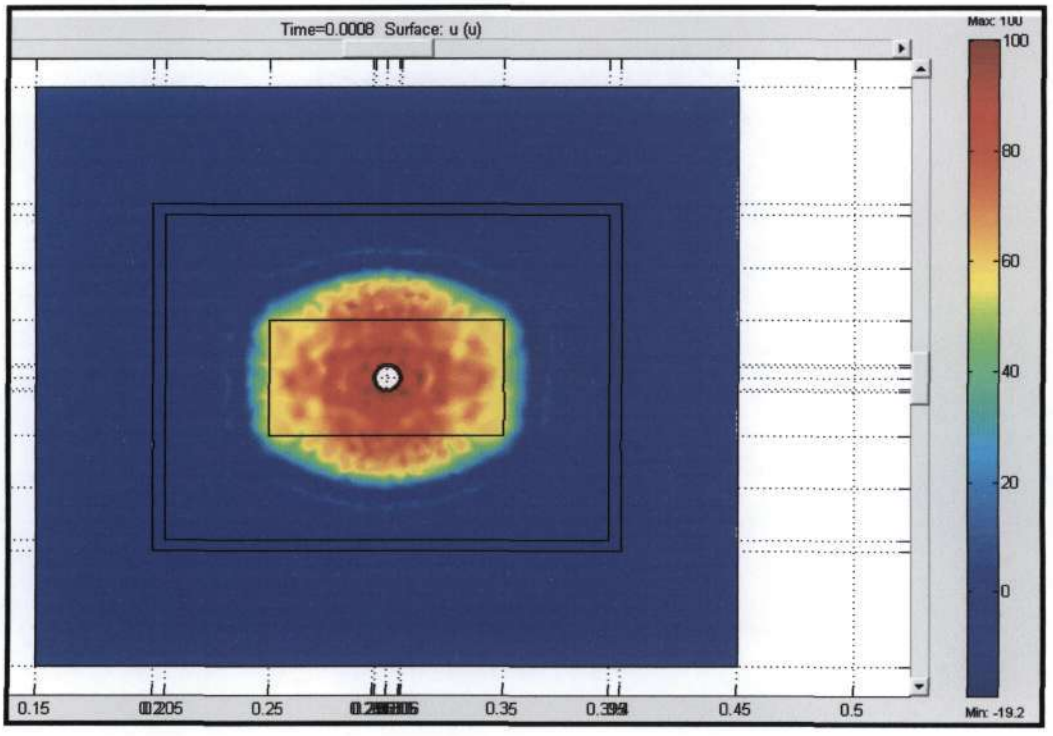

Figure B4 – Illustration of simulation at time = **800 μs**

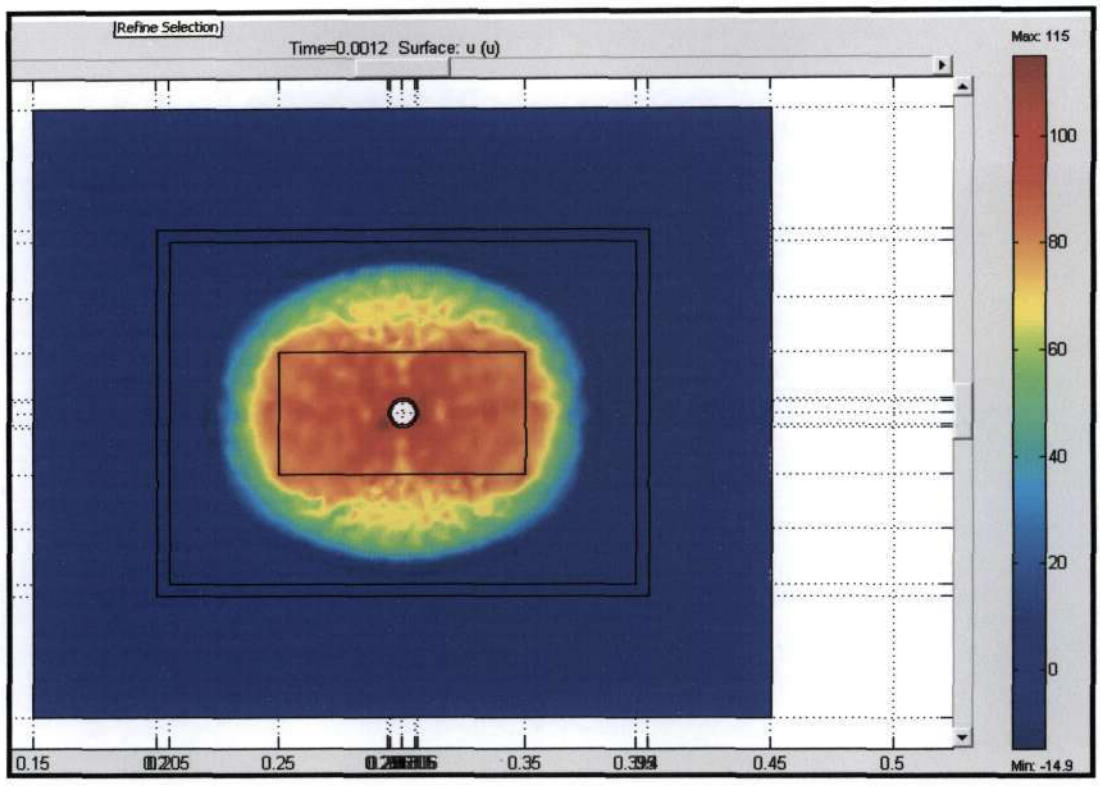

Figure B5 – Illustration of simulation at time = **1.2 ms**

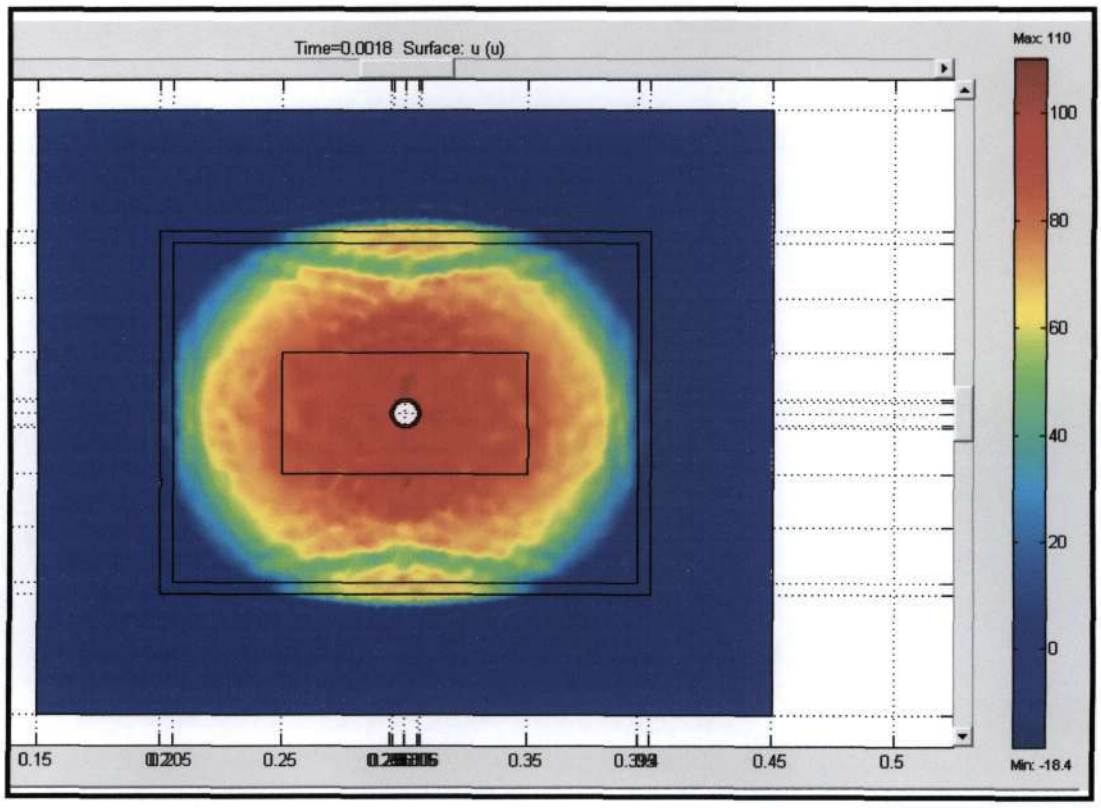

Figure B6 – Illustration of simulation at time = **1.8 ms**

Appendix C – Experimental results

Test: 1mm gap: Point to Plane

Flash Over

Oscilloscope Reading	**RMS kVolts**	**Barometer** 750		**Pressure Kpa** 100.00
1.4	20.79			
1.59	23.61	**Dry bulb**	**Wet bulb**	**Humidity. g/m3**
1.54	22.87	21	18.5	15
1.54	22.87			
1.4	20.79			
Average =	22.18			
Variation =	13.5%			
STD Deviation =	1.31			
Max. deviation from mean value =	6.43%			

Table (C1) – Test results: 1mm electrode gap spacing

Test: 2mm gap: Point to Plane

Flash Over

Oscilloscope Reading	**RMS kVolts**	**Barometer** 750		**Pressure Kpa** 100.00
1.73	25.69			
1.87	27.77	**Dry bulb**	**Wet bulb**	**Humidity. g/m3**
1.78	26.43	21	18.5	15
1.82	27.03			
1.82	27.03			
Average =	26.79			
Variation =	8.1%			
STD Deviation =	0.78			
Max. deviation from mean value =	4.10%			

Table (C2) – Test results: 2mm electrode gap spacing

Test: 3mm gap: Point to Plane

Flash Over

Oscilloscope Reading	**RMS kVolts**	**Barometer** 748		**Pressure Kpa** 99.73
2.71	40.24			
2.76	40.98	**Dry bulb**	**Wet bulb**	**Humidity. g/m3**
2.71	40.24	21	19	15.5
2.76	40.98			
2.81	41.73			
Average =	40.84			
Variation =	3.6%			
STD Deviation =	0.62			
Max. deviation from mean value =	2.18%			

Table (C3) – Test results: 3mm electrode gap spacing

Appendix D: Experimental results

Breakdown test results (with circulation and filtering)

Test: 1mm gap: Point to Plane:

Flash Over

Oscilloscope Reading	**RMS kVolts**	**% Variation (from mean)**	**Barometer** Direct		**Pressure Kpa** 102.20
2.71	26.16	10.37			
2.43	23.45	19.65	**Dry bulb**	**Wet bulb**	**Humidity. g/m3**
3.37	32.53	11.46	20	17	13
3.27	31.56	8.13			
3.34	32.23	10.43			
Average =	**29.19**				
STD Deviation =	**4.13**				
Max. deviation from mean value=	**19.65%**				

Figure (D1): Test results for breakdown testing: 1mm gap spacing (with filtering)

Test: 2mm gap: Point to Plane:

Flash Over

Oscilloscope Reading	**RMS kVolts**	**% Variation (from mean)**	**Barometer** Direct		**Pressure Kpa** 102.20
3.3	43.00	22.54			
2.09	31.03	11.56	**Dry bulb**	**Wet bulb**	**Humidity. g/m3**
2.53	37.57	7.06	20	17	13
2.15	31.93	9.02			
2.15	31.93	9.02			
Average =	**35.09**				
STD Deviation =	**5.13**				
Max. deviation from mean value=	**22.54%**				

Figure (D2): Test results for breakdown testing: 2mm gap spacing (with filtering)

Please see overleaf for 3mm results.....

Test: 3mm gap: Point to Plane:

Flash Over

Oscilloscope Reading	**RMS kVolts**	**% Variation (from mean)**	**Barometer** Direct		**Pressure Kpa** 102.20
4.53	67.27	2.17			
4.06	60.29	8.43	**Dry bulb**	**Wet bulb**	**Humidity. g/m3**
5.15	76.47	16.15	20	17	13
4.68	69.49	5.55			
3.75	55.68	15.43			
Average =	**65.84**				
STD Deviation =	**8.10**				
Max. deviation from mean value=	**16.15%**				

Figure (D3): Test results for breakdown testing: 3mm gap spacing (with filtering)

CHAPTER 18
BIBLIOGRAPHY

1) F.H Kreuger, Discharge Detection in High Voltage Equipment, Spottiswoode, Ballantyne and Co.Ltd.

2) Specification for unused mineral insulating oils for transformers and switchgear, IEC publication pp 296, 1982

3) E.Howells, E.T. Norton, Detection Of Partial Discharges in Transformers using Acoustic Emission Techniques, IEEE Trans. Pow. Appl. Sys. 97 (1978) pp 1538 -1549.

4) Train, D., Mercier, A., and Thorne D., The Detection Of Partial Discharges in High Voltage Potential Transformers in Service., IEEE Transaction on Power Apparatus and Systems, Vol. 93, Nov-Dec. 1974, pp. 1909-1916

5) Karsai K., Kerenyi D., Kiss L., Large Power Transformers, Elsevier Science Publishers. 1987.

6) Taylor W.T. High Voltage Power Transformers, Sir Isaac Pitman & Sons, Ltd, 1922

7) D.J. Allan, J.A.C. Forest, E.L. Howitt and A.B. Petchell, Electric and Acoustical Location of Discharges in Transformers, IEE Conference on Diagnostic Testing of High Voltage Power Apparatus in Service, March 6-8, 1973 Conference Publication Number 94, Part 1, pp 65-70

8) Mark MacAlpine, Zhao Zhiqiang, M. Suleyman Demokan, Development of a fibre-optic sensor for partial discharges in oil-filled power transformers, Electric Power Systems Research 63 (2002) pp 27 – 36.

9) Y. Lu, X. Tan and X. Hu. P.D. detection and localisation by acoustic measurements in an oil-filled transformer, IEE Proc.-Sci. Meas. Technology Vol 147, No.2, March 2000.

10) F.H Kreuger, Discharge Detection in High Voltage Equipment, Spottiswoode, Ballantyne and Co.Ltd.

11) L. Tang, W. Wang, Acoustic location of partial discharges in online power transformer, 6th Int. Symp. High Voltage Engineering, New Orleans, LA, 1989, Paper 22.09.

12) Kawada H., Honda M., Inoue T., Amemiya T., Partial Discharge Automatic Monitor for Oil-Filled Power Transformer, IEEE Trans. Power App. And Sys., Vol. PAS-103, No.2, February 1984.

13) Acoustic Emission Consulting, Inc. Partial Discharge Detection in Transformers. Ver : 4/24/01.

14) Lundgaard L.E., Partial Discharge – Part XIII : Acoustic Partial Discharge Detection – Fundamental Considerations, IEEE Electrical Insulation Magazine, July/August 1992-Vol :8, No :4

15) Eleftherion Peter M., Partial Discharge XXI : Acoustic Emission-Based P.D. Source Location In Transformers, IEEE Electrical Insulating Magazine, November/December 1995 –Vol :11, No.6

16) Lundgaard L.E., Partial Discharge – Part XIV: Acoustic Partial Discharge Detection – Practical Application, IEEE Electrical Insulation Magazine, September/October 1992 – Vol :8, No.5

17) Howells E.; Norton E.T., Parameters Affecting The Velocity Of Sound In Transformer Oil, IEEE Transactions on P.A.S., Vol. P.A.S-103, No.5, May 1984

18) Meunier Robert, Vaillancourt Georges H., Propagation behaviour of acoustic partial discharge signals in oil-filled transformers, Conference Record of the ICDL 1996, 12th International Conference on Conduction and Breakdown in Dielectric Liquids, Roma, Italy, July 15-19, 1996

19) Bengtsson T., Leijon M., Ming L., Jonsson B., Directivity of acoustic signals from partial discharges in oil, IEE Proc.-Sci.Meas, Technol., Vol.142, No.1, January 1995

20) Femlab, User's Guide and Introduction, Version 2.0, Comsol AB.

21) Femlab Model Library, Version 2.0, Comsol AB

22) SABS IEC 60270, Specification: High-voltage test techniques – Partial discharge measurements, 2000.

23) Blackburn T.R., James R.E., Su Q, Phung T.; An improved electric/acoustic method for the location of partial discharges in power transformers; Proceedings of the 3rd International Conference on Properties and Applications of Dielectric materials; 1991.

24) Kreuger F.H.; Gulski E., Krivda A.; Classification of Partial Discharges; IEEE Transactions on Electrical Insulation, Vol. 28, No 6, December 1993.

25) Phung B.T., Blackburn T.R., Liu Z.; Acoustic measurements of partial discharge signals; Journal of Electrical and Electronics Engineering, Australia; 2000.

26) Allan D.J., Forrest J.A.C., Howitt E.L., Petchell A.B.; Electric and Acoustic Location of discharges in transformers; Conference on Diagnostic testing of High Voltage Power Apparatus in Service; 6-8 March 1973.

27) Stricklett K.L., von Glahn P., Van Brunt R.J., Cheim L.A.V.; Correlations between Electrical and Acoustic Detection of Partial Discharges in Liquids and Implications for Continuous Data recording; IEEE Trans. Diel. Elec. Insul., Vol2, No 4, August 1995.

28) Menon R., Kolambekar S., Buch N.J., Ramamoorty M.; Correlation of Acoustic Emission Method and Electrical Method for Detection of Partial Discharges in Transformers; 2001 IEEE 7th International Conference on Solid Dielectrics, June 25-29, 2001, Eindhoven, the Netherlands.

29) Grossmann E., Feser I.K.; Comparison of the sensitivity of an Acoustical and Electrical P.D.-Measurement on Transformers in the Laboratory and On Site; 2000 Conference on Electrical Insulation and Dielectric Phenomena, 2000.

30) Tobazcon R.; Prebreakdown phenomena in dielectric liquids; IEEE Trans. Diel. Elec. Insul., Vol 1, No. 6, December 1994, pp 1132 – 1147.

31) Beroual A.; Electronics and Gaseous processes in the prebreakdown phenomena of dielectric liquids; Journal Of Applied Physics, Vol. 73(9), May 1 1993, pp 4528 – 4533.

32) Danikas M.G.; Breakdown Of Transformer Oil; IEEE Electrical Insulation Magazine; Vol.6, No. 5, Sept/Oct 1990, pp 27 – 34.

33) Watson P.K., Higham J.B.; Electric Breakdown of Transformer Oil; Proc. IEE, Vol. 100, 1953, pp 168-173.

34) Kattan R., Denat A., Bonifaci N.; Formation of Vapor Bubbles in Non-Polar Liquids Initiated by Current Pulse; IEEE Transactions on electrical Insulation; Vol. 26; No.4; August 1991; pp 656 – 662

35) Kattan R., Denat A., Lesaint O.; Generation, Growth, and Collapse of Vapor Bubbles in Hydrocarbons Liquids under a High Divergent Electric Field; J. Appl. Phys.; Vol. 66; 1989; pp. 4062-4066.

36) Naudé C.F., Ellis A.T.; On the Mechanism of Cavitation Damage by Nonhemispherical Bubbles Collapsing in Contact with a Solid Boundary; J. Basic Eng. Trans. ASME; Vol. 83; 1961; pp 648-656.

37) Lord Rayleigh; On the Pressure Developed in a Liquid during the Collapse of a Spherical Cavity; Phil. Mag.; Vol. 34; 1917; pp 94-98.

38) Hentschel W., Lauterborn W.; Acoustic Emission of Single Laser-produced Cavitation Bubbles and their Dynamics; Appl. Sci. Res.; Vol. 38; 1982; pp. 225-230.

39) Watson P.K., Chadband W.G., Mak W.Y.; Bubble Growth following a Localised Electrical Discharge and its relationship to the breakdown of Triggered Spark Gaps in Liquids; IEEE Trans. Electr. Insul; Vol. 20; 1985; pp. 275 – 280.

40) Strickett K.L., Fenimore C., Kelley E.F., Yamashit H., Pace M.O.,Blalock T.V, Wintenberg A.L., Alexeff I.; IEEE Trans. Electr. Insul.; Vol. 26; 1991.

41) Chadband W.G., Wright G.T.; Brit. J. Appl. Phys.; Vol. 16, 1965.

42) Haidara M., Bonifaci N., Denat A.; Corona Discharges in Liquid and Gaseous Hydrocarbons. Influence Of Pressure."; Proc. Gaseous Dielectrics VI, Knoxville (USA); September 23-27; 1990.

43) Cygan S., Laghari J.R.; Dependence of the Electric Strength on Thickness, Area and Volume of Polypropylene; IEEE Trans. On Elec. Insul.; Vol. EI-22; No. 6; pp 835 – 837; 1987.

44) Boggs S.; Analytical approach to breakdown under impulse conditions, IEEE Transactions on Dielectrics and Electrical Insulation; Vol. 11; No. 1; February 2004.

45) Beroual A., Zahn M., Badent A., Kist K., Schwabe A.J., Yamashita H., Yamazawa K., Danikas M., Chadband W.G., Torshin Y.; Propagation and structure of streamers in liquid dielectrics; IEEE Electrical Insulation Magazine; Vol. 14; no. 2; March/April 1998.

46) ASTM D 3300-00; ASTM International; Standard Test Method for Dielectric Breadkown Voltage of Insulating Oils of Petroleum Origin under Impulse Conditions; Dec 2000.

47) BP Lube Marketing, http://www.bpoil.co.za/products, 26 August 2004.

48) Forster E.O, Yamashita H., Mazzetti C., Pompili M., Caroli L., Patrissi S.; The effect of the electrode gap on breakdown in liquid dielectrics; IEEE Transactions on Dielectrics and Electrical Insulation; Vol. 1; No. 3; June 1994.

49) Nitta Y., Aihara Y.; Polarity effect on breakdown in Organic liquids; IEEE Trans. Elec. Ins.; Vol. 11; pp. 91-94; 1976.

50) Zaky A.; Effect of polarity and gap length on the breakdown characteristics of mineral oil for non-uniform fields; J. Phys. D: Appl. Phys.; Vol 9; pp. 77-79; 1976.

51) Yoshino K.; Electric properties of liquid perfluorocarbon breakdown characteristics; Technology report of the Osaka University; Vol. 28; No. 1471; 1979.

52) Yoshino K., Ohseko K., Shiraishi M., Terauchi M., Inuishi Y.; Dependence of polarity effect of dielectric breakdown on molecular structure of liquids; Proc. 7th Int. Conf. Conduction and breakdown in dielectric liquids; IEEE #81, CH 1594-1; pp. 236-240; 1981.

53) Fenimore C., Stricklett K.L., Yamashita H., Kawai H., Forster E.O., Pompili M.; The inception and structure of prebreakdown streamers in perfluoro polyethers; Conf. Record, 10th Int. Conf. Conduction and breakdown in dielectric liquids; IEEE #90 CH 2812-6; pp. 430-435; 1990.

54) Forster E.O., Mazzetti C., Pompili M., Cecere R.; The effect of molecular structure on the properties of dielectric fluids; IEEE trans. Elec. Ins.; Vol. 26; pp. 749-754; 1991.

55) Mazzetti C., Pompili M., Forster E.O.; Study of the time to breakdown in transformer oils under impulse conditions; IEEE Trans. Elec. Ins.; Vol. 25; pp. 1111-1116; 1990.

56) De Vos J.C., Vermeer J.; On the impulse-strength of a composite insulation; CIGRE' Report 226, 1960.